ENCLOSURE 4-3

Risk-Informed Closure of GSI-191

Volume 3

Engineering (CASA Grande) Analysis

South Texas Project Risk-Informed GSI-191 Evaluation

Volume 3

CASA Grande Analysis

Document: STP-RIGSI191-V03
Revision: 2
Date: November 6, 2013

Prepared by:
Timothy D. Sande, Enercon Services, Inc.
Bruce C. Letellier, Alion Science and Technology
Gilbert L. Zigler, Enercon Services, Inc.

Reviewed by:
Zahra Mohaghegh, University of Illinois, Urbana-Champaign
Seyed A. Reihani, University of Illinois, Urbana-Champaign

Approved by:
Ernest J. Kee, South Texas Project

The Risk-Informed GSI-191 Closure Pilot Program is piloted by the South Texas Project (STP) Nuclear Operating Company and jointly funded with several other licensees. It is a collaboration of experts from industry, academia, and a national laboratory. In general, all products are developed jointly and reviewed in regularly scheduled (monthly) Technical Team Meetings and weekly teleconferences as well as in specific review cycles by Independent Oversight (technical evaluation of all materials), STP Nuclear Operating Company project management, and STP Nuclear Operating Company quality management. The business entities, the main areas of investigation, and the principal investigators of the Pilot Program are summarized below.

STP Nuclear Operating Company

Project Management, Licensing, Quality Assurance

Steve Blossom; Rick Grantom (ret.); Ernie Kee; Wayne Harrison (ret.); Wes Schulz

Alion Science & Technology

Containment Accident Stochastic Analysis (CAS) Grande & GSI-191 Analysis & Methodology Implementation (GAMI)

Bruce Letellier, PhD[1]; Janet Leavitt, PhD[2];
Tim Sande[3]; Gil Zigler[3]; Austin Glover[3], Clint Shaffer, Joe Tezak[3]

The University of New Mexico

Corrosion/Head Loss Experiments (CHLE)

Kerry Howe, PhD

University of Illinois at Urbana Champaign

Independent Oversight

Zahra Mohaghegh, PhD[4]; Seyed Reihani, PhD[4]

Texas A&M University

Thermal Hydraulics (TH)

Yassin Hassan, PhD; Rodolfo Vaghetto, PhD; Saya Lee

The University of Texas at Austin

Uncertainty Quantification (UQ), Jet Formation

Elmira Popova, PhD (1962-2012); David Morton, PhD; Alex Galenko, PhD; Jeremy Tejada, PhD; Erich Schneider, PhD

ABS Consulting

Probabilistic Risk Assessment (PRA)

David Johnson, ScD; Don Wakefield; Tom Mikschl

Knf Consulting Services, LLC

Location-Specific Failure Damage Mechanism (DM)

Karl Fleming; Bengt Lydell (ScandPower)

[1] Previous to 2013, Los Alamos National Laboratory
[2] Previously, UNM
[3] From January 2013, Sande, Glover, Zigler, and Tezak, ENERCON
[4] Previous to 2013, Soteria Consultants, LLC

Revision History Log

Revision	Date	Description
0	1/30/2013	Original document.
1	6/6/2013	The following changes were made in this version of the report: • Miscellaneous editorial changes • Replaced proprietary information related to the fiberglass debris size distribution and fiberglass erosion fractions with references to specific tables that contain the same information in other documents. • Added a new section describing the information process flow in CASA Grande. • Added a description at the end of the conventional head loss section to clarify that the head loss values calculated with the NUREG/CR-6224 correlation were increased significantly to account for uncertainties in the correlation. • Replaced informal email reference for shedding parameters with a revised version of the UT technical report and updated parameter values.
2	See Cover page	Several changes were made to this version of the report to address inconsistencies that were discovered between the previous version and the actual implementation in CASA Grande. The changes to the report include: • Revised figures in Section 1 to reflect the final implementation. • Revised tables and figures in Section 2.1 to reflect the implemented relationship between various input parameters. • Revised discussion in LOCA frequency input section to describe interpolated values that were excluded from the LOCA frequency inputs, and updated tables to match the format of the reference document. • Deleted the equations and probability distributions for active water volume and pool level in Section 2.2 that were not implemented in CASA. • Revised footnotes to correct reference numbers. • Corrected total SI flow rate for 27.5-inch DEGB in Section 2.2 along with the associated figure and equation. • Added elevation difference below the containment floor for CS and LHSI pumps as well as the HHSI pumps in Section 2.2. • Deleted the figure in Section 2.2 showing several pool temperature

Revision	Date	Description
		profiles along with the interpolation scheme that was not implemented in CASA, and added a table showing the specific values that were implemented. • Added statements in the design input and debris generation analysis sections that the bounding LBLOCA qualified coatings quantities were used for all break sizes in CASA. Also added a footnote in Section 2.2 clarifying the basis for the qualified coatings quantities used. • Added an assumption that the qualified coatings debris is assumed to fail as 10 μm particles. • Deleted unqualified coatings figures and data in Section 2.2 that were not implemented in CASA. • Revised description of the treatment of unqualified coatings in the debris generation analysis section to clarify the CASA evaluation. • Deleted destruction pressures corresponding to the insulation ZOI sizes in Section 2.2. • Split assumption regarding linear interpolation of LOCA frequencies into two separate assumptions—one for the interpolation of the top-down frequencies and another for the interpolation of the bottom-up frequencies. • Made several corrections to the characteristic debris sizes and densities shown in the strainer head loss analysis section including: o Corrected the size and S_v for small and large pieces of fiberglass to match fiberglass fines. (Also deleted the corresponding assumption that small and large pieces of fiberglass can be treated as cubes for head loss calculations.) o Corrected the macroscopic density of Microtherm fiber from 15 lb_m/ft^3 to 2.4 lb_m/ft^3. o Corrected the densities for Microtherm TiO_2 and SiO_2, which were inadvertently switched in the previous revisions. o Corrected the size and S_v for epoxy fines from 6 μm to 6 mils (152 μm). o Corrected the S_v for epoxy chips, which was incorrectly calculated in previous revisions. o Added justification for specific values used. • Deleted discussion of initial pool chemistry, pool pH, and metal

Revision	Date	Description
		quantity inputs from Section 2.2. • The assumptions that there would be no washdown transport for breaks where sprays are not initiated, and that unqualified coatings would wash down to the pool immediately if they fail while the sprays are still on were both deleted. • A new assumption was added that the transport fractions for an LBLOCA in the steam generator compartments can be used for all breaks. • Updated the debris transport analysis section to more accurately describe specific transport fractions used in CASA Grande. • Deleted table of inputs for clean strainer head loss in Section 2.2 and replaced it with the maximum value. Also updated the clean strainer head loss analysis section to specify that the maximum clean strainer head loss was used for all breaks. • Revised penetration parameters in Section 2.2 to show η in units of min^{-1} rather than a dimensionless variable. Also deleted inaccurate equation in the debris penetration analysis section used to correct η from the test conditions to the plant conditions. • Edited assumption for hot leg switchover timing from 6 hours to a range from 5.75 to 6 hours. • Added a note stating that a 5 minute time increment was used in CASA. • Provided additional justification for the assumption that a combination of pumps failing in the same train is worse than the same combination of pumps failing in separate trains. • Modified assumption that spray erosion would occur prior to the start of recirculation to also include pool erosion. • Deleted assumption that the gas void at the pumps would be proportional to the pump flow split since the gas void fraction at the strainers was assumed to be the same as the gas void fraction at the pumps. • Deleted assumption regarding the effects of counter-current flow on debris buildup in the core. • Clarified assumption on small break boron precipitation to state that boron precipitation was not precluded for small breaks. • Revised illustration of sump failure criteria in Section 4.2 to correct the NPSH available equation. • Revised description of CASA Grande to clarify that it was not

Revision	Date	Description
		developed as a generic software package, but was simply used as an evaluation tool for the STP risk-informed GSI-191 calculations. • Revised the description of the LOCA frequency analysis. • Corrected the equation for the number of medium breaks sampled in the LOCA frequency analysis section. • Deleted chemical effects analysis section. • Edited strainer head loss analysis section to clarify that a bounding clean strainer head loss value was used rather than a flow and temperature dependent correlation. • Corrected typos in head loss correlation equations. • Revised head loss equation for calculating the composite S_V value from a geometric weighting by volume to a linear weighting by mass for consistency with the equation that was used in CASA. • Deleted Froude number equation for vortex formation in the air intrusion analysis section. • Deleted inaccurate equation describing the split in void fraction between pumps in air intrusion analysis section. • Added a note in the penetration analysis section to clarify that a strainer filtration efficiency of 100% was used for particulate debris. • Added footnote in the in-vessel downstream effects analysis section stating that preliminary results from additional thermal-hydraulic modeling has indicated that siphon effects are possible under specific conditions. • Added description of the strainer loading table in the strainer head loss analysis section and an assumption that debris loads uniformly on the strainer. Also added additional strainer geometry input to Section 2.2. • Replaced implicit friction factor equation in the strainer head loss analysis section with an explicit form. Also added the pipe roughness and suction pipe diameter input to Section 2.2. • Added a note to the parametric evaluation section to explain that the parametric cases were not rerun based on the current changes to CASA and therefore should only be used for qualitative insights. • Replaced example input deck in Appendix 1 with the new input decks. • Other miscellaneous editorial changes. Two types of changes were made to the CASA Grande program to support requantification of conditional failure probabilities reported in this revision.

Revision	Date	Description
		Changes involving the code structure or equation implementation were verified to have either no effect or incidental effect by comparing results from a baseline calculation before and after the modification. Changes involving input parameters were examined as sequential perturbations to a baseline calculation before adopting the entire suite for reevaluation. The code changes to CASA Grande include: • Implemented parallel optimization to increase efficiency. • Created external input file to support batch runs. • Optimized degasification routine for matrix evaluation. • Pulled NPSH required out of subroutine and up to the user input level for each pump type. • Corrected slopes of total injection flow rate to reflect change in summary table. • Corrected logic to allow one CS train off if and only if all three actuate. • Removed alternate polynomial evaluation of saturation pressure for degasification calculation and replaced with lookup table from NIST. • Optimized NPSH routine for matrix evaluation. • Fixed error in passing relative roughness to Colebrook friction equation caused by misinterpretation of published equation. The input changes to CASA Grande include: • Corrected pump failure definition for Case 9 to model two LHSI pump failures rather than two HHSI pump failures. • Revised break-dependent SI pump flow rates to match corrected flow rates described in Section 2.2. • Revised CS flow rates to match ranges described in Section 2.2. • Increased sampling resolution to 20 LHS replicates and 15 Johnson percentiles from 3 and 5 respectively. • Incorporated new material properties (size and density) consistent with the changes to the strainer head loss analysis section. • Imposed a 100% failure fraction for unqualified coatings. • Changed the failure of unqualified coatings to introduce 100% of the transportable coatings at a constant rate over the first 36 hours. • Corrected recirculation transport fraction for epoxy fine chips (changed from 21% to 41%).

Table of Contents

Revision History Log ... 3
Table of Contents ... 8
List of Figures ... 11
List of Tables ... 14
Definitions and Acronyms ... 16
1 Introduction ... 18
2 Design Input ... 24
2.1 General Description of Inputs Required ... 24
2.2 Specific Inputs Used ... 32
2.2.1 Timing for Key Plant Response Actions ... 32
2.2.2 Containment Geometry ... 33
2.2.3 LOCA Frequencies ... 33
2.2.4 Pump State Frequencies ... 43
2.2.5 Pool Water Level ... 45
2.2.6 Pool Temperature ... 45
2.2.7 Operating Trains ... 51
2.2.8 ECCS and CSS Flow Rates ... 51
2.2.9 Qualified Coatings Quantity ... 54
2.2.10 Unqualified Coatings Quantity ... 54
2.2.11 Crud Debris Quantity ... 55
2.2.12 Latent Debris Quantity ... 56
2.2.13 Miscellaneous Debris Quantity ... 56
2.2.14 Insulation Zones of Influence ... 56
2.2.15 Insulation Debris Size Distribution ... 56
2.2.16 Debris Characteristics ... 57
2.2.17 Blowdown Transport Fractions ... 58
2.2.18 Washdown Transport Fractions ... 59
2.2.19 Pool Fill Transport Fractions ... 60
2.2.20 Recirculation Transport Fractions ... 60
2.2.21 Debris Erosion ... 62
2.2.22 Strainer Geometry ... 63
2.2.23 Clean Strainer Head Loss ... 66
2.2.24 Pump NPSH Margin ... 66
2.2.25 Strainer Structural Margin ... 67
2.2.26 Vortex Air Ingestion ... 67
2.2.27 Bubble Transport ... 67
2.2.28 Pump Gas Limits ... 67
2.2.29 Fiberglass Penetration ... 67

2.2.30 Decay Heat Curve 69
2.2.31 Core Blockage Debris Limits 70
3 Assumptions 71
4 Methodology 83
4.1 GSI-191 Analysis Steps 87
4.2 Structured Information Process Flow 89
4.3 Uncertainty Quantification and Propagation 97
4.4 Verification and Validation 97
5 Analysis 98
5.1 Evaluation Scenarios (PRA Branch Fractions to Populate) 98
5.2 Containment CAD Model 101
5.3 LOCA Frequency 122
5.3.1 Relative Weight of Breaks in Specific Weld Categories 124
5.3.2 Weld Categories and Coordinates 127
5.3.3 Statistical Fit of NUREG-1829 LOCA Frequencies 147
5.3.4 Sample Epistemic Uncertainty of LOCA Frequencies 148
5.3.5 Sample Break Sizes at Each Weld Location 149
5.4 Debris Generation 151
5.4.1 ZOI Model 151
5.4.2 Insulation Debris Size Distribution Model 155
5.4.3 Insulation Debris 156
5.4.4 Qualified Coatings Debris 156
5.4.5 Unqualified Coatings Debris 157
5.4.6 Latent Debris 158
5.4.7 Miscellaneous Debris 158
5.4.8 Debris Characteristics 158
5.5 Debris Transport 158
5.5.1 Upstream Blockage 158
5.5.2 Blowdown Transport 159
5.5.3 Washdown Transport 160
5.5.4 Pool Fill Transport 160
5.5.5 Recirculation Transport 160
5.5.6 Debris Erosion 161
5.5.7 Strainer Transport 161
5.5.8 Time-Dependent Debris Arrival Model 173
5.6 Strainer Head Loss 174
5.6.1 Clean Strainer Head Loss 174
5.6.2 Conventional Debris Head Loss Model 175
5.6.3 Chemical Debris Head Loss Model 186
5.6.4 Strainer Head Loss 191

5.6.5 Acceptance Criterion: NPSH Margin Module 192
5.6.6 Acceptance Criterion: Structural Margin 197
5.7 Air Intrusion 197
5.7.1 Vortex Formation 198
5.7.2 Degasification 198
5.7.3 Gas Transport and Accumulation 203
5.7.4 Acceptance Criterion: Pump Gas Void Limits 206
5.8 Debris Penetration 206
5.9 Ex-Vessel Downstream Effects 212
5.9.1 Pump, Valve, Component Wear 212
5.9.2 System and Component Clogging/Blockage 213
5.10 In-Vessel Downstream Effects 214
5.10.1 Fuel Rod Debris Deposition (LOCADM) 214
5.10.2 Core Blockage Scenarios 215
5.10.3 Decay Heat Boil-Off Flow Rate 223
5.10.4 Time-Dependent Core Debris Accumulation 225
5.10.5 Acceptance Criteria: Debris Loads 226
5.11 Boron Precipitation 226
5.11.1 Time-Dependent Core Debris Accumulation 228
5.11.2 Acceptance Criteria: Debris Loads 228
5.12 Parametric Evaluations 228
6 Results 232
7 Conclusions 242
8 References 243
Appendix 1: CASA Grande Input Decks 1-1

List of Figures

Figure 1.1 – CASA Grande input variables 21
Figure 1.2 – CASA Grande calculation modules 22
Figure 1.3 – CASA Grande link to PRA 23
Figure 2.1.1 – Illustration of input variable relationships for debris generation analysis 27
Figure 2.1.2 – Illustration of input variable relationships for strainer head loss analysis 29
Figure 2.1.3 – Illustration of input variable relationships for gas intrusion analysis 30
Figure 2.1.4 – Illustration of input variable relationships for core blockage and boron precipitation analysis 31
Figure 2.2.1 – Temperature profiles implemented in CASA Grande 46
Figure 2.2.2 – Total SI flow rate vs. break size 52
Figure 2.2.3 – STP strainer Photo 1 (before protective grating was installed) 64
Figure 2.2.4 – STP strainer Photo 2 (after protective grating was installed) 65
Figure 2.2.5 – STP strainer Photo 3 65
Figure 2.2.6 – STP strainer Photo 4 66
Figure 4.1 – Example of realistic probability distribution for an input variable 84
Figure 4.2 – Risk-informed GSI-191 resolution path 86
Figure 4.2.1 – Illustration of a hypothetical DEGB spherical ZOI truncated by a wall 91
Figure 4.2.2 – Illustration of the processes local to the ECCS screen 93
Figure 4.2.3 – Illustration of the flow paths in the reactor vessel 94
Figure 4.2.4 – Illustration of sump failure criteria 95
Figure 4.2.5 – Illustration of processes local to the strainer with a direct impact on the performance thresholds 96
Figure 5.2.1 – Cross-section of steam generator compartment with Loops B and C 102
Figure 5.2.2 – Close-up view of steam generator compartment with Loops B and C 102
Figure 5.2.3 – Operating deck (Elevation 68'-0") 103
Figure 5.2.4 – Piping and equipment (View 1) 104
Figure 5.2.5 – Piping and equipment (View 2) 105
Figure 5.2.6 – Steam generator compartment floor (Elevation 19'0") 106
Figure 5.2.7 – Plan view of containment floor (Elevation -11'3") 107
Figure 5.2.8 – Isometric view of containment floor (Elevation -11'3") 108
Figure 5.2.9 – Plan view of major piping and equipment 109
Figure 5.2.10 – Section view of RCS Loop D (left) and Loop A (right) 110
Figure 5.2.11 – Section view of RCS Loop D (left) and Loop C (right) 111
Figure 5.2.12 – Nukon insulation on piping, pressurizer, pumps, and heat exchangers 112
Figure 5.2.13 – Thermal-Wrap insulation on steam generators 113
Figure 5.2.14 – Microtherm insulation in secondary shield wall penetrations 114
Figure 5.2.15 – Lead blankets on pipes 115
Figure 5.2.16 – Welds representing potential LOCA break locations (View 1) 116

Figure 5.2.17 – Welds representing potential LOCA break locations (View 2) 116
Figure 5.2.18 – Currently installed ECCS strainers 117
Figure 5.2.19 – Illustration of additional insulation modeled at hanger and valve locations 118
Figure 5.2.20 – Illustration of work points used to identify location of welds, hangers, and valves 119
Figure 5.2.21 – Example of CAD model text data output 120
Figure 5.2.22 – Concrete walls and floors exported from CAD model in STL format 121
Figure 5.2.23 – Geometry of piping and equipment insulation in CASA Grande 122
Figure 5.3.1 – Locations of Category 6B welds that were modeled 130
Figure 5.3.2 – Illustration of bounded Johnson fit for NUREG-1829 break frequencies 147
Figure 5.3.3 – Illustration of LOCA frequency vs. break size for 62nd percentile 149
Figure 5.3.4 – Example of non-uniform stratified sampling strategy for one weld case 151
Figure 5.4.1 – Illustration of 17D Nukon ZOI for a 31" DEGB 153
Figure 5.4.2 – Illustration of 17D Nukon ZOI for a 6" side-wall break 154
Figure 5.4.3 – Illustration of 17D Nukon ZOI for a 2" side-wall break 154
Figure 5.4.4 – Illustration of sub-zones used for fiberglass debris size distribution 155
Figure 5.4.5 – Distribution of potential fiberglass debris quantities 156
Figure 5.5.1 – Photograph of 30-inch vent hole in secondary shield wall 159
Figure 5.5.2 – Logic tree for LDFG fines showing total transport fraction implemented for all breaks ... 164
Figure 5.5.3 – Logic tree for LDFG small pieces showing total transport fraction implemented for all breaks 165
Figure 5.5.4 – Logic tree for LDFG large pieces showing total transport fraction implemented for all breaks 166
Figure 5.5.5 – Logic tree for Microtherm fines showing total transport fraction implemented for all breaks 166
Figure 5.5.6 – Logic tree for crud fines showing total transport fraction implemented for all breaks 167
Figure 5.5.7 – Logic tree for qualified coatings fines showing total transport fraction implemented for all breaks 168
Figure 5.5.8 – Logic tree for unqualified alkyd coatings fines showing total transport fraction implemented for all breaks 169
Figure 5.5.9 – Logic tree for unqualified epoxy coatings fines showing total transport fraction implemented for all breaks 169
Figure 5.5.10 – Logic tree for unqualified epoxy coatings fine chips showing total transport fraction implemented for all breaks 170
Figure 5.5.11 – Logic tree for unqualified epoxy coatings small chips showing total transport fraction implemented for all breaks 170
Figure 5.5.12 – Logic tree for unqualified epoxy coatings large chips showing total transport fraction implemented for all breaks 171
Figure 5.5.13 – Logic tree for unqualified epoxy coatings curled chips showing total transport fraction implemented for all breaks 171

Figure 5.5.14 – Logic tree for unqualified IOZ coatings fines showing total transport fraction implemented for all breaks 172
Figure 5.5.15 – Logic tree for latent fines showing total transport fraction implemented for all breaks 172
Figure 5.5.16 – Illustration of time-dependent transport 174
Figure 5.6.1 – Circumscribed strainer dimensions 180
Figure 5.6.3 – Exponential probability density function for chemical effects bump-up factors applied to SBLOCAs 189
Figure 5.6.4 – Exponential probability density function for chemical effects bump-up factors applied to MBLOCAs 190
Figure 5.6.5 – Exponential probability density function for chemical effects bump-up factors applied to LBLOCAs 191
Figure 5.6.6 – Typical sample of sump-strainer head loss histories generated under the assumption of exponential chemical effects factor and artificial head-loss inflation 192
Figure 5.6.7 – Illustration of parameters that affect pump NPSH 193
Figure 5.6.8 – Schematic of STP ECCS sump suction piping 195
Figure 5.7.1 – Isometric view of ECCS strainer 203
Figure 5.7.2 – Cross-section view of ECCS strainer and sump pit 204
Figure 5.7.3 – Illustration of air bubble accumulation and venting 206
Figure 5.8.1 – Illustration of direct passage and shedding 207
Figure 5.8.2 – Illustration of time-dependent parameters associated with debris accumulation on the strainer and core 208
Figure 5.10.1 – Deposit growth process assumed by LOCADM when core is boiling (63) 215
Figure 5.10.2 – Illustration of RCS at STP 216
Figure 5.10.3 – Large or medium hot leg break during cold leg injection with partial core blockage 217
Figure 5.10.4 – Large or medium hot leg break during hot leg injection 219
Figure 5.10.5 – Large or medium cold leg break during cold leg injection with partial core blockage 220
Figure 5.10.6 – Large or medium cold leg break during hot leg injection 221
Figure 5.10.7 – Small hot leg break during cold leg injection 222
Figure 5.10.8 – Time-dependent boil-off flow rate 225
Figure 5.11.1 – Amorphous precipitate formation on heated surface (96) 227
Figure 5.12.1 – STP ECCS strainer prior to upgrade 229
Figure 6.1 – Linear-linear interpolation of bounded Johnson extrema (solid) with non-uniform stratified random break-size profiles (dashed) 235
Figure 6.2 – Empirical distribution of total failure probability for Case 43 (one train operable) based on 15 discrete samples of the NUREG-1829 break-frequency uncertainty envelope 237

List of Tables

Table 2.1.1 – General input variables used in multiple aspects of the analysis 25
Table 2.1.2 – Input variables used primarily in debris generation analysis 25
Table 2.1.3 – Input variables used primarily in strainer head loss analysis 27
Table 2.1.4 – Input variables used primarily in gas intrusion analysis 29
Table 2.1.5 – Input variables used primarily in fiber penetration and in-vessel effects analysis 30
Table 2.2.1 – Sump switchover time 33
Table 2.2.2 – NUREG-1829 PWR current-day LOCA frequencies and fitted Johnson parameters 34
Table 2.2.3 – Relative frequencies vs. break size for hot leg, SG inlet, and cold leg welds (Categories 1A through 3B) 35
Table 2.2.4 – Relative frequencies vs. break size for cold leg and surge line welds (Categories 3C through 4D) 36
Table 2.2.5 – Relative frequencies vs. break size for pressurizer line welds (Categories 5A through 5F) .. 37
Table 2.2.6 – Relative frequencies vs. break size for pressurizer and small bore line welds (Categories 5F through 6B) 38
Table 2.2.7 – Relative frequencies vs. break size for safety injection and recirculation line welds (Categories 7A through 7F) 39
Table 2.2.8 – Relative frequencies vs. break size for safety injection and recirculation line welds (Categories 7F through 7L) 40
Table 2.2.9 – Relative frequencies vs. break size for accumulator injection and CVCS line welds (Categories 7M through 8C) 41
Table 2.2.10 – Relative frequencies vs. break size for CVCS line welds (Categories 8D through 8F) 42
Table 2.2.11 – Frequency of success pump combination states 43
Table 2.2.12 – Range of water volumes implemented in CASA Grande 45
Table 2.2.13 – Temperature profiles implemented in CASA Grande 46
Table 2.2.14 – Total SI flow rates 51
Table 2.2.15 – Containment spray flow rates 54
Table 2.2.16 – Quantity of qualified coatings debris 54
Table 2.2.17 – Quantity and location of potentially transportable unqualified coatings debris 55
Table 2.2.18 – Unqualified epoxy debris size distribution 55
Table 2.2.19 – Quantity of latent debris 56
Table 2.2.20 – Input variables used primarily in debris penetration and core blockage analysis 56
Table 2.2.21 – Material properties of debris 57
Table 2.2.22 – Blowdown transport fractions according to break location 59
Table 2.2.23 – Washdown transport fractions according to spray initiation 60
Table 2.2.24 – Pool fill transport fractions according to break location 60
Table 2.2.25 – Recirculation pool transport fractions according to break size and location (insulation) .. 61
Table 2.2.26 – Recirculation transport fractions according to break size and location (coatings, latent debris, crud, dirt/dust) 62

Table 2.2.27 – ECCS sump suction pipe diameters 67
Table 2.2.28 – Fitted filtration parameters for test module 68
Table 2.2.29 – Fitted filtration parameters for each ECCS strainer 68
Table 2.2.30 – Fitted shedding parameters 69
Table 2.2.31 – Decay heat generation rate based on 1979 ANS plus 2 sigma uncertainty 69
Table 3.1 – Strainer debris accumulation and approach velocity comparison 75
Table 3.2 – Strainer debris accumulation and approach velocity comparison for CS pump failures[14] 75
Table 3.3 – Core debris accumulation for various pump failures 76
Table 5.1.1 – Bounding or representative cases for highest frequency pump combination states 100
Table 5.3.1 – Description of weld categories 126
Table 5.3.2 – Comparison of LOCA frequency report and CAD model pipe sizes and weld counts 128
Table 5.3.3 – Weld data from component database and CAD model 131
Table 5.3.4 – Example calculation of LOCA frequencies vs. break size for 62nd Percentile 148
Table 5.5.1 – Blowdown transport fractions used in CASA Grande 159
Table 5.5.2 – Washdown transport fractions used in CASA Grande 160
Table 5.5.3 – Pool fill transport fractions used in CASA Grande 160
Table 5.5.4 – Recirculation transport fractions used in CASA Grande 161
Table 5.5.5 – Time-dependent transport 173
Table 5.6.1 – Head loss characteristics for fibrous debris 179
Table 5.6.2 – Head loss characteristics for non-fibrous debris 179
Table 5.6.3 – Strainer loading table 181
Table 5.6.4 – Exponential probability distribution parameters applied to chemical effects bump-up factors for each LOCA category 188
Table 5.7.1 – Semi-empirical correlation parameters to calculate Henry's constants in aqueous solvent (87) 199
Table 5.10.1 – Decay heat generation rate based on 1979 ANS plus 2 sigma uncertainty 224
Table 5.12.1 – Comparison of mean LBLOCA conditional failure probabilities before and after ECCS strainer replacement 231
Table 6.1 – Mean LBLOCA conditional failure probabilities for five states of pump availability 233
Table 6.2 – Distribution of total conditional failure for LBLOCAs under Case 43 (single train operable) 236
Table 6.3 – Cold leg split fractions conditioned on LOCA category for Case 43 238
Table 6.4 – Random itemization of 49 break events that lead to failure for plant state Case 43 239

Definitions and Acronyms

ARL	Alden Research Laboratory
BC	Branch Connection
BEP	Best Efficiency Point
B-F	Bimetallic Welds
B-J	Single Metal Welds
BWR	Boiling Water Reactor
CAD	Computer Aided Design
CASA	Containment Accident Stochastic Analysis
CCDF	Complementary Cumulative Distribution Function
CCW	Component Cooling Water
CDF	Core Damage Frequency
CHLE	Corrosion/Head Loss Experiments
CS	Containment Spray
CSHL	Clean Strainer Head Loss
CSS	Containment Spray System
CVCS	Chemical Volume Control System
D&C	Design and Construction Defects
DEGB	Double Ended Guillotine Break
DM	Degradation Mechanism
ECC	Emergency Core Cooling
ECCS	Emergency Core Cooling System
EOP	Emergency Operating Procedure
EPRI	Electric Power Research Institute
ESF	Engineered Safety Feature
FA	Fuel Assembly
GL 08-01	Generic Letter 2008-01
GSI-191	Generic Safety Issue 191
HHSI	High Head Safety Injection
HLSO	Hot Leg Switchover
IGSCC	Intergranular Stress Corrosion Cracking
LBLOCA	Large Break Loss of Coolant Accident
LDFG	Low Density Fiberglass
LERF	Large Early Release Frequency
LHS	Latin Hypercube Sampling
LHSI	Low Head Safety Injection
LOCA	Loss of Coolant Accident
MBLOCA	Medium Break Loss of Coolant Accident
NIST	National Institute of Standards and Technology
NPSH	Net Positive Suction Head

NRC	Nuclear Regulatory Commission
OD	Outer Diameter
PDF	Probability Density Function
PRA	Probabilistic Risk Assessment
PWR	Pressurized Water Reactor
PWROG	Pressurized Water Reactor Owner's Group
PWSCC	Primary Water Stress Corrosion Cracking
RCS	Reactor Coolant System
RHR	Residual Heat Removal
RI-ISI	Risk-Informed In-Service Inspection
RMI	Reflective Metal Insulation
RWST	Refueling Water Storage Tank
SBLOCA	Small Break Loss of Coolant Accident
SC	Stress Corrosion
SI	Safety Injection
SIR	Safety Injection and Recirculation
SRM	Staff Requirements Memorandum
STP	South Texas Project
STPNOC	South Texas Project Nuclear Operating Company
TAMU	Texas A&M University
TF	Thermal Fatigue
TGSCC	Transgranular Stress Corrosion Cracking
TSC	Technical Support Center
USI A-43	Unresolved Safety Issue A-43
UT	University of Texas (Austin)
V&V	Verification and Validation
VF	Vibration Fatigue
WCAP	Westinghouse Commercial Atomic Power
ZOI	Zone of Influence

1 Introduction

The emergency core cooling system (ECCS) and containment spray system (CSS) in a pressurized water reactor (PWR) are designed to safely shutdown the plant following a loss of coolant accident (LOCA) in accordance with 10CFR50.46. The assurance of long term core cooling in PWRs following a LOCA has a long history dating back to the Nuclear Regulatory Commission (NRC) studies of the mid 1980s associated with Unresolved Safety Issue (USI) A-43. Results of the NRC research on boiling water reactor (BWR) ECCS suction strainer blockage of the early 1990s identified new phenomena and failure modes that were not considered in the resolution of USI A-43. As a result of these concerns, Generic Safety Issue (GSI) 191 was identified in September 1996 related to debris clogging of the ECCS sump suction strainers at PWRs. Although plants have taken steps to prevent strainer clogging (by increasing the screen area, for example), satisfactory closure of this issue has proved elusive due to long term cooling issues and the effect of chemical precipitates on head loss. Previous investigators have identified bounding scenarios using conservative inputs, methods, and acceptance criteria. The acceptance criteria are applied in a "pass/fail" fashion that ignores the risk significance. That is, if the results are acceptable, the issue has been resolved. Otherwise, it is necessary to either redo the analysis with partial relaxation of analytical conservatisms or perform additional plant modifications to ensure that the acceptance criteria are met.

A sudden break in the reactor coolant system (RCS) piping at a PWR would result in a high energy, two-phase jet. Depending on the size and location of the break, it is possible for the jet to destroy a large quantity of insulation on nearby piping and equipment. During the RCS blowdown phase, some of the insulation debris may be blown to upper containment and some may be blown to lower regions of the containment.

Per plant design, the ECCS and CSS would be automatically initiated, drawing flow from the refueling water storage tank (RWST). The CSS would wash some debris from upper containment down to the containment floor. Debris on the containment floor could be transported by the high-velocity sheeting flow as the pool fills. Some debris may be transported into inactive cavities below the containment floor (such as the reactor cavity), or directly to the ECCS sump strainers as the sump cavities fill. After the RWST has been depleted, the ECCS and CSS pumps would be automatically switched over to recirculation. Some of the debris in the containment pool would be transported to the ECCS sumps where it would accumulate on the strainers. Some of the fine debris (particulate and fiberglass fines) would penetrate (i.e., pass through) the strainer.

As debris collects on the strainer, the head loss across the strainer would rise. Corrosion of various containment metals, and dissolution of insulation debris and other materials in the buffered and borated containment pool may result in the formation of chemical precipitates. These precipitates can accumulate on the strainer debris beds increasing the overall head loss. Some of the chemical precipitates may also penetrate the strainer. If the head loss across the strainer exceeds either the net positive suction head (NPSH) margin for the safety injection (SI) system, or the strainer structural margin, long-term core cooling may be compromised.

Debris that penetrates through the strainer can also cause downstream issues including blockage or wear of various downstream components, or more significantly blockage of the fuel channels within the reactor core.

The assurance of long-term post-LOCA core cooling must be fully addressed as required by the NRC in Generic Letter 2004-02 (1). All U.S. PWRs have worked through the required analyses using deterministic approaches. In 2006, the NRC commissioners issued a staff requirements memorandum (SRM) directing the staff and industry to make a concerted effort to look at resolution of the GSI-191 issue holistically (2). This proved to be challenging since the analyses were performed using bounding methods. Although there were known conservatisms in the analyses, there was no method for quantifying the overall margin associated with the conservatisms so that the effects of best-estimate assumptions could be put into proper perspective and compared to the conservative assumptions to holistically determine the overall level of margin.

In 2010, due to the ongoing challenges of resolving GSI-191, the NRC commissioners directed the staff to consider new and innovative resolution approaches (3). One of the approaches included in the SRM was the option of addressing GSI-191 using a risk-informed approach. In 2011, South Texas Project (STP) initiated a three-year effort as a pilot plant to define and implement a risk-informed approach to resolve GSI-191. An evaluation tool called CASA Grande[5] was developed to analyze the accident sequences in a realistic time-dependent manner with uncertainty propagation to determine the probabilities of various failures potentially leading to core damage from a spectrum of location-specific pipe breaks (i.e., LOCAs) for input into STP's plant-specific probabilistic risk assessment (PRA). The specific failure modes that need to be considered are:

1. Strainer head loss exceeds the NPSH margin for the pumps causing some or all of the ECCS and CSS pumps to fail.
2. Strainer head loss exceeds the strainer structural margin causing the strainer to fail, which could subsequently result in larger quantities and larger sizes of debris being ingested into the ECCS and CSS.
3. Air intrusion exceeds the limits of the ECCS and CSS pumps causing degraded pump performance or complete failure due to gas binding.
4. Debris penetration exceeds ex-vessel effects limits causing a variety of potential equipment and component failures due to wear or clogging.
5. Debris penetration exceeds in-vessel effects limits resulting in partial or full core blockage with insufficient flow to cool the core.

[5] CASA is an acronym for Containment Accident Stochastic Analysis

6. Buildup of oxides, crud, LOCA-generated debris, and chemical precipitates on fuel cladding exceeds the limits for heat transfer resulting in unacceptably high peak cladding temperatures.
7. Boron concentration in the core exceeds the solubility limit leading to boron precipitation and subsequently resulting in unacceptable flow blockage or impaired heat removal.

Failure Modes 4 and 6 have been conservatively addressed as part of the previous deterministic evaluation for STP with no issues of concern (see Sections 5.9 and 5.10.1), and are therefore not explicitly modeled in CASA Grande. The remaining failure modes are explicitly modeled.

This report provides a full description of the STP CASA Grande analysis including the input parameters, assumptions, methodology, and results. It also provides a description of the limited parametric evaluations that have been performed.

Figure 1.1 and Figure 1.2 illustrate the input variables and analytical modules used for CASA Grande, and Figure 1.3 illustrates the link between CASA Grande and the PRA.

Figure 1.1 – CASA Grande input variables

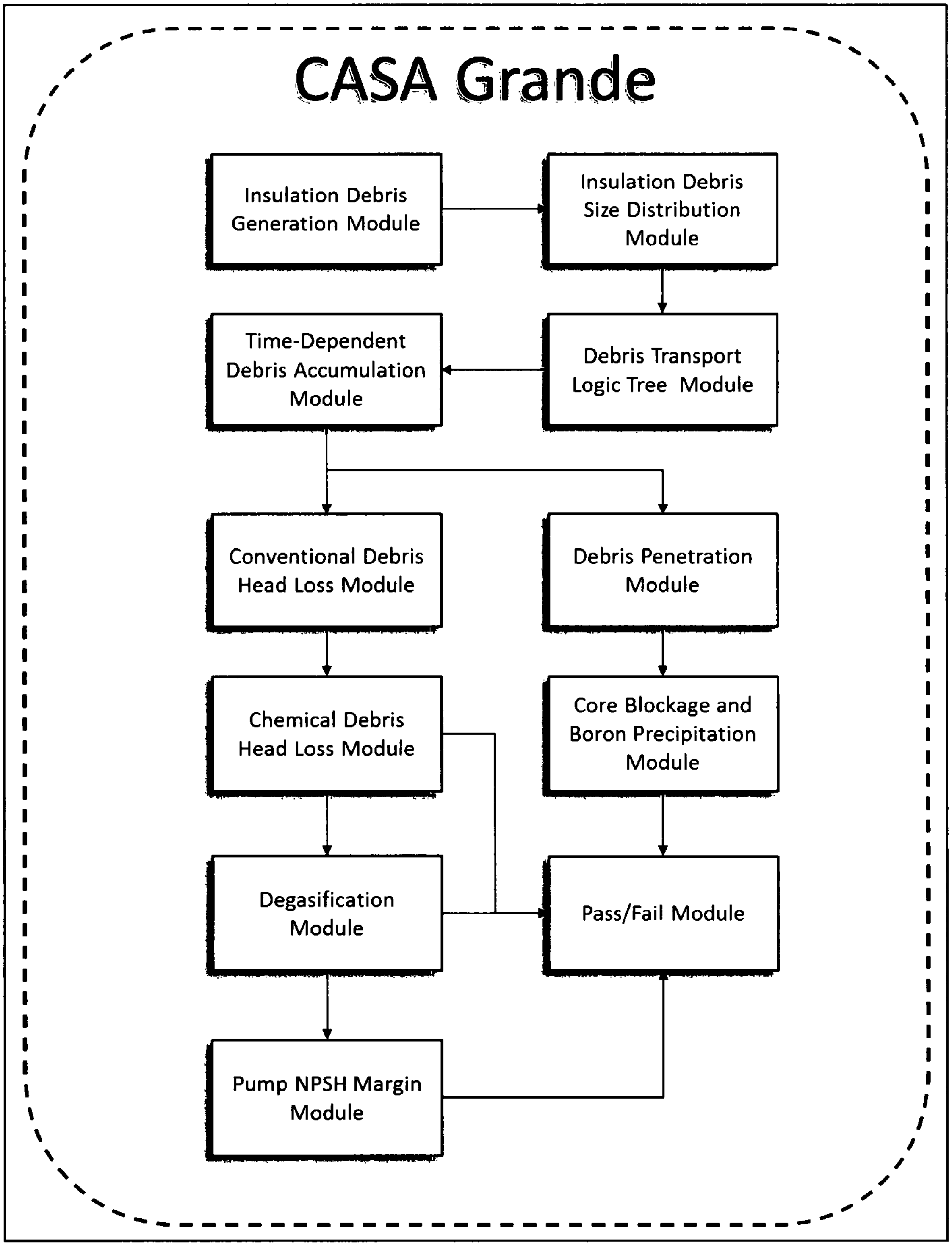

Figure 1.2 – CASA Grande calculation modules

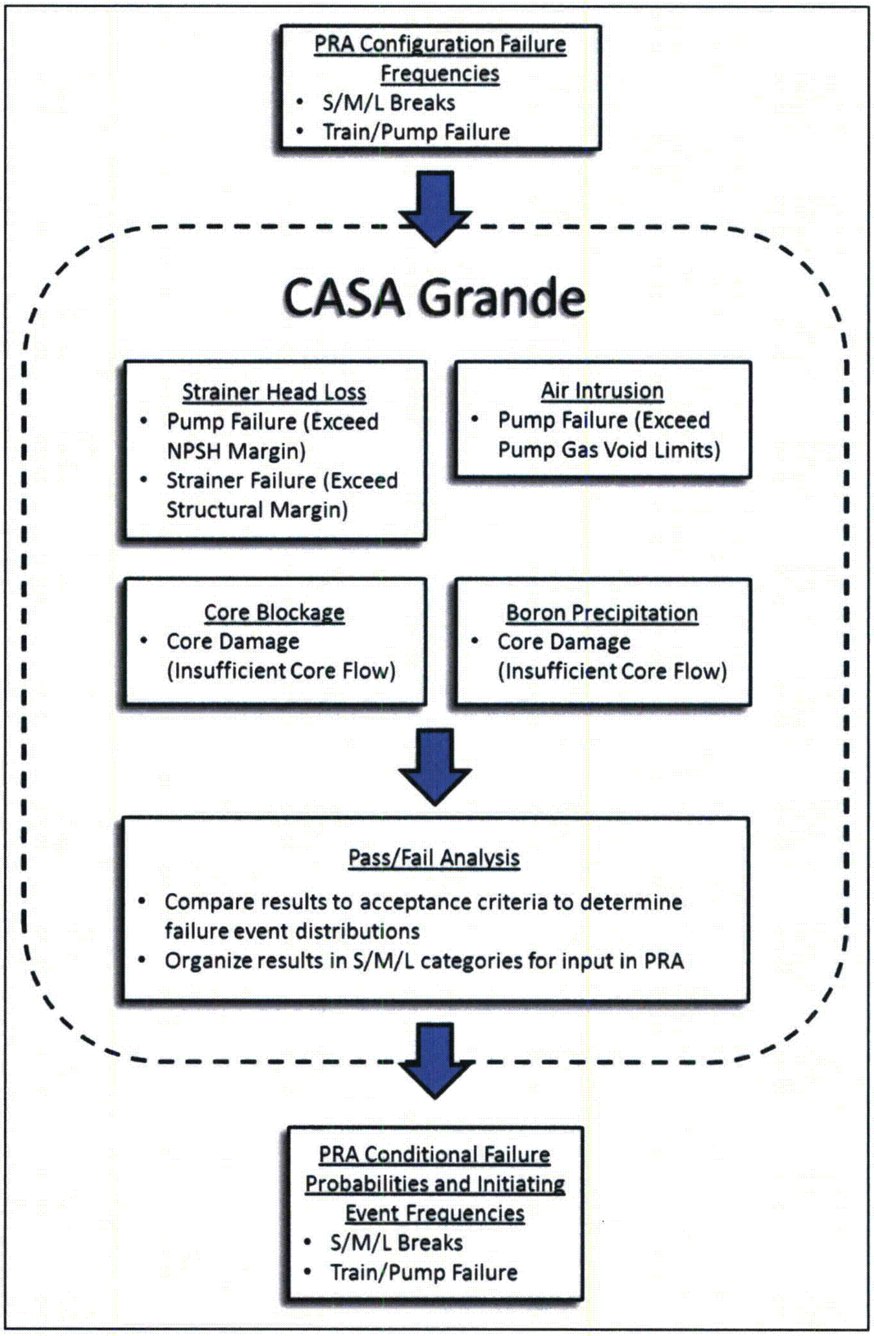

Figure 1.3 – CASA Grande link to PRA

2 Design Input

A wide range of input variables are used in the various GSI-191 analysis areas. In some cases, the input may consist of a single value, in other cases the input may have a probability distribution or change over time. Some inputs must be entered into CASA Grande as part of the input deck (e.g., containment pool temperature profiles), while other inputs may be calculated within CASA Grande (e.g., strainer head loss, which is directly calculated and then used as an input for the degasification calculation). Section 2.1 provides a general description of the relationship between the various input parameters, and Section 2.2 provides a description of the actual inputs used in the STP analysis.

The detailed analyses required to develop each of the design inputs are described in the referenced documents in Section 2.2. The majority of the significant input variables that were developed as part of the STP risk-informed GSI-191 evaluation project were developed under the following topical areas:

- Containment CAD Model (4)
- Thermal Hydraulics Modeling (5; 6)
- LOCA Frequency Evaluation (7; 8; 9)
- Jet Formation Modeling (10)
- Coatings and Crud Debris Calculations (11; 12; 13)
- Water Volume/Level Calculation (14)
- Chemical Effects Testing (15; 16; 17; 18; 19; 20; 21; 22)
- Debris Transport Calculation (23)
- Strainer Head Loss Testing (24)
- NPSH Calculation (25)
- Strainer Penetration Testing (26; 27; 28)
- In-vessel Effects Evaluation (29)

2.1 General Description of Inputs Required

Table 2.1.1 through Table 2.1.5 list the design input variables that go into a GSI-191 evaluation. They also show the relationship between other input and output variables, and whether the conservative direction is represented by a high or low value. Note that in many cases, input values may affect multiple outputs where in one situation it is conservative to assume a low value and in another situation it is conservative to assume a high value. Figure 2.1.1 through Figure 2.1.4 illustrate how the various input variables tie together in CASA Grande.

Table 2.1.1 – General input variables used in multiple aspects of the analysis

Design Input Variable	Conservative Direction	Preceding Direct-Input Variables	Proceeding Direct-Output Variables	Comments
Accident Time	N/A	N/A	Unqualified Coatings Failure, Spray Flow Rate, Sump Flow Rate, Strainer Accumulation, Containment Temperature, Fiber Penetration, Boil-off Flow Rate, Core Accumulation	
Break Location	N/A	LOCA Frequency	Debris Quantity, Debris Size Distribution, Core Accumulation	
Break Size	↑	LOCA Frequency	Pool Temperature, ZOI Size, Injection Flow Rate	
Pool Water Volume	↓	Break Size	Pool Water Level, Strainer Accumulation	
Pool Water Level	↓	Pool Water Volume	NPSH Available, Degasification	
Containment Pressure	↓	Pool Temperature, Accident Time	NPSH Available, Degasification	
Pool Temperature	↑↓	Break Size, Accident Time	Chemical Precipitation, Strainer Head Loss, NPSH Available, Degasification	
Operating Pumps	↑↓	N/A	Spray Flow Rate, Injection Flow Rate, Sump Flow Rate	
Spray Flow Rate	↑↓	Operating Pumps, Accident Time	Sump Flow Rate, Core Accumulation	
Injection Flow Rate	↑↓	Operating Pumps, Break Size	Sump Flow Rate, Core Accumulation	
Sump Flow Rate	↑	Spray Flow Rate, Injection Flow Rate	Strainer Approach Velocity, NPSH Available, Degasification, Fiber Penetration	

Table 2.1.2 – Input variables used primarily in debris generation analysis

Design Input Variable	Conservative Direction	Preceding Direct-Input Variables	Proceeding Direct-Output Variables	Comments
LOCA Frequency	↑	N/A	Break Location, Break Size	
Insulation Location	N/A	N/A	Debris Quantity, Size Distribution	
Qualified Coatings Quantity	↑	N/A	Debris Quantity	

Design Input Variable	Conservative Direction	Preceding Direct-Input Variables	Proceeding Direct-Output Variables	Comments
Unqualified Coatings Quantity	↑	N/A	Debris Quantity	
Unqualified Coatings Location	N/A	N/A	Debris Transport	
Unqualified Coatings Failure	↑	Accident Time	Debris Quantity, Debris Transport	
Latent Debris Quantity	↑	N/A	Debris Quantity	
Miscellaneous Debris Quantity	↑	N/A	Debris Quantity	
Destruction Pressure	↓	N/A	ZOI Size	
ZOI Size	↑	Break Size, Destruction Pressure	Debris Quantity	
Debris Size Distribution	↓	Break Location, Insulation Location	Debris Transport, Strainer Head Loss	
Debris Density	↑↓	N/A	Strainer Head Loss	Head loss increases with higher macroscopic density and lower microscopic density
Debris Quantity	↑	Break Location, Insulation Location, ZOI Size, Qualified Coatings Quantity, Unqualified Coatings Failure, Latent Debris Quantity, Miscellaneous Debris Quantity	Strainer Accumulation	

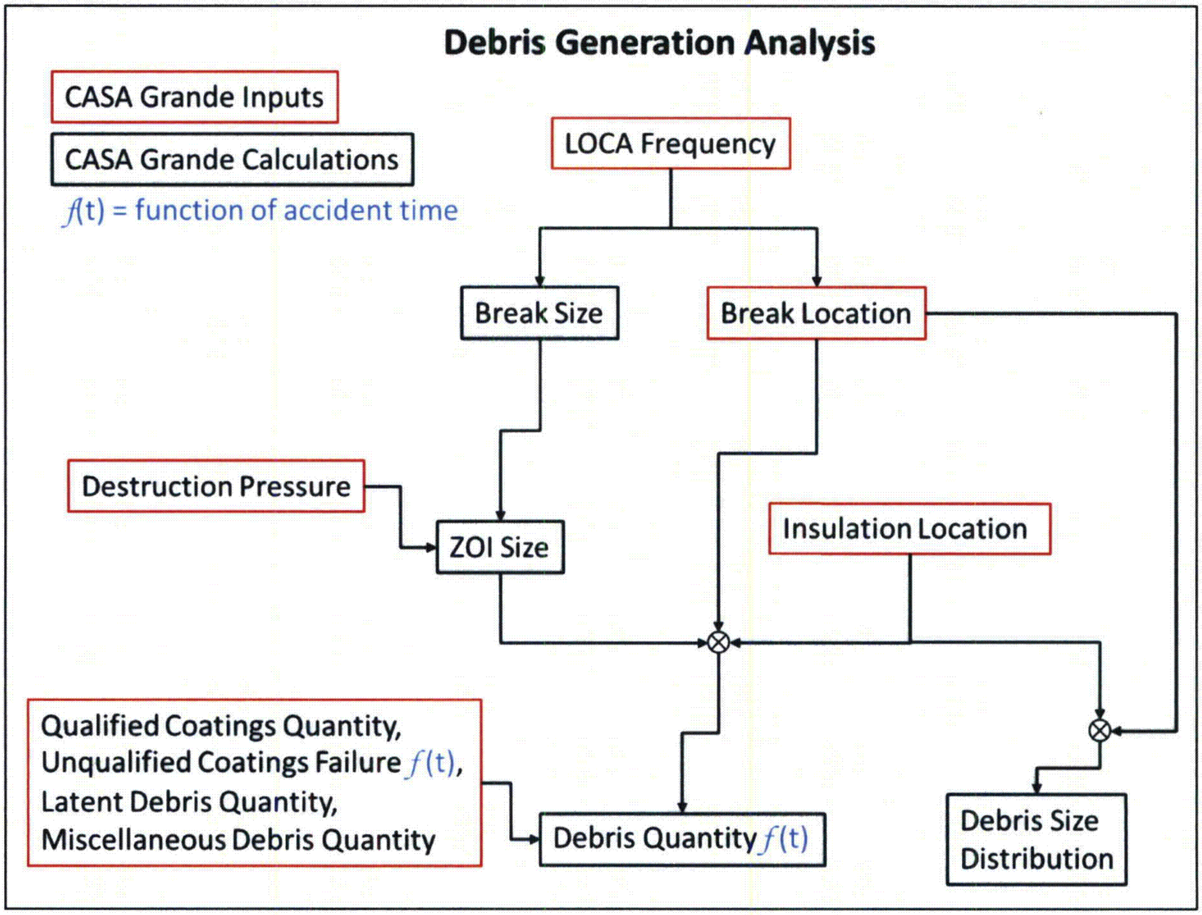

Figure 2.1.1 – Illustration of input variable relationships for debris generation analysis

Table 2.1.3 – Input variables used primarily in strainer head loss analysis

Design Input Variable	Conservative Direction	Preceding Direct-Input Variables	Proceeding Direct-Output Variables	Comments
Strainer Height	↑	N/A	Degasification	
Strainer Area	↓	N/A	Debris Bed Thickness, Strainer Approach Velocity, Fiber Penetration	
Strainer Interstitial Volume	↓	N/A	Debris Bed Thickness, Strainer Area	
Debris Transport	↑	Debris Size Distribution, Unqualified Coatings Location, Unqualified Coatings Failure	Strainer Accumulation	

Design Input Variable	Conservative Direction	Preceding Direct-Input Variables	Proceeding Direct-Output Variables	Comments
Strainer Accumulation	↑	Debris Quantity, Debris Transport, Sump Flow Rate, Pool Volume, Accident Time	Debris Bed Thickness, Fiber Penetration, Strainer Approach Velocity	
Debris Bed Thickness	↑↓	Strainer Accumulation, Strainer Area, Strainer Interstitial Volume	Strainer Head Loss	
Chemical Precipitation	↑	Pool Temperature	Strainer Head Loss	
Strainer Approach Velocity	↑	Sump Flow Rate, Strainer Area, Strainer Accumulation	Strainer Head Loss	
Clean Strainer Head Loss	↑	N/A	Strainer Head Loss	
Strainer Head Loss	↑	Pool Temperature, Strainer Approach Velocity, Clean Strainer Head Loss, Debris Bed Thickness, Debris Size Distribution, Chemical Precipitation	Degasification, Sump Failure	
NPSH Required	↑	Degasification	NPSH Margin	
NPSH Available	↓	Pool Water Level, Containment Pressure, Pool Temperature, Sump Flow Rate	NPSH Margin	
NPSH Margin	↓	NPSH Required, NPSH Available	Sump Failure	Acceptance criterion compared against strainer head loss
Structural Margin	↓	N/A	Sump Failure	Acceptance criterion compared against strainer head loss

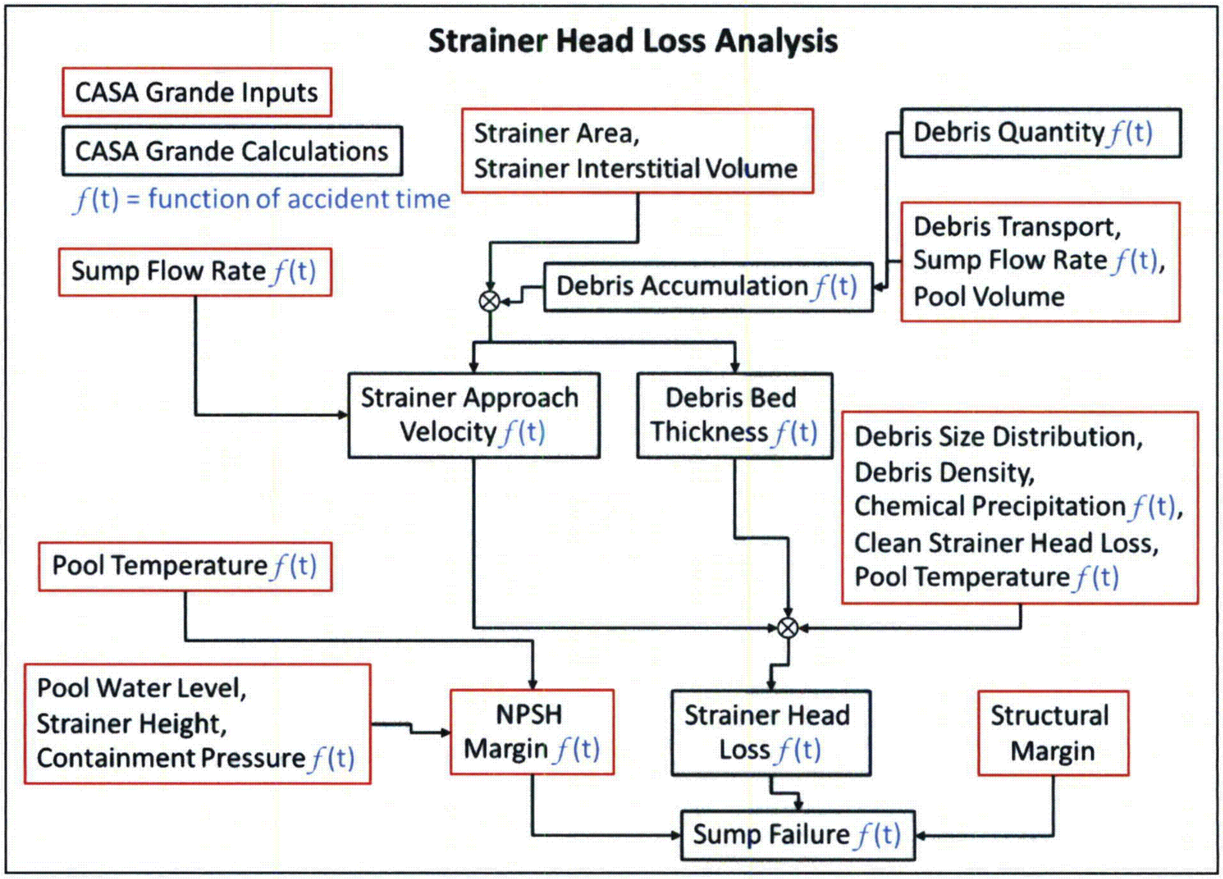

Figure 2.1.2 – Illustration of input variable relationships for strainer head loss analysis

Table 2.1.4 – Input variables used primarily in gas intrusion analysis

Design Input Variable	Conservative Direction	Preceding Direct-Input Variables	Proceeding Direct-Output Variables	Comments
Degasification	↑	Strainer Height, Pool Water Level, Containment Pressure, Pool Temperature, Sump Flow Rate, Strainer Head Loss	NPSH Required, Sump Failure	
Pump Gas Limits	↓	N/A	Sump Failure	Acceptance criterion compared against gas void fraction

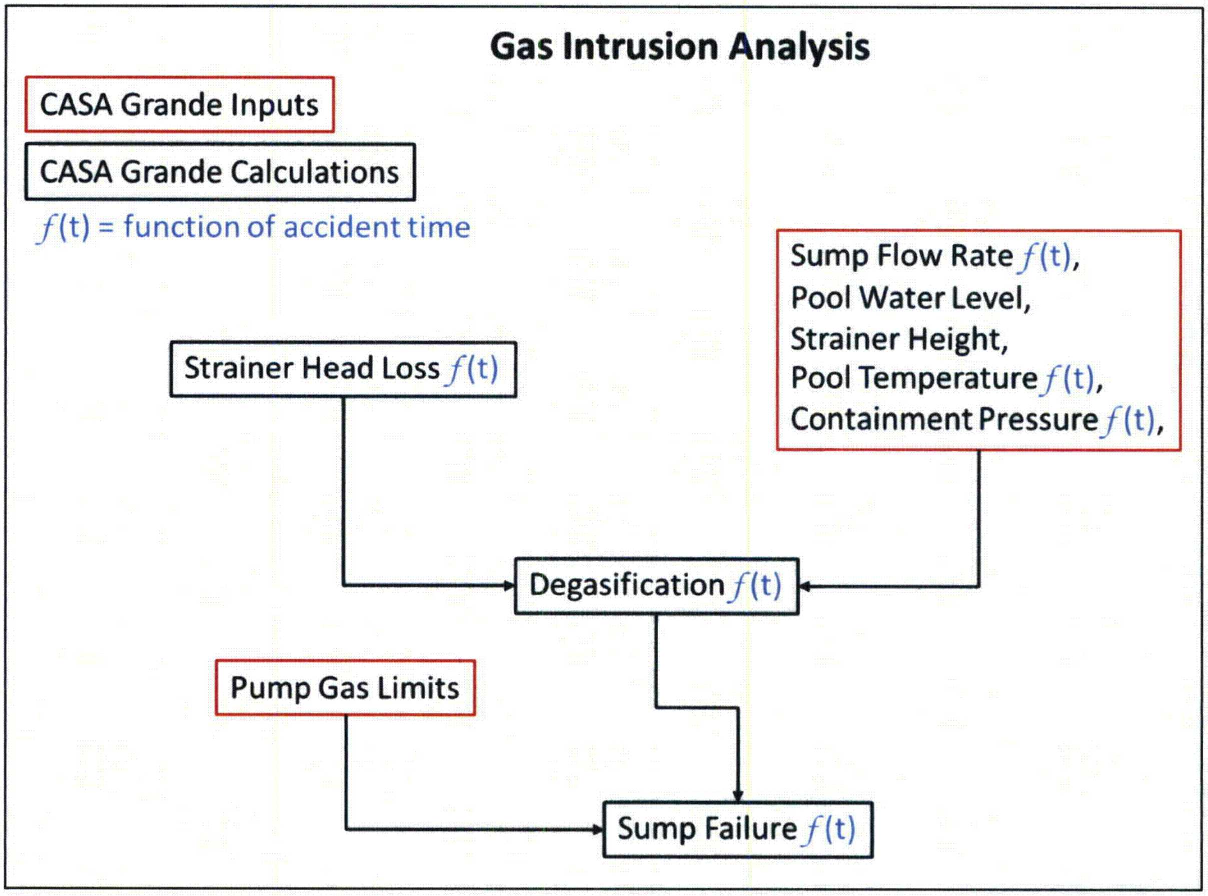

Figure 2.1.3 – Illustration of input variable relationships for gas intrusion analysis

Table 2.1.5 – Input variables used primarily in fiber penetration and in-vessel effects analysis

Design Input Variable	Conservative Direction	Preceding Direct-Input Variables	Proceeding Direct-Output Variables	Comments
Fiber Penetration	↑	Sump Flow Rate, Strainer Accumulation, Strainer Area, Accident Time	Core Accumulation	
Boil-off Flow Rate	↑	N/A	Core Accumulation	
Core Accumulation	↑	Break Location, Spray Flow Rate, Injection Flow Rate, Boil-off Flow Rate, Fiber Penetration, Accident Time	Core Blockage, Boron Precipitation	

Design Input Variable	Conservative Direction	Preceding Direct-Input Variables	Proceeding Direct-Output Variables	Comments
Core Blockage	↑	Core Accumulation	In-Vessel Failure	Core accumulation compared to core blockage acceptance criteria
Boron Precipitation	↑	Core Accumulation	In-Vessel Failure	Core accumulation compared to boron precipitation acceptance criteria

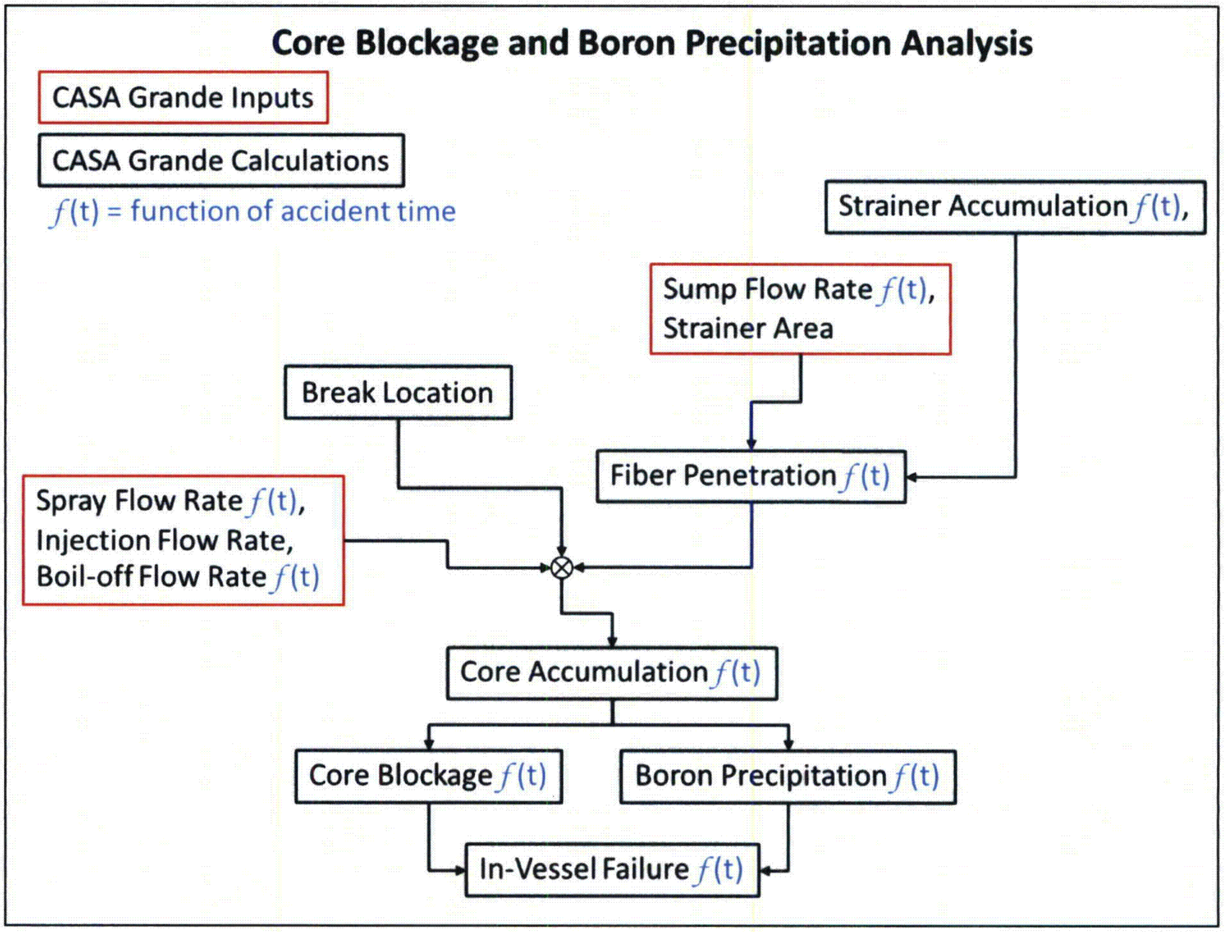

Figure 2.1.4 – Illustration of input variable relationships for core blockage and boron precipitation analysis

2.2 Specific Inputs Used

This section documents the specific design inputs used in the CASA Grande analysis. The actual input decks are provided in Appendix 1.

2.2.1 Timing for Key Plant Response Actions

There are a number of automated or proceduralized plant response actions that would occur following a LOCA event. The timing for these actions is important for the GSI-191 evaluation since the timing can have a significant impact on a variety of phenomena. Immediately after a LOCA, several things would occur: 1) the pressure in the accumulators ranges from 590 psig to 670 psig (30), so the accumulators would not inject their inventory unless the RCS pressure drops below approximately 600 psig, 2) the LHSI and HHSI pumps would start injecting water from the RWST into the cold legs after the RCS pressure drops below the shutoff head, and 3) the CS pumps would start injecting water from the RWST into the containment spray headers if the containment pressure rises above 9.5 psig (31). Note that for breaks smaller than 2-inches, the accumulators would not inject since the RCS pressure would not drop below 600 psig before the accumulators are secured, and the sprays would not be initiated since the containment pressure would not rise above 9.5 psig (5).

Other important longer-term actions include:

- Securing one CS pump if all three CS pumps are successfully initiated
- Securing all CS pumps later in the event
- Switchover to ECCS sump recirculation after the RWST has been drained
- Switchover to hot leg injection

Per procedure, if all three trains of containment spray are successfully initiated, one of the three pumps would be manually secured (32; 33). Since this is a continuous action step that is intended to conserve the RWST, the third train of containment spray would be secured early in the event prior to switchover to recirculation.

In general, the remaining two trains of sprays would be on for a minimum of 6.5 hours for medium and large breaks. The termination criteria are 1) up to 6.5 hours has passed since the beginning of the event, 2) containment pressure has dropped below 6.5 psig, 3) the iodine levels are low enough to support the 30-day habitability limits, and 4) the Technical Support Center (TSC) staff has agreed that the sprays can be terminated (34). Typically, the pressure will drop below 6.5 psig in less than an hour (5), and the iodine levels would be relatively low given that there is no core damage early in the LOCA event. According to the STP operators (35), the decision to terminate containment sprays would probably be made as soon as the pressure drops below 6.5 psig (well before reaching 6.5 hours). However, 6.5 hours was used as a reasonably conservative time for securing containment sprays.

The timing for switchover to recirculation is dependent on the volume of water in the RWST and the total ECCS and CSS flow rate. Table 2.2.1 shows the sump switchover timing as a function of break size[6] (5).

Table 2.2.1 – Sump switchover time

Break Size (in)	Sump Switchover Time (s)[7]	Sump Switchover Time (min)
1.5"	20,239	337
2"	4,750	79
4"	3,353	56
6"	2,653	44
8"	2,268	38
12"	1,873	31
27.5" DEGB	1,773	30

Switchover to hot leg injection is started 5.5 hours after the beginning of the event (32; 36). As discussed in Assumption 1.j, the switchover steps are assumed to be completed between 5.75 and 6 hours after the beginning of the event.

2.2.2 Containment Geometry

Containment geometry data includes potential break locations (i.e., pipe welds), insulation quantities and locations, robust barrier locations, etc. This information is included in the STP containment computer aided design (CAD) model, which has been formally prepared, reviewed, and approved for use in safety-related applications (4).

Additional description of the CAD model is provided in Section 5.2.

2.2.3 LOCA Frequencies

The LOCA frequency input for CASA Grande is taken from two sources—a top-down evaluation of the overall frequencies for different break sizes, and a bottom-up evaluation of the relative frequencies at various locations based on specific degradation mechanisms (DMs). The overall frequencies for different

[6] This is based on best-estimate conditions where all pumps are available. However, these results can be conservatively applied to scenarios where some pumps fail to start since a reduction in the overall ECCS and CSS flow rates would delay sump switchover, thereby delaying strainer head loss and core blockage as the pump NPSH margin increases and the required core flow rate decreases.

[7] Note that the switchover time in seconds is consistent with the results of the thermal-hydraulic calculation data spreadsheets. However, the thermal-hydraulic report (5) presents the values in units of minutes or hours, which introduces some rounding error.

break sizes are based on the values provided in NUREG-1829 (37), which were fit using a bounded Johnson distribution as shown in Table 2.2.2 (8).

Table 2.2.2 – NUREG-1829 PWR current-day LOCA frequencies and fitted Johnson parameters

Size (in)	NUREG-1829 Quantiles				Fitted Johnson Parameters			
	5th	Median	Mean	95th	γ	δ	ξ	λ
0.5	6.80E-05	6.30E-04	1.90E-03	7.10E-03	1.650950	5.256964E-01	4.117000E-05	1.420E-02
1.625	5.00E-06	8.90E-05	4.20E-04	1.60E-03	1.646304	4.593913E-01	2.530000E-06	3.200E-03
2[8]	3.69E-06	6.57E-05	3.10E-04	1.18E-03	1.646308	4.593851E-01	1.870000E-06	2.361E-03
3	2.10E-07	3.40E-06	1.60E-05	6.10E-05	1.646605	4.589467E-01	1.200000E-07	1.220E-04
6[8]	6.30E-08	1.08E-06	5.20E-06	1.98E-05	1.646403	4.566256E-01	3.000000E-08	3.965E-05
7	1.40E-08	3.10E-07	1.60E-06	6.10E-06	1.645739	4.487957E-01	6.023625E-09	1.220E-05
14	4.10E-10	1.20E-08	2.00E-07	5.80E-07	1.645211	3.587840E-01	2.892430E-10	1.160E-06
31	3.50E-11	1.20E-09	2.90E-08	8.10E-08	1.645072	3.343493E-01	2.636770E-11	1.600E-07

The relative frequencies of breaks in various weld locations are based on specific DMs for categories of welds as shown in Table 2.2.3 through Table 2.2.10 (7). There are a total of 45 different categories that are considered. Note that several of the values in this table were based on logarithmic interpolation of the adjacent values. Since linear interpolation was used for the other portions of the LOCA frequency evaluation (see Assumption 3.d and Assumption 3.e), the logarithmically interpolated values were filtered out and not used in the evaluation.

Additional details on the LOCA Frequencies are provided in Section 5.3.

[8] The quantiles are not explicitly defined in NUREG-1829 for 2-inch and 6-inch breaks. However, these values were linearly interpolated from the 1-5/8-inch, 3-inch, and 7-inch break categories. The fitted Johnson parameters were determined using the same optimization process that was used for the original set of data in NUREG-1829 (8).

Table 2.2.3 – Relative frequencies vs. break size for hot leg, SG inlet, and cold leg welds (Categories 1A through 3B)

Category	1A		1B		1C		2		3A		3B	
System	Hot Leg		Hot Leg		Hot Leg		SG Inlet		Cold Leg		Cold Leg	
Pipe Size (in)	29		29		29		29		27.5		31	
DEGB (in)	41.01		41.01		41.01		41.01		38.89		43.84	
Weld Type	B-F		B-J		B-J		B-F		B-F		B-F	
DM	SC, D&C		D&C		TF, D&C		SC, D&C		SC, D&C		SC, D&C	
No. Welds	4		11		1		4		4		4	
	Break Size, X (in)	**F(LOCA≥X)**	**Break Size, X (in)**	**F(LOCA≥X)**	**Break Size, X (in)**	**F(LOCA≥X)**	**Break Size, X (in)**	**F(LOCA≥X)**	**Break Size, X (in)**	**F(LOCA≥X)**	**Break Size, X (in)**	**F(LOCA≥X)**
	0.50	4.02E-07	0.50	1.95E-09	0.50	1.25E-08	0.50	1.98E-06	0.50	1.51E-07	0.50	1.51E-07
	1.50	9.25E-08	1.50	4.49E-10	1.50	2.87E-09	1.50	4.59E-07	1.50	3.43E-08	1.50	3.43E-08
	2.00	6.92E-08	2.00	3.36E-10	2.00	2.15E-09	2.00	3.45E-07	2.00	2.38E-08	2.00	2.38E-08
	3.00	4.61E-08	3.00	2.24E-10	3.00	1.43E-09	3.00	2.31E-07	3.00	1.42E-08	3.00	1.42E-08
	4.00	3.19E-08	4.00	1.55E-10	4.00	9.90E-10	4.00	1.60E-07	4.00	9.49E-09	4.00	9.49E-09
	6.00	1.89E-08	6.00	9.19E-11	6.00	5.89E-10	6.00	9.52E-08	6.00	5.39E-09	6.00	5.39E-09
	6.75	1.61E-08	6.75	7.83E-11	6.75	5.01E-10	6.75	8.12E-08	6.75	4.53E-09	6.75	4.53E-09
	14.00	7.01E-09	14.00	3.40E-11	14.00	2.18E-10	14.00	3.35E-08	14.00	2.01E-09	14.00	2.01E-09
	20.00	3.70E-09	20.00	1.80E-11	20.00	1.15E-10	20.00	1.81E-08	20.00	1.15E-09	20.00	1.15E-09
	29.00	1.90E-09	29.00	9.24E-12	29.00	5.92E-11	29.00	9.57E-09	27.50	6.96E-10	27.50	6.96E-10
	31.50	1.64E-09	31.50	7.97E-12	31.50	5.11E-11	31.50	8.30E-09	31.50	5.63E-10	31.50	5.63E-10
	41.01	1.04E-09	41.01	5.03E-12	41.01	3.22E-11	41.01	5.24E-09	38.89	4.12E-10	43.80	3.38E-10

Table 2.2.4 – Relative frequencies vs. break size for cold leg and surge line welds (Categories 3C through 4D)

Category	3C		3D		4A		4B		4C		4D	
System	Cold Leg		Cold Leg		Surge Line		Surge Line		Surge Line		Surge Line	
Pipe Size (in)	27.5		31		16		16		16		2.5	
DEGB (in)	38.89		43.84		22.63		22.63		22.63		3.54	
Weld Type	B-J		B-J		B-F		B-J		BC		B-J	
DM	D&C		D&C		SC, TF, D&C		TF, D&C		TF, D&C		TF, D&C	
No. Welds	12		24		1		7		2		6	
	Break Size, X (in)	**F(LOCA≥X)**	**Break Size, X (in)**	**F(LOCA≥X)**	**Break Size, X (in)**	**F(LOCA≥X)**	**Break Size, X (in)**	**F(LOCA≥X)**	**Break Size, X (in)**	**F(LOCA≥X)**	**Break Size, X (in)**	**F(LOCA≥X)**
	0.50	2.79E-09	0.50	2.79E-09	0.50	9.75E-06	0.50	7.44E-08	0.50	1.21E-07	0.50	7.44E-08
	1.50	6.33E-10	1.50	6.33E-10	1.50	3.30E-06	1.50	2.52E-08	1.50	4.11E-08	1.50	2.52E-08
	2.00	4.39E-10	2.00	4.39E-10	2.00	2.43E-06	2.00	1.85E-08	2.00	3.02E-08	2.00	1.85E-08
	3.00	2.62E-10	3.00	2.62E-10	3.00	1.58E-06	3.00	1.20E-08	3.00	1.97E-08	3.00	1.20E-08
	4.00	1.75E-10	4.00	1.75E-10	4.00	1.03E-06	4.00	7.82E-09	4.00	1.28E-08	3.54	9.42E-09
	6.00	9.95E-11	6.00	9.95E-11	6.00	5.58E-07	6.00	4.26E-09	6.00	6.94E-09		
	6.75	8.36E-11	6.75	8.36E-11	6.75	4.68E-07	6.75	3.57E-09	6.75	5.82E-09		
	14.00	3.70E-11	14.00	3.70E-11	14.00	1.18E-07	14.00	9.03E-10	14.00	1.47E-09		
	20.00	2.11E-11	20.00	2.11E-11	16.00	9.19E-08	16.00	7.02E-10	16.00	1.15E-09		
	27.50	1.28E-11	27.50	1.28E-11	20.00	6.14E-08	20.00	4.69E-10	20.00	7.65E-10		
	31.50	1.04E-11	31.50	1.04E-11	22.63	4.77E-08	22.63	3.64E-10	22.63	5.93E-10		
	38.89	7.60E-12	43.80	6.23E-12								

Table 2.2.5 – Relative frequencies vs. break size for pressurizer line welds (Categories 5A through 5F)

Category	5A		5B		5C		5D		5E		5F	
System	Pressurizer		Pressurizer		Pressurizer		Pressurizer		Pressurizer		Pressurizer	
Pipe Size (in)	6		3		4		3		6		6	
DEGB (in)	8.49		4.24		5.66		4.24		8.49		8.49	
Weld Type	B-J		B-J		B-J		B-J		B-J		B-F	
DM	TF, D&C		TF, D&C		D&C		D&C		D&C		SC, TF, D&C	
No. Welds	29		14		53		4		29		0	
	Break Size, X (in)	**F(LOCA≥X)**	**Break Size, X (in)**	**F(LOCA≥X)**	**Break Size, X (in)**	**F(LOCA≥X)**	**Break Size, X (in)**	**F(LOCA≥X)**	**Break Size, X (in)**	**F(LOCA≥X)**	**Break Size, X (in)**	**F(LOCA≥X)**
	0.50	4.59E-08	0.50	4.59E-08	0.50	1.72E-08	0.50	1.72E-08	0.50	1.72E-08	0.50	5.09E-06
	0.75	2.76E-08	0.75	2.76E-08	0.75	1.03E-08	0.75	1.03E-08	0.75	1.03E-08	0.75	3.06E-06
	1.00	1.96E-08	1.00	1.96E-08	1.00	7.33E-09	1.00	7.33E-09	1.00	7.33E-09	1.00	2.17E-06
	1.50	1.24E-08	1.50	1.24E-08	1.50	4.64E-09	1.50	4.64E-09	1.50	4.64E-09	1.50	1.38E-06
	2.00	6.64E-09	2.00	6.64E-09	2.00	2.49E-09	2.00	2.49E-09	2.00	2.49E-09	2.00	7.36E-07
	3.00	2.75E-09	3.00	2.75E-09	3.00	1.03E-09	3.00	1.03E-09	3.00	1.03E-09	3.00	3.05E-07
	4.24	1.30E-09	4.24	1.30E-09	4.24	4.87E-10	4.24	4.87E-10	4.24	4.87E-10	4.24	1.44E-07
	5.66	6.26E-10			5.66	2.34E-10			5.66	2.34E-10	5.66	6.94E-08
	6.00	5.47E-10							6.00	2.05E-10	6.00	6.06E-08
	6.75	4.16E-10							6.75	1.56E-10	6.75	4.61E-08
	8.49	2.64E-10							8.49	9.89E-11	8.49	2.93E-08

Table 2.2.6 – Relative frequencies vs. break size for pressurizer and small bore line welds (Categories 5F through 6B)

Category	5G		5H		5I		5J		6A		6B	
System	Pressurizer		Pressurizer		Pressurizer		Pressurizer		Small Bore		Small Bore	
Pipe Size (in)	6		6		4		2		2		1	
DEGB (in)	8.49		8.49		5.66		2.83		2.83		1.41	
Weld Type	B-F		B-F		BC		B-J		B-J		B-J	
DM	SC, D&C		D&C (Weld Overlay)		D&C		TF, D&C		VF, SC, D&C		VF, SC, D&C	
No. Welds	0		4		2		2		16		193	
	Break Size, X (in)	**F(LOCA≥X)**	**Break Size, X (in)**	**F(LOCA≥X)**	**Break Size, X (in)**	**F(LOCA≥X)**	**Break Size, X (in)**	**F(LOCA≥X)**	**Break Size, X (in)**	**F(LOCA≥X)**	**Break Size, X (in)**	**F(LOCA≥X)**
	0.50	5.01E-06	0.50	1.74E-08	0.50	1.72E-08	0.50	4.59E-08	0.50	1.22E-06	0.50	1.22E-06
	0.75	3.01E-06	0.75	1.05E-08	0.75	1.03E-08	0.75	2.76E-08	0.75	7.18E-07	0.75	7.18E-07
	1.00	2.13E-06	1.00	7.42E-09	1.00	7.33E-09	1.00	1.96E-08	1.00	5.00E-07	1.00	5.00E-07
	1.50	1.35E-06	1.50	4.70E-09	1.50	4.64E-09	1.50	1.24E-08	1.40	3.30E-07	1.40	3.30E-07
	2.00	7.24E-07	2.00	2.52E-09	2.00	2.49E-09	2.00	6.64E-09	1.50	3.08E-07		
	3.00	3.00E-07	3.00	1.04E-09	3.00	1.03E-09	2.83	3.13E-09	1.99	1.75E-07		
	4.24	1.42E-07	4.24	4.94E-10	4.24	4.87E-10			2.00	1.73E-07		
	5.66	6.83E-08	5.66	2.37E-10	5.66	2.34E-10			2.80	8.66E-08		
	6.00	5.96E-08	6.00	2.07E-10								
	6.75	4.54E-08	6.75	1.58E-10								
	8.49	2.88E-08	8.49	1.00E-10								

Table 2.2.7 – Relative frequencies vs. break size for safety injection and recirculation line welds (Categories 7A through 7F)

Category	7A		7B		7C		7D		7E		7F	
System	SIR		SIR		SIR		SIR		SIR		SIR	
Pipe Size (in)	12		8		8		12		12		10	
DEGB (in)	16.97		11.31		11.31		16.97		16.97		14.14	
Weld Type	B-J		B-J		B-J		B-J		BC, B-J		B-J	
DM	TF, D&C		TF, D&C		SC, TF, D&C		SC, D&C		D&C		D&C	
No. Welds	21		9		3		3		57		30	
	Break Size, X (in)	**F(LOCA≥X)**	**Break Size, X (in)**	**F(LOCA≥X)**	**Break Size, X (in)**	**F(LOCA≥X)**	**Break Size, X (in)**	**F(LOCA≥X)**	**Break Size, X (in)**	**F(LOCA≥X)**	**Break Size, X (in)**	**F(LOCA≥X)**
	0.50	2.78E-06	0.50	2.78E-06	0.50	3.10E-06	0.50	3.54E-07	0.50	1.14E-08	0.50	1.14E-08
	0.75	1.67E-06	0.75	1.67E-06	0.75	1.86E-06	0.75	2.12E-07	0.75	6.84E-09	0.75	6.84E-09
	1.00	1.18E-06	1.00	1.18E-06	1.00	1.32E-06	1.00	1.51E-07	1.00	4.85E-09	1.00	4.85E-09
	1.50	7.48E-07	1.50	7.48E-07	1.50	8.34E-07	1.50	9.54E-08	1.50	3.07E-09	1.50	3.07E-09
	2.00	4.01E-07	2.00	4.01E-07	2.00	4.48E-07	2.00	5.12E-08	2.00	1.65E-09	2.00	1.65E-09
	2.83	1.67E-07	2.83	1.67E-07	2.83	1.86E-07	2.83	2.13E-08	2.83	6.85E-10	2.83	6.85E-10
	4.00	8.50E-08	4.00	8.50E-08	4.00	9.48E-08	4.00	1.08E-08	4.00	3.49E-10	4.00	3.49E-10
	4.24	7.41E-08	4.24	7.41E-08	4.24	8.26E-08	4.24	9.45E-09	4.24	3.04E-10	4.24	3.04E-10
	5.66	3.79E-08	5.66	3.79E-08	5.66	4.23E-08	5.66	4.84E-09	5.66	1.56E-10	5.66	1.56E-10
	6.00	3.31E-08	6.00	3.31E-08	6.00	3.70E-08	6.00	4.23E-09	6.00	1.36E-10	6.00	1.36E-10
	6.75	2.52E-08	6.75	2.52E-08	6.75	2.81E-08	6.75	3.22E-09	6.75	1.04E-10	6.75	1.04E-10
	7.20	2.22E-08	7.20	2.22E-08	7.20	2.48E-08	7.20	2.83E-09	7.20	9.12E-11	7.20	9.12E-11
	8.49	1.60E-08	8.49	1.60E-08	8.49	1.79E-08	8.49	2.04E-09	8.49	6.58E-11	8.49	6.58E-11
	10.00	1.16E-08	10.00	1.16E-08	10.00	1.29E-08	10.00	1.47E-09	10.00	4.75E-11	10.00	4.75E-11
	11.31	9.11E-09	11.31	9.11E-09	11.31	1.02E-08	11.31	1.16E-09	11.31	3.74E-11	11.31	3.74E-11
	14.14	5.93E-09					14.14	7.56E-10	14.14	2.44E-11	14.14	2.44E-11
	16.97	4.05E-09					16.97	5.16E-10	16.97	1.66E-11		

Table 2.2.8 – Relative frequencies vs. break size for safety injection and recirculation line welds (Categories 7F through 7L)

Category	7G		7H		7I		7J		7K		7L	
System	SIR		SIR		SIR		SIR		SIR		SIR	
Pipe Size (in)	8		6		4		3		2		1.5	
DEGB (in)	11.31		8.49		5.66		4.24		2.83		2.12	
Weld Type	BC, B-J		B-J		BC		BC		BC		B-J	
DM	D&C		D&C		D&C		D&C		D&C		D&C	
No. Welds	42		23		5		9		10		0	
	Break Size, X (in)	**F(LOCA≥X)**	**Break Size, X (in)**	**F(LOCA≥X)**	**Break Size, X (in)**	**F(LOCA≥X)**	**Break Size, X (in)**	**F(LOCA≥X)**	**Break Size, X (in)**	**F(LOCA≥X)**	**Break Size, X (in)**	**F(LOCA≥X)**
	0.50	1.14E-08	0.50	1.14E-08	0.50	1.14E-08	0.50	1.14E-08	0.50	1.14E-08	0.50	1.14E-08
	0.75	6.84E-09	0.75	6.84E-09	0.75	6.84E-09	0.75	6.84E-09	0.75	6.84E-09	0.75	6.84E-09
	1.00	4.85E-09	1.00	4.85E-09	1.00	4.85E-09	1.00	4.85E-09	1.00	4.85E-09	1.00	4.85E-09
	1.50	3.07E-09	1.50	3.07E-09	1.50	3.07E-09	1.50	3.07E-09	1.50	3.07E-09	1.50	3.07E-09
	2.00	1.65E-09	2.00	1.65E-09	2.00	1.65E-09	2.00	1.65E-09	2.00	1.65E-09	2.00	1.65E-09
	2.83	6.85E-10	2.83	6.85E-10	2.83	6.85E-10	2.83	6.85E-10	2.83	6.85E-10		
	4.00	3.49E-10	4.00	3.49E-10	4.00	3.49E-10	4.00	3.49E-10				
	4.24	3.04E-10	4.24	3.04E-10	4.24	3.04E-10	4.24	3.04E-10				
	5.66	1.56E-10	5.66	1.56E-10	5.66	1.56E-10						
	6.00	1.36E-10	6.00	1.36E-10								
	6.75	1.04E-10	6.75	1.04E-10								
	7.20	9.12E-11	7.20	9.12E-11								
	8.49	6.58E-11	8.49	6.58E-11								
	10.00	4.75E-11										
	11.31	3.74E-11										

Table 2.2.9 – Relative frequencies vs. break size for accumulator injection and CVCS line welds (Categories 7M through 8C)

Category	7M		7N		7O		8A		8B		8C	
System	ACC		ACC		ACC		CVCS		CVCS		CVCS	
Pipe Size (in)	12		12		12		2		4		2	
DEGB (in)	16.97		16.97		16.97		2.83		5.66		2.83	
Weld Type	B-J		B-J		BC, B-J		B-J		B-J		B-J	
DM	SC, D&C		TF, D&C		D&C		TF, VF, D&C		TF, VF, D&C		VF, D&C	
No. Welds	0		35		15		10		19		47	
	Break Size, X (in)	**F(LOCA≥X)**	**Break Size, X (in)**	**F(LOCA≥X)**	**Break Size, X (in)**	**F(LOCA≥X)**	**Break Size, X (in)**	**F(LOCA≥X)**	**Break Size, X (in)**	**F(LOCA≥X)**	**Break Size, X (in)**	**F(LOCA≥X)**
	0.50	3.54E-07	0.50	5.18E-08	0.50	6.26E-09	0.50	4.28E-08	0.50	4.28E-08	0.50	1.87E-08
	0.75	2.12E-07	0.75	3.11E-08	0.75	3.75E-09	0.75	2.57E-08	0.75	2.57E-08	0.75	1.12E-08
	1.00	1.51E-07	1.00	2.21E-08	1.00	2.66E-09	1.00	1.82E-08	1.00	1.82E-08	1.00	7.97E-09
	1.50	9.54E-08	1.50	1.40E-08	1.50	1.69E-09	1.50	1.15E-08	1.50	1.15E-08	1.50	5.04E-09
	2.00	5.12E-08	2.00	7.49E-09	2.00	9.04E-10	2.00	6.03E-09	2.00	6.03E-09	2.00	2.64E-09
	2.83	2.13E-08	2.83	3.12E-09	2.83	3.76E-10	3.00	2.42E-09	3.00	2.42E-09	3.00	1.06E-09
	4.00	1.08E-08	4.00	1.67E-09	4.00	2.02E-10			4.00	1.26E-09		
	4.24	9.45E-09	5.66	7.09E-10	5.66	8.55E-11			5.66	5.77E-10		
	5.66	4.84E-09	6.00	6.19E-10	6.00	7.47E-11						
	6.00	4.23E-09	6.80	4.71E-10	6.80	5.69E-11						
	6.75	3.22E-09	7.20	4.14E-10	7.20	5.00E-11						
	7.20	2.83E-09	10.00	2.16E-10	10.00	2.61E-11						
	8.49	2.04E-09	14.14	1.11E-10	14.14	1.34E-11						
	10.00	1.47E-09	16.97	7.56E-11	16.97	9.12E-12						
	11.31	1.16E-09										
	14.14	7.56E-10										
	16.97	5.16E-10										

Table 2.2.10 – Relative frequencies vs. break size for CVCS line welds (Categories 8D through 8F)

Category	8D		8E		8F	
System	CVCS		CVCS		CVCS	
Pipe Size (in)	4		4		4	
DEGB (in)	5.66		5.66		5.66	
Weld Type	B-J		BC		BC	
DM	VF, D&C		TF, D&C		D&C	
No. Welds	6		4		1	
	Break Size, X (in)	**F(LOCA≥X)**	**Break Size, X (in)**	**F(LOCA≥X)**	**Break Size, X (in)**	**F(LOCA≥X)**
	0.50	1.87E-08	0.50	7.98E-08	0.50	1.87E-08
	0.75	1.12E-08	0.75	4.79E-08	0.75	1.12E-08
	1.00	7.97E-09	1.00	3.40E-08	1.00	7.97E-09
	1.50	5.04E-09	1.50	2.15E-08	1.50	5.04E-09
	2.00	2.64E-09	2.00	1.12E-08	2.00	2.64E-09
	3.00	1.06E-09	3.00	4.51E-09	3.00	1.06E-09
	4.00	5.49E-10	4.00	2.34E-09	4.00	5.49E-10
	5.66	2.52E-10	5.66	1.08E-09	5.66	2.52E-10

2.2.4 Pump State Frequencies

The frequency of various pump state combinations was determined based on the STP PRA model as shown in Table 2.2.11 (38). Note that these frequencies are based on the PRA without considering failure related to GSI-191 phenomena. Only sequences ending in success, as opposed to core damage, are included in the pump combination state frequencies since only those sequences are candidates to transition to core damage when GSI-191 failure phenomena are considered.

Table 2.2.11 – Frequency of success pump combination states

Case	Working HHSI Pumps	Working LHSI Pumps	Working CS Pumps	Pump State Frequency (year^{-1})
1	3	3	3	2.64E-04
2	3	3	2	3.32E-06
3	3	3	1	7.53E-08
4	3	3	0	9.77E-09
5	3	2	3	3.49E-06
6	3	2	2	4.38E-08
7	3	2	1	9.80E-10
8	3	2	0	1.25E-10
9	3	1	3	3.22E-08
10	3	1	2	3.95E-10
11	3	1	1	7.59E-12
12	3	1	0	9.85E-13
13	3	0	3	<1E-14
14	3	0	2	<1E-14
15	3	0	1	<1E-14
16	3	0	0	<1E-14
17	2	3	3	1.94E-06
18	2	3	2	2.44E-08
19	2	3	1	5.39E-10
20	2	3	0	6.95E-11
21	2	2	3	1.17E-07
22	2	2	2	9.16E-06
23	2	2	1	7.81E-08
24	2	2	0	1.19E-09
25	2	1	3	7.65E-10
26	2	1	2	6.03E-08
27	2	1	1	4.93E-10
28	2	1	0	6.16E-12

Case	Working HHSI Pumps	Working LHSI Pumps	Working CS Pumps	Pump State Frequency ($year^{-1}$)
29	2	0	3	<1E-14
30	2	0	2	<1E-14
31	2	0	1	<1E-14
32	2	0	0	<1E-14
33	1	3	3	2.67E-08
34	1	3	2	3.26E-10
35	1	3	1	6.18E-12
36	1	3	0	8.02E-13
37	1	2	3	6.43E-10
38	1	2	2	3.54E-08
39	1	2	1	2.84E-10
40	1	2	0	3.01E-12
41	1	1	3	9.96E-12
42	1	1	2	1.63E-09
43	1	1	1	4.34E-08
44	1	1	0	1.76E-10
45	1	0	3	<1E-14
46	1	0	2	<1E-14
47	1	0	1	<1E-14
48	1	0	0	<1E-14
49	0	3	3	5.84E-11
50	0	3	2	6.24E-13
51	0	3	1	<1E-14
52	0	3	0	<1E-14
53	0	2	3	4.92E-13
54	0	2	2	3.50E-11
55	0	2	1	<1E-14
56	0	2	0	<1E-14
57	0	1	3	<1E-14
58	0	1	2	<1E-14
59	0	1	1	3.89E-11
60	0	1	0	<1E-14
61	0	0	3	<1E-14
62	0	0	2	<1E-14
63	0	0	1	<1E-14
64	0	0	0	<1E-14

2.2.5 Pool Water Level

The active water volume is based on the total volume of water in containment (from the RWST, RCS, and accumulators) minus any water sequestered in inactive regions. The pool volume is equal to the active water volume minus the transitory water volume (i.e., water circulating through the ECCS and CSS piping, containment sprays falling through the air or migrating down to the pool, condensation on walls and other surfaces, water still in the RCS, etc.). These values were calculated at bounding conditions as shown in Table 2.2.12 (14), and the pool volume for small, medium, and large breaks was sampled in CASA Grande based on these ranges.

Table 2.2.12 – Range of water volumes implemented in CASA Grande

Break Size	Minimum Volume (ft^3)	Maximum Volume (ft^3)
LBLOCA	45,201	69,263
MBLOCA	39,533	69,444
SBLOCA	43,464	61,993

The pool water level is calculated using the following equation:

$$H_{pool} = \frac{V_{pool}}{A_{pool}} \quad \text{Equation 1}$$

where:

H_{pool} = Height above the containment floor at Elevation -11'3"
V_{pool} = Pool volume
A_{pool} = Pool area

The area of the pool at STP is 12,301 ft^2 (14).

2.2.6 Pool Temperature

The pool temperature profiles were determined for different break sizes based on thermal-hydraulic modeling. The temperature profiles for breaks that are 6 inches and larger have a similar trends, and the larger breaks have a higher peak temperature early in the event and then drop down to a lower overall temperature later in the event (5).

The 6-inch break temperature profile was used to represent all small and medium breaks and the 27.5-inch DEGB temperature profile was used to represent all large breaks (see Assumption 1.k). The 6-inch break temperature profile was based on an extended simulation that went out to 30 days, and the 27.5-inch DEGB temperature profile was logarithmically extrapolated from 10 hours to 30 days as described in Assumption 1.l. The two temperature profiles that were used in the CASA evaluation are shown in Figure 2.2.1 and Table 2.2.13 (5). Note that the initial temperature transient prior to the start of recirculation is not shown in Figure 2.2.1 since temperature only affects models that are important after the start of recirculation (e.g., the NPSH model).

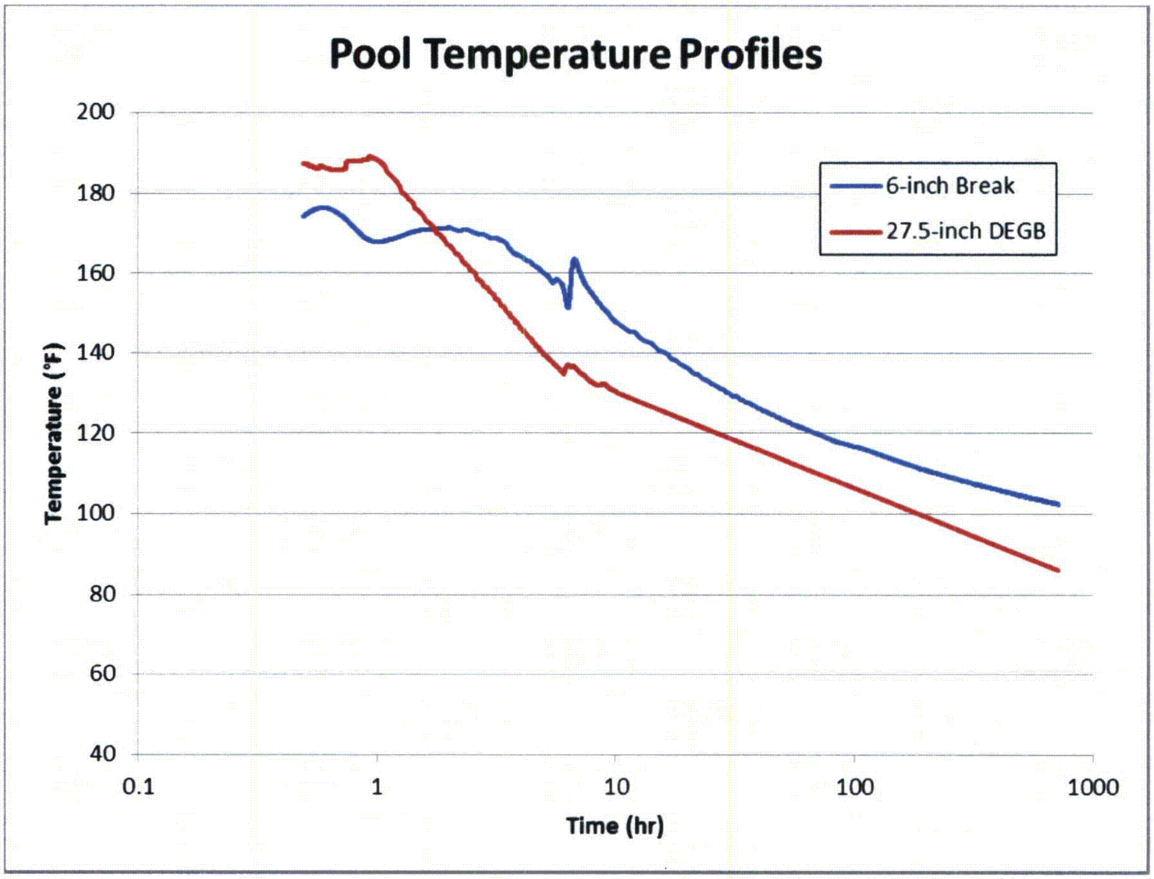

Figure 2.2.1 – Temperature profiles implemented in CASA Grande

Table 2.2.13 – Temperature profiles implemented in CASA Grande

Time (hr)	Temperature for 6-inch Break (°F)	Temperature for 27.5-inch DEGB (°F)
0	119.6	119.8113
0.0847	131.2987	213.9295

Time (hr)	Temperature for 6-inch Break (°F)	Temperature for 27.5-inch DEGB (°F)
0.0864	140.1689	242.3104
0.0881	150.3314	255.0268
0.0897	156.124	255.7907
0.0914	159.2343	253.1617
0.0931	162.1567	252.9372
0.0947	164.568	252.539
0.0964	166.6937	251.9023
0.0981	168.5685	250.9733
0.0997	170.2457	249.7169
0.1014	171.7175	245.8894
0.1031	172.9577	235.9856
0.1047	174.0415	224.0051
0.1064	174.957	212.9495
0.1081	175.7084	203.5499
0.1097	176.3081	195.7225
0.1139	177.5299	179.5894
0.1306	164.4935	199.8048
0.1472	132.7076	174.8143
0.1639	124.0848	174.8276
0.1806	123.6914	177.3518
0.1972	123.5988	180.7405
0.2139	123.5641	183.2333
0.2306	123.5529	185.1644
0.2472	124.4938	186.4925
0.2639	127.6399	187.2579
0.2806	129.7484	187.827
0.2972	131.0391	188.1924
0.3139	149.8002	188.4266
0.3306	158.2393	188.5605
0.3472	162.7694	188.5934
0.3639	165.496	188.5042
0.3806	167.3851	188.3375
0.3972	168.6688	189.3187
0.4139	169.7687	189.757
0.4306	170.9814	189.0923
0.4472	171.9993	188.5202
0.4639	172.8771	188.0148
0.4806	173.715	187.5621
0.4972	174.4595	187.4103
0.5139	175.0903	187.0671
0.5306	175.6074	186.733

Time (hr)	Temperature for 6-inch Break (°F)	Temperature for 27.5-inch DEGB (°F)
0.5472	176.0061	186.4249
0.5639	176.2923	186.1559
0.5806	176.4625	186.764
0.5972	176.4855	186.5012
0.6139	176.3916	186.2557
0.6306	176.2055	186.0555
0.6472	175.9468	185.9119
0.6639	175.6184	185.8265
0.6806	175.2411	185.8062
0.6972	174.8243	185.8495
0.7139	174.3902	185.9526
0.7306	173.9374	186.1092
0.7472	173.4284	187.8900
0.7639	172.8459	187.9673
0.7806	172.2319	187.9196
0.7972	171.6143	187.9119
0.8139	171.0143	187.9385
0.8306	170.4548	187.9954
0.8472	169.9507	188.0710
0.8639	169.5034	188.1647
0.8806	169.1086	188.2538
0.8972	168.7661	188.3385
0.9139	168.4824	188.4003
0.9306	168.2551	189.0996
0.9472	168.0847	188.9199
0.9639	167.9707	188.7439
0.9806	167.9020	188.5614
0.9972	167.8705	188.3622
1.0139	167.8665	188.1314
1.0306	167.8947	187.8597
1.0472	167.9451	187.5387
1.0639	168.0131	187.1667
1.0806	168.0978	186.7559
1.3611	170.0607	178.4091
1.6944	170.9606	171.8762
2.0278	171.4105	166.5421
2.3611	170.8721	162.2238
2.6944	169.8110	158.1410
3.0278	168.7942	154.9818
3.3611	168.1132	151.7673
3.6944	165.3090	148.9234

Time (hr)	Temperature for 6-inch Break (°F)	Temperature for 27.5-inch DEGB (°F)
4.0278	164.1228	146.0834
4.3611	163.0112	143.7967
4.6944	161.4436	141.6054
5.0278	159.9385	139.5251
5.3611	158.1298	137.9892
5.6944	158.4517	136.4819
6.0278	156.5706	134.8865
6.3611	151.6937	136.9000
6.6944	163.7090	136.6489
7.0278	160.9624	135.3569
7.3611	158.1118	134.3103
7.6944	156.1579	133.2941
8.0278	154.6151	132.4453
8.3611	153.2333	131.9467
8.6944	151.9641	132.0536
9.0278	150.8191	132.1915
9.3611	149.7667	131.3055
9.6944	148.7924	130.7946
10.0278	147.8649	130.2765
20.0833	136.208	123.0489
32.0833	129.023	118.1991
44.0833	124.979	114.9095
56.0833	122.145	112.4170
68.0833	120.131	110.4096
80.0833	118.471	108.7290
92.0833	117.316	107.2834
104.0833	116.498	106.0152
116.0833	115.616	104.8855
128.0833	114.710	103.8671
140.0833	113.896	102.9399
152.0833	113.173	102.0890
164.0833	112.521	101.3027
176.0833	111.924	100.5720
188.0833	111.358	99.8894
200.0833	110.859	99.2491
212.0833	110.393	98.6461
224.0833	109.993	98.0763
236.0833	109.577	97.5362
248.0833	109.209	97.0229
260.0833	108.910	96.5339
272.0833	108.593	96.0669

Time (hr)	Temperature for 6-inch Break (°F)	Temperature for 27.5-inch DEGB (°F)
283.3333	108.281	95.6474
297.2222	107.968	95.1520
308.3333	107.710	94.7720
319.4444	107.473	94.4055
333.3333	107.162	93.9649
344.4444	106.943	93.6254
355.5556	106.715	93.2967
369.4444	106.477	92.9000
380.5556	106.250	92.5932
391.6667	106.124	92.2953
402.7778	105.893	92.0057
416.6667	105.666	91.6547
427.7778	105.541	91.3822
438.8889	105.316	91.1168
452.7778	105.193	90.7942
463.8889	105.069	90.5432
475.0000	104.844	90.2982
488.8889	104.725	89.9998
500.0000	104.607	89.7671
511.1111	104.377	89.5396
525.0000	104.366	89.2620
536.1111	104.140	89.0452
547.2222	104.023	88.8328
561.1111	103.905	88.5733
572.2222	103.791	88.3703
583.3333	103.673	88.1712
597.2222	103.566	87.9276
608.3333	103.452	87.7368
619.4444	103.335	87.5494
633.3333	103.145	87.3198
644.4444	103.100	87.1398
655.5556	102.913	86.9628
669.4444	102.868	86.7457
680.5556	102.681	86.5753
691.6667	102.645	86.4076
702.7778	102.525	86.2427
716.6667	102.516	86.0401

CASA Grande evaluates water properties by using the current pool temperature to enter a lookup table based on the National Institute of Standards and Technology (NIST) reference property database (39).

2.2.7 Operating Trains

In the event of a LOCA, all three trains of ECCS would be automatically initiated due to a safety injection actuation signal and would begin to draw flow from the RWST (40). As discussed in Section 2.2.1, the three trains of CS would also be automatically initiated if the containment pressure rises above 9.5 psig. If all three CS pumps start successfully, operators would (per procedure) manually secure one of the three CS pumps (33). Once the RWST has been drained down to the Lo-Lo RWST level, the recirculation mode of ECCS and CS operation would be automatically initiated through the three ECCS sumps (40).

A variety of train or pump failure combinations are possible (many of which go beyond traditional design basis analyses). This is discussed in more detail in Section 5.1.

2.2.8 ECCS and CSS Flow Rates

The maximum flow rates per train are 2,800 gpm for the low head safety injection (LHSI) flow (41), 1,620 gpm for the high head safety injection (HHSI) flow (41), and 2,600 gpm for the containment spray (CS) flow (41). This gives a maximum total sump flow of 7,020 gpm per train. The maximum total flow rates are only possible for LBLOCA conditions. For SBLOCA conditions, containment sprays would not be initiated due to the small increase in containment pressure (5), the LHSI may not inject due to high RCS pressure, and the HHSI flow rate would vary from 0 gpm to 1,620 gpm per train depending on the actual size of the break and number of trains operating. For MBLOCA conditions, the sprays would be initiated, but the combined LHSI and HHSI flow would range up to 4,420 gpm per train (41) depending on the actual size of the break. Table 2.2.14 provides a summary of the total SI flow rates for different break sizes based on thermal-hydraulic modeling[9] (5).

Table 2.2.14 – Total SI flow rates

Break Size (in)	Nominal Total SI Flow (gpm)
1.5"	1,231
2"	2,076
4"	4,120
6"	7,951
8"	10,285
15"	11,780
27.5" DEGB	11,988

The data in Table 2.2.14 is plotted in Figure 2.2.2 with the 27.5-inch DEGB plotted with the equivalent break size of 38.9 inches. As shown in this figure, the SI flow rate can be approximated using two linear

[9] These flow rates are based on simulations using nominal operating conditions (i.e., all ECCS trains operating, all fan coolers operating, and nominal CCW heat exchanger temperatures).

curves (see Equation 2). The reason that the slope changes for breaks greater than approximately 9 inches is that the break size is large enough for the LHSI and HHSI pumps to operate at essentially maximum capacity. For smaller breaks, the reduced break size causes back-pressure in the RCS that limits the total SI pump flow.

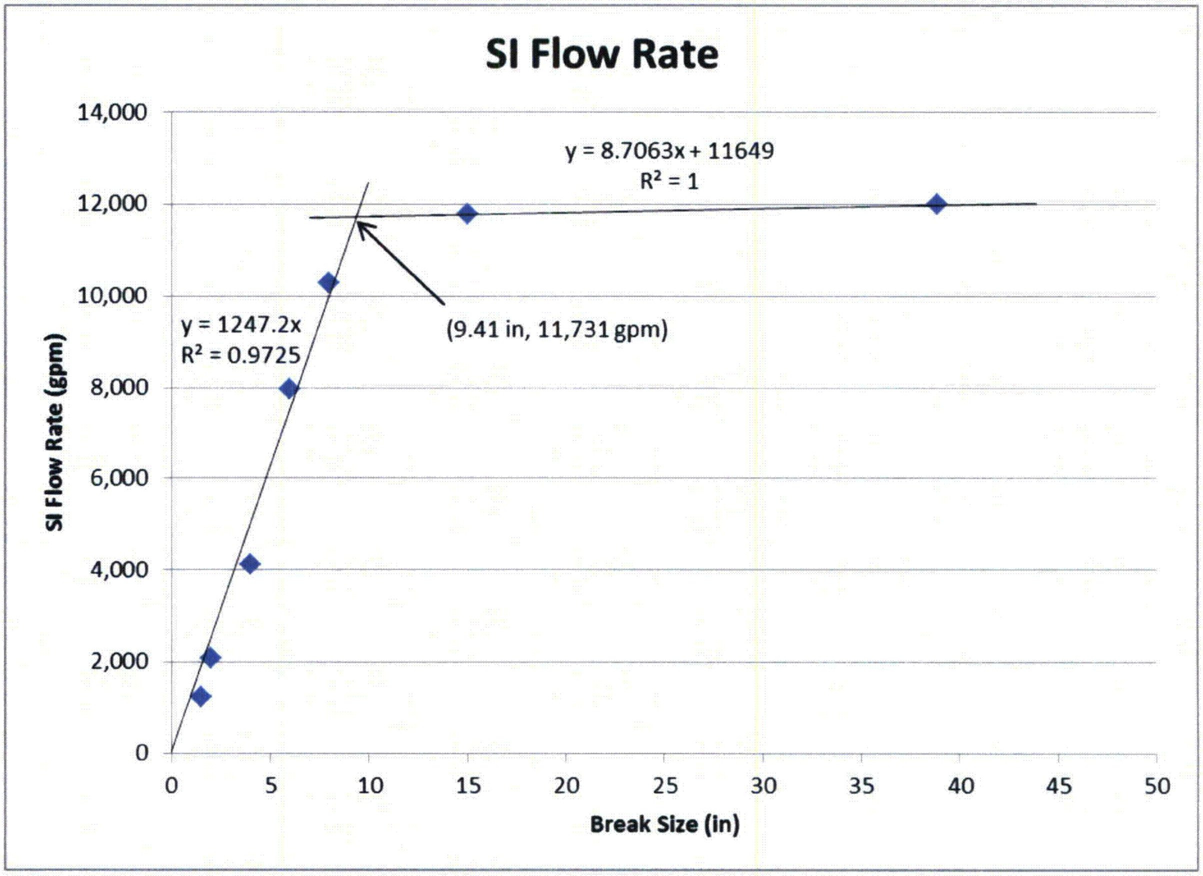

Figure 2.2.2 – Total SI flow rate vs. break size

$$Q_{TSI} = 1{,}247.2\, {}^{gpm}/_{in} \cdot D_{break} \qquad \text{if } D_{break} < 9.41 \text{ in}$$
$$Q_{TSI} = 8.706\, {}^{gpm}/_{in} \cdot D_{break} + 11{,}649 gpm \qquad \text{if } D_{break} \geq 9.41 \text{ in}$$

Equation 2

where:

Q_{TSI} = Total SI flow rate (combined LHSI and HHSI pump flow rates from all trains)
D_{break} = Break diameter (equivalent break diameter for DEGB)

Note, however, that the total SI flow rate cannot be greater than the maximum capacity of the operating pumps. Therefore, the following criterion is defined for the total SI flow rate based on a maximum LHSI pump flow rate of 2,800 gpm, and a maximum HHSI pump flow rate of 1,620 gpm (41):

$$Q_{TSI} \leq 2{,}800gpm \cdot N_{LHSI} + 1{,}620gpm \cdot N_{HHSI} \quad \text{Equation 3}$$

where:

N_{LHSI} = Number of operating LHSI pumps
N_{HHSI} = Number of operating HHSI pumps

For any given scenario, the flow rate for individual SI pumps within each train can be estimated based on a ratio of the maximum pump capacities, as well as the number of LHSI and HHSI pumps that are running (assuming at least one LHSI pump and one HHSI pump are running). This is shown in the following equations:

$$Q_{LHSI} = Q_{TSI} \cdot \left[\frac{2{,}800gpm}{2{,}800gpm \cdot N_{LHSI} + 1{,}620gpm \cdot N_{HHSI}}\right] \quad \text{Equation 4}$$

$$Q_{HHSI} = Q_{TSI} \cdot \left[\frac{1{,}620gpm}{2{,}800gpm \cdot N_{LHSI} + 1{,}620gpm \cdot N_{HHSI}}\right] \quad \text{Equation 5}$$

where:

Q_{LHSI} = LHSI pump flow rate for an individual train
Q_{HHSI} = HHSI pump flow rate for an individual train

If containment sprays are initiated, the flow rate is not dependent on the size of the break. However, it would vary depending on the number of trains in operation. As discussed above, the maximum spray flow rate for a single train is 2,600 gpm. If all three trains are operating, the maximum flow rate is approximately 2,060 gpm per train (41). If two trains are operating, the maximum flow rate is approximately 2,350 gpm per train (42). The minimum probable CS flow rates are approximately 1,657 gpm per train for three train operation and 1,932 gpm per train for two train operation (42). The minimum spray flow rate for one train operation was not available in STP documentation, but was assumed to be 80% of the maximum flow rate consistent with the range of flow rates for two and three train operation (see Assumption 1.i). This gives a minimum spray flow rate of 2,080 gpm for single train operation. Table 2.2.15 provides a summary of the range of containment spray flow rates.

Table 2.2.15 – Containment spray flow rates

Number of Operating Spray Pumps	Minimum Spray Flow per Train (gpm)	Maximum Spray Flow per Train (gpm)
One Train	2,080	2,600
Two Trains	1,932	2,350
Three Trains	1,657	2,060

2.2.9 Qualified Coatings Quantity

The total quantity of qualified coatings debris is a function of break size, location, surface area of coated concrete and steel within the ZOI, and coating thickness. The quantity of qualified coatings debris generated was conservatively calculated for four break sizes as shown in Table 2.2.16 (11). The break sizes include a 2-inch break, a 6-inch break, a 15-inch break, and a 31-inch double-ended guillotine break (DEGB). The results can be conservatively applied for breaks in any location that are less than or equal to break sizes listed (e.g., the 15-inch quantities can be used for any breaks between 6 and 15 inches in diameter). To simplify the evaluation, however, the quantity of qualified coatings debris for a 31-inch DEGB was applied to all breaks.

Table 2.2.16 – Quantity of qualified coatings debris[10]

Coatings Type	31-inch DEGB Quantity (lb_m)	15-inch Break Quantity (lb_m)	6-inch Break Quantity (lb_m)	2-inch Break Quantity (lb_m)
Qualified Epoxy	105	25	3	0
Qualified IOZ	39	3	0	0

2.2.10 Unqualified Coatings Quantity

The total quantity and locations of potentially transportable unqualified coatings are shown in Table 2.2.17 (12). Note that these coatings are listed as potentially transportable since unqualified coatings in upper containment would not transport if they fail after containment sprays are secured, and

[10] Note that some breaks analyzed had a slightly higher quantity of qualified epoxy or IOZ coatings (11). However, this table presents the maximum combined quantity of qualified epoxy and IOZ coatings debris for each break size. The most significant difference in the results of the qualified coatings calculation is that the bounding crossover leg break has 105 lb_m epoxy + 39 lb_m IOZ (144 lb_m total) compared to the bounding cold leg break with 129 lb_m epoxy + 8 lb_m IOZ (137 lb_m total) (11). These two breaks represent the bounding quantities of qualified epoxy and IOZ debris for all other breaks. The epoxy and IOZ debris quantities from the crossover leg break were selected for this evaluation since this represents the maximum total quantity of qualified coatings debris. It is possible that adjusting the quantity of epoxy up by 24 lb_m and the quantity of IOZ down by 31 lb_m could make the answer slightly worse since the density of epoxy is lower than the density of IOZ, and lower density has a conservative effect on head loss. However, since the bounding LBLOCA coatings debris quantities were used for all breaks, the overall treatment of qualified coatings is very conservative.

unqualified coatings in the reactor cavity would not transport for breaks outside the reactor cavity. This is discussed in more detail in Section 2.2.20 and Section 5.5. The percentages shown in Table 2.2.17 were calculated based on the quantity in each location divided by the total quantity.

Table 2.2.17 – Quantity and location of potentially transportable unqualified coatings debris

Coatings Type	Upper Containment Quantity (lb_m)	Lower Containment Quantity (lb_m)	Reactor Cavity Quantity (lb_m)	Total Quantity (lb_m)
Unqualified Epoxy	295 (15%)	36 (2%)	1,574 (83%)	1,905
Unqualified IOZ	305 (83%)	64 (17%)	0 (0%)	369
Unqualified Alkyd	146 (54%)	125 (46%)	0 (0%)	271
Unqualified Baked Enamel	0 (0%)	267 (100%)	0 (0%)	267
Unqualified Intumescent	0 (0%)	2 (100%)	0 (0%)	2

The quantity of unqualified coatings debris that transports to the strainers is dependent on the failure fraction and failure timing. It is possible that some unqualified coatings would experience significantly less than 100% failure. For example, the unqualified epoxy in the reactor cavity at STP is actually a qualified coatings system, and would likely remain fully intact under post-LOCA conditions. However, these coatings are conservatively assumed to be unqualified due to higher radiation exposure (12). All of the unqualified coatings were conservatively assumed to have a failure fraction of 100%. The intumescent coatings are assumed to be negligible (see Assumption 4.c). The unqualified coatings failure timing shows that approximately 6% of the unqualified coatings would fail in the first 24 hours (12).

The unqualified alkyd and IOZ coatings would fail as fines, but the unqualified epoxy coatings would fail in the distribution shown in Table 2.2.18 (12).

Table 2.2.18 – Unqualified epoxy debris size distribution

Size Designation	Size Range (inches)	Percentage of Total Mass
Fines (particles)	0.006	12.28%
Flat Fine Chips	0.0156	37.23%
Flat Small Chips	0.125-0.5	9.43%
Flat Large Chips	0.5-2.0	20.53%
Curled Chips	0.5-2.0	20.53%

2.2.11 Crud Debris Quantity

The maximum quantity of RCS crud debris that would be released in a LOCA is 24 lb_m (13).

2.2.12 Latent Debris Quantity

The total quantity of latent debris is shown in Table 2.2.19 (43).

Table 2.2.19 – Quantity of latent debris

Coatings Type	Quantity (all breaks) (lb_m)
Latent Fiber	30
Dirt/Dust	170

2.2.13 Miscellaneous Debris Quantity

The total quantity of unqualified tags, labels, plastic signs, tie wraps, etc. at STP is bounded by a total surface area of 100 ft^2 (43).

2.2.14 Insulation Zones of Influence

The insulation zones of influence (ZOIs) used for this analysis are based on the standard deterministic approach described in NEI 04-07 Volumes 1 and 2, where the ZOI size for each type of insulation is based on the destruction pressure (44; 45). Table 2.2.20 lists the ZOI sizes for each type of insulation at STP.

Table 2.2.20 – Input variables used primarily in debris penetration and core blockage analysis

Insulation Type	ZOI Radius / Break Diameter	Reference
Transco RMI	2.0	(45)
Unjacketed Nukon, Jacketed Nukon with standard bands	17.0	(45)
Thermal-Wrap; assumed to be the same as Nukon (see Assumption 1.d)	17.0	(45)
Microtherm; assumed to be the same as Min-K (see Assumption 4.a)	28.6	(45)

2.2.15 Insulation Debris Size Distribution

The debris size distribution used for low density fiberglass (LDFG) insulation (Nukon and Thermal-Wrap) is based on a proprietary methodology report where debris that is generated closest to the break consists of a larger fraction of fines and small pieces, and debris generated at the outer portion of the ZOI consists of a larger fraction of large pieces and intact blankets. The fiberglass size distribution that was implemented in CASA Grande is shown in Table 4.1 of the Alion debris size distribution report (46).

The Microtherm debris was assumed to fail as 100% fines, but was split into the following categories based on the manufacturing data: 58% SiO_2, 39% TiO_2, and 3% fibers (43).

2.2.16 Debris Characteristics

Table 2.2.21 provides the material properties (size and density) for insulation (43; 46; 45), qualified coatings (11; 43), unqualified coatings (12), crud (13), and latent debris (43) at STP.

Table 2.2.21 – Material properties of debris

Debris Type	Debris Size	Macroscopic Density	Microscopic Density
Nukon	Fines: 7 µm fibers Small Pieces: <6 inches Large Pieces: >6 inches Jacketed Large Pieces: Intact Blankets	2.4 lb_m/ft^3	175 lb_m/ft^3
Thermal-Wrap	Fines: 7 µm fibers Small Pieces: <6 inches Large Pieces: >6 inches Jacketed Large Pieces: Intact Blankets	2.4 lb_m/ft^3	159 lb_m/ft^3
Microtherm	Fines: 6 µm fibers	15 lb_m/ft^3	165 lb_m/ft^3
	Fines: 20 µm SiO_2 particles		137 lb_m/ft^3
	Fines: 2.5 µm TiO_2 particles		262 lb_m/ft^3
Qualified Epoxy	Fines: 10 µm particles	-	94 lb_m/ft^3
Qualified IOZ	Fines: 10 µm particles	-	208 lb_m/ft^3
Unqualified Epoxy	Fines: 6 mil particles Fine Chips: 0.0156"×15 mil Small Chips: 0.125"-0.5"×15 mil Large Chips: 0.5"-2.0"×15 mil Curled Chips: 0.5"-2.0"×15 mil	-	124 lb_m/ft^3
Unqualified Alkyd	Fines: 4 - 20 µm particles	-	207 lb_m/ft^3
Unqualified IOZ	Fines: 4 - 20 µm particles	-	244 lb_m/ft^3
Unqualified Baked Enamel	Fines: 4 - 20 µm particles	-	93 lb_m/ft^3
Crud	Fines: 8 - 63 µm particles	-	325 - 556 lb_m/ft^3
Latent Fiber	Fines: 7 µm fibers	2.4 lb_m/ft^3	175 lb_m/ft^3
Dirt/Dust	Fines: 17.3 µm particles	-	169 lb_m/ft^3

2.2.17 Blowdown Transport Fractions

The blowdown transport fractions were calculated based on the break location, size of debris, upper and lower containment volumes, and the locations of grating. The appropriate blowdown transport fractions are shown for each break location and debris size in Table 2.2.22 (23).

The types of debris that would be subject to the blowdown forces include Nukon, Microtherm, qualified coatings, and crud. As discussed in Section 5.4.2, the Nukon debris would fail as fines, small pieces, large pieces, and intact blankets. The Microtherm, qualified coatings, and crud debris would all fail as fine debris and would transport similar to the Nukon fines. Since the intact blankets would not transport readily, this debris was not included in the transport analysis (see Assumption 6.a).

Based on the weld locations and transport potential, all LOCA breaks were binned in the following location categories:

1. Steam generator compartments: Weld locations inside the secondary shield wall above Elevation 19'-0".
2. Reactor cavity: Weld locations inside the primary shield wall.
3. Below Steam Generator Compartments: Weld locations inside the secondary shield wall below Elevation 19'-0".
4. Pressurizer compartment: Weld locations inside the pressurizer compartment (excluding the surge line).
5. Pressurizer surge line: Weld locations on the surge line outside the secondary shield wall.
6. RHR compartments: Weld locations inside the RHR compartments.
7. Annulus: Weld locations in the annulus (excluding the surge line).

Table 2.2.22 – Blowdown transport fractions according to break location

Break Location	Debris Type and Size	Blowdown Transport Fractions		
		Upper Containment	Lower Containment	Remaining in Compartments
1. Steam Generator Compartments	Fines	70%	30%	0%
	Small LDFG	33-60%	13-25%	15-54%
	Large LDFG	0-22%	0%	78-100%
2. Reactor Cavity	Fines	70%	30%	0%
	Small LDFG	33-60%	13-25%	15-54%
	Large LDFG	0-22%	0%	78-100%
3. Below Steam Generator Compartments	Fines	70%	30%	NA
	Small LDFG	21-50%	50-79%	NA
	Large LDFG	0%	100%	NA
4. Pressurizer Compartment	Fines	70%	30%	0%
	Small LDFG	26-66%	11-28%	6-63%
	Large LDFG	16-26%	1-11%	63-83%
5. Pressurizer Surge Line	Fines	70%	30%	NA
	Small LDFG	3-36%	64-97%	NA
	Large LDFG	0%	100%	NA
6. RHR Compartments	Fines	70%	30%	0%
	Small LDFG	3-45%	1-19%	36-96%
	Large LDFG	0%	0-10%	90-100%
7. Annulus	Fines	70%	30%	0%
	Small LDFG	6-37%	13-25%	38-81%
	Large LDFG	0%	0%	100%

2.2.18 Washdown Transport Fractions

The washdown transport fractions were calculated based on the spray flow distribution, the size of debris, and the number of grating levels that debris would be washed through. The appropriate washdown transport fractions are shown for each debris size depending on whether sprays are initiated in Table 2.2.23 (23). Note that the washdown transport fractions do not depend on the location of the break, but only whether sprays are initiated. Since unqualified coatings debris may fail later in the event, this debris would only be washed down to the pool if the sprays are initiated and the coatings fail before the sprays are secured.

Table 2.2.23 – Washdown transport fractions according to spray initiation

Sprays Initiated?	Debris Type	Washdown Transport Fractions	
		Washed Down in Annulus	Washed Down inside Secondary Shield Wall
Yes	Fines	47%	53%
	Small LDFG	7-19%	21-27%
	Large LDFG	0%	0%
No	All	0%	0%

2.2.19 Pool Fill Transport Fractions

The pool fill transport fractions were calculated based on the size of debris, the break location, the volume of the inactive cavities and sump cavities, and the pool volume at the time when these cavities would be filled. The appropriate pool fill transport fractions are shown for each break location and debris size in Table 2.2.24 (23).

Table 2.2.24 – Pool fill transport fractions according to break location

Break Location	Debris Type	Pool Fill Transport Fraction	
		Each Sump	Inactive Cavities
Breaks Inside the Secondary Shield Wall (Locations 1-3)	Fines (all)	2%	5%
	Small LDFG	0%	0%
	Large LDFG	0%	0%
Break Outside the Secondary Shield Wall (Locations 4-7)	Fines (all)	3%	9%
	Small LDFG	0%	0%
	Large LDFG	0%	0%

2.2.20 Recirculation Transport Fractions

The transport of debris during the recirculation phase is dependent on the break location, water level, and flow rate. The transport fractions were calculated based on CFD modeling of the recirculation pool. Since it is not practical to run CFD simulations for all possible scenarios to investigate the effects of differing water levels and flow rates, a limited number of simulations were completed to determine recirculation transport fractions for various groups of breaks. The appropriate recirculation transport fractions are shown for each break location and debris size in Table 2.2.25 and Table 2.2.26 (23). Note that the unqualified epoxy coatings in the reactor cavity would not transport for any breaks outside the reactor cavity. In the case of a reactor cavity break, the transport fractions for the unqualified epoxy in the reactor cavity are the same as the unqualified epoxy outside the reactor cavity (23).

Table 2.2.25 – Recirculation pool transport fractions according to break size and location (insulation)

Break Location	Break Size	Debris Type	Recirculation Transport Fractions		
			Debris in Lower Containment	Washed in Annulus	Washed inside Secondary Shield Wall
1: Steam Generator Compartments	SBLOCA	Fines	100%	100%	100%
		Small LDFG	27%	20%	27%
		Large LDFG	0%	NA	NA
	MBLOCA LBLOCA	Fines	100%	100%	100%
		Small LDFG	64%	58%	64%
		Large LDFG	0%	NA	NA
2: Reactor Cavity	SBLOCA MBLOCA LBLOCA	Fines	100%	100%	100%
		Small LDFG	64%	58%	64%
		Large LDFG	0%	NA	NA
3: Below Steam Generator Compartments	SBLOCA	Fines	100%	100%	100%
		Small LDFG	27%	20%	27%
		Large LDFG	0%	NA	NA
	MBLOCA LBLOCA	Fines	100%	100%	100%
		Small LDFG	64%	58%	64%
		Large LDFG	0%	NA	NA
4: Pressurizer Compartment	SBLOCA MBLOCA LBLOCA	Fines	100%	100%	100%
		Small LDFG	61%	55%	16%
		Large LDFG	0%	NA	NA
5: Pressurizer Surge Line	SBLOCA MBLOCA LBLOCA	Fines	100%	100%	100%
		Small LDFG	61%	55%	16%
		Large LDFG	0%	NA	NA
6: RHR Compartments	SBLOCA MBLOCA LBLOCA	Fines	100%	100%	100%
		Small LDFG	61%	55%	16%
		Large LDFG	26%	NA	NA
7: Annulus	SBLOCA MBLOCA LBLOCA	Fines	100%	100%	100%
		Small LDFG	61%	55%	16%
		Large LDFG	NA	NA	NA

Table 2.2.26 – Recirculation transport fractions according to break size and location (coatings, latent debris, crud, dirt/dust)

Break Location	Break Size	Debris Type	Size	Recirculation Transport Fraction: Debris in Lower Containment	Recirculation Transport Fraction: Washed in Annulus	Recirculation Transport Fraction: Washed inside Secondary Shield Wall
Breaks Inside the Secondary Shield Wall (Locations 1-3)	SBLOCA	Qual. Coatings	Fines	100%	100%	100%
		Unqual. Coatings	Fines	100%		
		Unqual. Epoxy	Fine Chips	21%		
			Small Chips	0%		
			Large Chips	0%		
			Curled Chips	100%		
		Crud	Fines	100%	100%	100%
		Dirt/Dust	Fines	100%	100%	100%
		Latent Fiber	Fines	100%	100%	100%
	MBLOCA LBLOCA	Qual. Coatings	Fines	100%	100%	100%
		Unqual. Coatings	Fines	100%		
		Unqual. Epoxy	Fine Chips	41%		
			Small Chips	0%		
			Large Chips	0%		
			Curled Chips	100%		
		Crud	Fines	100%	100%	100%
		Dirt/Dust	Fines	100%	100%	100%
		Latent Fiber	Fines	100%	100%	100%
Breaks Outside the Secondary Shield Wall (Locations 4-7)	MBLOCA LBLOCA	Qual. Coatings	Fines	100%	100%	100%
		Unqual. Coatings	Fines	100%		
		Unqual. Epoxy	Fine Chips	31%		
			Small Chips	0%		
			Large Chips	0%		
			Curled Chips	100%		
		Crud	Fines	100%	100%	100%
		Dirt/Dust	Fines	100%	100%	100%
		Latent Fiber	Fines	100%	100%	100%

2.2.21 Debris Erosion

Small or large pieces of fiberglass debris retained on grating in upper containment would be subject to erosion by containment sprays. Small or large pieces of fiberglass debris that settle in the containment pool would also be subject to erosion by the flow of water moving past the debris. The erosion fraction for fiberglass debris retained in upper containment would be 1%, and the average erosion fraction for fiberglass debris that settles in the recirculation pool would be a value below 10% as documented in Table 6.6 of the STP debris transport calculation (23).

The spray erosion would occur relatively quickly in the event, and can be assumed to occur during the pool fill phase (23). However, the erosion of fiberglass debris in the pool would be a more gradual process. As shown in Table 6.6 of the STP debris transport calculation, the majority of erosion would occur within the first 24 hours, but some erosion would continue at reduced rates over the duration of the event (23).

2.2.22 Strainer Geometry

The strainers at STP are PCI Sure-Flow stacked disk strainers. The gap thickness between the strainer disks is 1 inch (47). The total surface area of each strainer is 1,818.5 ft^2 per train, the interstitial volume is 81.8 ft^3 per train, and the circumscribed strainer area is 419.0 ft^2 per train (48). The height of the strainers above the containment floor is 28.5 inches[11] (49), and the center of the strainers is 15.4 inches above the floor (49). The height of each strainer module is 25 inches, and the width of each module is 28 inches (47). The bottom of the strainer modules are 2.25 inches above the floor (47). Since the core tube is at the center of the strainer and has a diameter of 10-7/8 inches (47), the minimum water level required to flow through the bottom of the strainer core tube and fill the sump pits is 10 inches. The strainer hole size is 0.095 inches (50). The inner diameter of the ECCS sump suction pipes is 15.25 inches (51; 52). The length and width of the sump pits are 10 ft by 4 ft (49).

The total length of the strainers (based on the dimensions of Strainer C) was determined using the following parameters:

- Active module length (A): 16-13/16" (47)
- Number of active modules: 11 on one side, 9 on the other (49)
- Core tube length (C): 21-5/16" (47)
- Gap between the middle module and active module (G): 6-3/4" (49)
- Middle module length (M): 24" (49)

Based on these parameters, the total strainer length was calculated as shown in Equation 6.

[11] Note that the strainer height was inadvertently entered into CASA Grande as 39 inches. This is conservative since the strainer height is used to calculate the average submergence within the degasification model. Because the average strainer height was overestimated, the average submergence was reduced and the gas void fraction was overestimated.

$$
\begin{aligned}
L &= 2\cdot\left[9\cdot C + 2\cdot\left(C-\frac{C-A}{2}\right) + 2\cdot G + M\right] \\
&= 2\cdot\left[9\cdot 21.31in + 2\cdot\left(21.31in - \frac{21.31in - 16.81in}{2}\right) + 2\cdot 6.75in + 24in\right] \\
&= 535\ in\cdot\frac{1\ ft}{12\ in} = 44.6\ ft
\end{aligned}
\qquad \text{Equation 6}
$$

Figure 2.2.3 through Figure 2.2.6 show photos of the STP strainers. As shown in Figure 2.2.4, protective grating was installed in front of the exposed strainer area to prevent inadvertent damage during outages. The location of the strainers in containment is shown in Section 5.2 (Figure 5.2.7).

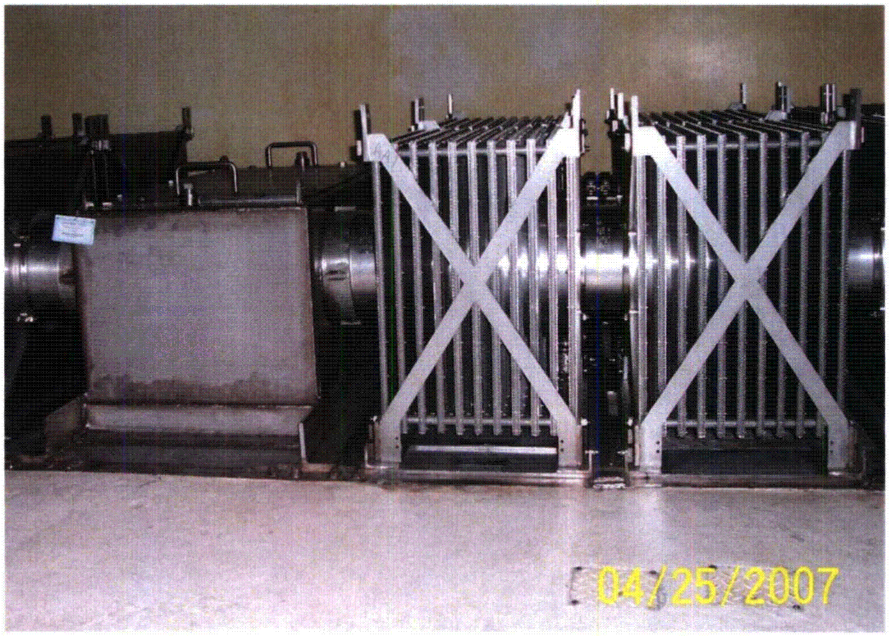

Figure 2.2.3 – STP strainer Photo 1 (before protective grating was installed)

Figure 2.2.4 – STP strainer Photo 2 (after protective grating was installed)

Figure 2.2.5 – STP strainer Photo 3

Figure 2.2.6 – STP strainer Photo 4

2.2.23 Clean Strainer Head Loss

Clean strainer head loss (CSHL) is a function of the strainer geometry, sump flow rate, and pool temperature. The maximum CSHL measured under bounding test conditions is 0.220 ft based on a test module flow rate of 530.1 gpm (equivalent to 10,543 gpm full strainer flow rate[12]) at 115.9 °F (53).

2.2.24 Pump NPSH Margin

The NPSH required for the HHSI, LHSI, and CS pumps is 12 ft (25). The difference in elevation between the containment floor and the pump impellers is 25.65 ft for the HHSI pumps and 25.83 ft for the LHSI and CS pumps (25).

The pipe roughness used to calculate the NPSH available is 0.00015 ft (25).

The diameters for the various segments of the suction pipes are shown in the table below (25). The definition of each pipe segment is provided in Section 5.6.5.

[12] The full strainer flow rate was calculated by scaling the test flow rate up using the test module surface area of 91.44 ft^2 (53) and the full strainer surface area of 1,818.5 ft^2 (48).

Table 2.2.27 – ECCS sump suction pipe diameters

Pipe Segment	Diameter (ft)
AB	1.27
BC	0.99
BD	1.27
DE	0.84
DF	1.27
FG	0.99

2.2.25 Strainer Structural Margin

The strainers have been structurally qualified for head losses up to 4.00 psi differential pressure at 128 °F (54; 55), which is equivalent to a head loss of 9.35 ft.

2.2.26 Vortex Air Ingestion

Vortex formation is precluded based on the design of the STP strainers (56).

2.2.27 Bubble Transport

Partial bubble transport can occur in a horizontal pipe when the Froude number is greater than 0.35, and full transport will occur when the Froude number is greater than 0.55 (57). For vertical pipes, partial transport will occur when the Froude number is greater than 0.35, and full transport will occur when the Froude number is greater than 1.0 (57).

2.2.28 Pump Gas Limits

The HHSI, LHSI, and CS pumps at STP can withstand gas voids up to 10% for up to 5 seconds depending on the pump flow rate compared to the best efficiency point (BEP) for the pump (58). The acceptance criterion for a steady-state gas void fraction at the pump suction inlet is 2% (59).

2.2.29 Fiberglass Penetration

The input parameters for filtration and shedding of fiberglass debris at the strainer were defined based on prototype strainer module testing (60). The filtration efficiency can be described as shown in Equation 7.

$$f(M^S) = \begin{cases} mM^S + b & if\ 0 \leq M^S \leq M_c \\ f(M_c) + \left(1 - f(M_c)\right)\left(1 - e^{-\delta(M^S - M_c)}\right) & if\ M^S > M_c \end{cases} \quad \text{Equation 7}$$

where:

f = Filtration efficiency
M^S = Mass of fiber on strainer
m, b, M_c, δ = Fitted filtration parameters

The range of filtration coefficients from the test are shown in Table 2.2.28

Table 2.2.28 – Fitted filtration parameters for test module

	m_{test} (g^{-1})	b	δ_{test} (g^{-1})	$M_{c,test}$ (g)
Lower	0.0003391	0.656	0.001308	880
Center	0.0003263	0.689	0.001125	930
Upper	0.0003723	0.706	0.031787	790

To use the test results, it is necessary to scale the parameters back to the plant conditions. Parameter b (the filtration efficiency at clean strainer conditions) is dimensionless. However, m, δ, and M_c have to be scaled proportional to the scaled strainer area. Given a test module area of 91.44 ft^2 and a strainer area of 1,818.5 ft^2 per train, the test parameters can be scaled to the plant conditions using the following equations. Table 2.2.29 shows the adjusted parameters.

$$m_{strainer} = m_{test} \cdot \frac{A_{module}}{A_{strainer}} = m_{test} \cdot \frac{91.44 ft^2}{1{,}818.5 ft^2} \quad \text{Equation 8}$$

$$\delta_{strainer} = \delta_{test} \cdot \frac{A_{module}}{A_{strainer}} = \delta_{test} \cdot \frac{91.44 ft^2}{1{,}818.5 ft^2} \quad \text{Equation 9}$$

$$M_{c,strainer} = M_{c,test} \cdot \frac{A_{strainer}}{A_{module}} = M_{c,test} \cdot \frac{1{,}818.5 ft^2}{91.44 ft^2} \quad \text{Equation 10}$$

Table 2.2.29 – Fitted filtration parameters for each ECCS strainer

	m (lb_m^{-1})	b	δ (lb_m^{-1})	M_c (lb_m)
Lower	0.007741	0.656	0.02968	38.5
Center	0.007449	0.689	0.02511	40.7
Upper	0.008499	0.706	0.7259	34.6

The shedding coefficients determined from the testing (results of Tests 5-7) are shown in Table 2.2.30 (60).

Table 2.2.30 – Fitted shedding parameters

	v	η (min^{-1})
Minimum	0.0096	0.0082
Average	0.0152	0.0313
Maximum	0.0196	0.0546

2.2.30 Decay Heat Curve

As shown in Table 2.2.31, the decay heat generation rate was taken from the 1979 ANS plus 2 sigma uncertainty (61). The rated thermal power for STP is 3,853 MW (62).

Table 2.2.31 – Decay heat generation rate based on 1979 ANS plus 2 sigma uncertainty

Time (s)	**Decay Heat Generation Rate (Btu/Btu)**
10	0.053876
15	0.050401
20	0.048018
40	0.042401
60	0.039244
80	0.037065
100	0.035466
150	0.032724
200	0.030936
400	0.027078
600	0.024931
800	0.023389
1,000	0.022156
1,500	0.019921
2,000	0.018315
4,000	0.014781
6,000	0.013040
8,000	0.012000
10,000	0.011262
15,000	0.010097
20,000	0.009350

Time (s)	Decay Heat Generation Rate (Btu/Btu)
40,000	0.007778
60,000	0.006958
80,000	0.006424
100,000	0.006021
150,000	0.005323
400,000	0.003770
600,000	0.003201
800,000	0.002834
1,000,000	0.002580

2.2.31 Core Blockage Debris Limits

Based on conservative testing by the PWR Owner's Group (PWROG), debris loads greater than 15 grams per fuel assembly (g/FA) may cause issues with core blockage (63). STP has a total of 193 fuel assemblies (64). Therefore, the total fiber quantity required to meet the 15 g/FA limit is 2,895 g (6.4 lb_m).

3 Assumptions

This section lists the major assumptions made in the CASA Grande analysis.

1. General Assumptions
    a. It was assumed that a LOCA that occurs during full power operation (i.e., Mode 1) is equivalent or bounding compared to the other operating modes. This is a reasonable assumption since the RCS pressure and temperature (key inputs affecting the ZOI size) would either be approximately the same or significantly lower for Modes 2 through 6. Also, the flow rate required to cool the core (a key input affecting core blockage) would be significantly reduced for low power or shutdown modes.
    b. It was assumed that containment would be isolated at the time of an accident. Although containment overpressure was not credited (see Assumption 1.c), this is a best-estimate assumption that allows the containment pool temperature to be greater than 212 °F. In general, assuming a higher pool temperature at the beginning of the event is also conservative since corrosion and dissolution would be higher, NPSH margin would be lower, and degasification would be higher.
    c. Containment pressure was assumed to be 14.7 psia for all cases except when the pool temperature is higher than the boiling temperature. In cases where the pool temperature is above 212 °F, the containment pressure was assumed to be equal to the saturation pressure. This is a conservative assumption since neglecting containment overpressure reduces the ECCS pump NPSH margin and increases the amount of degasification at the strainer.
    d. It was assumed that Thermal-Wrap is identical to Nukon for GSI-191 analysis purposes. This is a reasonable assumption since both are LDFG products with similar properties (44).
    e. It was assumed that qualified coatings debris would fail as 10 μm particles. This is consistent with the deterministic debris generation calculation (43) and the guidance in NEI 04-07 (45).
    f. It was assumed that small and large pieces of fiberglass that are predicted to transport to the strainer can be treated as fine debris with respect to both the transport timing and subsequent effects on head loss and penetration. This is a conservative assumption since in reality, the pieces of insulation debris would tend to transport more slowly, would be less likely to penetrate the strainer, and would not form as uniform a debris bed on the strainer resulting in lower head losses.
    g. The only reflective metal insulation (RMI) in containment at STP is stainless steel Transco RMI that is installed on the reactor vessel (43). It was assumed that the RMI can be neglected in the STP GSI-191 analysis. This is a reasonable assumption since 1) the quantity of RMI debris would be relatively small since the ZOI size for Transco RMI is only 2.0D (45), 2) stainless steel foils are chemically inert, 3) the majority of RMI debris generated would not reach the strainers since the transport paths from the reactor cavity through the secondary shield wall to the strainers are tortuous and not conducive

to transport of the relatively heavy RMI debris (65), and 4) RMI has a minor effect on debris head loss for strainers that are sitting above the floor elevation (RMI can actually reduce head loss by breaking up the uniform accumulation of a fiber debris bed) (66).

h. It was assumed that the failure of permanently installed lead blankets within various break ZOIs can be neglected. This is a reasonable assumption since there are only a few pipes with lead blankets at STP, a limited number of breaks would be close enough to these pipes to damage the lead blankets, and the lead debris that is generated would not be likely to transport or cause any significant problems. Note, however, that the fiberglass insulation underneath the lead shielding on the piping within the appropriate ZOI is considered for the debris generation calculation.

i. It was assumed that the minimum spray flow rate for single train operation is 80% of the maximum spray flow rate for single train operation. This is a reasonable assumption since the minimum spray flow rate for two train operation is 82% of the maximum spray flow rate for two train operation, and the minimum spray flow rate for three train operation is 80% of the maximum spray flow rate for three train operation (see Section 2.2.8).

j. It was assumed that switchover to hot leg injection would occur between 5.75 and 6 hours after the start of the event. This is a reasonably assumption since the switchover procedure is started 5.5 hours after the start of the event and according to plant personnel, switchover for both trains can be completed within 15 minutes (67).

k. As shown in Table 2.1.1, the pool temperature has an effect on many aspects of the overall GSI-191 evaluation including chemical effects (material release rates and solubility limits), debris transport, strainer head loss, NPSH margin, degasification, and in-vessel effects. For some aspects of the analysis, a higher temperature profile is more conservative (e.g., NPSH margin and degasification), whereas a lower temperature profile is more conservative for other aspects of the analysis (e.g., strainer head loss and debris transport). Due to the competing effects and the complexity of the overall evaluation, it is not possible to pre-determine whether a higher or lower pool temperature profile would be more limiting. However, several aspects of the evaluation were analyzed independently and implemented in CASA without a direct link to the temperature profile. The effects of temperature on the various aspects of the evaluation are described below:

    I. The chemical effects evaluation includes both an analysis of the release rates and the solubility limits. Release rates increase with increasing temperature, and solubility decreases with decreasing temperature (with the exception of products that exhibit retrograde solubility), so it is difficult to say which direction is conservative overall for chemical effects. However, since the STP CHLE testing wasn't fully completed prior to the submittal, a simplified approach was used to address chemical effects where chemical head loss was (mostly) decoupled from the temperature profile in CASA. As discussed in Section 5.6.3, chemical precipitation was assumed to occur when the pool temperature drops below 140 °F. Therefore, minimizing the temperature profile would be conservative.

II. The debris settling and tumbling velocities are lower at lower temperatures due to the higher viscosity, so minimizing the temperature profile would be conservative. However, this effect has been decoupled from the temperature profile in CASA since the debris transport fractions were conservatively determined based on transport testing that was generally conducted at room temperature conditions (23).

III. The clean strainer head loss and conventional debris bed head loss are higher at lower temperatures, so minimizing the temperature profile would maximize the overall strainer head loss. Note, however, that a single bounding value was used for the clean strainer head loss in CASA (see Section 2.2.23).

IV. The pump NPSH margin is lower at higher temperatures, so maximizing the temperature profile would be conservative. However, the strainer structural margin is lower than the NPSH margin for essentially the entire event except very early in the event when the pool temperature is near or above 212 °F.

V. The quantity of gas released at the strainer is larger at higher temperatures, so maximizing the temperature profile would tend to be conservative. However, degasification is also larger for larger pressure drops, which increases at lower temperatures, so these two factors are competing. In general, the void fraction does not change significantly over the range of prototypical long-term temperature profiles where the debris bed head loss would be more likely to be high enough for significant degasification to occur (i.e., due to the increase in head loss from chemical precipitates and failed unqualified coatings). Although additional sensitivity analysis would be necessary to fully understand the effects of the temperature profile on failures due to degasification, this was not considered to be a significant driver.

VI. The boil-off rate (along with the corresponding SI flow split and debris transport to the core for a cold leg break during cold leg injection) increases with increasing temperature, so a higher temperature during the cold leg injection period is conservative. However, this effect has been decoupled from the temperature profile implemented in CASA since the SI flow entering the vessel was assumed to be at saturation conditions (see Section 5.10.3).

Based on this evaluation, it was assumed that all small and medium breaks less than 6 inches can be conservatively represented by a nominal 6-inch break containment pool temperature profile, and all large breaks greater than 6 inches can be represented by a nominal 27.5-inch DEGB temperature profile. These two temperature profiles tend to maximize the temperature early in the event (i.e., the first 1-2 hours), and then minimize the temperature for the remainder of the event (5). This is generally conservative since the strainer debris head loss and chemical precipitation timing are the most significant parameters affected by the temperature profile and will be maximized if the temperature profile is minimized.

l. It was assumed that the temperature profiles developed from the thermal-hydraulic modeling can be logarithmically extrapolated from the temperature at the end of the simulations to the nominal component cooling water (CCW) temperature at 30 days—86 °F (5). This minimizes the long-term temperature profile since the containment pool temperature will never drop below the CCW temperature and is likely to be higher than the CCW temperature at the end of 30 days. As discussed in Assumption 1.k, minimizing the temperature profile is conservative.

m. It was assumed that a 36-hr run time for the CASA Grande simulations is sufficient to predict the scenarios that would proceed to failure. This is a reasonable assumption since most of the dominant time-dependent phenomena occur within the first 24 hours. Note that a 5 minute time increment was used to evaluate each of the time-dependent models in CASA.

2. Equipment Failure Assumptions (prior to the start of recirculation)

   a. It was assumed that pump failures in one train are indistinguishable from identical failures in another train. For example, a failure of the LHSI and CS pumps in Train A (with no other failures) is assumed to be identical to a failure of the LHSI and CS pumps in Train C (with no other failures). This is a reasonable assumption since the strainer area and pump flow rates are essentially the same for all three trains, and the trains are physically located in the same area in containment. Therefore, there would be negligible differences in debris transport, head loss, penetration, etc. for cases with identical failures in different trains.

   b. It was assumed that a combination of pumps failing in the same train is worse than the same combination of pumps failing in separate trains. For example, given a scenario where one LHSI, one HHSI, and one CS pump all fail, the scenario where all three pumps fail in Train A is worse in terms of strainer failures than the scenario where the HHSI and LHSI pumps fail in Train A and the CS pump fails in Train B. The total CS and SI flow would be the same for these two cases. In the first case, however, Trains B and C would be operating at maximum flow, whereas in the second case, only Train C would be operating at maximum flow and the remaining flow would be split between Trains A and B. As illustrated in Table 3.1, by splitting the flow between Trains A and B, the likelihood of either Train A or Train B failing due to high head loss or degasification is significantly reduced. Note that this assumption is not necessarily conservative in terms of vessel failures since the additional strainer surface area from one or two extra trains operating could increase the total amount of debris that arrives at the core. However, since it is more likely for a full train to fail than it would be for an LHSI pump, HHSI pump, and CS pump to fail in separate trains[13], this assumption is reasonable.

[13] This is illustrated by the pump state frequencies in Table 5.1.1, which shows that the failure for one HHSI pump and one CS pump is 2.44E-08 yr^{-1} compared to a single train failure frequency of 9.16E-06 yr^{-1} (i.e., the failure of all three pumps in one train is over two orders of magnitude more likely than a random failure of one HHSI pump and one CS pump in any of the trains).

Table 3.1 – Strainer debris accumulation and approach velocity comparison[14]

Train/Parameters		Scenario 1 (LHSI A, HHSI A, CS A)	Scenario 2 (LHSI A, HHSI A, CS B)
Train A	Debris Accumulation	0%	19%
	Approach Velocity	0 ft/s	0.0032 ft/s
Train B	Debris Accumulation	50%	31%
	Approach Velocity	0.0086 ft/s	0.0054 ft/s
Train C	Debris Accumulation	50%	50%
	Approach Velocity	0.0086 ft/s	0.0086 ft/s

c. It was assumed that the failure of various combinations of pumps can be bounded in terms of strainer failures by other scenarios that have an equal or higher approach velocity and an equal or higher debris accumulation on any one strainer. This assumption is appropriate based on the conservative assumptions that failure of one pump or train is equivalent to the failure of all pumps and trains (see Assumption 12.a through Assumption 12.c). This is illustrated in Table 3.2 using CS pump failures as an example. In this example, Train C in Scenario 3 has the most limiting conditions with the combination of highest debris accumulation and highest approach velocity, and therefore would be the most likely fail.

Table 3.2 – Strainer debris accumulation and approach velocity comparison for CS pump failures[14]

Train/Parameters		Scenario 1 (no failures)	Scenario 2 (CS A)	Scenario 3 (CS A, CS B)	Scenario 4 (CS A, CS B, CS C)
Train A	Debris Accumulation	33.3%	24%	28%	33.3%
	Approach Velocity	0.0086 ft/s	0.0054 ft/s	0.0054 ft/s	0.0054 ft/s
Train B	Debris Accumulation	33.3%	38%	28%	33.3%
	Approach Velocity	0.0086 ft/s	0.0086 ft/s	0.0054 ft/s	0.0054 ft/s
Train C	Debris Accumulation	33.3%	38%	44%	33.3%
	Approach Velocity	0.0086 ft/s	0.0086 ft/s	0.0086 ft/s	0.0054 ft/s

d. It was assumed that the failure of various combinations of pumps can be bounded in terms of in-vessel failures by other scenarios that have a higher flow split to the core with an equal number of trains in operation. The flow split to the core is dependent on the flow split to the SI pumps vs. the total sump flow rate (Q_{SI}/Q_{total}), and the boil-off flow split to the core vs. the total SI flow rate for cold leg breaks (Q_{boil}/Q_{SI}). An example calculation is illustrated in the table below.

[14] Calculated using a strainer area of 1,818.5 ft^2 per strainer and flow rates of 2,800 gpm per LHSI pump, 1,620 gpm per HHSI pump, and 2,600 gpm per CS pump. Note that changes in the flow rates due to break size or other effects would change the specific percentages, but the relative effects between break cases would be consistent with the values shown above.

Table 3.3 – Core debris accumulation for various pump failures[15]

Flow Splits	Scenario 1 (1 CS)	Scenario 2 (1 LHSI, 1CS)	Scenario 3 (1 HHSI, 1CS)	Scenario 3 (2 CS)	Scenario 3 (2 LHSI, 1 CS)
SI Flow Split	71.8%	66.8%	69.1%	83.6%	59.6%
Core Flow Split	4.5%	5.7%	5.2%	4.5%	7.8%
Total Split	3.3%	3.8%	3.6%	3.8%	4.7%

e. It was assumed that failure of equipment other than pumps does not need to be explicitly linked to the PRA equipment failure probabilities. Failures of fan coolers and heat exchangers can have a significant impact on the containment pool temperature. However, rather than modeling the explicit equipment failure scenarios postulated in the PRA, the range of equipment failures was considered in the development of the containment pool temperature profiles (5).

f. It was assumed that pump configurations with a frequency less than 2E-09/yr would result in failure of at least one of the GSI-191 acceptance criteria. This is a conservative assumption since some of these cases would not proceed to failure.

3. LOCA Frequency Assumptions

a. It was assumed that the geometric mean aggregation of LOCA frequencies in NUREG-1829 (37) is the most appropriate set of results to use for this evaluation. As described in Section 5.3, the NUREG-1829 data must be fit to appropriately determine the epistemic uncertainty associated with LOCA frequency estimates. Based on an evaluation of the relative merits of the arithmetic mean and geometric mean, the geometric mean aggregation was determined to be more representative of the overall consensus of the panelists (68).

b. It was assumed that the current-day LOCA frequencies are more appropriate to use for this evaluation than the end-of-plant-license frequencies. This is a reasonable assumption for the base analysis, although the effect of using end-of-plant-license frequencies can be evaluated as a sensitivity case.

c. It was assumed that breaks on non-weld locations can be excluded from the evaluation. This is a reasonable assumption since the break frequency for non-weld locations would be significantly smaller than weld locations, and would not generate significantly different quantities of debris from the weld breaks. It was also assumed that isolable breaks can be excluded from the evaluation since isolable breaks would not lead to recirculation.

d. Linear-linear interpolation of top-down LOCA frequencies from NUREG-1829 was used to preserve uniform probability density between expert elicitation points provided in

[15] Calculated for cold leg break conditions with three train operation using flow rates of 2,800 gpm per LHSI pump, 1,620 gpm per HHSI pump, 2,600 gpm per CS pump, and a 600 gpm boil-off flow rate. Note that changes in the flow rates due to break size or other effects would change the specific percentages, but the relative effects between break cases would be consistent with the values shown above.

the tables. Uniform probability density avoids any attribution of behavior that the panel did not intend and generally shifts probability density to larger break sizes.

e. It was also assumed that the bottom-up LOCA frequencies that are used to assign relative frequencies to the individual weld locations can be linearly interpolated. This does not necessarily introduce conservatism to the analysis since the bottom-up frequencies are scaled to match the top-down NUREG-1829 frequencies. However, it is a reasonable approach given an incomplete understanding of the physical behavior of the LOCA frequency curve between the established values.

f. Out of 193 welds on small bore (0.75-inch and 1-inch) pipes, only 35 were modeled with 3 welds modeled on 1-inch pipes and 32 welds modeled on 0.75-inch pipes (4). It was assumed that the overall break frequency for the 193 welds can be distributed across the 35 welds (176 welds assumed to be 0.75-inch and 17 welds assumed to be 1-inch). This is a reasonable assumption since breaks of this size are generally insignificant with respect to GSI-191 phenomena. Also, since the 35 welds that were modeled are scattered around containment, it is not likely that the weld locations that were not modeled would have any significant differences with respect to the quantity of debris that would be generated or transported from the locations that were modeled.

g. With exception to the small bore weld count discussed in Assumption 3.f, it was assumed that the weld count in the CAD model (4) is more accurate than the weld count in the LOCA frequency report (7) in any cases where there are deviations (see Section 5.3.2). This is a reasonable assumption since the CAD model includes specific references to the source drawings and is consistent with the component database (9).

4. Debris Generation Assumptions

   a. It was assumed that the ZOI size for Microtherm is identical to the ZOI size for Min-K. This is a reasonable assumption since the two insulation types are essentially the same (44).

   b. It was assumed that 100% of the miscellaneous debris (tags, labels, etc.) would fail at the beginning of the event. This is a conservative assumption since the majority of the miscellaneous debris would be outside the ZOI and may not fail at all during the event.

   c. It was assumed that the quantity of unqualified intumescent coatings is negligible and can be excluded from the analysis. This is a reasonable assumption since the total transportable quantity is only 2 lb_m (see Section 2.2.10).

5. Chemical Effects Assumptions

   a. It was assumed that chemical products would not form before the pool temperature drops below 140 °F. This is a reasonable assumption for the purposes of this evaluation since the solubility limit for aluminum precipitates increases significantly at higher temperatures, and calcium precipitates are not expected to form in large quantities for most of the scenarios evaluated (20). Note that the temperature profiles used in the CASA Grande evaluation conservatively minimize the temperature and therefore minimize the time that it would take for chemical products to form.

6. Debris Transport Assumptions

   a. It was assumed that there would be no significant transport of intact blanket debris. This is a reasonable assumption since the intact blankets are large pieces that would be easily held up on structures and would be too heavy to transport readily in the containment pool (69).

   b. It was assumed that miscellaneous tags, labels, etc. are all located in lower containment and would fall directly in the containment pool. It was also assumed that all of the miscellaneous debris would transport to the strainers at the start of recirculation. This is a conservative assumption since some of the miscellaneous debris would be in locations above the pool where it would not transport. Also, based on previous testing, miscellaneous debris would not be likely to transport in the recirculation pool (53).

   c. It was assumed that all latent debris is on the containment floor at the beginning of the event. This assumption results in an increased transport fraction to inactive cavities, but neglects any retention of latent debris above the pool where much of it could be shielded from containment sprays.

   d. It was assumed that debris washed down from upper containment reaches the pool after the inactive and sump cavities are filled, but before recirculation is initiated. This is a conservative assumption since it neglects transport of any washdown debris to inactive cavities during pool fill, but accelerates the time that debris would reach the strainer during the recirculation phase.

   e. It was assumed that the debris transport to each of the strainers is proportional to the flow rate through each strainer divided by the total flow rate through all of the strainers. This is a reasonable assumption since the debris transports with the flow.

   f. It was assumed that the fine debris that is initially in the pool at the start of recirculation as well as the fine debris that transports to the pool during recirculation would be uniformly distributed in the pool. This is a reasonable assumption since the fine debris in lower containment prior to the start of recirculation would be well mixed in the pool as it fills, and the fine debris washed down from upper containment during recirculation would be well mixed due to the dispersed locations where containment sprays enter the pool.

   g. It was assumed that fiberglass debris erosion caused by flow in the pool or by containment sprays would occur prior to the start of recirculation. This is a conservative assumption since it accelerates the time that erosion fines would reach the strainers.

   h. It was assumed that the overall transport fractions for each type of debris can be represented by the bounding transport fractions for an LBLOCA in the steam generator compartments. This is a reasonably conservative recommendation based on the following points (see Section 2.2.17 through Section 2.2.21):

      I. Worst case values were selected from the transport fraction ranges for steam generator compartment blowdown and washdown.

      II. Transport fractions for LBLOCAs are equivalent or bounding for MBLOCAs and SBLOCAs.

III. Sprays are always assumed to be activated (even for SBLOCAs) in the implemented transport fractions.

IV. Unqualified epoxy coatings in the reactor cavity never transport (even for reactor cavity breaks) in the implemented transport fractions.

V. Pool fill transport to the strainers assumes that all three strainers are active (even for cases where only one or two trains are operating) in the implemented transport fractions.

VI. Steam generator compartment blowdown transport fractions for small and large pieces of fiberglass are not necessarily bounding for other break locations.

VII. Washdown transport fractions are applicable to all break locations.

VIII. Inactive cavity transport fractions for breaks inside the secondary shield wall are bounding compared to breaks in the annulus.

IX. Steam generator compartment recirculation transport fractions are bounding for all other break locations.

X. The transport calculation used to determine all of the debris transport fractions includes several conservatisms (23).

7. Head Loss Assumptions

   a. It was assumed that miscellaneous debris would partially overlap and would fully block strainer flow over an area equivalent to 75% of the miscellaneous debris surface area. This assumption is consistent with the guidance in NEI 04-07 (45).

   b. It was assumed that all coatings materials would have a packing fraction similar to acrylic coatings. It was also assumed that non-coatings particulate debris would have a packing fraction similar to iron oxide sludge. These assumptions are based on engineering judgment due to limited data.

   c. It was assumed that a fiber bed of at least 1/16th of an inch is necessary to capture chemical precipitates. This is a reasonable assumption since a thinner debris bed would not fully cover the strainer and would not support appreciable head losses due to chemical debris.

   d. It was assumed that 100% of the transported particulate debris would be captured on the strainer at the time of arrival. This assumption does not imply that no particulate would penetrate the strainer. However, since the in-vessel effects acceptance criteria that were implemented in CASA are independent of the particulate quantity, this assumption is conservative.

   e. It was assumed that the debris on the strainers would be homogenously mixed. This is a reasonable assumption since much of the debris would arrive at the strainer simultaneously.

   f. It was assumed that fiberglass debris would accumulate uniformly on the strainers with a density of 2.4 lb_m/ft^3. This is consistent with the assumptions used in NUREG/CR-6224

(70). For the purposes of developing the strainer loading table (see Section 5.6.2), the pool height was assumed to always be sufficient to allow debris to accumulate on the top of the strainer, but debris accumulation on the bottom of the strainer was limited to 2 inches to account for the height of the strainer above the floor. Assuming that the pool height is greater than the debris accumulation on the top of the strainer is not necessarily accurate for cases where the water level is relatively low and the debris load is large. However, for the majority of cases, the debris load would not be large enough to accumulate a fiber bed that exceeds the submergence level.

8. Degasification Assumptions

   a. It was assumed that Henry's Law is applicable for degasification calculations. Henry's Law essentially states that the solubility of a gas in a liquid is proportional to the partial pressure of the gas above the liquid. At the equilibrium saturation level, the number of gas molecules moving into and out of solution is constant. The initial saturation of gas in the containment pool would have sufficient time to reach equilibrium. Due to the short time that it would take for flow to pass through the debris bed on the ECCS strainers, there may not be sufficient time to reach equilibrium and all of the gas to come out of solution in the debris bed itself. However, it is expected that equilibrium conditions would be reached downstream of the strainer. Therefore, Henry's law is considered to be applicable for calculating the air released.

   b. It was assumed that the temperature upstream and downstream of the strainers is constant. This is a reasonable assumption since the water temperature would not change significantly as the water flows through the strainer.

   c. It was assumed that the air in containment would be essentially the same as atmospheric air. For example, the addition of nitrogen from the accumulators and the formation of hydrogen due to chemical reactions in the containment pool were not considered. These and other sources of non-condensable gasses in containment are likely minor compared to the total initial free volume of air in containment.

   d. It was assumed that air behaves as an ideal gas. This is a reasonable assumption since the correction factor for non-ideal behavior at low pressures is essentially negligible (71). For example, the z-factor for air at 5 bar (72.5 psi) and 350 K (170 °F) is 1.0002 (72).

   e. It was assumed that the relative humidity of the containment atmosphere is 100%[16]. This is a reasonable assumption given the amount of steam released into containment during a LOCA.

   f. It was assumed that the relative humidity of the gas voids downstream of the ECCS strainers is 100%. This is a reasonable assumption since the gas bubbles that are formed would be fully surrounded by water. Note also that this assumption is conservative since maximizing the humidity downstream of the strainer minimizes the partial pressure of the air, and therefore reduces the equilibrium concentration of dissolved air downstream of the strainer.

[16] Note that a lower relative humidity in containment would increase the concentration of dissolved air in the containment pool, resulting in a larger quantity of air released.

g. It was assumed that the average submergence depth (from the surface of the pool to the center of the strainer) can be used for the hydrostatic head. This is a reasonable assumption since the STP strainers are designed for uniform flow distribution.

h. It was assumed that any gas voids caused by degasification would be transported to the ECCS pumps. This is a conservative assumption since it maximizes potential pump failures due to air ingestion, and also maximizes the NPSH required.

i. The void fraction at the pumps was assumed to be the same as the void fraction downstream of the sump strainers. This is a conservative assumption since it neglects the decreased bubble size due to the higher static pressure.

9. Penetration Assumptions

   a. It was assumed that the debris beds on the strainers would not be disrupted after the debris initially accumulates. This is a reasonable assumption since the strainers are not located in the immediate vicinity of any potential breaks where the break flow could impinge the strainers and shear off a portion of the debris.

   b. It was assumed that debris that penetrates the strainers would be uniformly distributed in the flow and would transport proportional to the flow split to the SI pumps vs. CS pumps (γ) and the flow split to the core vs. bypass paths (λ). This is a reasonable assumption since the fiber that penetrates the strainer would be very fine and would easily transport with the flow.

   c. It was assumed that all debris that penetrates the strainer and transports through the core would be trapped on the core (i.e., 100% filtration efficiency). This is a conservative assumption since it maximizes the debris load on the core.

   d. It was assumed that all debris that penetrates the strainer and bypasses the core (either through the containment sprays or directly out the break) would immediately be transported back to the containment pool. This is a conservative assumption since it neglects potential hold-up of debris in various locations and neglects the time that it would take for debris to transport through the systems and wash back to the pool.

10. Core Blockage Assumptions

   a. It was assumed that a debris bed would not form at the top of the core (blocking flow to the core) during the hot leg injection phase. This is a reasonable assumption since debris blockage would result in boiling in the core, which would disrupt the debris bed.

   b. To calculate the boil-off flow rate for a cold leg break during cold leg injection, it was assumed that the RCS pressure is 14.7 psia, and the SI flow entering the reactor vessel is saturated liquid (i.e., 212 °F). This assumption conservatively maximizes the boil-off flow rate since a lower inlet temperature and/or a higher RCS pressure would increase the enthalpy required to boil the water.

11. Boron Precipitation Assumptions

   a. It was assumed that the current STP design basis evaluation methodology used to calculate the required hot leg switchover timing is appropriate with the exception of GSI-191 related phenomenon (i.e., formation of a debris bed on the core). This is an appropriate assumption since the generic boron precipitation issues not related to GSI-191 are being separately addressed by the PWROG and do not need to be evaluated for GSI-191 closure.

b. It was assumed that for a medium or large cold leg break during cold leg injection, a fiber debris load of at least 7.5 g/FA would form a debris bed that would prevent the natural mixing processes credited in the design basis hot leg switchover calculation resulting in boron precipitation prior to switchover. This is a conservative assumption since a debris bed of 15 g/FA was necessary to capture chemical precipitates and cause significant blockage concerns.

c. It was assumed that boron precipitation would not be an issue for small breaks. This is a reasonable assumption since natural circulation would maintain a relatively steady concentration of boron in the core. Boron precipitation failures were not explicitly precluded for small breaks (i.e., the same acceptance criteria were used for all break sizes). However, no boron precipitation failures were observed to occur for small breaks.

d. It was assumed that boron precipitation would not be an issue for medium and large hot leg breaks. This is a reasonable assumption since at least one train would be injecting in the cold leg throughout the event. This flow would pass through the core and maintain a relatively steady concentration of boron. Even if significant core blockage occurs, some flow would still pass through the debris bed and flush through the core.

12. Acceptance Criteria Assumptions

a. It was assumed that failure of one pump in any train due to loss of NPSH margin is equivalent to the failure of all pumps in all trains. This is a conservative assumption since the NPSH margin is not the same for all pumps, and if one pump failed, the sump flow rate would be reduced making it less likely that a second pump would fail. Also, since the trains are independent, failure of one train would not affect the other trains except that suspended debris in the pool after the failure would only accumulate on the remaining trains that are still active.

b. It was assumed that structural failure of one strainer would allow sufficient debris ingestion to result in complete failure of the ECCS. This is a conservative assumption since it is possible that the ECCS could continue to operate even with large quantities of debris ingested.

c. It was assumed that failure of one pump in any train due to excess air ingestion is equivalent to the failure of all pumps in all trains. This is a conservative assumption since one train or one pump in a given train may ingest significantly more air than the other trains or pumps resulting in the failure of only one train or pump.

4 Methodology

The methodology for performing a deterministic GSI-191 evaluation is provided in NEI 04-07 Volume 1 (44) as approved by the NRC in their safety evaluation documented in NEI 04-07 Volume 2 (45).

To account for any uncertainties associated with the analysis and plant-specific conditions where they exist, conservative assumptions are adopted in deterministic models. Insulation debris quantities are calculated based on the maximum possible break size at the worst case break location. Debris transport is calculated based on maximum flow rates, minimum water level, and smallest debris size distributions. Chemical precipitation is calculated based on maximum pool temperature and pH, maximum pool volume, maximum debris quantities, and maximum spray duration. Strainer head loss is calculated based on maximum quantities of debris generated and transported, minimum debris penetration, maximum flow rate, and minimum pool temperature. The maximum strainer head loss is compared against the minimum NPSH margin, which is calculated based on maximum flow rate and maximum pool temperature. Core head loss is calculated based on maximum debris penetration, maximum flow rate, and worst case flow configurations. The core head loss is also compared to conservative acceptance criteria based on the minimum available driving head.

Although the deterministic methodology is relatively well defined, the conservatism in the overall result is compounded by the numerous conservatisms introduced in each portion of the analysis. Also, as identified above, several conservatisms are mutually exclusive, such as the use of a minimum water level for debris transport and a maximum pool volume for chemical precipitation, or use of a minimum temperature for strainer head loss and a maximum temperature for strainer NPSH margin.

In each area of a deterministic analysis, it is permissible to implement analytical refinements to reduce the level of conservatism. The appendices to NEI 04-07 Volume 2 contain several refinement options such as CFD modeling to reduce debris transport in the containment pool (45). However, every refinement that is applied must be justified to show that some level of conservatism is maintained, and the analysis still provides bounding results.

For a risk-informed analysis of GSI-191, it is necessary to postulate all possible events that require recirculation through the ECCS strainers. To calculate the probability associated with core damage or a subsequent large early release, it is necessary to estimate the frequency of the various initiating events, and determine the outcome for a representative sample of the events (this may require analysis of thousands of different scenarios). Rather than analyzing these scenarios in a conservative and bounding manner like the deterministic approach, it is necessary to perform the analysis using realistic inputs, methods, and acceptance criteria.

For some input variables, a best-estimate value may be adequate for a realistic analysis (this could be true for parameters that have a tight range between the minimum and maximum values or for parameters where the results of the analysis are relatively insensitive to large variations in the parameter values). However, some input variables may require probability distributions. Figure 4.1 shows an example probability distribution for water volume. Depending on the specific analysis, either the calculated minimum or calculated maximum water volume would be used as an input for a deterministic evaluation.[17] For a risk-informed evaluation, the input probability distribution can be sampled to determine the actual impact on the results with an appropriate probability weight carried through the analysis for the extreme conditions associated with the minimum and maximum values.

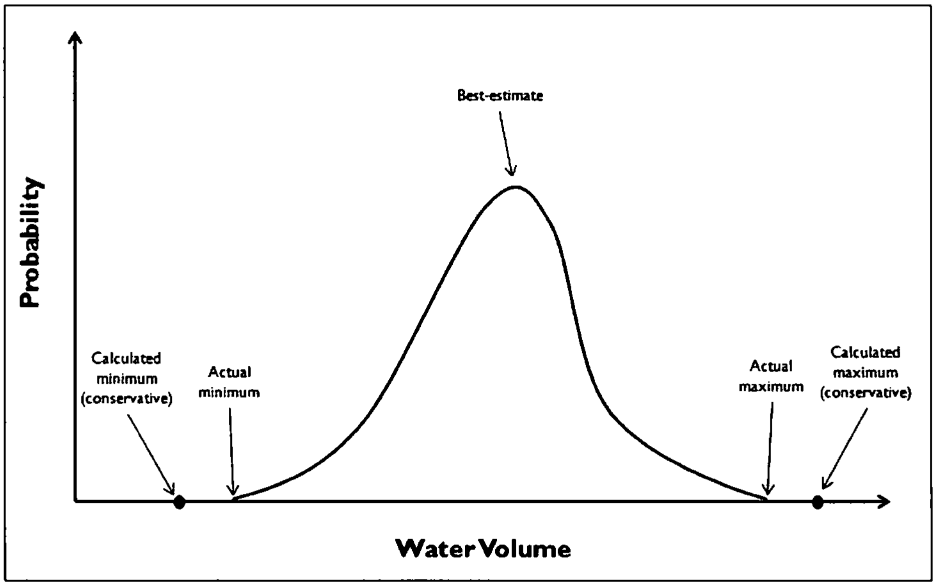

Figure 4.1 – Example of realistic probability distribution for an input variable

In addition to using realistic inputs, it is also important to perform a time-dependent evaluation to capture the time-dependent factors and events that are significant to GSI-191. This includes time-dependent failure for unqualified coatings, time-dependent transport of debris to the strainers, time-dependent precipitation of chemical products, time-dependent operator actions such as securing pumps or switching over to hot leg injection, etc.

For a risk-informed evaluation, the uncertainties associated with the various input parameters and models must also be estimated and carried through the evaluation.

[17] Note that a deterministic refinement could be applied by reducing the level of conservatism in the minimum or maximum water volume calculation. This may provide significant improvement, but using a bounding value for the water volume input still produces results that are unrealistically biased in the conservative direction.

The conditional failure probabilities determined from CASA Grande for the three basic events (small, medium, and large break LOCAs), along with the initiating event frequencies, are used as inputs for the plant-specific PRA. The PRA results are then compared to a hypothetically perfect plant configuration with respect to ECCS performance to calculate the change in core damage frequency (CDF) and large early release frequency (LERF). If the ΔCDF and ΔLERF values are within Region 3 as defined in Regulatory Guide 1.174 (73), the risk associated with GSI-191 is considered very small. If the ΔCDF and ΔLERF values are within Region 2 or Region 1, the risk is more significant, and would require more extensive compensating measures to reduce the risk.

Figure 4.2 provides a simplified high level picture of the risk-informed GSI-191 resolution process.

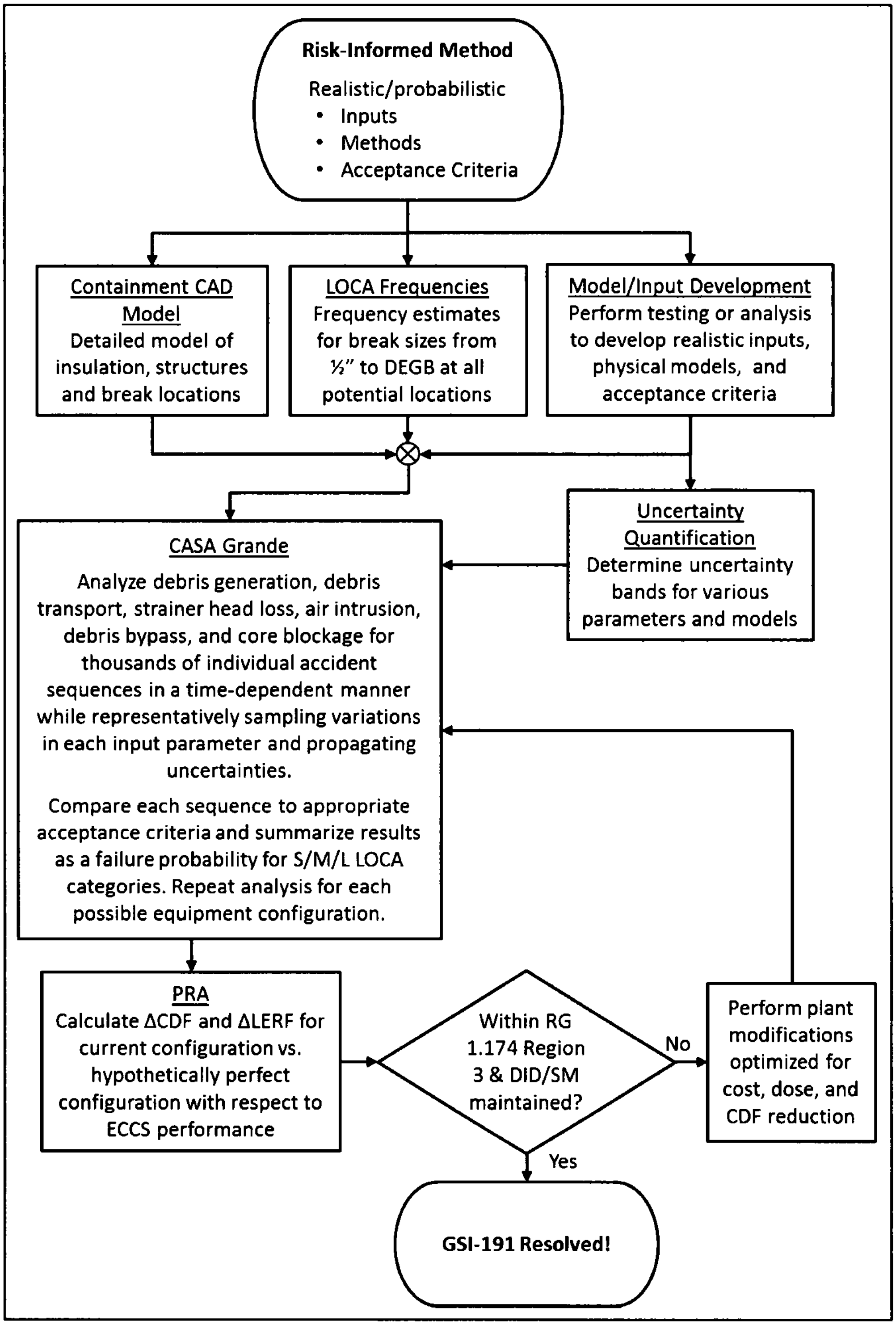

Figure 4.2 – Risk-informed GSI-191 resolution path

4.1 GSI-191 Analysis Steps

The risk-informed analysis of the physical phenomena associated with GSI-191 includes the following general steps:

1. Identify the scenarios that must be evaluated. This includes essentially all events that lead to ECCS sump recirculation from a primary or secondary side break during any mode of operation. This also includes different equipment failure combinations consistent with the PRA.
2. Develop a detailed containment building CAD model. The model should include concrete structures, grating, insulation on equipment and piping, and potential break locations on welds.
3. Estimate the frequency of the initiating events. This requires an assessment of the frequency associated with breaks ranging from a ½-inch hole to a full DEGB at each potential break location, based on the following steps:
    a. Determine the relative probability of breaks in each weld category based on specific degradation mechanisms and distribute total LOCA frequency to each weld location based on relative weight between weld cases.
    b. Identify appropriate weld category for each weld location.
    c. Statistically fit the NUREG-1829 LOCA frequency data.
    d. Sample the epistemic uncertainty in the NUREG-1829 frequencies using the statistical fit.
    e. Sample a variety of break sizes at each weld location and record the appropriate frequency for each sampled break.
4. Determine the type, quantity, and characteristics of debris that is generated. This includes the following steps:
    a. Determine the appropriate ZOI size for each material based on the destruction pressure and break size.
    b. Determine the appropriate size distribution for each type of insulation debris based on the insulation type and distance from the break location.
    c. Calculate the quantity of each type and size of insulation debris based on the ZOI size, insulation location, and break location.
    d. Calculate the quantity of each type of qualified coatings debris based on the ZOI size, break location, and coatings location.
    e. Determine the quantity of unqualified coatings debris based on plant walkdowns and logs. Also determine the timing for the coatings failure.
    f. Determine the quantity of latent debris based on plant walkdowns.
    g. Determine the quantity of miscellaneous debris based on plant walkdowns.
    h. Define the debris characteristics (size and density) for each type of debris.
5. Analyze debris transport during each phase of the event. This includes the following steps:
    a. Evaluate potential blockage upstream of the strainer.

   b. Calculate debris transport during the blowdown phase based on the type and size of debris generated inside the ZOI, the break location, and the grating locations.
   c. Calculate debris transport during the washdown phase based on the type and size of debris in upper containment, the spray distribution, and the grating locations.
   d. Calculate debris transport during the pool fill-up phase based on the type and size of debris in lower containment at the end of the blowdown phase, the break and spray flow rate, the cavity volumes below the containment floor elevation, and the pool volume at the time when the cavities would be filled.
   e. Calculate debris transport during the recirculation phase based on the type and size of debris in the pool, the initial debris distribution at the beginning of recirculation, the pool water level, and the break, spray, and sump flow rates.
   f. Determine debris erosion fractions based on the type, size, and location of non-transporting pieces of debris.
   g. Calculate total debris transport to the strainers for each type and size of debris based on the transport fractions for blowdown, washdown, pool fill, recirculation, and erosion.
   h. Determine the time-dependent arrival of debris at the strainers based on time-dependent failure and transport considerations.
6. <u>Determine overall head loss at the strainer and compare to the NPSH and structural margin.</u> This includes the following steps:
   a. Determine the clean strainer head loss.
   b. Calculate the conventional head loss due to fiber and particulate debris based on the flow rate and temperature.
   c. Account for the increase in head loss due to chemical effects.
   d. Calculate the total head loss at the strainer based on the CSHL and debris bed head loss.
   e. Determine the strainer NPSH margin based on the pool temperature, flow rate, and gas void fraction, and compare results to the total strainer head loss.
   f. Compare the strainer structural margin to the total strainer head loss.
7. <u>Analyze air intrusion at the strainer.</u> This includes the following steps:
   a. Determine the potential for vortex formation.
   b. Calculate the quantity of degasification at the strainer based on the containment pressure, strainer submergence, strainer head loss, flow rate, and temperature.
   c. Determine whether gas would transport through the strainer modules and ECCS suction piping to the pumps.
   d. Determine the impact of gas voids on the ECCS and CSS pumps.
8. <u>Determine the time-dependent quantity of debris that penetrates the strainer.</u>
9. <u>Evaluate ex-vessel downstream effects issues.</u> This includes the following steps:
   a. Evaluate wear on pumps, valves, and other components from the penetrated debris.
   b. Evaluate potential clogging of small orifices from the penetrated debris.
10. <u>Evaluate in-vessel downstream effects issues.</u> This includes the following steps:
   a. Analyze heat transfer issues associated with deposition of debris on the fuel rods.

   b. Identify cases where full blockage at the bottom of the core during cold leg injection would not lead to core damage.
   c. Determine the boil-off flow rate required to remove decay heat from the core.
   d. For cases where blockage at the bottom of the core could lead to core damage, calculate time-dependent transport of debris to the core based on time-dependent penetration, SI and CS pump flow split, and core bypass flow split.
   e. Determine core blockage acceptance criteria based on fuel blockage test results.
11. <u>Boron precipitation</u>
   a. Identify cases where a debris bed could accelerate the onset of boron precipitation prior to hot leg injection.
   b. Determine boron precipitation acceptance criteria based on debris load necessary to block natural mixing processes.
12. <u>Parametric evaluations</u>
   a. Modify input parameter(s) of interest.
   b. Rerun CASA Grande and compare results to base case to determine influence of parameter(s).

4.2 Structured Information Process Flow

The basic event for a LOCA scenario consists of a single accident progression that is initiated by a broken pipe and continues for 30 days. The following outline provides a high level description of the process flow for evaluating independent LOCA scenarios. Unlike predictive physics models (like RELAP), which enumerate field equations and constitutive relationships, CASA Grande embodies only mass conservation in the form of a first-order rate equation to track debris fractions in the containment pool. Energy balance is addressed in principle by external calculations (e.g., the pool temperature profiles developed from the thermal-hydraulic modeling). In this respect, CASA Grande is primarily an uncertainty propagation tool, but the timeline of the accident progression is determined by tracking debris through the system circulation history. The timeline supports externally calculated parameters such as decay heat, pool temperature, operational configurations, chemical product formation, and coatings degradation. It also provides a basis for comparison to time-dependent performance metrics like NPSH available, and core debris loading relative to the timing for switchover to hot leg injection.

1. Set plant failure state (number of trains and specific pumps available). The failure state determines available flow rates through each train and guides operator actions via EOP.

2. Randomly select a weld type/case based on relative frequency of break occurrence. The relative frequencies reflect susceptibility to failure.

3. Randomly select a specific weld from this type/case assuming equal probability among all welds of the same type/case. The weld location defines *P(x,y,z)*, whether it is a hot leg or cold leg

break condition, and the specific compartment in containment. Each weld location has a pre-defined list of insulation targets that can be "seen" in every direction. Concrete walls are the only feature that is credited for shielding insulation from potential damage since pipes and large equipment are assumed to have no effect on a ZOI.

4. Conditional upon having a break for this specific weld type/case, sample a break diameter that is consistent with NUREG-1829:

   $$D_{break} \sim F_{D_{break}|weld\ case} \qquad \text{Equation 11}$$

   Record break contribution to SBLOCA, MBLOCA, or LBLOCA category. The designation of SBLOCA, MBLOCA, or LBLOCA becomes an explicit correlation for many following physical variables.

5. Randomly select a complete temperature history *T(t)* from appropriate correlations of thermal-hydraulic trends for SBLOCA, MBLOCA, or LBLOCA events.

6. Calculate radii $R_{i,j,k}$ of the three damage zones indexed by i = 1,2,3, debris sizes (fines, small pieces, large pieces, or intact blankets) indexed by j = 1,2,3,4, and target type indexed by k, where $k \in K$ indexes insulation products in containment. The three sets are indexed by k: K denotes insulation products, $\mathcal{F}$ denotes fiber-based insulation, and $\mathcal{L}$ denotes all types of debris including insulation and other debris such as unqualified coatings and crud particulate; so, $\mathcal{F} \subset K \subset \mathcal{L}$. The $R_{i,j,k}$ damage zones for Nukon are scaled to the maximum damage radius for insulation k. Figure 4.2.1 is an illustration that shows the nomenclature of damage for a hypothetical break that has its damage radii truncated by a wall.

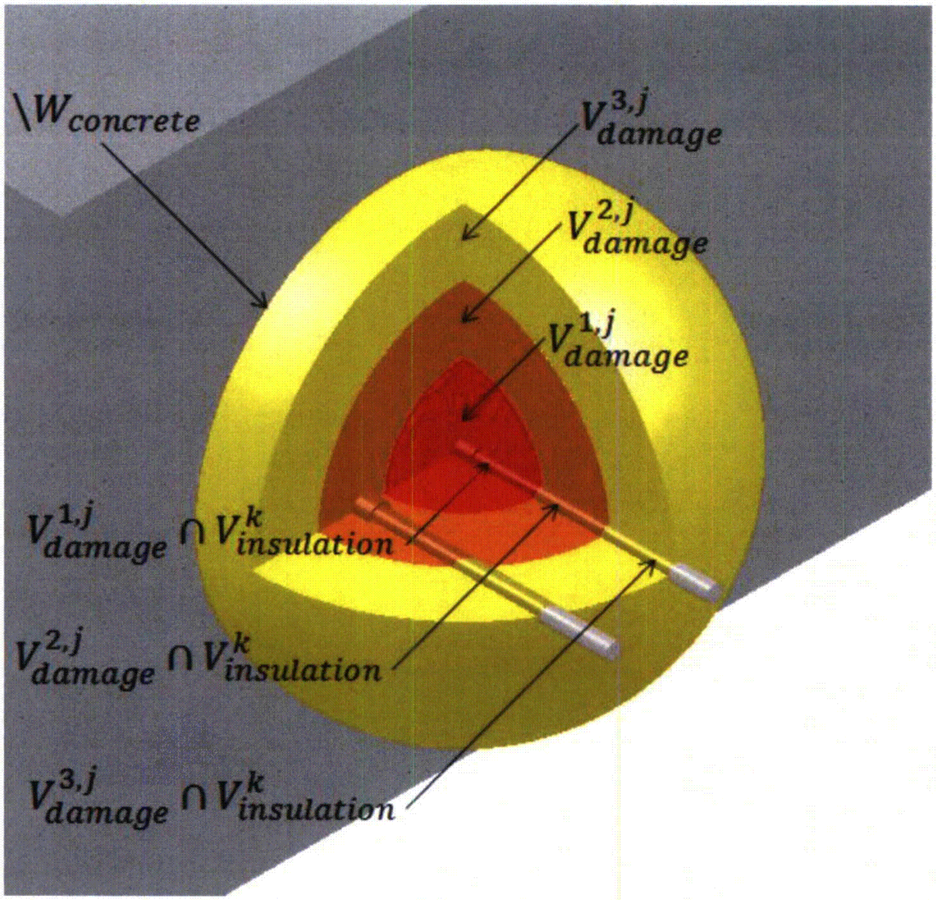

Figure 4.2.1 – Illustration of a hypothetical DEGB spherical ZOI truncated by a wall

7. If $D_{break} < D_{pipe}$, choose a random direction perpendicular to the pipe according to $\phi \sim U(0,2\pi)$. Else, ϕ is assigned a flag that indicates a spherical ZOI.

8. Calculate intersection of damage zones with insulation targets and clip by concrete walls to obtain the amount of debris in each damage radius and debris size (*i,j,k*), and convert volume to mass:

$$M_{i,j,k} = \rho_k \left| \left(V^{i,j}_{damage}(\phi) \cap V^{k}_{insulation}\right) \setminus W_{concrete} \right| \quad \text{Equation 12}$$

Here, the "$\backslash W_{concrete}$" designates exclusion of those insulation targets not damaged due to structural concrete blocking the break jet.

9. Apply transport logic to obtain all ZOI-generated debris mass arrival at the pool as a function of break size and compartment location. Complex transport logic is represented here via the operator $F_{transport}$:

$$m^P(0) = F_{transport} \otimes M \quad \text{Equation 13}$$

The transport logic captures things like erosion of fibers from large pieces to fines in transforming the vector M of $M_{i,j,k}$ to the vector $m^P(t)$ of $m^P_{i,j,k}(t)$ $t = 0$.

10. Introduce fixed quantities of non-ZOI debris types (those in $\mathcal{L}$ but not K and not addressed above) like crud particulate, latent debris, and unqualified coatings debris.

11. Apply fill up transport fraction F^{ℓ}_{fill}, to train ℓ's strainer sump cavity. This mass of debris is initially resident on each strainer, in addition to all other debris constituents that arrive over time:

$$m^{\ell}_{i,j,k}(0) = F^{\ell}_{fill} m^P_{i,j,k}(0) \quad \text{Equation 14}$$

12. At each time t, assume homogenous mixing in the pool:

$$C^P_{i,j,k}(t) = m^P_{i,j,k}(0)/V^P(t) \quad \text{Equation 15}$$

While this form is never used explicitly, it is helpful to think about debris mixing, transport, and accumulation in terms of concentration.

13. Solve coupled differential equations for mass in the pool, mass on the strainer, and mass on the core (see Figure 4.2.2 and Figure 4.2.3 for the nomenclature setting):

$$\frac{d}{dt} m^P_k(t) = S_k(t) - \sum_{\ell=A,B,C} \frac{d}{dt} m^{\ell}_k(t) - \frac{d}{dt} m^{core}_k(t)\bigg|_{k\in\mathcal{F}}, \forall k \in \mathcal{L}$$

$$\frac{d}{dt} m^{\ell}_k(t) = f\left(\sum_{k\in\mathcal{L}} m^{\ell}_k(t)\right)\left(\frac{Q^{\ell}(t)}{V^P(t)}\right) m^P_k(t) - \eta\nu m^{\ell}_k(t), \qquad \forall k \in \mathcal{L} \quad \text{Equation 16}$$

$$\frac{d}{dt} m^{core}_k(t) = \lambda\eta \sum_{\ell=A,B,C} \gamma_{\ell} m^{\ell}_k(t), \qquad \forall k \in \mathcal{F}$$

where sources $S_k(t)$ of debris type k can be time-dependent, flow split λ is the fraction of ECCS injection that passes through the fuel, and flow split γ is the fraction of total strainer flow that is injected. The complement (1 – γ) is the fraction of total strainer flow passed to containment spray, and the complement (1 – λ) is the fraction of ECCS injection that bypasses the core. For cold leg breaks, λ is determined based on the time-dependent boil-off rate. For hot leg breaks, λ = 1. For simplicity in writing the equations here, the additional subscripts are suppressed and the masses are indexed by debris type $k \in \mathcal{L}$. That said, the other indices matter in implementation. For example, the last term in Equation 16 is only present when the k index indicates fiber, but it is also only present when the size index indicates fines.

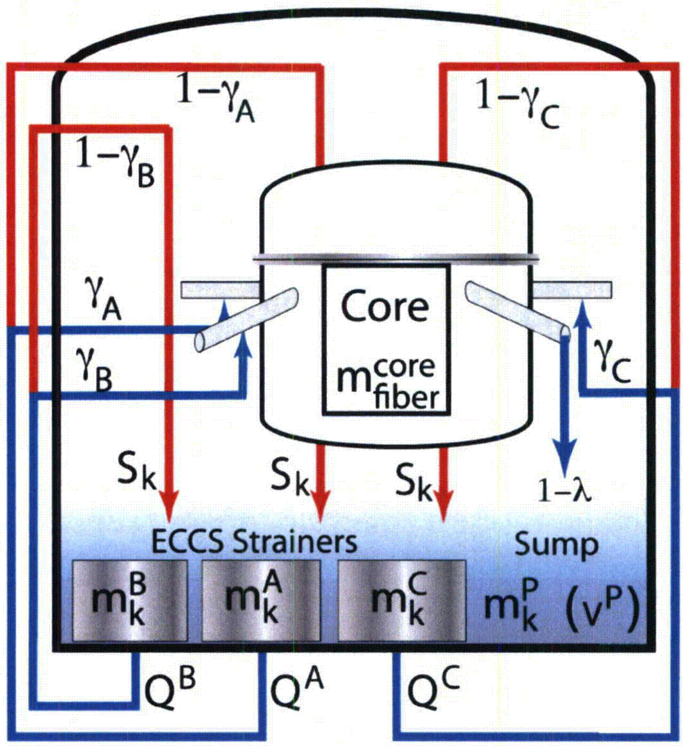

Figure 4.2.2 – Illustration of the processes local to the ECCS screen

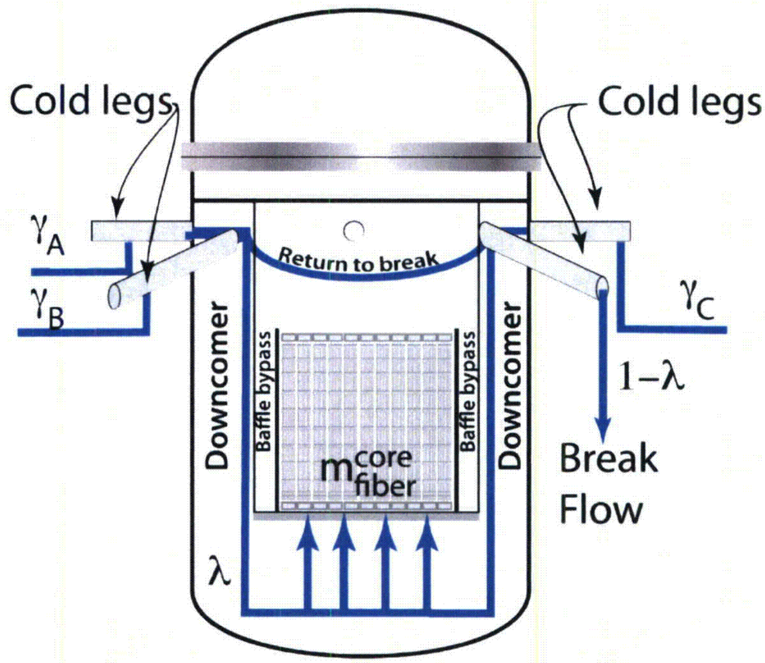

Figure 4.2.3 – Illustration of the flow paths in the reactor vessel

14. Given histories of fiber and particulate debris thickness $\delta(t)$ on the strainer, compute time-dependent head loss across each strainer according to:

$$\Delta P^{\ell}(t) = H\left(m^{\ell}(t), Q^{\ell}(t)\right) N(5,1) \Phi_{ch}(t) \qquad \text{Equation 17}$$

where the function H is given by NUREG/CR-6224 with arguments given by the vector $m^{\ell}(t)$ of $m_k^{\ell}(t)$ for all $k \in \mathcal{L}$, and velocity via the flow rate $Q^{\ell}(t)$, where $N(5,1)$ is a truncated random variable with a mean of 5 and unit variance, and where

$$\Phi_{ch}(t) = H\begin{cases} 1, \delta(t) < 1/16" \; or \; T(t) > N(140,5) \\ \varepsilon, otherwise \end{cases} \qquad \text{Equation 18}$$

Here, the chemical head loss Φ_{ch} takes a value of 1 if the thickness is below 1/16th of an inch or the temperature exceeds the specified normal random variable, centered on 140 °F. Otherwise, Φ_{ch} takes the value of a shifted, and truncated, exponential random variable, which is denoted by ε.

15. Compare time-dependent head loss to time-dependent NPSH margin and record the scenario as a failure if:

$$\max_{t,\ell}\left[\Delta P^{\ell}(t) - NPSH_{margin}(t)\right] > 0$$ Equation 19

In other words, a failure is recorded for this scenario if anywhere along the 30-day time history the head loss exceeds the NPSH margin for any strainer $\ell = A, B, C$. The strainer head loss and NPSH margin and other sump failure criteria are illustrated in Figure 4.2.4.

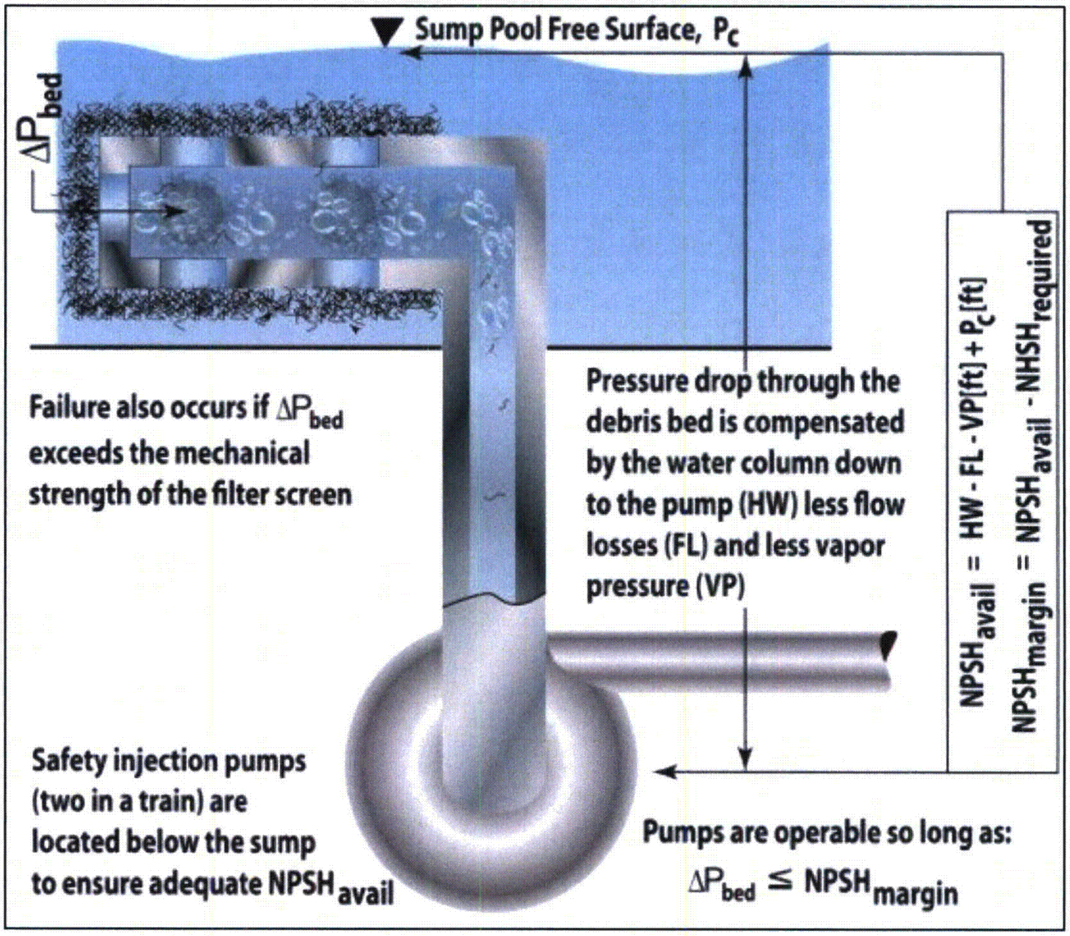

Figure 4.2.4 – Illustration of sump failure criteria

16. Compare time-dependent head loss to the strainer structural margin and record the scenario as a failure if:

$$\max_{t,\ell} \Delta P^{\ell}(t) > \Delta P_{mech}$$ Equation 20

where ΔP_{mech} is the design strainer structural strength in terms of pressure drop across the strainer.

17. Given time-dependent head loss, calculate time-dependent gas evolution and record the scenario as a failure if:

$$\max_{t,\ell} F_{void}\left(\Delta P^{\ell}(t)\right) > 2\% \qquad \text{Equation 21}$$

18. For cold leg breaks, compare the time-dependent fiber accumulation on the core against the assumed 7.5 g/FA threshold. Record the scenario as a failure if $\max_t m^{core}(t) > 7.5g/FA$.

19. For hot leg breaks, record the scenario as a success in terms of the core blockage and boron precipitation criteria.

20. If any performance threshold is exceeded for the scenario, then record a failure.

Figure 4.2.5 is an illustration of the processes listed above that need to be evaluated in GSI-191 for ECCS performance during the recirculation phase.

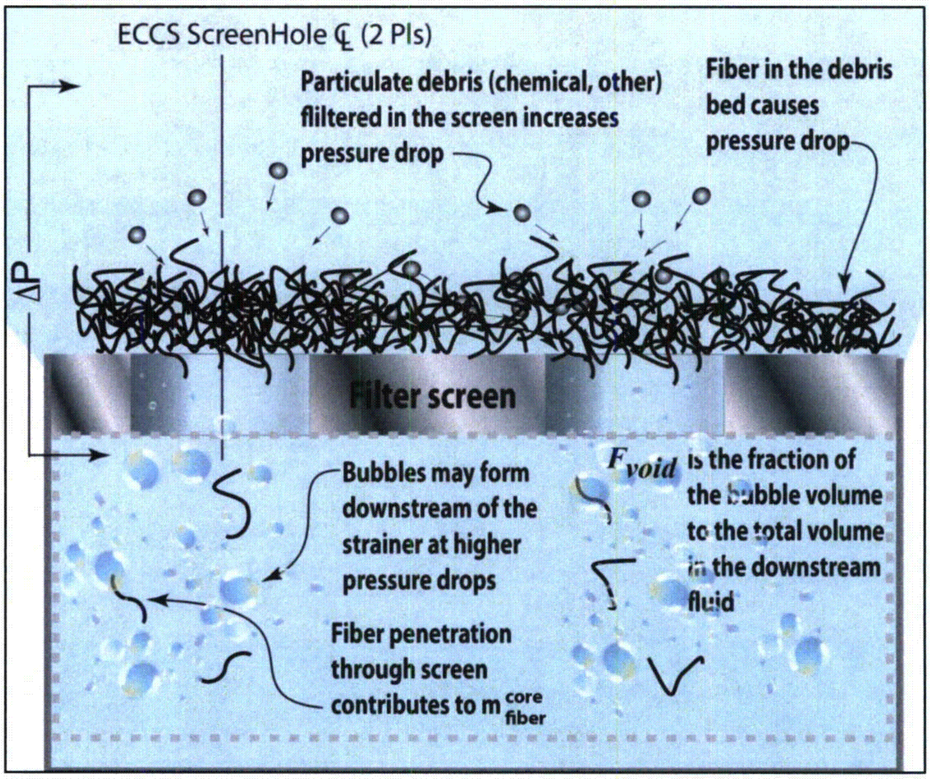

Figure 4.2.5 – Illustration of processes local to the strainer with a direct impact on the performance thresholds

4.3 Uncertainty Quantification and Propagation

As discussed above, the steps listed in Section 4.2 provide a high level illustration of the calculations within CASA Grande for a single scenario. That specific scenario includes numerous random realizations including the selection of the specific weld location where the break occurs, the effective size of the break, the direction of the break on the pipe, etc. Although it is not always explicitly stated in the Section 4.2 description, many of the steps outlined depend on the specifics of the scenario. To construct a Monte Carlo estimator of the failure probability, these steps would be replicated many times. However, CASA Grande does not simply construct a so-called naïve Monte Carlo estimator. Rather, techniques are used to reduce the variability of the failure probability calculations and to propagate uncertainties (such as the epistemic uncertainty in the initiating frequency) to the PRA, where these failure probabilities become branch fractions at the top event.

GSI-191 evaluations include complex calculations with numerous areas of uncertainty. In some cases, conservative values were selected for input parameters, but in many cases, probability distributions were developed to evaluate the full realistic range of conditions. The probability distributions for each parameter were sampled and propagated with the appropriate weighting to realistically determine the risk associated with GSI-191 phenomena. The detailed methodology for uncertainty quantification and propagation is described in a report by UT Austin (74).

4.4 Verification and Validation

A verification and validation (V&V) process is used to ensure that software fulfills the intended purpose. Verification tests are performed to ensure that the software has been correctly programmed (i.e., it correctly solves the equations that it is intended to solve). Validation tests are performed to ensure that the software correctly models the conditions and physical phenomena (i.e., the equations accurately represent reality).

Since CASA Grande was not developed as a generic software package, but was simply used as an evaluation tool for the STP risk-informed GSI-191 calculations, it was not put through a formal V&V process. However, it was independently checked and reviewed following an approach similar to a typical engineering calculation. This review included a series of hand and alternate software calculations that were compared to the results of CASA Grande (75)[18].

[18] Note that the verification report has not been updated to reflect the recent changes to CASA and Volume 3.

5 Analysis

This section describes the physical models used in CASA Grande and the calculations performed to determine debris generation, debris transport, strainer head loss, chemical effects, air intrusion, strainer debris penetration, ex-vessel downstream effects, core blockage, and boron precipitation.

5.1 Evaluation Scenarios (PRA Branch Fractions to Populate)

The STP PRA evaluates LOCA scenarios that fall into the categories of small breaks (up to 2 inches), medium breaks (2 to 6 inches) and large breaks (greater than 6 inches). The PRA also evaluates a variety of equipment failure scenarios and different operating modes. To populate specific PRA branch fractions related to GSI-191 phenomena, it is necessary to evaluate the full range of potential scenarios.

As discussed in Assumption 1.a, the CASA Grande evaluation was only performed for full power operation (Mode 1). The full spectrum of break sizes was evaluated and subsequently binned into the small, medium, and large categories. Potential equipment failures that can affect the GSI-191 analyses include pump failures (either individual pumps or full trains) and fan cooler failures. The most significant variable affected by the failure of fan coolers is the containment pool temperature. This is evaluated as part of the thermal-hydraulic analysis (5), but was not explicitly evaluated in CASA Grande. Pump failures, on the other hand, are much more important to the overall GSI-191 analysis, and therefore were directly evaluated by running multiple scenarios with different combinations of pump failures.

STP has a configuration of three trains with one sump per train. Each train has 3 pumps, an LHSI pump, an HHSI pump, and a CS pump. The maximum pump flow rates are 2,800 gpm for each of the LHSI pumps, 1,620 gpm for each of the HHSI pumps, and 2,600 gpm for each of the CS pumps (see Section 2.2.8). Variations in the pump flow rates affect several important areas of the overall GSI-191 evaluation, so pump failure scenarios must be carefully evaluated. The following list provides the primary areas that are impacted by pump flow rates:

1. Washdown Transport: Washdown transport is a function of the total CS flow rate for all pumps. However, based on Assumption 6.h, the washdown transport fractions were assumed to be constant for all breaks.
2. Recirculation Transport: Recirculation transport is a function of the total break flow rate (HHSI plus LHSI) and the total CS flow rate. Higher pump flow rates would increase the pool turbulence in the locations where the break and spray flow enters the pool, and would also increase the pool velocities in the approach paths to the strainers. However, since large pieces of debris would not reach the pool for most scenarios (e.g., breaks inside the SG compartments), and fine debris would transport to the strainers even at relatively low flow rates, flow rate variations on recirculation transport would essentially only affect the transport fraction for small pieces of

fiberglass debris. Based on Assumption 6.h, however, the recirculation transport fractions were assumed to be constant for all breaks.

3. Debris Accumulation: Since fine debris would be transported in suspension, the accumulation on the strainers would be proportional to the flow split (i.e., if one sump has twice as much flow as another sump, the debris load on that sump strainer will be twice as high as the other strainer).
4. Approach Velocity: The approach velocity for each strainer is equal to the sump flow divided by the strainer area for each train.
5. Strainer Head Loss: The head loss for each strainer is a function of the quantity of debris on the strainer and the strainer approach velocity.
6. Degasification: The quantity of air released from solution for each sump is a function of the strainer head loss and the flow rate through the strainer for each train.
7. Strainer Debris Penetration: The quantity of fiber debris that penetrates each strainer is a function of the debris quantity that reaches the strainer and the penetration timing is a function of the flow rate through the strainer.
8. Reactor Vessel Debris Quantity: The quantity of fiber debris that reaches the reactor vessel is a function of the strainer debris penetration and the flow split between the CS pumps and the SI pumps for each train.
9. Core Accumulation: The fraction of the debris entering the reactor vessel that accumulates on the core in cold leg breaks is the ratio of the core boil-off rate due to decay heat to the flow entering the vessel.

These effects are discussed in more detail in the following sections. Any combination of pumps could fail due to mechanical problems, giving a total of 512 possible combinations for the STP configuration. However, the number of cases that need to be analyzed can be reduced if certain assumptions are made. By applying Assumption 2.a (failures in one train are indistinguishable from failures in another train) and Assumption 2.b (combination of pump failures in one train is worse than the same combination of pump failures in separate trains), the total number of pump combination states can be reduced to 64. The frequency for each of these pump combination states is provided in Section 2.2.4. Since the pump combination states with a frequency less than 2E-09 would have a negligible impact on the overall CDF and LERF, these cases can be conservatively assumed to all go to failure without significantly affecting the overall results (see Assumption 2.f). This eliminates 48 low frequency pump combination states. Table 5.1.1 shows the sixteen pump combination states that have a frequency higher than 2E-09.

By applying Assumption 2.c (bounding strainer debris accumulation and approach velocity) and Assumption 2.d (bounding core accumulation), the total number of cases can be reduced to five pump combination states that need to be evaluated. Note that since one CS pump is procedurally secured whenever all three CS pumps are confirmed to be operating (before the start of recirculation), cases with 2 CS pumps operating are essentially identical to cases with all 3 CS pumps operating.

Table 5.1.1 – Bounding or representative cases for highest frequency pump combination states

Case	Working HHSI Pumps	Working LHSI Pumps	Working CS Pumps	Pump State Frequency (yr^{-1})	Bounding Case for Strainer Failure	Bounding Case for Vessel Failure	Comments
1	3	3	3	2.64E-04	Case 1	Case 1	One CS pump procedurally secured
2	3	3	2	3.32E-06	Case 1	Case 1	Identical to Case 1
3	3	3	1	7.53E-08	Case 22	Case 9	
4	3	3	0	9.77E-09	Case 1	Case 9	
5	3	2	3	3.49E-06	Case 22	Case 9	One CS pump procedurally secured
6	3	2	2	4.38E-08	Case 22	Case 9	Identical to Case 5
9	3	1	3	3.22E-08	Case 9	Case 9	One CS pump procedurally secured
17	2	3	3	1.94E-06	Case 22	Case 9	One CS pump procedurally secured
18	2	3	2	2.44E-08	Case 22	Case 9	Identical to Case 17
21	2	2	3	1.17E-07	Case 22	Case 22	One CS pump procedurally secured, Identical to Case 22
22	2	2	2	9.16E-06	Case 22	Case 22	Single train failure
23	2	2	1	7.81E-08	Case 26	Case 26	
26	2	1	2	6.03E-08	Case 26	Case 26	
33	1	3	3	2.67E-08	Case 22	Case 9	One CS pump procedurally secured
38	1	2	2	3.54E-08	Case 26	Case 26	
43	1	1	1	4.34E-08	Case 43	Case 43	Dual train failure

The scenarios that were explicitly evaluated in CASA Grande were:

- Case 1: Full train operation
- Case 22: Single train failure
- Case 43: Dual train failure
- Case 9: Two LHSI pump failures
- Case 26: Single train failure with failure of one additional LHSI pump

All other high frequency pump state cases are bounded by these five pump combination states as shown in Table 5.1.1.

5.2 Containment CAD Model

A CAD model of the STP containment building was developed to perform a variety of GSI-191 calculations as well as to define the geometry in CASA Grande (4). The details included in the CAD model and specific containment features are illustrated in Figure 5.2.1 through Figure 5.2.20.

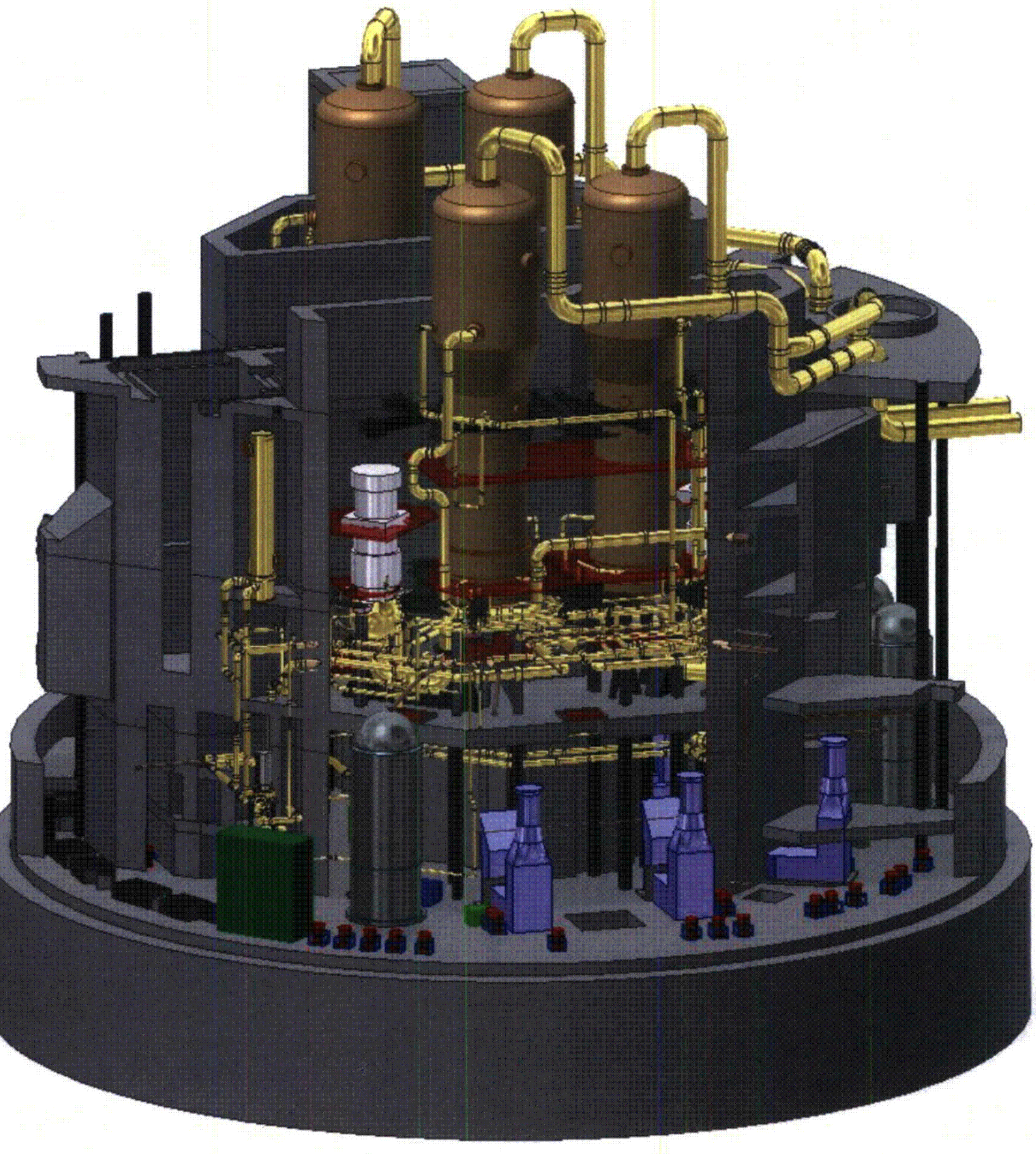

Figure 5.2.1 – Cross-section of steam generator compartment with Loops B and C

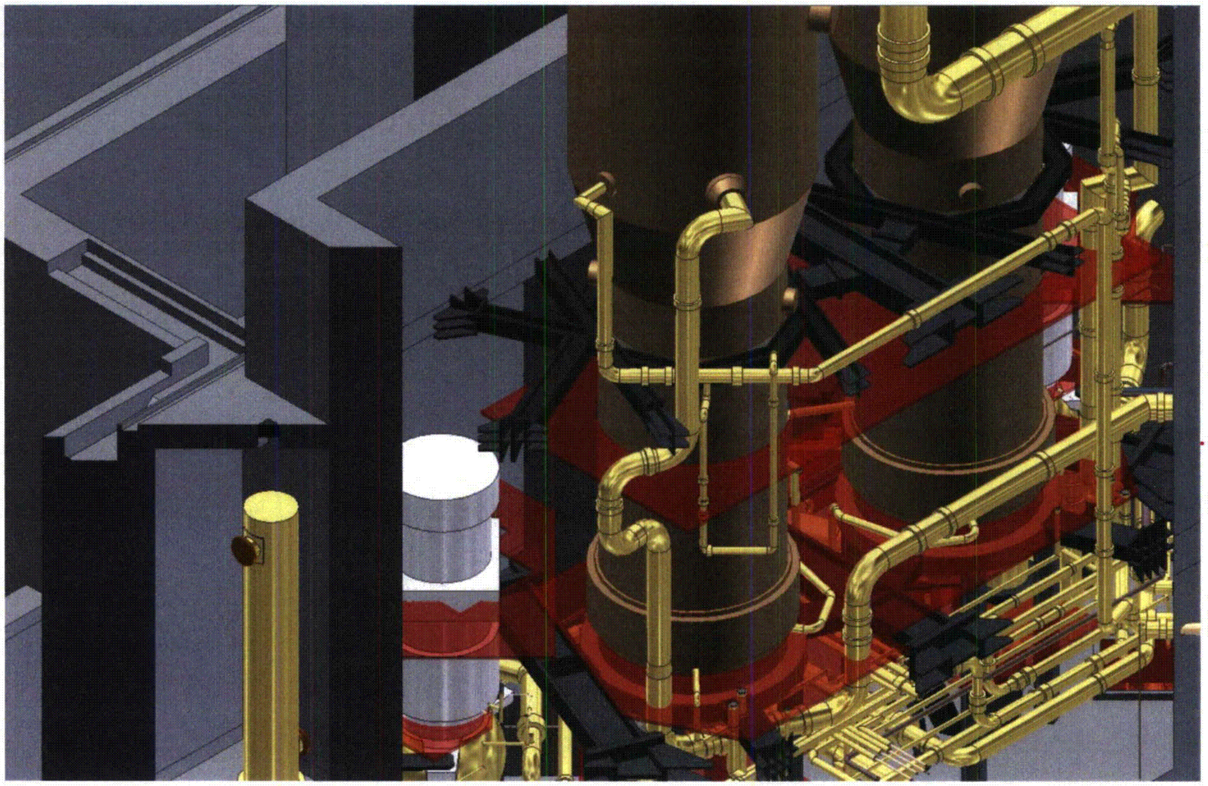

Figure 5.2.2 – Close-up view of steam generator compartment with Loops B and C

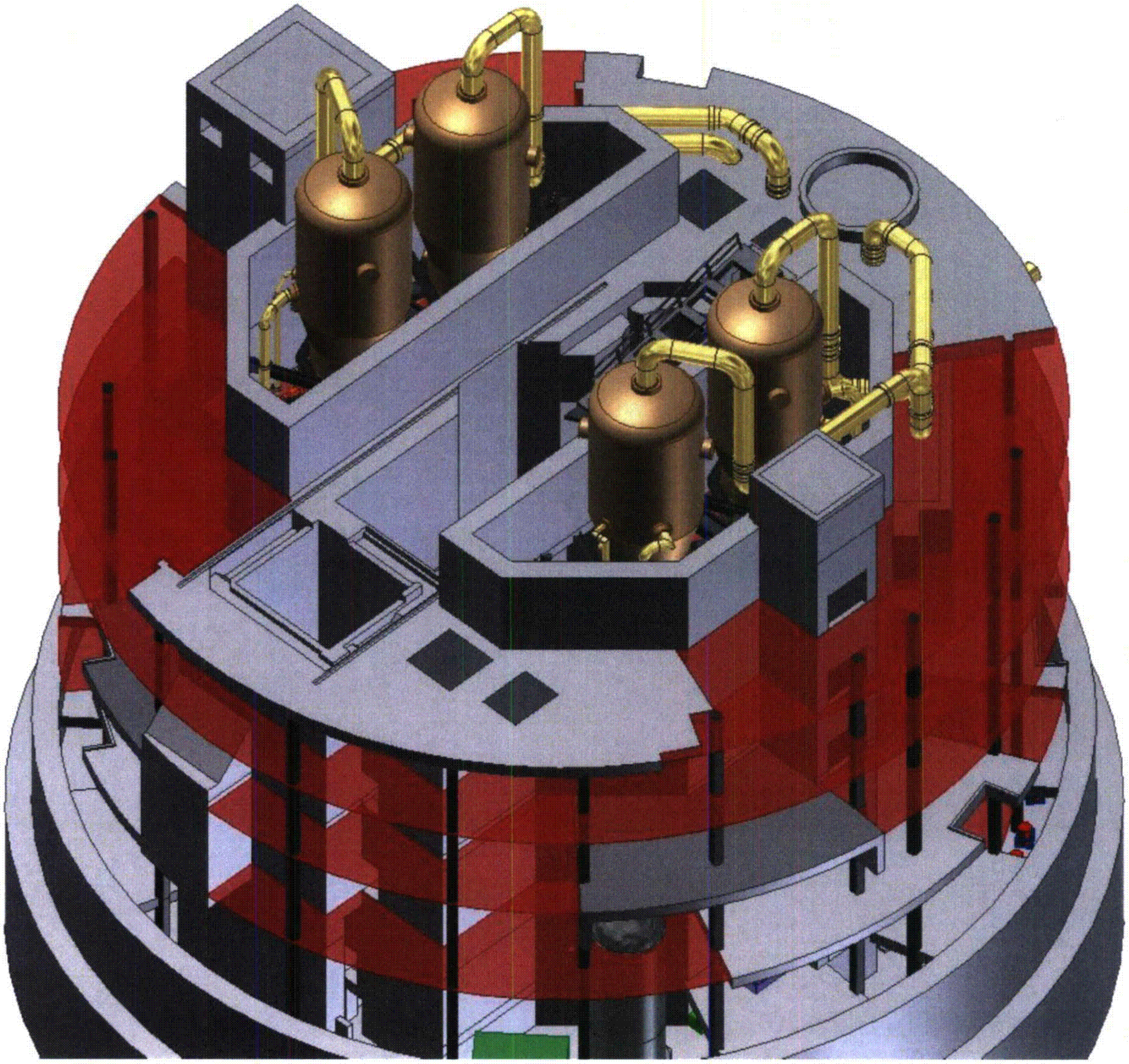

Figure 5.2.3 – Operating deck (Elevation 68'-0")

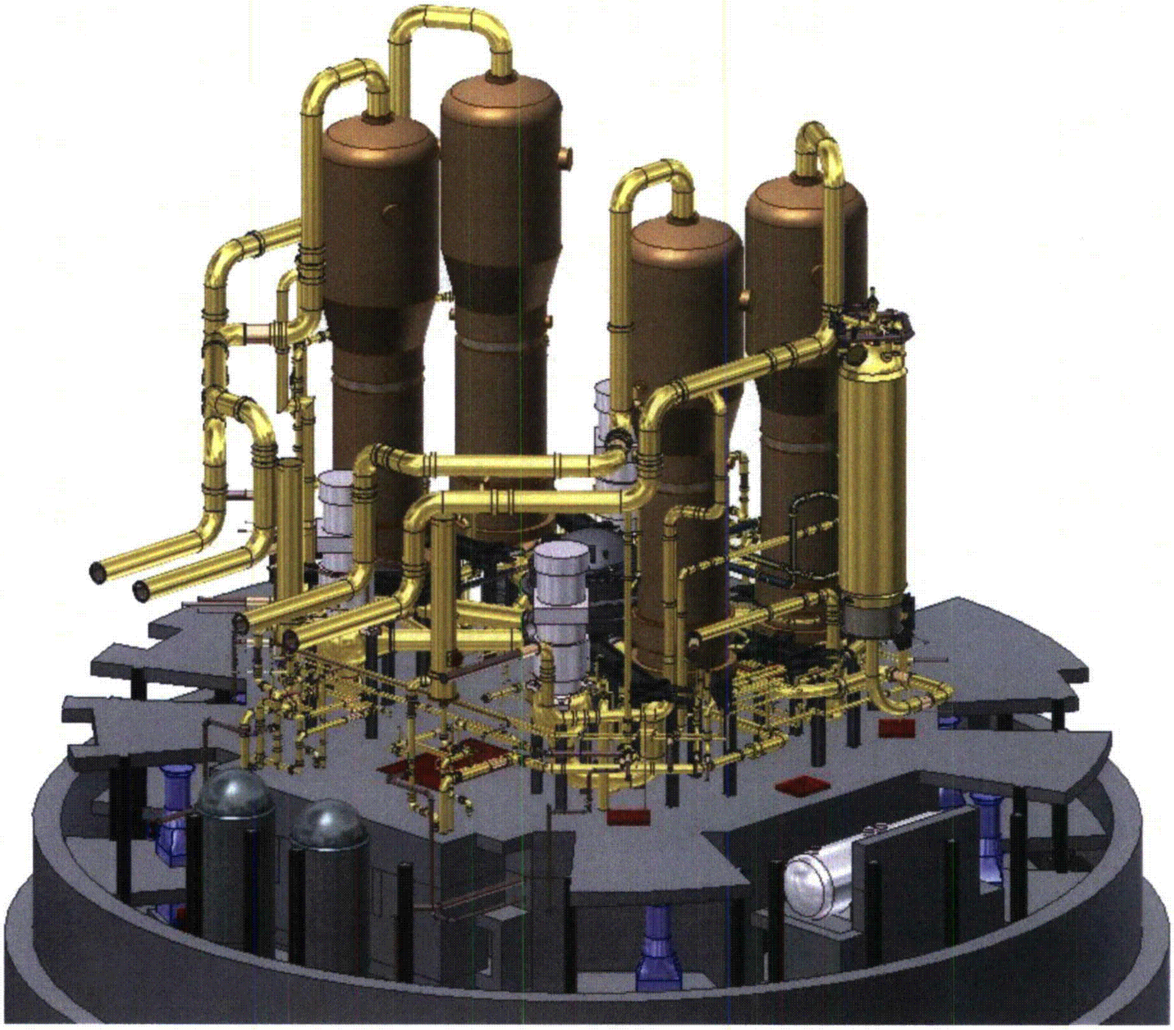

Figure 5.2.4 – Piping and equipment (View 1)

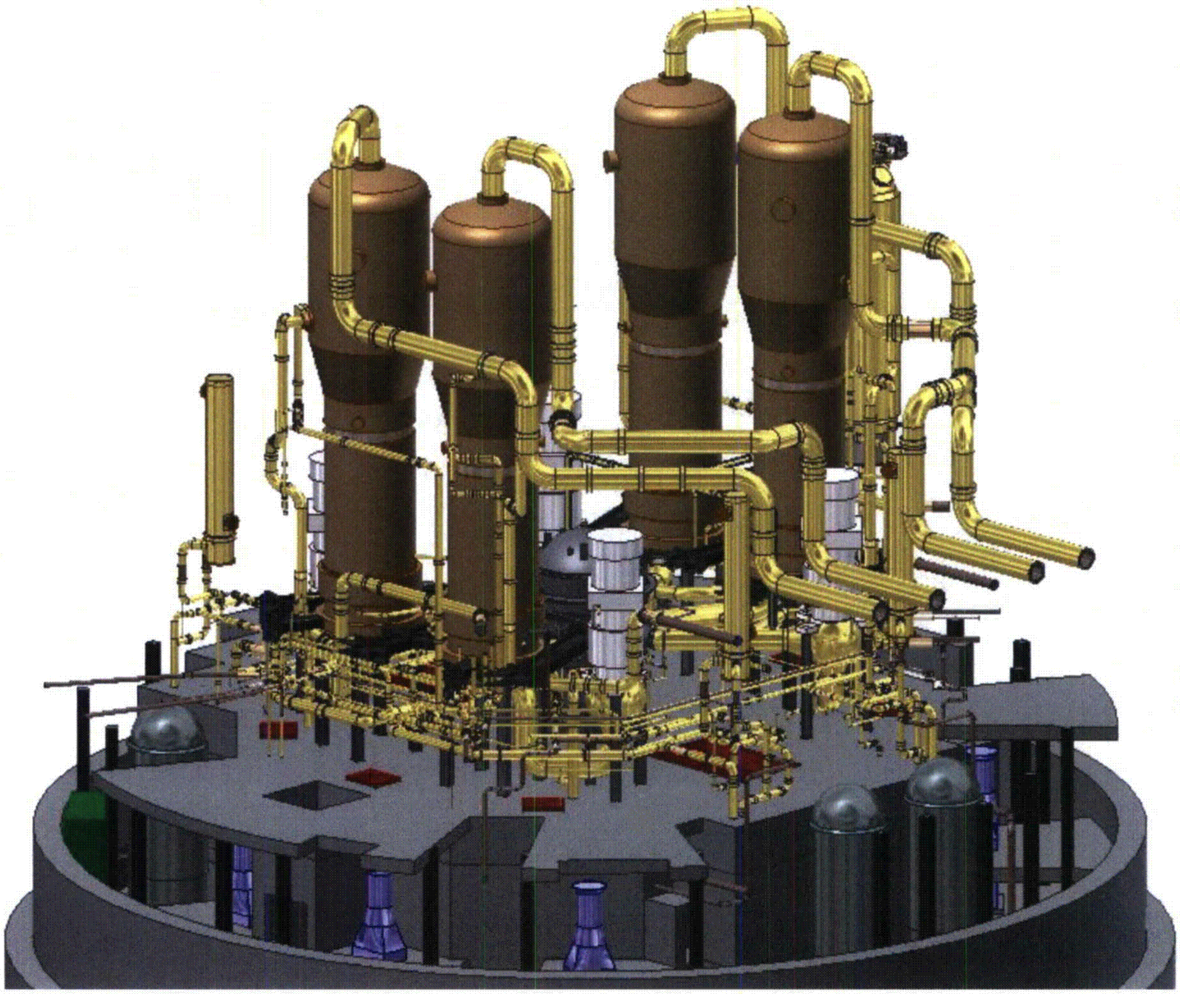

Figure 5.2.5 – Piping and equipment (View 2)

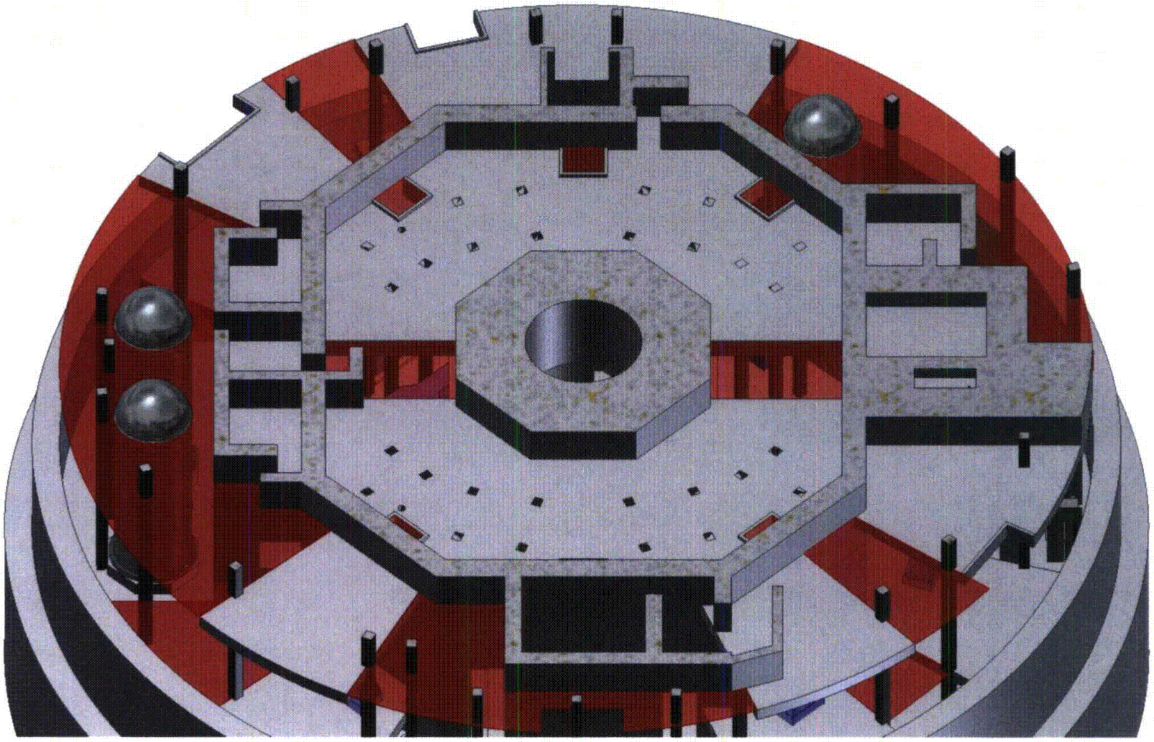

Figure 5.2.6 – Steam generator compartment floor (Elevation 19'0")

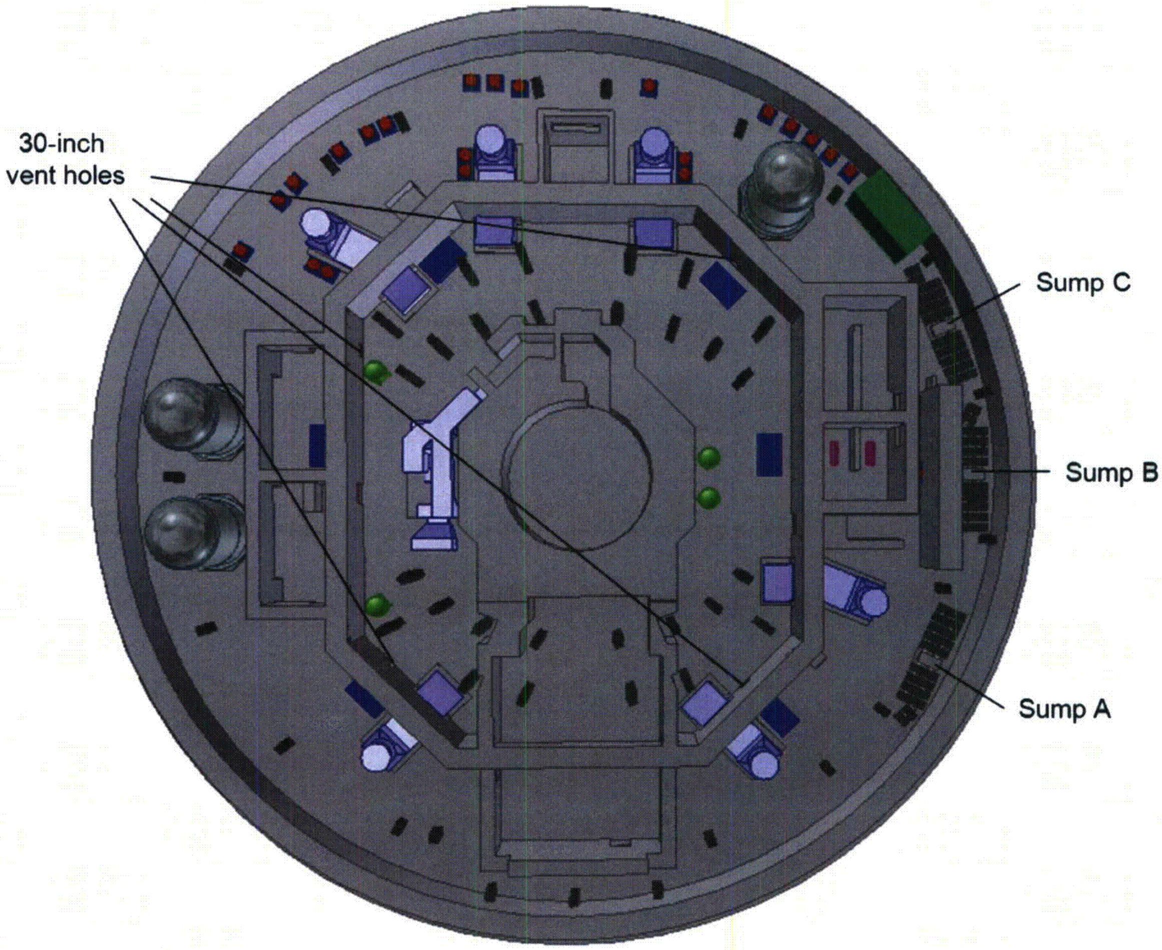

Figure 5.2.7 – Plan view of containment floor (Elevation -11'3")

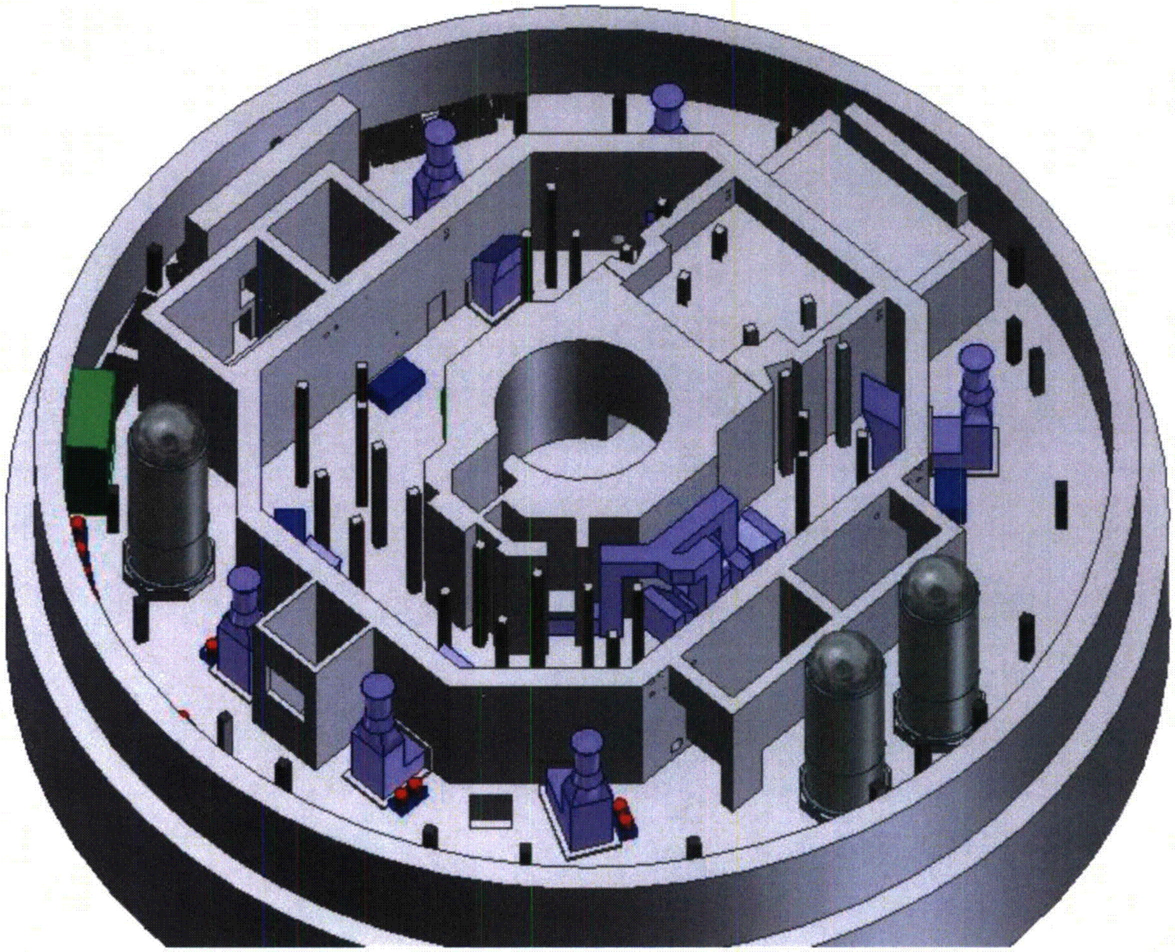

Figure 5.2.8 – Isometric view of containment floor (Elevation -11'3")

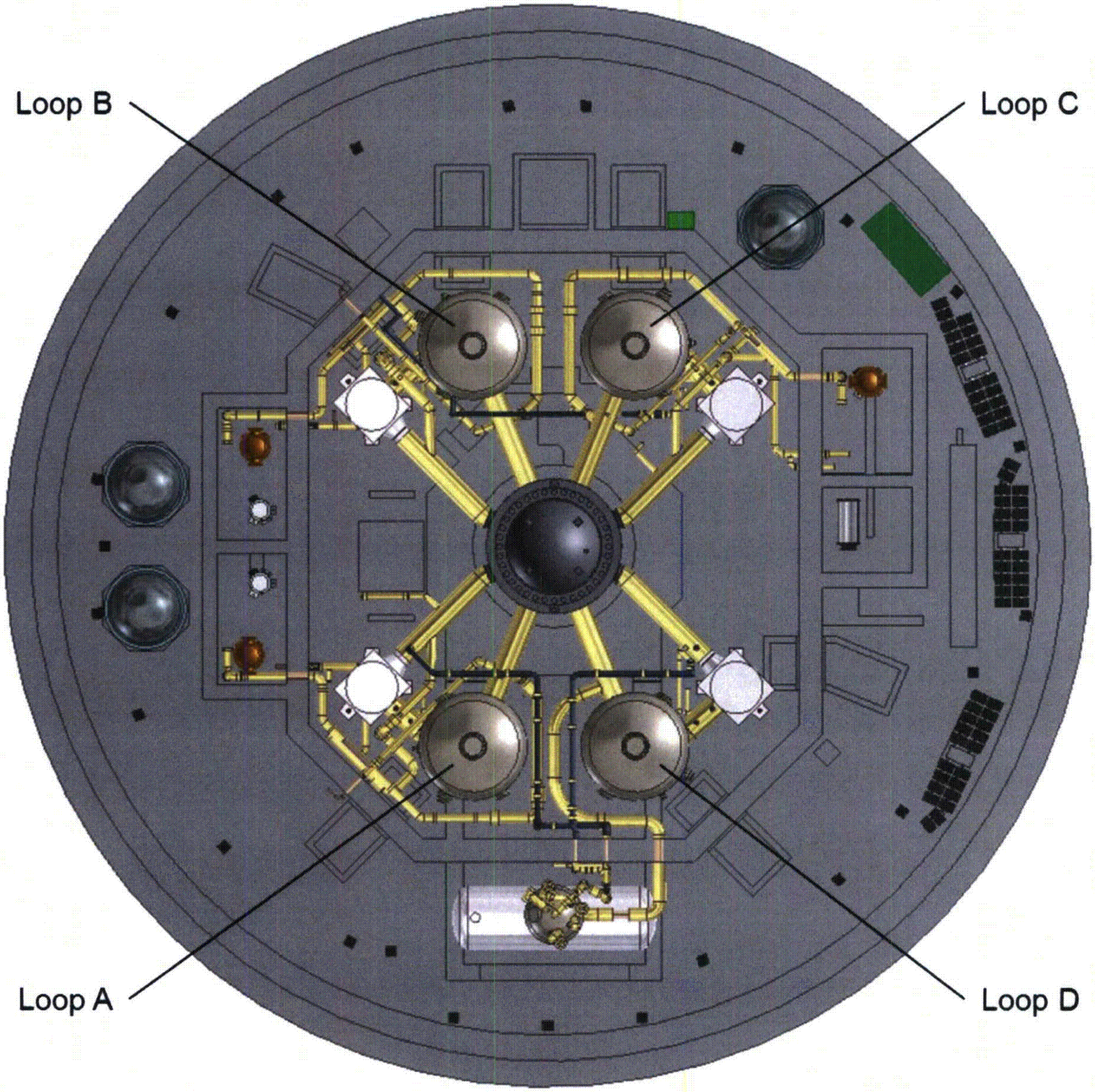

Figure 5.2.9 – Plan view of major piping and equipment

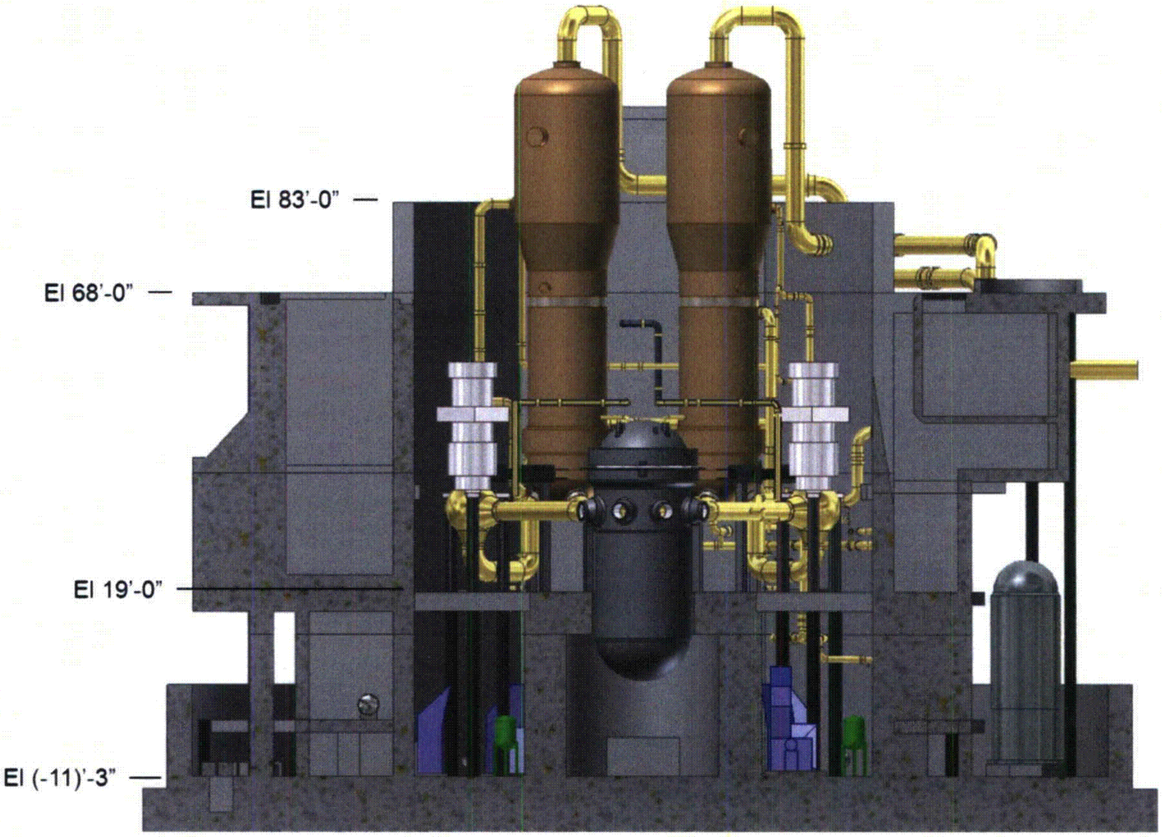

Figure 5.2.10 – Section view of RCS Loop D (left) and Loop A (right)

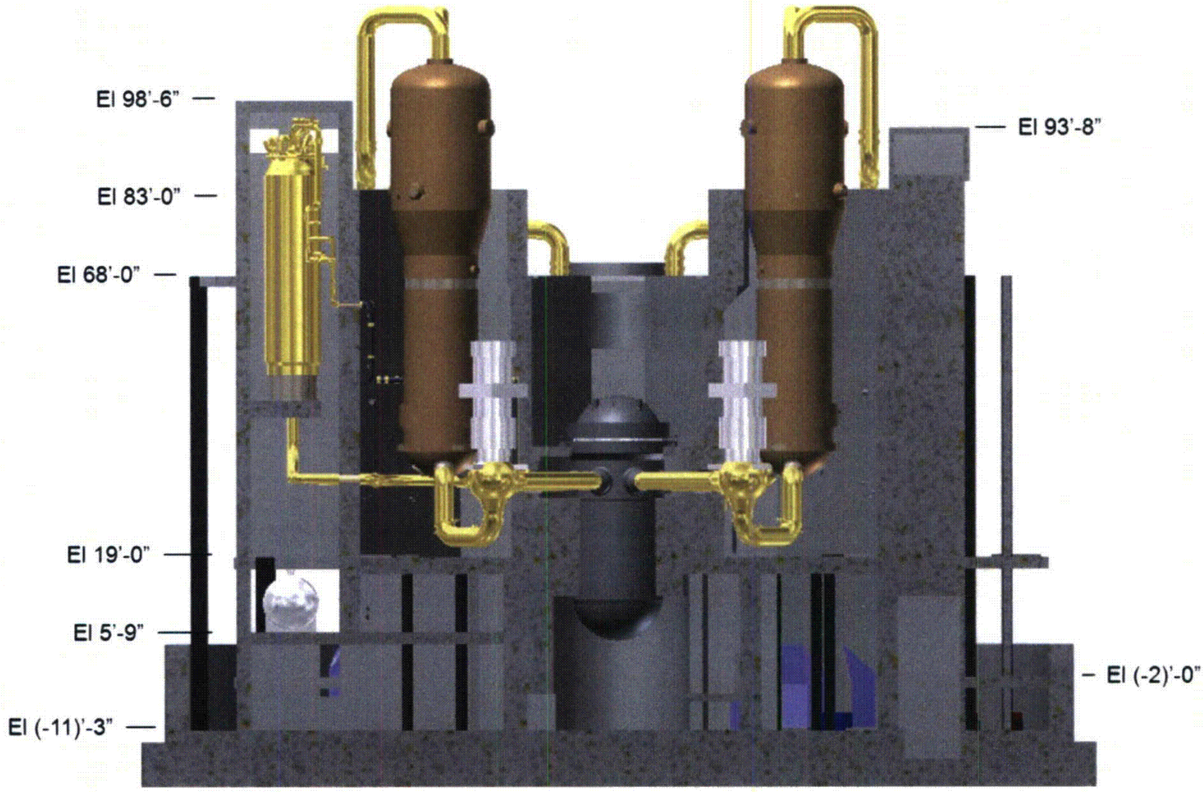

Figure 5.2.11 – Section view of RCS Loop D (left) and Loop C (right)

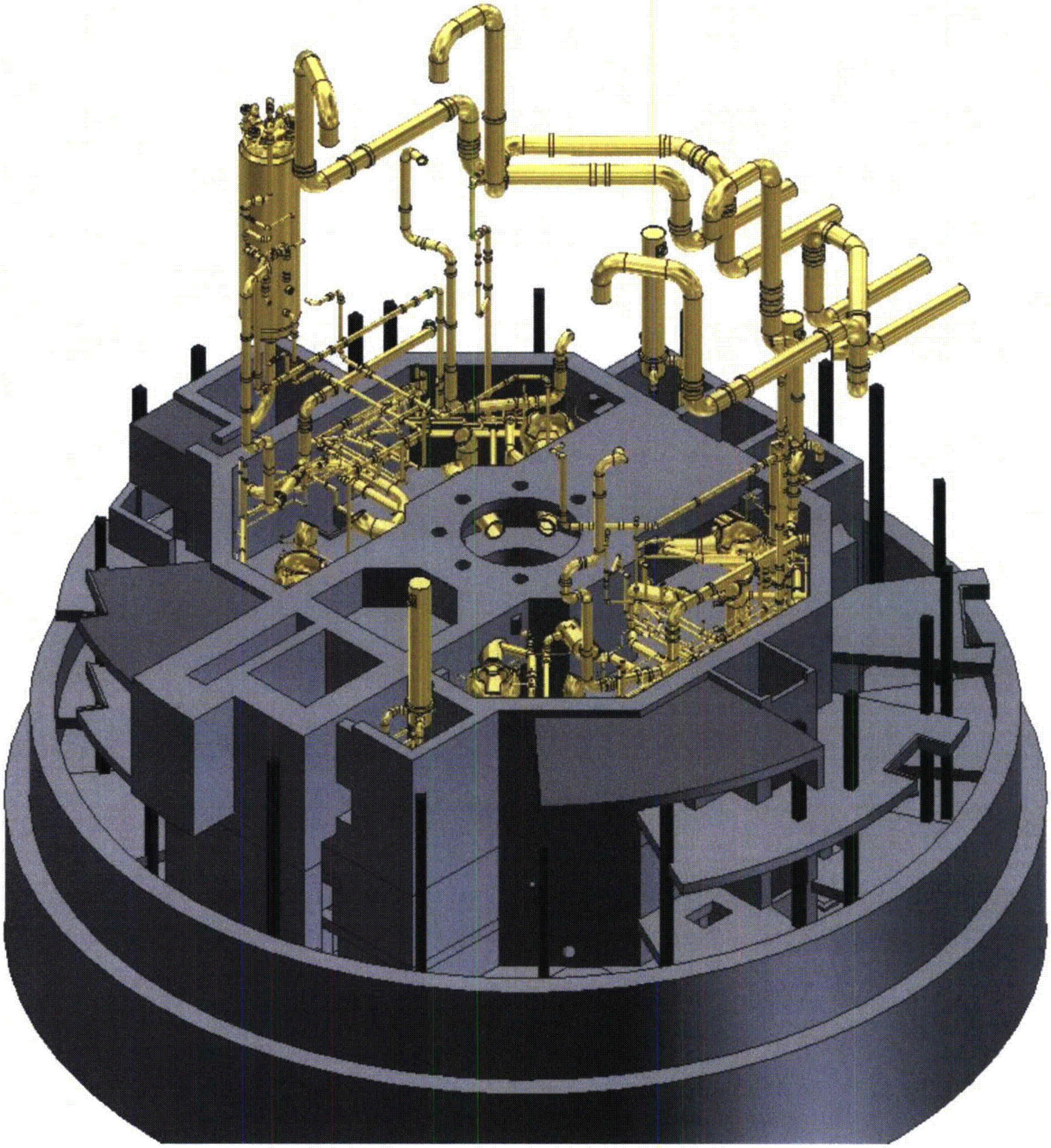

Figure 5.2.12 – Nukon insulation on piping, pressurizer, pumps, and heat exchangers

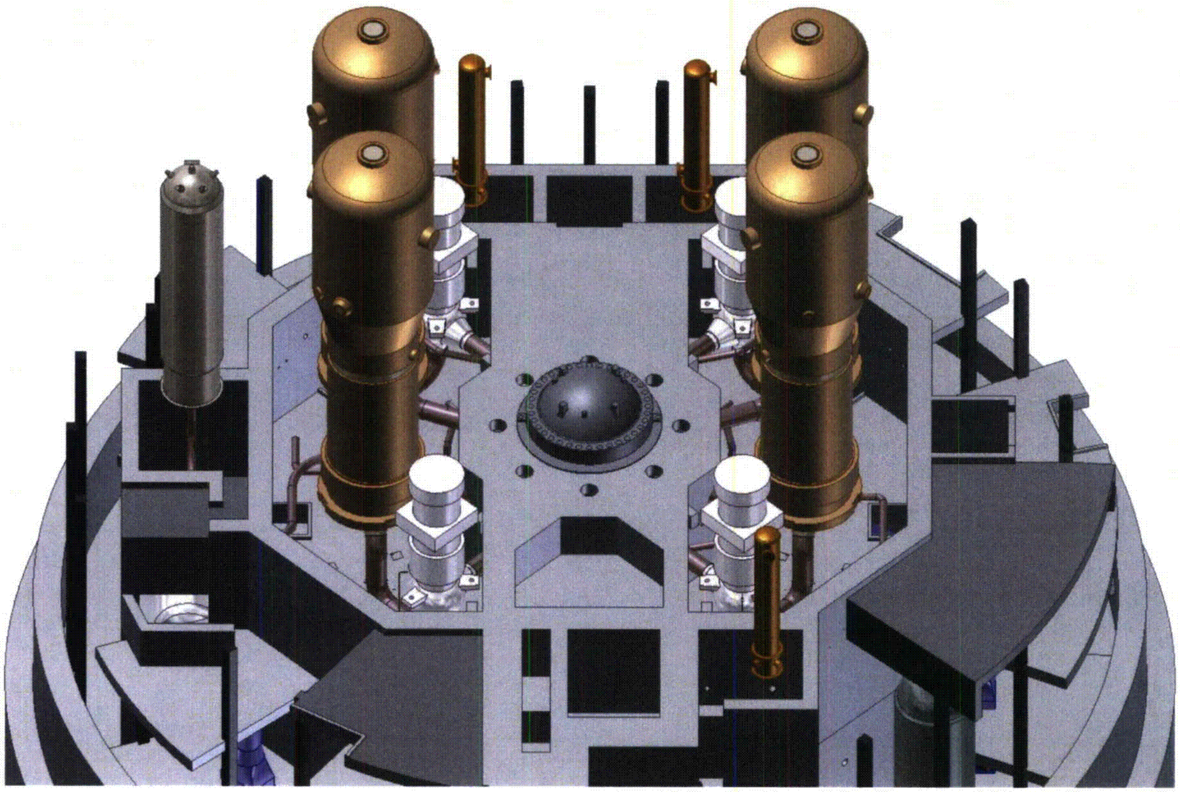

Figure 5.2.13 – Thermal-Wrap insulation on steam generators

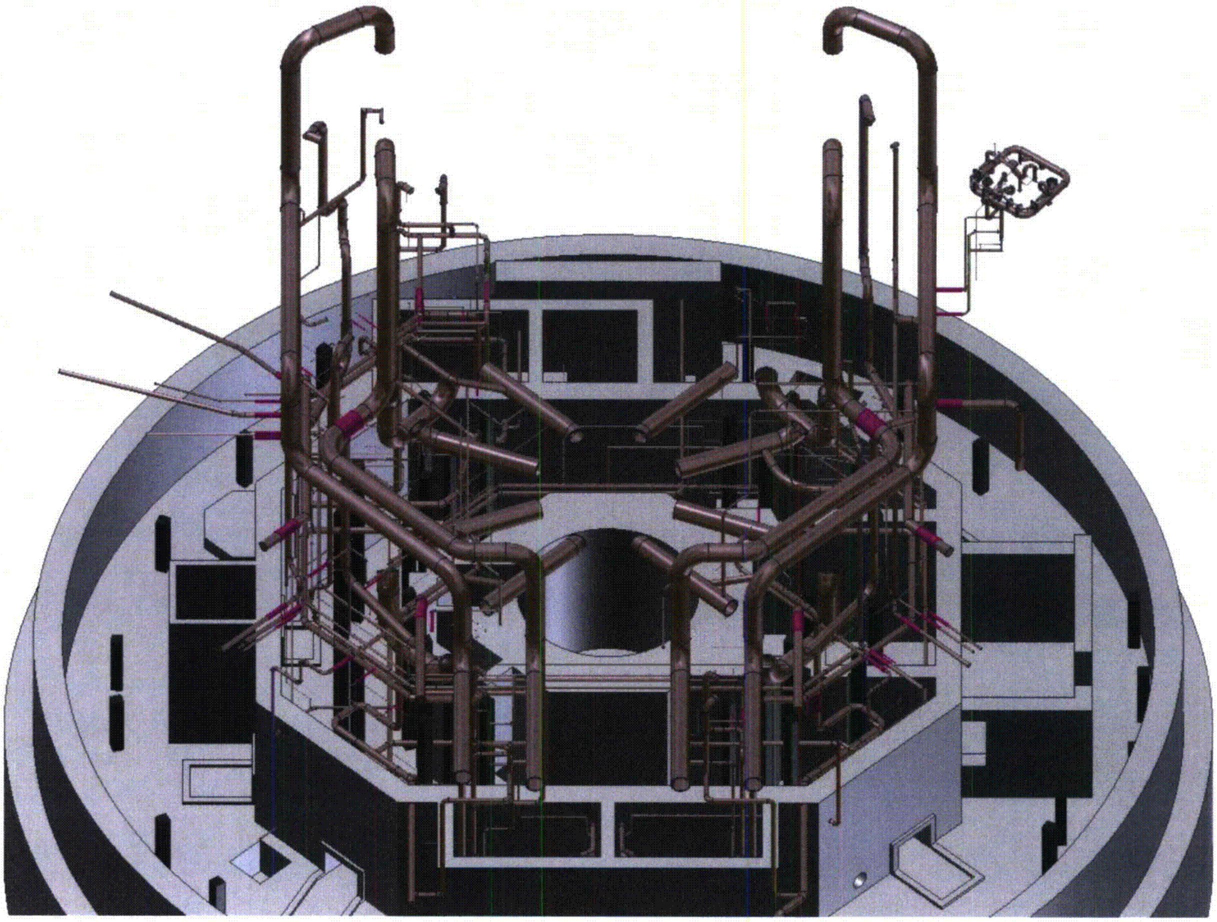

Figure 5.2.14 – Microtherm insulation in secondary shield wall penetrations

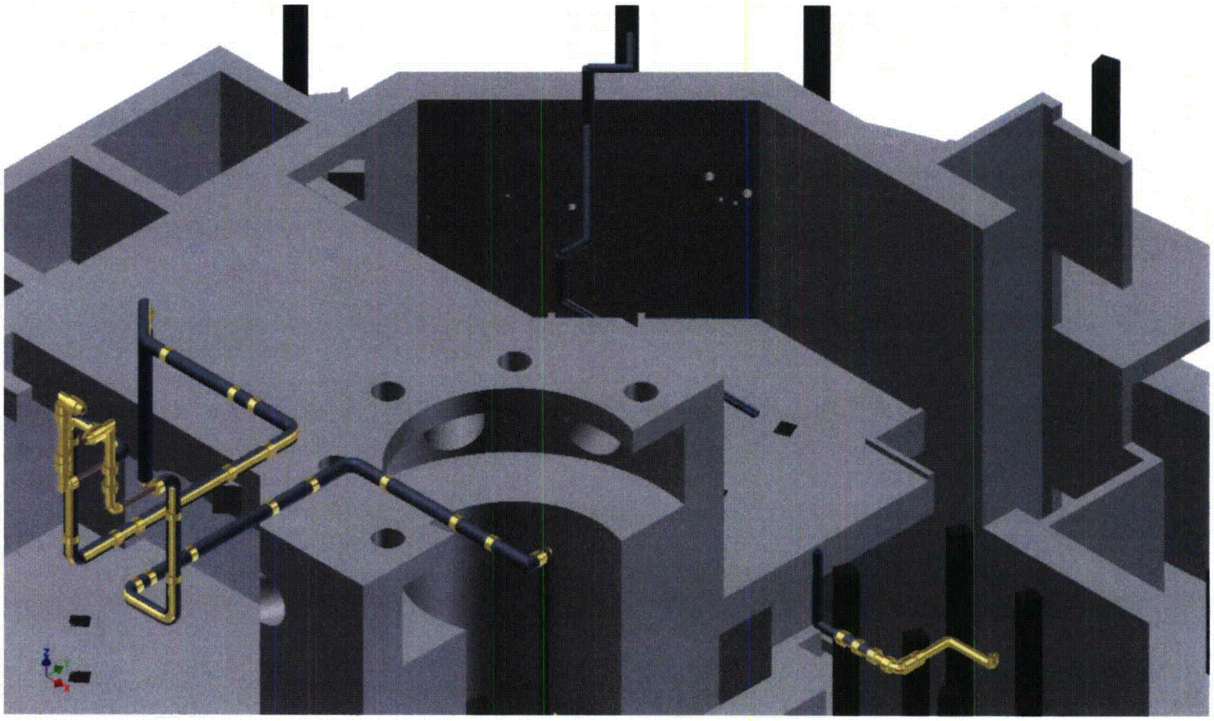

Figure 5.2.15 – Lead blankets on pipes

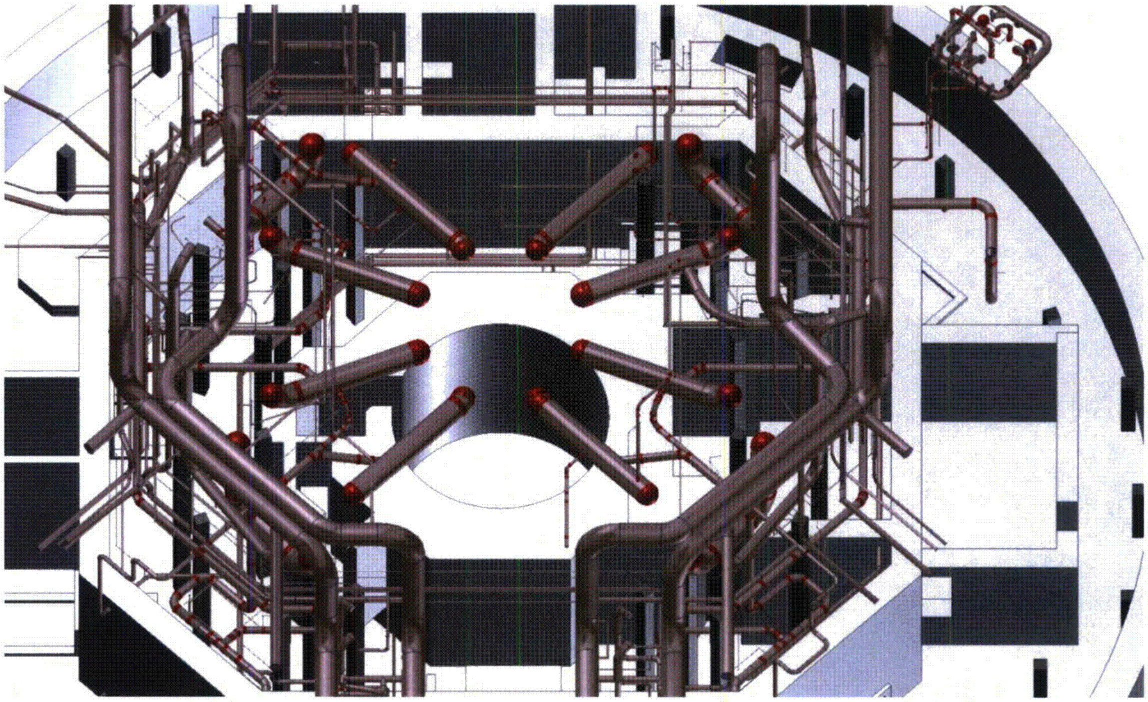

Figure 5.2.16 – Welds representing potential LOCA break locations (View 1)

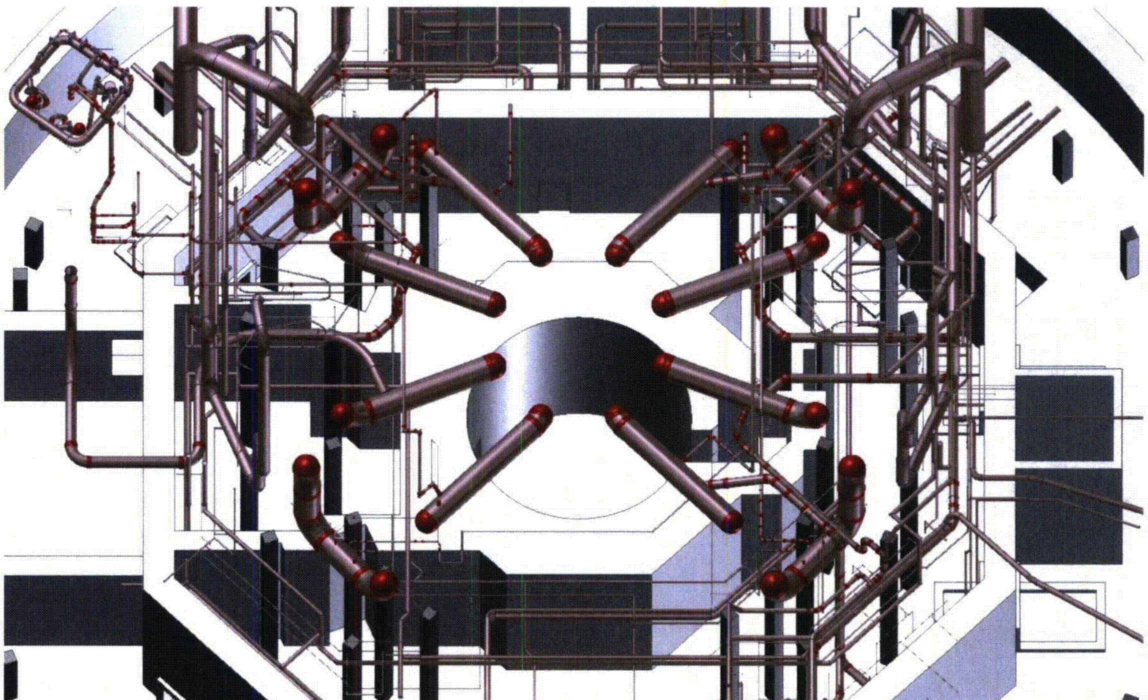

Figure 5.2.17 – Welds representing potential LOCA break locations (View 2)

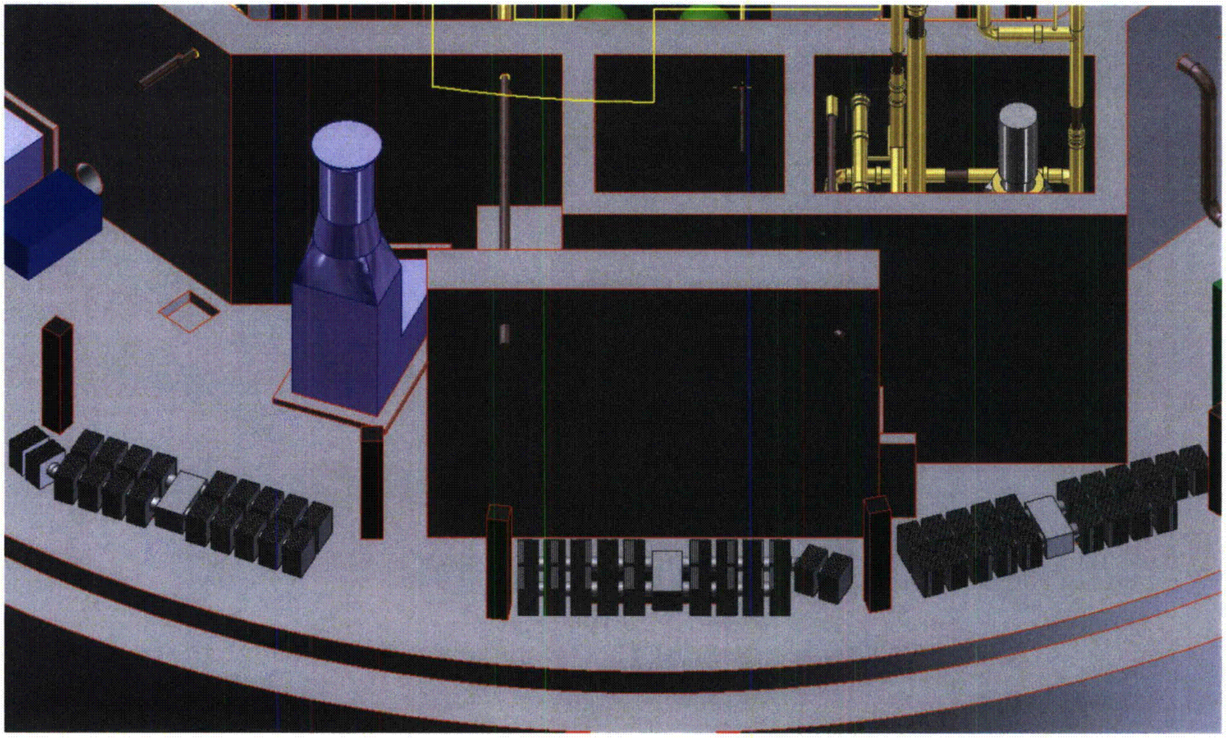

Figure 5.2.18 – Currently installed ECCS strainers

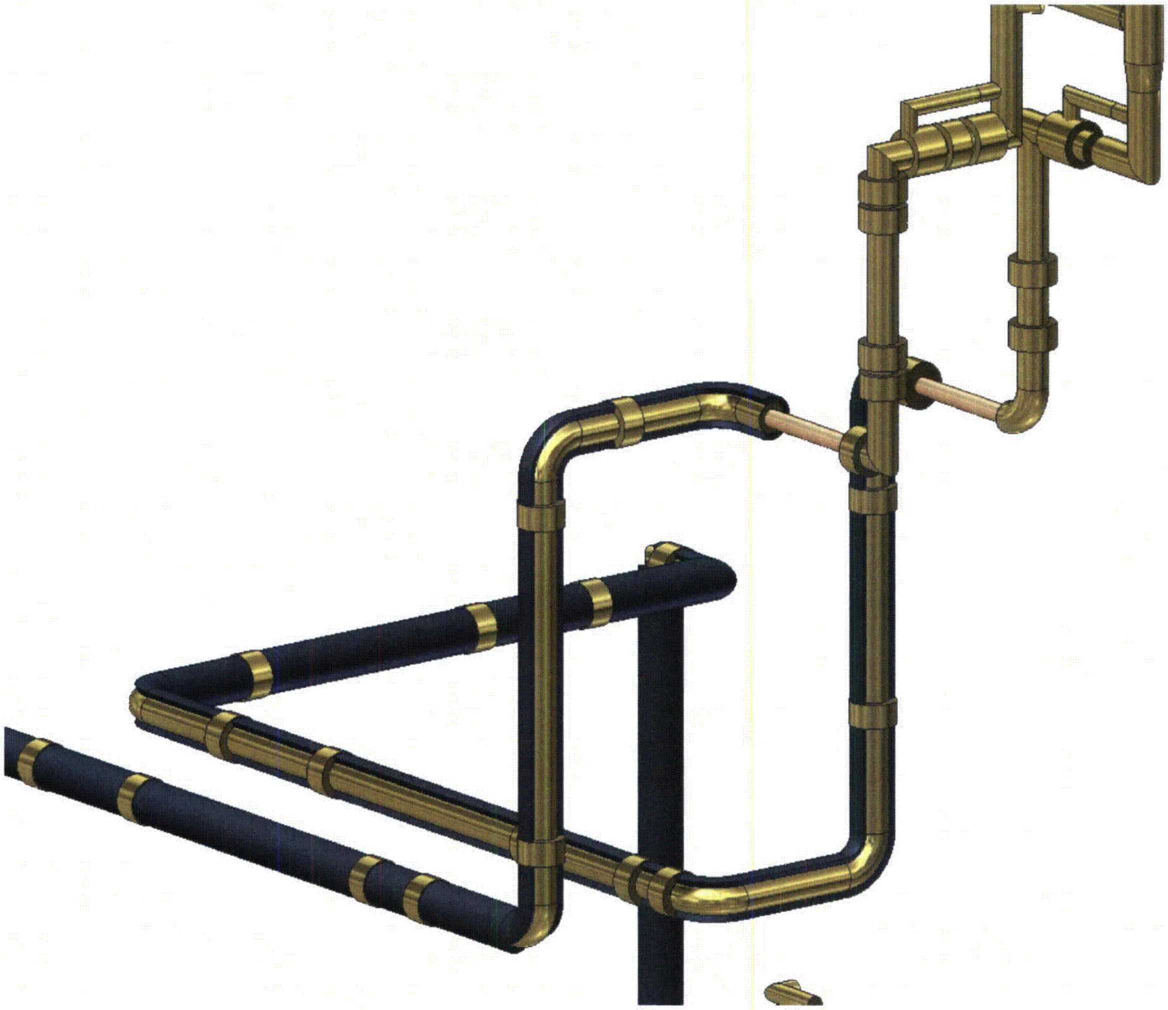

Figure 5.2.19 – Illustration of additional insulation modeled at hanger and valve locations

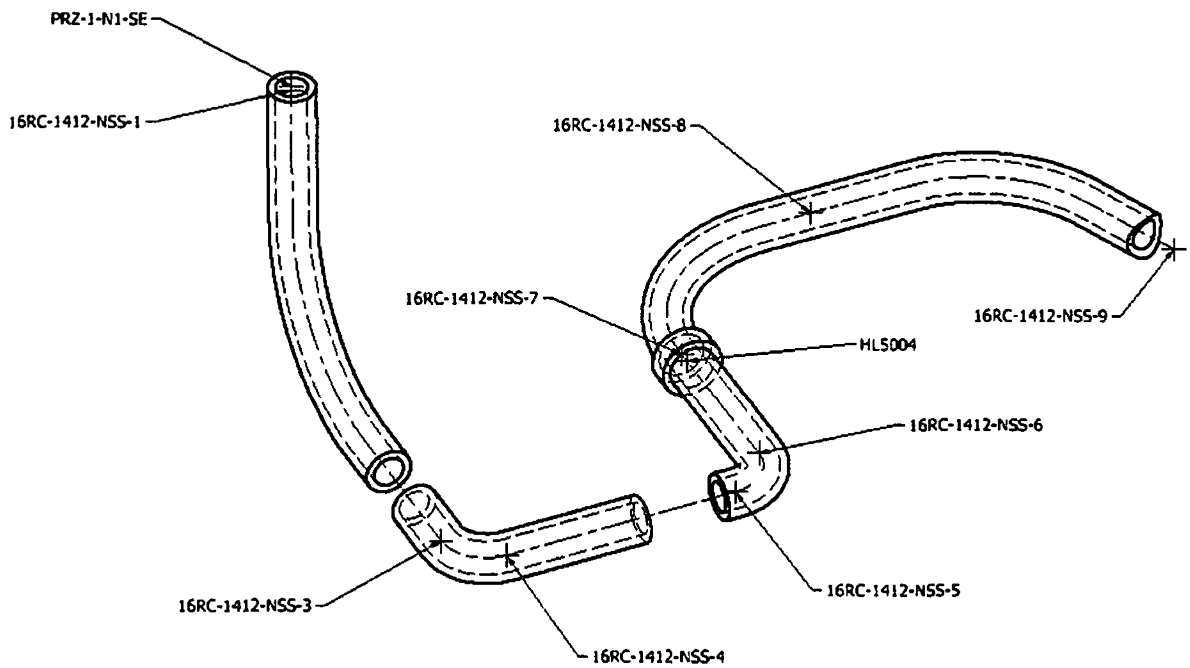

Figure 5.2.20 – Illustration of work points used to identify location of welds, hangers, and valves

The geometrical details of the pipes, pipe insulation, and work points (weld, hanger, and valve locations) were exported from the CAD model to a text format. As shown in Figure 5.2.21, the text data includes the part name (which specifies the line number and insulation type if applicable), the coordinates for the junction of each pipe segment, the bend radius for curved portions of the pipe, the inner and outer diameters (either of the pipe or insulation depending on the part), and a text identifier for any work points that are included on the line. The text data was imported into CASA Grande to define the geometry of the piping and associated insulation.

The insulation associated with the equipment (steam generators, pumps, and pressurizer) was defined by creating primitive shapes based on the dimensions of significant features of the equipment defined in the CAD model.

The concrete walls and floors were exported from the CAD model and imported into CASA Grande in stereolithography (STL) format to define robust barriers that would protect some insulation from the break jet. The concrete STL file is shown in Figure 5.2.22.

```
11-09-21 South Texas Plant.iam
Number of Points = 3. Number of Straights = 1. Unit of Length = Inches.
.ipt Name,Point,X,Y,Z,Rad,ID,OD,WP
0.75RC-1002-BB2 [NUKON]:1,0,97.81,-594.19,998,0,1.05,5.05,
0.75RC-1002-BB2 [NUKON]:1,1,94.56,-594.19,998,0,1.05,5.05,FW0002
0.75RC-1002-BB2 [NUKON]:1,2,86.06,-594.19,998,0,1.05,5.05,FW0001
Point to Point Length: 11.75

11-09-21 South Texas Plant.iam
Number of Points = 3. Number of Straights = 2. Unit of Length = Inches.
.ipt Name,Point,X,Y,Z,Rad,ID,OD,WP
0.75RC-1006-BB1 [NUKON]:1,0,28.6,-725.86,1199.92,0,1.05,6.05,
0.75RC-1006-BB1 [NUKON]:1,1,21.71,-720.48,1199.92,0,1.05,6.05,
0.75RC-1006-BB1 [NUKON]:1,2,21.71,-720.48,1209.19,0,1.05,6.05,
Point to Point Length: 18.02

11-09-21 South Texas Plant.iam
Number of Points = 14. Number of Straights = 11. Unit of Length = Inches.
.ipt Name,Point,X,Y,Z,Rad,ID,OD,WP
0.75RC-1007-BD7 [NUKON]:1,0,2.43,-606,1173.07,0,1.05,6.05,
0.75RC-1007-BD7 [NUKON]:1,1,2.43,-606,1181.82,0,1.05,6.05,
0.75RC-1007-BD7 [NUKON]:1,2,15.83,-616.47,1181.82,0,1.05,6.05,
0.75RC-1007-BD7 [NUKON]:1,3,15.83,-616.47,1199.92,0,1.05,6.05,
0.75RC-1007-BD7 [NUKON]:1,4,83.5,-669.34,1199.92,0,1.05,6.05,
0.75RC-1007-BD7 [NUKON]:1,5,35.27,-731.07,1199.92,0,1.05,6.05,
0.75RC-1007-BD7 [NUKON]:1,6,28.6,-725.86,1199.92,0,1.05,6.05,
Point to Point Length: 216.52

0.75RC-1007-BD7 [NUKON]:1,0,53.95,-646.25,1199.92,0,1.05,6.05,
0.75RC-1007-BD7 [NUKON]:1,1,48.71,-652.95,1199.92,0,1.05,6.05,
0.75RC-1007-BD7 [NUKON]:1,2,6.2,-619.73,1199.92,0,1.05,6.05,
0.75RC-1007-BD7 [NUKON]:1,3,0.38,-627.18,1199.92,0,1.05,6.05,
Point to Point Length: 71.91

0.75RC-1007-BD7 [NUKON]:1,0,59.58,-699.94,1199.92,0,1.05,6.05,
0.75RC-1007-BD7 [NUKON]:1,1,46.16,-689.46,1199.92,0,1.05,6.05,
0.75RC-1007-BD7 [NUKON]:1,2,51.55,-682.56,1199.92,0,1.05,6.05,
Point to Point Length: 25.78
```

Figure 5.2.21 – Example of CAD model text data output

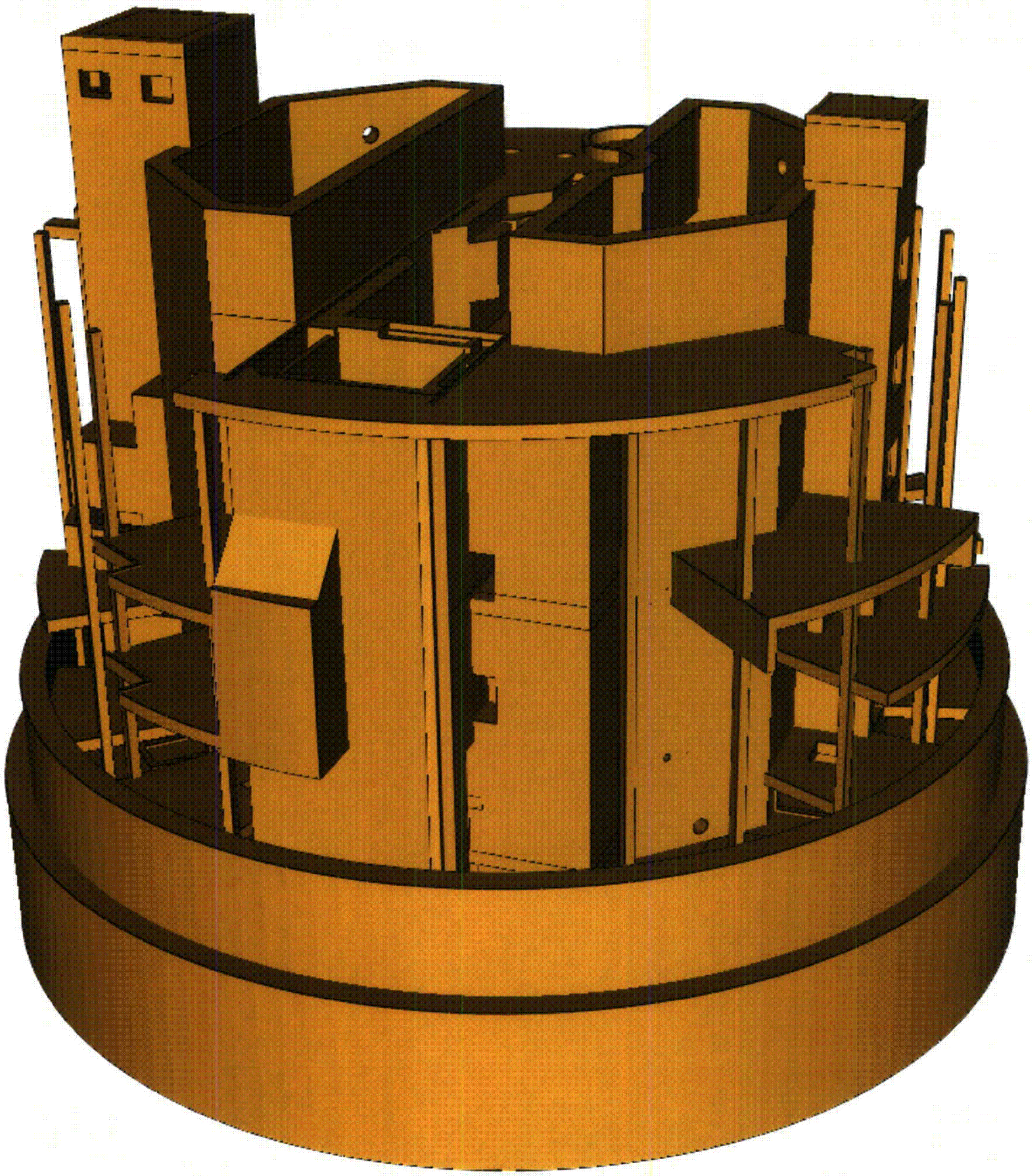

Figure 5.2.22 – Concrete walls and floors exported from CAD model in STL format

Figure 5.2.23 shows the geometry of the piping and equipment insulation in CASA Grande.

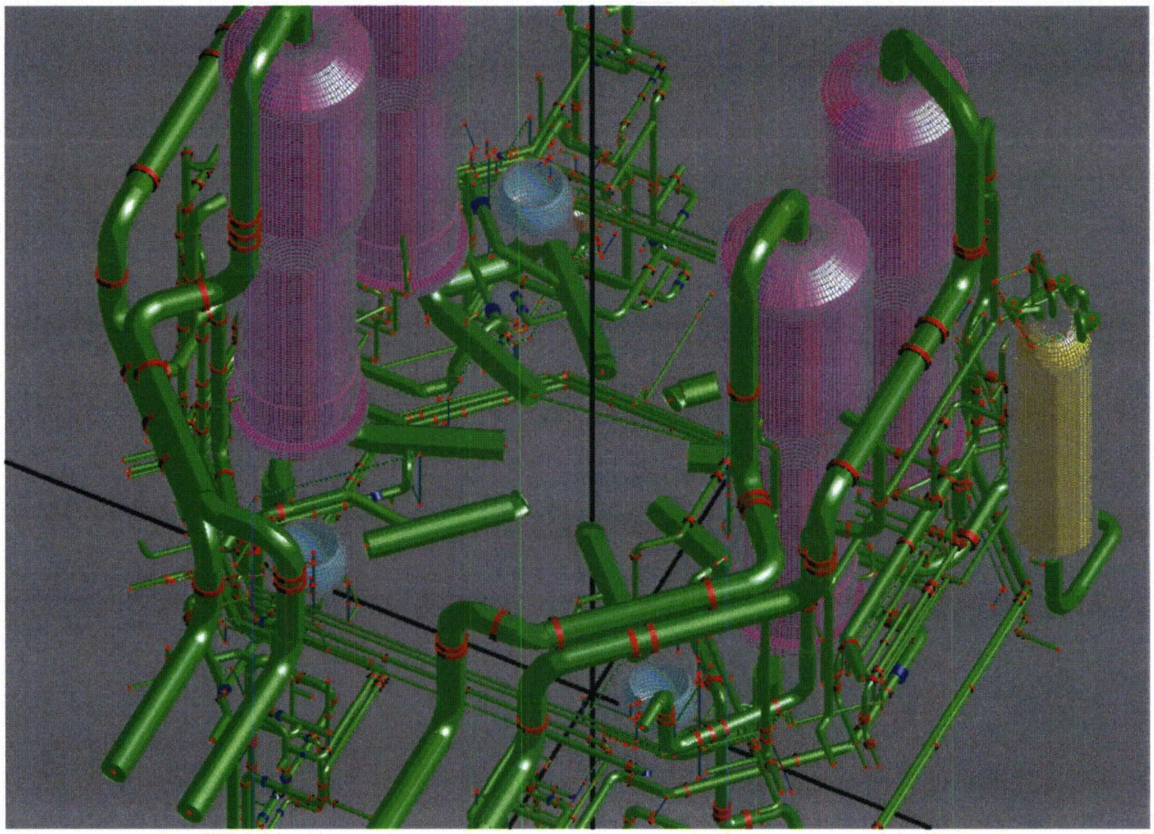

Figure 5.2.23 – Geometry of piping and equipment insulation in CASA Grande

5.3 LOCA Frequency

Determining the initiating event frequency is a key requirement in performing a risk-informed evaluation. Estimating the frequencies for LOCA pipe breaks, particularly larger breaks, is challenging since there is limited data from operating experience (due to the very low probabilities of these breaks occurring). The best generic estimates for LOCA frequencies are based on an expert elicitation process that was documented in NUREG-1829 (37). NUREG-1829 provides LOCA frequencies as a function of break size for both BWR and PWR plants. These values are total frequencies that include all potential primary-side break locations. However, since two equivalent-size breaks in different locations may have a significantly different likelihood of occurrence as well as a significantly different effect on GSI-191 related phenomena (e.g., quantity of debris generated, transport fractions, in-vessel flow paths, etc.), the total frequencies for all possible break locations must be broken down into the specific frequencies for each break location. The LOCA frequencies must then be appropriately sampled to evaluate the full range of potential LOCA scenarios. This was done using the following steps, each of which is explained in further detail in subsequent sections:

A. Calculate the relative weight of breaks for specific weld categories based on pipe size, weld type, applicable degradation mechanisms, etc., and distribute total LOCA frequency to each weld location based on relative weight between weld cases.
B. Identify applicable weld category and spatial coordinates for each weld location.
C. Statistically fit the NUREG-1829 frequencies (5th, Median, and 95th) using a bounded Johnson distribution for each size category. These fits represent the epistemic uncertainty associated with LOCA frequencies.
D. Sample epistemic uncertainty (e.g., 62nd percentile) and determine the corresponding total frequency curve based on the bounded Johnson fits (assuming linear interpolation between size categories).
E. Sample break sizes at each weld location and proceed with the GSI-191 analysis carrying the appropriate probability weight with each break scenario.

Table 2.2.3 through Table 2.2.10 define the annual frequency of breaks as a function of size for each of the weld cases. The tables are accepted as input to CASA Grande as an Excel file, which includes a reference list that assigns every weld in containment to one of the defined cases. The units of any pair of columns defining a weld case are break size in inches (Column 1 of a pair) and annual break frequency in number of breaks per year of size greater than *x* per weld (Column 2 of a pair), where *x* is any break size in Column 1. The purpose of the information in the break-frequency table is to support hybrid break frequency assignment (8) by defining relative proportions of break frequency across the weld types within any break size range of interest. Table 2.2.3 through Table 2.2.10 provide the link between aggregate annual break frequencies defined by NUREG-1829 and the assignment of breaks to specific locations in containment.

Table 2.2.3 through Table 2.2.10 incorporate industry data on break size and weld failure modes in the bottom-up approach for break frequency estimation. Many of the values in Table 2.2.3 through Table 2.2.10 were populated using a log-log interpolation scheme based on arguments invoking fracture mechanics and distributions of observed break sizes. However, as discussed in Assumption 3.e, all break-frequency interpolation was consistently performed using linear-linear interpolation. Therefore, it was necessary to filter out log-log interpolated values from each weld case. Interpolated values were identified as co-linear points in log-log space and eliminated from each weld case table.

The respective break frequencies were scaled by multiplying by the number of welds in each case and dividing all break frequency entries by the annual total frequency, including all sizes and all weld cases. The number of welds in each case was carefully verified to be consistent with the weld count in the STP CAD model (see Section 5.3.1). Division by the total annual break frequency is not strictly required, but it emphasizes that the purpose of the table is to define the joint probability distribution that exists between break size and weld type. A weld case provides a categorical representation of location within the plant as specified by the CAD model.

All break-size intervals needed to support the Latin hypercube sampling (LHS) design were determined across all weld categories and linear-linear interpolation was used to populate each weld category at a common list of break sizes. There can be a very long list of unique size bins that is determined by the LHS design size, but recall that the sample design preserves the definition of LOCA categories so that break-size intervals never span the LOCA-bin limits.

The hybrid break frequency assignment (8) was implemented. Each uncertainty percentile sampled from the Johnson break-size frequency envelope (see Section 5.3.4) was first divided by the total annual break frequency to form a conditional probability distribution, and the probability of experiencing a break within each bin of the common break-size interval list was calculated. The probability of experiencing a break within each interval was then distributed across all weld cases that can support a break of the given size. Relative probabilities between weld cases supporting the break-size interval determine the proportion assigned to each weld case. Thus, the aggregate frequency specified by the top-down approach of NUREG-1829 is preserved while the distribution of breaks among weld types specified by the bottom-up approach is also preserved. This equivalence is the essence of the hybrid methodology. Examples of the hybrid method (8) and the CASA implementation differ only in the number of size categories that are manipulated.

The frequencies for each weld location were determined by assigning an equal probability of experiencing a given break size for every weld assigned to a given weld case (for each sample of the Johnson uncertainty envelope).

The rebalanced table resulting from systematic mapping of each break-size bin across the weld cases was used to calculate LHS sample weights associated with every break scenario that was evaluated. The hybrid break frequency assignment was repeated as necessary for each sample of the Johnson uncertainty profile that was propagated through the evaluation. A description of the process for selecting specific break sizes from each weld category is provided in Section 5.3.5.

5.3.1 Relative Weight of Breaks in Specific Weld Categories

As discussed in Section 2.2.3, the relative weight of breaks in various weld locations are based on specific degradation mechanisms for categories of welds. These frequencies were determined from an analysis of DM-dependent weld failure rates based on service data, a Bayes method for uncertainty treatment developed in the EPRI risk-informed in-service inspection (RI-ISI) program, and estimates of conditional probability versus break size using information developed in NUREG-1829. The resulting weld-specific LOCA frequencies are used to establish the relative probabilities of break size and location that are subsequently normalized against the NUREG-1829 frequencies. Descriptions of the 45 unique categories are provided in Table 2.2.3 through Table 2.2.10, and summarized in Table 5.3.1.

Note that the pipe size listed in Table 5.3.1 is the nominal diameter, which is treated the same as the inner diameter. The DEGB size is the diameter of an equivalent hole with twice the inner area of the pipe (i.e., the equivalent break size given a fully offset DEGB with jets emanating from both sides of the broken pipe), and is calculated using the following equation:

$$D_{DEGB} = \sqrt{2} \cdot D_i \qquad \text{Equation 22}$$

where:

D_{DEGB} = Equivalent DEGB break size diameter assuming full pipe offset
D_i = Pipe inner diameter

For the hot and cold leg piping, the nominal diameter is equal to the inner diameter. However, the nominal diameter is larger (and in some cases significantly larger) for the higher schedule/thicker walled pipes that are 16 inches and smaller. For example, the surge line is a 16-inch, Schedule 160 pipe, which has an inner diameter of 12.81 inches. Therefore, the actual DEGB size would be 18.12 inches rather than 22.63 inches as shown in Table 5.3.1.

The weld types include:

- ASME XI Category B-F welds (bimetallic)
- ASME XI Category B-J welds (single metal)
- Branch connection (BC) welds, which are B-J welds used at branch connections

The degradation mechanisms include:

- Design and construction defects (D&C)
- Intergranular stress corrosion cracking (IGSCC)
- Transgranular stress corrosion cracking (TGSCC)
- Primary water stress corrosion cracking (PWSCC)
- Thermal fatigue (TF)
- Vibration fatigue (VF)

As discussed in Section 5.3.2 and Assumption 3.g, the weld count provided in Section 2.2.3 are not consistent with the CAD model for all break categories. Therefore, the weld counts were modified slightly in Table 5.3.1, and the values that were modified are marked with an asterisk. Also, Category 6B contains two weld sizes (nominal 0.75-inch and 1-inch pipes), and Categories 6A and 8C contain two weld sizes (nominal 1.5-inch and 2-inch). As noted in the tables, the different weld sizes were captured as subcategories.

Table 5.3.1 – Description of weld categories

Category	System	Nominal Pipe Size (in)	Actual Pipe Size (in)	DEGB (in)	Weld Type	DM	No. Welds
6B-1	Small Bore	0.75*	0.614	0.87	B-J	VF, SC, D&C	176
6B-2		1	0.815	1.15			17
7L	SIR	1.5	N/A	N/A	B-J	D&C	0
5J	Pressurizer	2	1.689	2.38	B-J	TF, D&C	2
6A-1	Small Bore	1.5*	1.338	1.89	B-J	VF, SC, D&C	1*
6A-2		2	1.689	2.38			23*
7K	SIR	2	1.689	2.38	BC	D&C	11*
8A	CVCS	2	1.689	2.38	B-J	TF, VF, D&C	10
8C-1	CVCS	1.5*	1.338	1.89	B-J	VF, D&C	8
8C-2		2	1.689	2.38			39
4D	Surge Line	2.5	2.125	3.01	B-J	TF, D&C	6
5B	Pressurizer	3	2.626	3.71	B-J	TF, D&C	14
5D	Pressurizer	3	2.626	3.71	B-J	D&C	4
7J	SIR	3	2.626	3.71	BC	D&C	8*
5C	Pressurizer	4	3.438	4.86	B-J	D&C	53
5I	Pressurizer	4	3.438	4.86	BC	D&C	2
7I	SIR	4	3.438	4.86	BC	D&C	5
8B	CVCS	4	3.438	4.86	B-J	TF, VF, D&C	19
8D	CVCS	4	3.438	4.86	B-J	VF, D&C	6
8E	CVCS	4	3.438	4.86	BC	TF, D&C	4
8F	CVCS	4	3.438	4.86	BC	D&C	1
5A	Pressurizer	6	5.189	7.34	B-J	TF, D&C	28*
5E	Pressurizer	6	5.189	7.34	B-J	D&C	29
5F	Pressurizer	6	5.189	7.34	B-F	SC, TF, D&C	4*
5G	Pressurizer	6	N/A	N/A	B-F	SC, D&C	0
5H	Pressurizer	6	5.189	7.34	B-F	D&C (Weld Overlay)	4
7H	SIR	6	5.189	7.34	B-J	D&C	23
7B	SIR	8	6.813	9.64	B-J	TF, D&C	9
7C	SIR	8	6.813	9.64	B-J	SC, TF, D&C	3
7G	SIR	8	6.813	9.64	BC, B-J	D&C	42
7F	SIR	10	8.500	12.02	B-J	D&C	30
7A	SIR	12	10.126	14.32	B-J	TF, D&C	21
7D	SIR	12	10.126	14.32	B-J	SC, D&C	3
7E	SIR	12	10.126	14.32	BC, B-J	D&C	57
7M	ACC	12	N/A	N/A	B-J	SC, D&C	0
7N	ACC	12	10.126	14.32	B-J	TF, D&C	35
7O	ACC	12	10.126	14.32	BC, B-J	D&C	15
4A	Surge Line	16	12.814	18.12	B-F	SC, TF, D&C	1

Category	System	Nominal Pipe Size (in)	Actual Pipe Size (in)	DEGB (in)	Weld Type	DM	No. Welds
4B	Surge Line	16	12.814	18.12	B-J	TF, D&C	7
4C	Surge Line	16	12.814	18.12	BC	TF, D&C	2
3A	Cold Leg	27.5	27.500	38.89	B-F	SC, D&C	4
3C	Cold Leg	27.5	27.500	38.89	B-J	D&C	12
1A	Hot Leg	29	29.000	41.01	B-F	SC, D&C	4
1B	Hot Leg	29	29.000	41.01	B-J	D&C	11
1C	Hot Leg	29	29.000	41.01	B-J	TF, D&C	1
2	SG Inlet	29	29.000	41.01	B-F	SC, D&C	4
3B	Cold Leg	31	31.000	43.84	B-F	SC, D&C	4
3D	Cold Leg	31	31.000	43.84	B-J	D&C	24
Total							**786***

5.3.2 Weld Categories and Coordinates

The weld categories and locations for each weld were determined based on a LOCA frequency component database (9) and the containment building CAD model (4). Both the database and CAD model are based on STP's in-service inspection (ISI) drawings. Table 5.3.3 shows the relevant weld data from these two sources. Note that there were a few discrepancies between the LOCA frequency report (7), the component database (9), and the CAD model (4). The discrepancies are listed below and were corrected in Table 5.3.3. Note that the corrections are marked with an asterisk.

- Weld 31-RC-1102-NSS-5 is listed in the database as Category 7J on a 3-inch pipe. However, according to the CAD model, this is a 2-inch pipe and therefore the weld falls within Category 7K.
- The component database was updated with a modification to the weld category identifiers after the LOCA frequency report was issued. Category 5G corresponds to B-J welds on 6-inch pressurizer piping susceptible to failures from D&C and PWSCC damage mechanisms. Four welds at STP that fit this category have weld overlays that eliminate the PWSCC damage mechanism. This was evaluated as a Category 5G sensitivity in the component database, but was included as Category 5H in the LOCA frequency report. Similarly, Categories 5H and 5I in the component database correspond to Categories 5I and 5J in the LOCA frequency report. To clear this up, the welds falling in these categories were adjusted in Table 5.3.3 to match the categories identified in the LOCA frequency report.
- Twenty-one 2-inch welds that are included in the CAD model were not explicitly identified in the component database. These welds were assigned to Category 6A.
- As discussed in Section 5.3.1, the pipe size provided in the LOCA frequency report is the nominal pipe diameter. The actual pipe diameter is typically smaller than the nominal diameter, which

also affects the equivalent DEGB size. The pipe diameter differences between the LOCA frequency report and the CAD model are shown in Table 5.3.2.

- There are also a few differences between the weld count provided in the LOCA frequency report and the CAD model as shown in Table 5.3.2. The most notable difference is the weld count for Category 6B. The LOCA frequency report lists 193 welds in this category, but the CAD model and the component database only contain a total of 35 of these welds. Upon review, the missing welds appear to be locations where 0.75-inch pipes (drain lines, etc.) are connected to larger piping. As shown in Figure 5.3.1, the 35 welds that were modeled are scattered throughout containment. Given the scattered distribution, and the relatively low significance with respect to GSI-191 phenomena for this size of breaks, it is reasonable to distribute the overall break frequency for the 193 welds to the 35 welds that were modeled (see Assumption 3.f). For other weld categories, the weld count in the CAD model was assumed to be more accurate than the weld count in the LOCA frequency report (see Assumption 3.g).

Table 5.3.2 – Comparison of LOCA frequency report and CAD model pipe sizes and weld counts

Category	Report Pipe Size (in)	CAD Pipe Size (in)	Report DEGB (in)	CAD DEGB (in)	Report Weld Count	CAD Weld Count
6B-1	1	0.614	1.41	0.87	193	32
6B-2		0.815		1.15		3
7L	1.5	N/A	2.12	N/A	0	0
5J	2	1.689	2.83	2.38	2	2
6A-1	2	1.338	2.83	1.89	16	1
6A-2		1.689		2.38		23
7K	2	1.689	2.83	2.38	10	11
8A	2	1.689	2.83	2.38	10	10
8C-1	2	1.338	2.83	1.89	47	8
8C-2		1.689		2.38		39
4D	2.5	2.125	3.54	3.01	6	6
5B	3	2.626	4.24	3.71	14	14
5D	3	2.626	4.24	3.71	4	4
7J	3	2.626	4.24	3.71	9	8
5C	4	3.438	5.66	4.86	53	53
5I	4	3.438	5.66	4.86	2	2
7I	4	3.438	5.66	4.86	5	5
8B	4	3.438	5.66	4.86	19	19
8D	4	3.438	5.66	4.86	6	6
8E	4	3.438	5.66	4.86	4	4
8F	4	3.438	5.66	4.86	1	1
5A	6	5.189	8.49	7.34	29	28
5E	6	5.189	8.49	7.34	29	29
5F	6	5.189	8.49	7.34	0	4
5G	6	N/A	8.49	N/A	0	0

Category	Report Pipe Size (in)	CAD Pipe Size (in)	Report DEGB (in)	CAD DEGB (in)	Report Weld Count	CAD Weld Count
5H	6	5.189	8.49	7.34	4	4
7H	6	5.189	8.49	7.34	23	23
7B	8	6.813	11.31	9.64	9	9
7C	8	6.813	11.31	9.64	3	3
7G	8	6.813	11.31	9.64	42	42
7F	10	8.500	14.14	12.02	30	30
7A	12	10.126	16.97	14.32	21	21
7D	12	10.126	16.97	14.32	3	3
7E	12	10.126	16.97	14.32	57	57
7M	12	N/A	16.97	N/A	0	0
7N	12	10.126	16.97	14.32	35	35
7O	12	10.126	16.97	14.32	15	15
4A	16	12.814	22.63	18.12	1	1
4B	16	12.814	22.63	18.12	7	7
4C	16	12.814	22.63	18.12	2	2
3A	27.5	27.500	38.89	38.89	4	4
3C	27.5	27.500	38.89	38.89	12	12
1A	29	29.000	41.01	41.01	4	4
1B	29	29.000	41.01	41.01	11	11
1C	29	29.000	41.01	41.01	1	1
2	29	29.000	41.01	41.01	4	4
3B	31	31.000	43.84	43.84	4	4
3D	31	31.000	43.84	43.84	24	24
Total					**775**	**628**

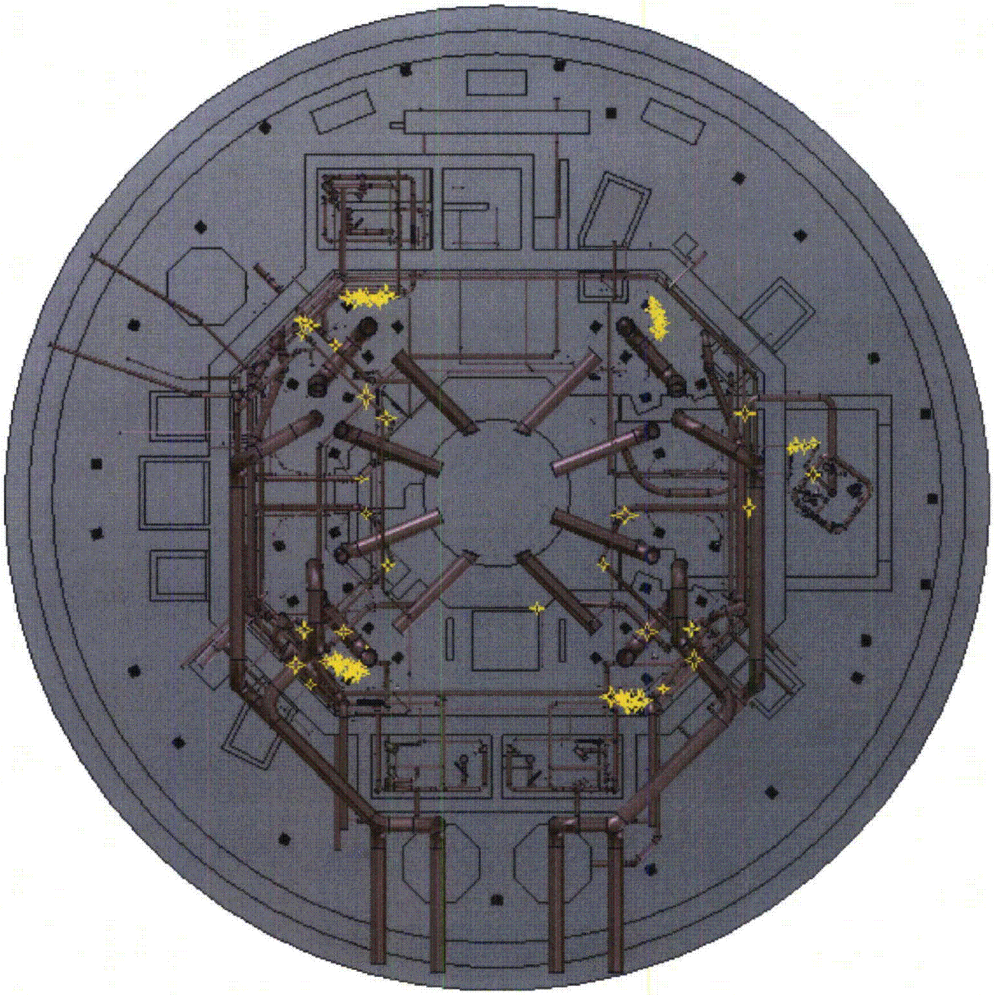

Figure 5.3.1 – Locations of Category 6B welds that were modeled

Table 5.3.3 – Weld data from component database and CAD model

No.	Line Number	Location Name	System	Category	Pipe ID	X	Y	Z	Side	Compartment
1	2-CV-1122-BB1	0.75-CV-1122-BB1-1	CV Small Bore	6B-1	0.614	-391.858	-245.642	497.125	Cold	SG Compartment
2	2-CV-1122-BB1	0.75-CV-1122-BB1-2	CV Small Bore	6B-1	0.614	-391.858	-260.642	513	Cold	SG Compartment
3	2-CV-1124-BB1	0.75-CV-1124-BB1-1	CV Small Bore	6B-1	0.614	-334.812	342.313	513	Cold	SG Compartment
4	2-CV-1124-BB1	0.75-CV-1124-BB1-2	CV Small Bore	6B-1	0.614	-334.812	329.313	525	Cold	SG Compartment
5	2-CV-1126-BB1	0.75-CV-1126-BB1-1	CV Small Bore	6B-1	0.614	399	269.313	477	Cold	SG Compartment
6	2-CV-1126-BB1	0.75-CV-1126-BB1-2	CV Small Bore	6B-1	0.614	399	260.313	513	Cold	SG Compartment
7	2-CV-1128-BB1	0.75-CV-1128-BB1-1	CV Small Bore	6B-1	0.614	350.702	-324.25	563.438	Cold	SG Compartment
8	2-CV-1128-BB1	0.75-CV-1128-BB1-2	CV Small Bore	6B-1	0.614	341.702	-324.25	563.438	Cold	SG Compartment
9	4-RC-1003-BB1	0.75-RC-1001-BB1-1	RC Small Bore	6B-1	0.614	108.001	-648.001	998	Cold	PZR Compartment
10	4-RC-1000-BB1	0.75-RC-1002-BB2-1	RC Small Bore	6B-1	0.614	97.812	-594.189	998	Cold	PZR Compartment
11	12-RC-1112-BB1	0.75-RC-1112-BB1-1	RC Small Bore	6B-1	0.614	-30.55	-261.662	456.035	Hot	SG Compartment
12	8-RC-1114-BB1	0.75-RC-1114-BB1-1	RC Small Bore	6B-1	0.614	-141.33	-226.374	483	Hot	SG Compartment
13	12-RC-1125-BB1	0.75-RC-1125-BB1-1	SI-ACC-CL1 Small Bore	6B-1	0.614	-270.999	-310.539	548.204	Cold	SG Compartment
14	12-RC-1125-BB1	0.75-RC-1125-BB1-2	SI-ACC-CL1 Small Bore	6B-1	0.614	-265.077	-384.343	273.017	Cold	Below SG Compartment
15	4-RC-1126-BB1	0.75-RC-1126-BB1-1	RC Small Bore	6B-1	0.614	-236	-91.56	507	Cold	SG Compartment
16	12-RC-1212-BB1	0.75-RC-1212-BB1-1	RC Small Bore	6B-1	0.614	-30.551	261.636	456.007	Hot	SG Compartment
17	8-RC-1214-BB1	0.75-RC-1214-BB1-1	RC Small Bore	6B-1	0.614	-143.269	225.591	483	Hot	SG Compartment
18	12-RC-1221-BB1	0.75-RC-1221-BB1-1	SI-ACC-CL2 Small Bore	6B-1	0.614	-270.999	310.309	548.169	Cold	SG Compartment
19	12-RC-1221-BB1	0.75-RC-1221-BB1-2	SI-ACC-CL2 Small Bore	6B-1	0.614	-265.077	384.113	273.006	Cold	Below SG Compartment
20	12-RC-1312-BB1	0.75-RC-1312-BB1-1	RC Small Bore	6B-1	0.614	54.55	261.662	455.999	Hot	SG Compartment
21	8-RC-1324-BB1	0.75-RC-1324-BB1-1	RC Small Bore	6B-1	0.614	165.148	223.469	492	Hot	SG Compartment
22	4-RC-1422-BB1	0.75-RC-1423-BB1-1	RC Small Bore	6B-1	0.614	108.001	-612.751	984	Cold	PZR Compartment
23	8-SI-1108-BB1	0.75-SI-1130-BB2-1	RC Small Bore	6B-1	0.614	-310.37	-395.39	483	Hot	SG Compartment
24	12-SI-1125-BB1	0.75-SI-1132-BB1-1	RC Small Bore	6B-1	0.614	-390.942	-354.644	273.017	Cold	Below SG Compartment
25	12-SI-1218-BB1	0.75-SI-1218-BB1-1	SI Small Bore	6B-1	0.614	-364.072	381.285	273.006	Cold	Below SG Compartment
26	8-SI-1208-BB1	0.75-SI-1223-BB2-1	RC Small Bore	6B-1	0.614	-313.12	395.46	483	Hot	SG Compartment
27	12-SI-1315-BB1	0.75-SI-1315-BB1-1	SI-ACC Small Bore	6B-1	0.614	312.427	331.154	548.194	Cold	SG Compartment
28	12-SI-1315-BB1	0.75-SI-1323-BB1-1	SI-ACC Small Bore	6B-1	0.614	345.971	364.697	191.014	Cold	Below SG Compartment
29	6-SI-1327-BB1	0.75-SI-1327-BB1-1	SI Small Bore	6B-1	0.614	361.366	383.719	491.924	Hot	SG Compartment
30	8-SI-1327-BB1	0.75-SI-1327-BB1-2	SI Small Bore	6B-1	0.614	335.604	393.925	540	Hot	SG Compartment
31	8-SI-1327-BB1	0.75-SI-1327-BB1-3	SI Small Bore	6B-1	0.614	200.944	259.265	492	Hot	SG Compartment
32	8-SI-1327-BB1	0.75-SI-1328-BB2-1	SI Small Bore	6B-1	0.614	360.352	397.461	491.924	Hot	SG Compartment
33	6-RC-1003-BB1	1-RC-1003-BB1-1	RC Small Bore	6B-2	0.815	53.272	-636.728	1263	Cold	PZR Compartment
34	4-RC-1123-BB1	1-RC-1123-BB1-1	RC Small Bore	6B-2	0.815	-18.187	-516.189	807	Cold	SG Compartment
35	4-RC-1422-BB1	1-RC-1422-BB1-1	RC Small Bore	6B-2	0.815	108.001	-607.626	984	Cold	PZR Compartment
36	16-RC-1412-NSS	1.5-RC-1412-NSS-1	RC	6A-1	1.338	165.003	-507	526.221	Hot	SG Compartment
37	2(1.5)-CV-1122-BB1	2(1.5)-CV-1122-BB1-1	CV - RCP1A	8C-1	1.338	-391.86	-260.64	551.44	Cold	SG Compartment
38	2(1.5)-CV-1122-BB1	2(1.5)-CV-1122-BB1-2	CV - RCP1A	8C-1	1.338	-381.8	-260.64	563.44	Cold	SG Compartment
39	2(1.5)-CV-1124-BB1	2(1.5)-CV-1124-BB1-1	CV - RCP1B	8C-1	1.338	-334.81	323.31	563.44	Cold	SG Compartment

No.	Line Number	Location Name	System	Category	Pipe ID	X	Y	Z	Side	Compartment
40	2(1.5)-CV-1124-BB1	2(1.5)-CV-1124-BB1-2	CV - RCP1B	8C-1	1.338	-334.81	311.44	563.44	Cold	SG Compartment
41	2(1.5)-CV-1126-BB1	2(1.5)-CV-1126-BB1-1	CV - RCP1C	8C-1	1.338	393	260.31	563.44	Cold	SG Compartment
42	2(1.5)-CV-1126-BB1	2(1.5)-CV-1126-BB1-2	CV - RCP1C	8C-1	1.338	385.94	260.31	563.44	Cold	SG Compartment
43	2(1.5)-CV-1128-BB1	2(1.5)-CV-1128-BB1-1	CV - RCP1D	8C-1	1.338	332.7	-318.12	563.44	Cold	SG Compartment
44	2(1.5)-CV-1128-BB1	2(1.5)-CV-1128-BB1-2	CV - RCP1D	8C-1	1.338	332.7	-309.56	563.44	Cold	SG Compartment
45	2-CV-1121-BB1	2-CV-1121-BB1-1	CV - PZR Auxiliary Spray Line	8A	1.689	11	-588.25	984	Cold	PZR Compartment
46	2-CV-1121-BB1	2-CV-1121-BB1-2	CV - PZR Auxiliary Spray Line	8A	1.689	44.93	-588.25	1062	Cold	PZR Compartment
47	2-CV-1121-BB1	2-CV-1121-BB1-3	CV - PZR Auxiliary Spray Line	8A	1.689	108	-621.5	1062	Cold	PZR Compartment
48	2-CV-1122-BB1	2-CV-1122-BB1-1	CV - RCP1A	8C-2	1.689	-391.86	-212.64	497.12	Cold	SG Compartment
49	2-CV-1122-BB1	2-CV-1122-BB1-2	CV - RCP1A	8C-2	1.689	-391.86	-221.64	497.12	Cold	SG Compartment
50	2-CV-1122-BB1	2-CV-1122-BB1-3	CV - RCP1A	8C-2	1.689	-391.86	-229.64	497.12	Cold	SG Compartment
51	2-CV-1122-BB1	2-CV-1122-BB1-4	CV - RCP1A	8C-2	1.689	-391.86	-242.64	497.12	Cold	SG Compartment
52	2-CV-1122-BB1	2-CV-1122-BB1-5	CV - RCP1A	8C-2	1.689	-391.86	-248.64	497.12	Cold	SG Compartment
53	2-CV-1122-BB1	2-CV-1122-BB1-6	CV - RCP1A	8C-2	1.689	-391.86	-260.64	548.44	Cold	SG Compartment
54	2-CV-1124-BB1	2-CV-1124-BB1-1	CV - RCP1B	8C-2	1.689	-325.97	377.65	513	Cold	SG Compartment
55	2-CV-1124-BB1	2-CV-1124-BB1-2	CV - RCP1B	8C-2	1.689	-332.69	370.93	513	Cold	SG Compartment
56	2-CV-1124-BB1	2-CV-1124-BB1-3	CV - RCP1B	8C-2	1.689	-334.81	365.81	513	Cold	SG Compartment
57	2-CV-1124-BB1	2-CV-1124-BB1-4	CV - RCP1B	8C-2	1.689	-334.81	359.31	513	Cold	SG Compartment
58	2-CV-1124-BB1	2-CV-1124-BB1-5	CV - RCP1B	8C-2	1.689	-334.81	351.31	513	Cold	SG Compartment
59	2-CV-1124-BB1	2-CV-1124-BB1-6	CV - RCP1B	8C-2	1.689	-334.81	345.31	513	Cold	SG Compartment
60	2-CV-1124-BB1	2-CV-1124-BB1-7	CV - RCP1B	8C-2	1.689	-334.81	339.31	513	Cold	SG Compartment
61	2-CV-1124-BB1	2-CV-1124-BB1-8	CV - RCP1B	8C-2	1.689	-334.81	332.31	513	Cold	SG Compartment
62	2-CV-1124-BB1	2-CV-1124-BB1-9	CV - RCP1B	8C-2	1.689	-334.81	329.31	516	Cold	SG Compartment
63	2-CV-1124-BB1	2-CV-1124-BB1-10	CV - RCP1B	8C-2	1.689	-334.81	329.31	522	Cold	SG Compartment
64	2-CV-1124-BB1	2-CV-1124-BB1-11	CV - RCP1B	8C-2	1.689	-334.81	329.31	528	Cold	SG Compartment
65	2-CV-1124-BB1	2-CV-1124-BB1-12	CV - RCP1B	8C-2	1.689	-334.81	329.31	560.44	Cold	SG Compartment
66	2-CV-1124-BB1	2-CV-1124-BB1-13	CV - RCP1B	8C-2	1.689	-334.81	326.31	563.44	Cold	SG Compartment
67	2-CV-1126-BB1	2-CV-1126-BB1-1	CV - RCP1C	8C-2	1.689	399	293.81	477	Cold	SG Compartment
68	2-CV-1126-BB1	2-CV-1126-BB1-2	CV - RCP1C	8C-2	1.689	399	286.81	477	Cold	SG Compartment
69	2-CV-1126-BB1	2-CV-1126-BB1-3	CV - RCP1C	8C-2	1.689	399	278.81	477	Cold	SG Compartment
70	2-CV-1126-BB1	2-CV-1126-BB1-4	CV - RCP1C	8C-2	1.689	399	272.81	477	Cold	SG Compartment
71	2-CV-1126-BB1	2-CV-1126-BB1-5	CV - RCP1C	8C-2	1.689	399	266.31	477	Cold	SG Compartment
72	2-CV-1126-BB1	2-CV-1126-BB1-6	CV - RCP1C	8C-2	1.689	399	263.31	477	Cold	SG Compartment
73	2-CV-1126-BB1	2-CV-1126-BB1-7	CV - RCP1C	8C-2	1.689	399	260.31	480	Cold	SG Compartment
74	2-CV-1126-BB1	2-CV-1126-BB1-8	CV - RCP1C	8C-2	1.689	399	260.31	510	Cold	SG Compartment
75	2-CV-1126-BB1	2-CV-1126-BB1-9	CV - RCP1C	8C-2	1.689	399	260.31	516	Cold	SG Compartment
76	2-CV-1126-BB1	2-CV-1126-BB1-10	CV - RCP1C	8C-2	1.689	399	260.31	560.44	Cold	SG Compartment
77	2-CV-1126-BB1	2-CV-1126-BB1-11	CV - RCP1C	8C-2	1.689	396	260.31	563.44	Cold	SG Compartment
78	2-CV-1128-BB1	2-CV-1128-BB1-1	CV - RCP1D	8C-2	1.689	379.7	-324.25	563.44	Cold	SG Compartment
79	2-CV-1128-BB1	2-CV-1128-BB1-2	CV - RCP1D	8C-2	1.689	367.7	-324.25	563.44	Cold	SG Compartment
80	2-CV-1128-BB1	2-CV-1128-BB1-3	CV - RCP1D	8C-2	1.689	359.7	-324.25	563.44	Cold	SG Compartment

No.	Line Number	Location Name	System	Category	Pipe ID	X	Y	Z	Side	Compartment
81	2-CV-1128-BB1	2-CV-1128-BB1-3A	CV - RCP1D	8C-2	1.689	353.7	-324.25	563.44	Cold	SG Compartment
82	2-CV-1128-BB1	2-CV-1128-BB1-3B	CV - RCP1D	8C-2	1.689	347.7	-324.25	563.44	Cold	SG Compartment
83	2-CV-1128-BB1	2-CV-1128-BB1-4	CV - RCP1D	8C-2	1.689	344.7	-324.25	563.44	Cold	SG Compartment
84	2-CV-1128-BB1	2-CV-1128-BB1-5	CV - RCP1D	8C-2	1.689	338.7	-324.25	563.44	Cold	SG Compartment
85	2-CV-1128-BB1	2-CV-1128-BB1-6	CV - RCP1D	8C-2	1.689	335.7	-324.25	563.44	Cold	SG Compartment
86	2-CV-1128-BB1	2-CV-1128-BB1-7	CV - RCP1D	8C-2	1.689	332.7	-321.12	563.44	Cold	SG Compartment
87	2-CV-1141-BB1	2-CV-1141-BB1-1	CV - RC Crossover-4	8A	1.689	243	-209.06	372	Cold	SG Compartment
88	2-CV-1141-BB1	2-CV-1141-BB1-2	CV - RC Crossover-4	8A	1.689	255	-186.06	372	Cold	SG Compartment
89	2-RC-1003-BB1	2-RC-1003-BB1-1	PZR Auxiliary Spray Line	5J*	1.689	108	-621.5	1062	Cold	PZR Compartment
90	2-RC-1003-BB1	2-RC-1003-BB1-2	PZR Auxiliary Spray Line	5J*	1.689	108	-630	1062	Cold	PZR Compartment
91	2-RC-1120-BB1	2-RC-1120-BB1-1	RC	7K	1.689	-252	-323	429.14	Cold	SG Compartment
92	2-RC-1120-BB1	2-RC-1120-BB1-2	RC	6A-2*	1.689	-252	-323.001	433	Cold	SG Compartment
93	2-RC-1121-BB1	2-RC-1121-BB1-1	RC	6A-2*	1.689	-271.125	-306.08	380.001	Cold	SG Compartment
94	2-RC-1121-BB1	2-RC-1121-BB1-2	RC	6A-2*	1.689	-228	-293.08	372.001	Cold	SG Compartment
95	2-RC-1121-BB1	2-RC-1121-BB1-3	RC	6A-2*	1.689	-228	-287.187	372.001	Cold	SG Compartment
96	2-RC-1121-BB1	2-RC-1121-BB1-3A	RC Drain	6A-2	1.689	-228	-283.19	372	Cold	SG Compartment
97	2-RC-1121-BB1	2-RC-1121-BB1-3B	RC Drain	6A-2	1.689	-228	-275.19	372	Cold	SG Compartment
98	2-RC-1121-BB1	2-RC-1121-BB1-4	RC	6A-2*	1.689	-228	-269.187	372.001	Cold	SG Compartment
99	2-RC-1219-BB1	2-RC-1219-BB1-1	RC	7K	1.689	-249.25	325.43	429.08	Cold	SG Compartment
100	2-RC-1219-BB1	2-RC-1219-BB1-2	RC	6A-2*	1.689	-249.25	325.434	433	Cold	SG Compartment
101	2-RC-1220-BB1	2-RC-1220-BB1-1	RC	6A-2*	1.689	-271.146	306.062	379.001	Cold	SG Compartment
102	2-RC-1220-BB1	2-RC-1220-BB1-2	RC	6A-2*	1.689	-228	293	369.751	Cold	SG Compartment
103	2-RC-1220-BB1	2-RC-1220-BB1-3	RC	6A-2*	1.689	-228	284.5	369.751	Cold	SG Compartment
104	2-RC-1220-BB1	2-RC-1220-BB1-4	RC	6A-2*	1.689	-228	275.5	369.751	Cold	SG Compartment
105	2-RC-1319-BB1	2-RC-1319-BB1-1	RC	7K	1.689	272.81	325.82	427.58	Cold	SG Compartment
106	2-RC-1319-BB1	2-RC-1319-BB1-2	RC	6A-2*	1.689	272.812	325.821	433	Cold	SG Compartment
107	2-RC-1321-BB1	2-RC-1321-BB1-1	RC	6A-2*	1.689	244.134	288.072	372.313	Cold	SG Compartment
108	2-RC-1321-BB1	2-RC-1321-BB1-4	RC	6A-2*	1.689	256.509	276.822	372.313	Cold	SG Compartment
109	2-RC-1321-BB1	2-RC-1321-BB1-5	RC	6A-2*	1.689	256.509	268.322	372.313	Cold	SG Compartment
110	2-RC-1321-BB1	2-RC-1321-BB1-6	RC	6A-2*	1.689	256.509	259.322	372.313	Cold	SG Compartment
111	2-RC-1417-BB1	2-RC-1417-BB1-1	RC	7K	1.689	273.37	-325.32	429.33	Cold	SG Compartment
112	2-RC-1417-BB1	2-RC-1417-BB1-2	RC	6A-2*	1.689	273.375	-325.323	433	Cold	SG Compartment
113	2-RC-1418-BB1	2-RC-1418-BB1-1	RC	6A-2*	1.689	295.146	-306.062	379.293	Cold	SG Compartment
114	2-RC-1418-BB1	2-RC-1418-BB1-2	CV - RC Crossover-4	8A	1.689	262.02	-306.06	372	Cold	SG Compartment
115	2-RC-1418-BB1	2-RC-1418-BB1-3	CV - RC Crossover-4	8A	1.689	258.02	-302.06	372	Cold	SG Compartment
116	2-RC-1418-BB1	2-RC-1418-BB1-4	RC	6A-2*	1.689	258.021	-294.812	372	Cold	SG Compartment
117	2-RC-1418-BB1	2-RC-1418-BB1-5	RC	6A-2*	1.689	258.021	-284.812	372	Cold	SG Compartment
118	2-RC-1418-BB1	2-RC-1418-BB1-6	RC	6A-2*	1.689	258.021	-271.312	372	Cold	SG Compartment
119	2-RC-1419-BB1	2-RC-1419-BB1-1	CV - RC Crossover-4	8A	1.689	254.02	-306.06	372	Cold	SG Compartment
120	2-RC-1419-BB1	2-RC-1419-BB1-2	CV - RC Crossover-4	8A	1.689	243	-294.81	372	Cold	SG Compartment
121	2-RC-1419-BB1	2-RC-1419-BB1-3	CV - RC Crossover-4	8A	1.689	243	-284.81	372	Cold	SG Compartment

No.	Line Number	Location Name	System	Category	Pipe ID	X	Y	Z	Side	Compartment
122	2-RC-1419-BB1	2-RC-1419-BB1-4	RC	6A-2*	1.689	243	-218.312	372	Cold	SG Compartment
123	2.5-RC-1003-BB1	2.5-RC-1003-BB1-1	Pressurizer Surge Line	4D	2.125	46.2	-643.8	1266	Cold	PZR Compartment
124	2.5-RC-1003-BB1	2.5-RC-1003-BB1-2	Pressurizer Surge Line	4D	2.125	46.2	-643.8	1272.31	Cold	PZR Compartment
125	2.5-RC-1003-BB1	2.5-RC-1003-BB1-3	Pressurizer Surge Line	4D	2.125	44.08	-645.92	1275.31	Cold	PZR Compartment
126	2.5-RC-1003-BB1	2.5-RC-1003-BB1-4	Pressurizer Surge Line	4D	2.125	41.25	-648.75	1275.31	Cold	PZR Compartment
127	2.5-RC-1003-BB1	2.5-RC-1003-BB1-5	Pressurizer Surge Line	4D	2.125	32.19	-657.81	1275.31	Cold	PZR Compartment
128	2.5-RC-1003-BB1	2.5-RC-1003-BB1-6	Pressurizer Surge Line	4D	2.125	30.07	-659.93	1275.31	Cold	PZR Compartment
129	3-RC-1003-BB1	3-RC-1003-BB1-1	PZR Auxiliary Spray Line	5B	2.626	108	-636	1062	Cold	PZR Compartment
130	3-RC-1003-BB1	3-RC-1003-BB1-2	PZR Auxiliary Spray Line	5B	2.626	108	-645	1062	Cold	PZR Compartment
131	3-RC-1015-NSS	3-RC-1015-NSS-1	Pressurizer PORV Line	5D	2.626	-44.11	-652.56	1262.06	Cold	PZR Compartment
132	3-RC-1015-NSS	3-RC-1015-NSS-2	Pressurizer PORV Line	5D	2.626	-46.2	-655.24	1260.66	Cold	PZR Compartment
133	3-RC-1015-NSS	3-RC-1015-NSS-3	Pressurizer PORV Line	5B	2.626	-48.29	-657.91	1259.25	Cold	PZR Compartment
134	3-RC-1015-NSS	3-RC-1015-NSS-4	Pressurizer PORV Line	5B	2.626	-54.45	-665.79	1259.25	Cold	PZR Compartment
135	3-RC-1015-NSS	3-RC-1015-NSS-5	Pressurizer PORV Line	5B	2.626	-59.99	-672.89	1259.25	Cold	PZR Compartment
136	3-RC-1015-NSS	3-RC-1015-NSS-6	Pressurizer PORV Line	5B	2.626	-69.2	-684.67	1259.25	Cold	PZR Compartment
137	3-RC-1015-NSS	3-RC-1015-NSS-7	Pressurizer PORV Line	5B	2.626	-68.43	-691.14	1259.25	Cold	PZR Compartment
138	3-RC-1015-NSS	3-RC-1015-NSS-8	Pressurizer PORV Line	5B	2.626	-48.48	-706.73	1259.25	Cold	PZR Compartment
139	3-RC-1015-NSS	3-RC-1015-NSS-9	Pressurizer PORV Line	5D	2.626	-26.26	-629.71	1262.06	Cold	PZR Compartment
140	3-RC-1015-NSS	3-RC-1015-NSS-10	Pressurizer PORV Line	5D	2.626	-24.16	-627.04	1260.66	Cold	PZR Compartment
141	3-RC-1015-NSS	3-RC-1015-NSS-11	Pressurizer PORV Line	5B	2.626	-22.08	-624.36	1259.25	Cold	PZR Compartment
142	3-RC-1015-NSS	3-RC-1015-NSS-12	Pressurizer PORV Line	5B	2.626	-15.92	-616.48	1259.25	Cold	PZR Compartment
143	3-RC-1015-NSS	3-RC-1015-NSS-13	Pressurizer PORV Line	5B	2.626	-10.38	-609.39	1259.25	Cold	PZR Compartment
144	3-RC-1015-NSS	3-RC-1015-NSS-14	Pressurizer PORV Line	5B	2.626	-1.17	-597.6	1259.25	Cold	PZR Compartment
145	3-RC-1015-NSS	3-RC-1015-NSS-15	Pressurizer PORV Line	5B	2.626	5.33	-596.8	1259.25	Cold	PZR Compartment
146	3-RC-1015-NSS	3-RC-1015-NSS-16	Pressurizer PORV Line	5B	2.626	25.24	-612.36	1259.25	Cold	PZR Compartment
147	3-RC-1106-BB1	3-RC-1106-BB1-25	SI - Capped	7J	2.626	-278.44	-299.61	430.31	Cold	SG Compartment
148	3-RC-1206-BB1	3-RC-1206-BB1-28	SI - Capped	7J	2.626	-278.44	299.61	430.31	Cold	SG Compartment
149	3-RC-1306-BB1	3-RC-1306-BB1-28	SI - Capped	7J	2.626	302.44	299.61	430.31	Cold	SG Compartment
150	3-RC-1406-BB1	3-RC-1406-BB1-25	SI - Capped	7J	2.626	302.44	-299.61	430.31	Cold	SG Compartment
151	4-CV-1001-BB1	4-CV-1001-BB1-1	CV - RC Crossover-3	8B	3.438	204.13	243.01	372.31	Cold	SG Compartment
152	4-CV-1001-BB1	4-CV-1001-BB1-2	CV - RC Crossover-3	8B	3.438	182.13	243.01	372.31	Cold	SG Compartment
153	4-CV-1118-BB1	4-CV-1118-BB1-1	CV - RC Coldleg 1	8B	3.438	-328	-91.56	507	Cold	SG Compartment
154	4-CV-1118-BB1	4-CV-1118-BB1-2	CV - RC Coldleg 1	8B	3.438	-269	-91.56	507	Cold	SG Compartment
155	4-CV-1120-BB1	4-CV-1120-BB1-1	CV - RC Coldleg 3	8B	3.438	181.59	196.84	522	Cold	SG Compartment
156	4-CV-1120-BB1	4-CV-1120-BB1-2	CV - RC Coldleg 3	8B	3.438	190.07	205.33	522	Cold	SG Compartment
157	4-RC-1000-BB1	4-RC-1000-BB1-1	Pressurizer Spray	5C	3.438	82.44	-594.19	984	Cold	PZR Compartment
158	4-RC-1000-BB1	4-RC-1000-BB1-2	Pressurizer Spray	5C	3.438	91.81	-594.19	984	Cold	PZR Compartment
159	4-RC-1000-BB1	4-RC-1000-BB1-3	Pressurizer Spray	5C	3.438	97.81	-594.19	990	Cold	PZR Compartment
160	4-RC-1000-BB1	4-RC-1000-BB1-4	Pressurizer Spray	5C	3.438	97.81	-594.19	1023	Cold	PZR Compartment
161	4-RC-1000-BB1	4-RC-1000-BB1-5	Pressurizer Spray	5C	3.438	100.64	-597.02	1029	Cold	PZR Compartment
162	4-RC-1000-BB1	4-RC-1000-BB1-6	Pressurizer Spray	5C	3.438	105.17	-601.55	1029	Cold	PZR Compartment

No.	Line Number	Location Name	System	Category	Pipe ID	X	Y	Z	Side	Compartment
163	4-RC-1000-BB1	4-RC-1000-BB1-7	Pressurizer Spray	5C	3.438	108	-608.38	1029	Cold	PZR Compartment
164	4-RC-1000-BB1	4-RC-1000-BB1-8	Pressurizer Spray	5C	3.438	108	-636	1029	Cold	PZR Compartment
165	4-RC-1003-BB1	4-RC-1003-BB1-1	Pressurizer Spray	5C	3.438	108	-635	984	Cold	PZR Compartment
166	4-RC-1003-BB1	4-RC-1003-BB1-2	Pressurizer Spray	5C	3.438	108	-642	984	Cold	PZR Compartment
167	4-RC-1003-BB1	4-RC-1003-BB1-3	Pressurizer Spray	5C	3.438	108	-648	990	Cold	PZR Compartment
168	4-RC-1003-BB1	4-RC-1003-BB1-4	Pressurizer Spray	5C	3.438	108	-648	1008	Cold	PZR Compartment
169	4-RC-1123-BB1	4-RC-1123-BB1-1	Pressurizer Spray	5I*	3.438	-252.54	-190.08	545.88	Cold	SG Compartment
170	4-RC-1123-BB1	4-RC-1123-BB1-2	Pressurizer Spray	5C	3.438	-252.54	-190.08	708	Cold	SG Compartment
171	4-RC-1123-BB1	4-RC-1123-BB1-3	Pressurizer Spray	5C	3.438	-252.54	-190.08	723	Cold	SG Compartment
172	4-RC-1123-BB1	4-RC-1123-BB1-4	Pressurizer Spray	5C	3.438	-244.06	-198.57	735	Cold	SG Compartment
173	4-RC-1123-BB1	4-RC-1123-BB1-5	Pressurizer Spray	5C	3.438	-211.95	-230.67	735	Cold	SG Compartment
174	4-RC-1123-BB1	4-RC-1123-BB1-6	Pressurizer Spray	5C	3.438	-203.47	-234.19	735	Cold	SG Compartment
175	4-RC-1123-BB1	4-RC-1123-BB1-7	Pressurizer Spray	5C	3.438	-30.19	-234.19	735	Cold	SG Compartment
176	4-RC-1123-BB1	4-RC-1123-BB1-8	Pressurizer Spray	5C	3.438	-18.19	-246.27	735	Cold	SG Compartment
177	4-RC-1123-BB1	4-RC-1123-BB1-9	Pressurizer Spray	5C	3.438	-18.19	-372.19	735	Cold	SG Compartment
178	4-RC-1123-BB1	4-RC-1123-BB1-10	Pressurizer Spray	5C	3.438	-18.19	-504.19	735	Cold	SG Compartment
179	4-RC-1123-BB1	4-RC-1123-BB1-11	Pressurizer Spray	5C	3.438	-18.19	-516.19	747	Cold	SG Compartment
180	4-RC-1123-BB1	4-RC-1123-BB1-12	Pressurizer Spray	5C	3.438	-18.19	-516.19	879	Cold	SG Compartment
181	4-RC-1123-BB1	4-RC-1123-BB1-13	Pressurizer Spray	5C	3.438	-6.19	-516.19	891	Cold	SG Compartment
182	4-RC-1123-BB1	4-RC-1123-BB1-14	Pressurizer Spray	5C	3.438	38.99	-516.19	891	Cold	SG Compartment
183	4-RC-1123-BB1	4-RC-1123-BB1-15	Pressurizer Spray	5C	3.438	50.81	-528.19	891	Cold	SG Compartment
184	4-RC-1123-BB1	4-RC-1123-BB1-16	Pressurizer Spray	5C	3.438	50.81	-588.19	891	Cold	PZR Compartment
185	4-RC-1123-BB1	4-RC-1123-BB1-17	Pressurizer Spray	5C	3.438	50.81	-594.19	897	Cold	PZR Compartment
186	4-RC-1123-BB1	4-RC-1123-BB1-18	Pressurizer Spray	5C	3.438	50.81	-594.19	978	Cold	PZR Compartment
187	4-RC-1123-BB1	4-RC-1123-BB1-19	Pressurizer Spray	5C	3.438	56.81	-594.19	984	Cold	PZR Compartment
188	4-RC-1123-BB1	4-RC-1123-BB1-20	Pressurizer Spray	5C	3.438	75.62	-594.19	984	Cold	PZR Compartment
189	4-RC-1126-BB1	4-RC-1126-BB1-1	CV - RC Coldleg 1	8B	3.438	-255	-91.56	507	Cold	SG Compartment
190	4-RC-1126-BB1	4-RC-1126-BB1-2	CV - RC Coldleg 1	8B	3.438	-228	-91.56	507	Cold	SG Compartment
191	4-RC-1126-BB1	4-RC-1126-BB1-3	CV - RC Coldleg 1	8B	3.438	-222	-91.56	513	Cold	SG Compartment
192	4-RC-1126-BB1	4-RC-1126-BB1-4	CV - RC Coldleg 1	8B	3.438	-222	-91.56	516	Cold	SG Compartment
193	4-RC-1126-BB1	4-RC-1126-BB1-5	CV - RC Coldleg 1	8B	3.438	-217.76	-95.8	522	Cold	SG Compartment
194	4-RC-1126-BB1	4-RC-1126-BB1-6	CV - RC Coldleg 1	8E	3.438	-205.01	-108.55	522	Cold	SG Compartment
195	4-RC-1320-BB1	4-RC-1320-BB1-1	CV - RC Crossover-3	8F	3.438	295.13	306.07	381.31	Cold	SG Compartment
196	4-RC-1320-BB1	4-RC-1320-BB1-2	CV - RC Crossover-3	8D	3.438	295.13	306.07	377.31	Cold	SG Compartment
197	4-RC-1320-BB1	4-RC-1320-BB1-3	CV - RC Crossover-3	8D	3.438	290.13	306.07	372.31	Cold	SG Compartment
198	4-RC-1320-BB1	4-RC-1320-BB1-4	CV - RC Crossover-3	8D	3.438	246.13	306.07	372.31	Cold	SG Compartment
199	4-RC-1320-BB1	4-RC-1320-BB1-5	CV - RC Crossover-3	8D	3.438	241.13	301.07	372.31	Cold	SG Compartment
200	4-RC-1320-BB1	4-RC-1320-BB1-6	CV - RC Crossover-3	8D	3.438	241.13	291.07	372.31	Cold	SG Compartment
201	4-RC-1320-BB1	4-RC-1320-BB1-7	CV - RC Crossover-3	8D	3.438	241.13	285.07	372.31	Cold	SG Compartment
202	4-RC-1320-BB1	4-RC-1320-BB1-8	CV - RC Crossover-3	8B	3.438	241.13	274.01	372.31	Cold	SG Compartment
203	4-RC-1320-BB1	4-RC-1320-BB1-9	CV - RC Crossover-3	8B	3.438	241.13	258.01	372.31	Cold	SG Compartment

No.	Line Number	Location Name	System	Category	Pipe ID	X	Y	Z	Side	Compartment
204	4-RC-1320-BB1	4-RC-1320-BB1-10	CV - RC Crossover-3	8B	3.438	241.13	248.01	372.31	Cold	SG Compartment
205	4-RC-1320-BB1	4-RC-1320-BB1-11	CV - RC Crossover-3	8B	3.438	236.13	243.01	372.31	Cold	SG Compartment
206	4-RC-1320-BB1	4-RC-1320-BB1-12	CV - RC Crossover-3	8B	3.438	220.13	243.01	372.31	Cold	SG Compartment
207	4-RC-1323-BB1	4-RC-1323-BB1-1	CV - RC Coldleg 3	8B	3.438	171.7	186.93	522	Cold	SG Compartment
208	4-RC-1323-BB1	4-RC-1323-BB1-2	CV - RC Coldleg 3	8B	3.438	164.64	179.85	522	Cold	SG Compartment
209	4-RC-1323-BB1	4-RC-1323-BB1-3	CV - RC Coldleg 3	8B	3.438	164.65	172.78	522	Cold	SG Compartment
210	4-RC-1323-BB1	4-RC-1323-BB1-4	CV - RC Coldleg 3	8E	3.438	195.67	141.82	522	Cold	SG Compartment
211	4-RC-1420-BB1	4-RC-1420-BB1-1	SI	7I	3.438	273.56	-187.1	548	Cold	SG Compartment
212	4-RC-1422-BB1	4-RC-1422-BB1-1	Pressurizer Spray	5I*	3.438	252.15	-188.74	538.31	Cold	SG Compartment
213	4-RC-1422-BB1	4-RC-1422-BB1-2	Pressurizer Spray	5C	3.438	249	-191.89	542.76	Cold	SG Compartment
214	4-RC-1422-BB1	4-RC-1422-BB1-3	Pressurizer Spray	5C	3.438	250.24	-199.13	547	Cold	SG Compartment
215	4-RC-1422-BB1	4-RC-1422-BB1-4	Pressurizer Spray	5C	3.438	259.44	-208.33	547	Cold	SG Compartment
216	4-RC-1422-BB1	4-RC-1422-BB1-5	Pressurizer Spray	5C	3.438	263.68	-212.57	553	Cold	SG Compartment
217	4-RC-1422-BB1	4-RC-1422-BB1-6	Pressurizer Spray	5C	3.438	263.68	-212.57	729	Cold	SG Compartment
218	4-RC-1422-BB1	4-RC-1422-BB1-7	Pressurizer Spray	5C	3.438	263.68	-218.57	735	Cold	SG Compartment
219	4-RC-1422-BB1	4-RC-1422-BB1-8	Pressurizer Spray	5C	3.438	263.68	-228	735	Cold	SG Compartment
220	4-RC-1422-BB1	4-RC-1422-BB1-9	Pressurizer Spray	5C	3.438	257.68	-234	735	Cold	SG Compartment
221	4-RC-1422-BB1	4-RC-1422-BB1-10	Pressurizer Spray	5C	3.438	57	-234	735	Cold	SG Compartment
222	4-RC-1422-BB1	4-RC-1422-BB1-11	Pressurizer Spray	5C	3.438	45	-246	735	Cold	SG Compartment
223	4-RC-1422-BB1	4-RC-1422-BB1-12	Pressurizer Spray	5C	3.438	45	-384	735	Cold	SG Compartment
224	4-RC-1422-BB1	4-RC-1422-BB1-13	Pressurizer Spray	5C	3.438	45	-504.07	735	Cold	SG Compartment
225	4-RC-1422-BB1	4-RC-1422-BB1-14	Pressurizer Spray	5C	3.438	57	-516	735	Cold	SG Compartment
226	4-RC-1422-BB1	4-RC-1422-BB1-15	Pressurizer Spray	5C	3.438	96.03	-516	735	Cold	SG Compartment
227	4-RC-1422-BB1	4-RC-1422-BB1-16	Pressurizer Spray	5C	3.438	108	-516	747	Cold	SG Compartment
228	4-RC-1422-BB1	4-RC-1422-BB1-17	Pressurizer Spray	5C	3.438	108	-516	879	Cold	SG Compartment
229	4-RC-1422-BB1	4-RC-1422-BB1-18	Pressurizer Spray	5C	3.438	108	-528	891	Cold	SG Compartment
230	4-RC-1422-BB1	4-RC-1422-BB1-19	Pressurizer Spray	5C	3.438	108	-582	891	Cold	SG Compartment
231	4-RC-1422-BB1	4-RC-1422-BB1-20	Pressurizer Spray	5C	3.438	108	-594	903	Cold	PZR Compartment
232	4-RC-1422-BB1	4-RC-1422-BB1-21	Pressurizer Spray	5C	3.438	108	-594	972	Cold	PZR Compartment
233	4-RC-1422-BB1	4-RC-1422-BB1-22	Pressurizer Spray	5C	3.438	108	-606	984	Cold	PZR Compartment
234	4-RC-1422-BB1	4-RC-1422-BB1-23	Pressurizer Spray	5C	3.438	108	-621.38	984	Cold	PZR Compartment
235	6-RC-1003-BB1	6-RC-1003-BB1-1	Pressurizer Spray	5E	5.189	108	-648	1017	Cold	PZR Compartment
236	6-RC-1003-BB1	6-RC-1003-BB1-2	Pressurizer Spray	5E	5.189	108	-648	1025	Cold	PZR Compartment
237	6-RC-1003-BB1	6-RC-1003-BB1-3	Pressurizer Spray	5E	5.189	108	-648	1033	Cold	PZR Compartment
238	6-RC-1003-BB1	6-RC-1003-BB1-4	Pressurizer Spray	5A	5.189	108	-648	1058	Cold	PZR Compartment
239	6-RC-1003-BB1	6-RC-1003-BB1-5	Pressurizer Spray	5A	5.189	108	-648	1066	Cold	PZR Compartment
240	6-RC-1003-BB1	6-RC-1003-BB1-6	Pressurizer Spray	5A	5.189	108	-648	1083	Cold	PZR Compartment
241	6-RC-1003-BB1	6-RC-1003-BB1-7	Pressurizer Spray	5A	5.189	97.58	-642.05	1095	Cold	PZR Compartment
242	6-RC-1003-BB1	6-RC-1003-BB1-8	Pressurizer Spray	5A	5.189	76.42	-629.95	1095	Cold	PZR Compartment
243	6-RC-1003-BB1	6-RC-1003-BB1-9	Pressurizer Spray	5A	5.189	66	-624	1107	Cold	PZR Compartment
244	6-RC-1003-BB1	6-RC-1003-BB1-9A	Pressurizer Spray	5A	5.189	66	-624	1128	Cold	PZR Compartment

No.	Line Number	Location Name	System	Category	Pipe ID	X	Y	Z	Side	Compartment
245	6-RC-1003-BB1	6-RC-1003-BB1-9B	Pressurizer Spray	5A	5.189	66	-624	1149	Cold	PZR Compartment
246	6-RC-1003-BB1	6-RC-1003-BB1-10	Pressurizer Spray	5A	5.189	66	-624	1251	Cold	PZR Compartment
247	6-RC-1003-BB1	6-RC-1003-BB1-11	Pressurizer Spray	5A	5.189	57.51	-632.49	1263	Cold	PZR Compartment
248	6-RC-1003-BB1	6-RC-1003-BB1-11A	Pressurizer Spray	5A	5.189	49.03	-640.97	1263	Cold	PZR Compartment
249	6-RC-1003-BB1	6-RC-1003-BB1-11B	Pressurizer Spray	5A	5.189	43.37	-646.63	1263	Cold	PZR Compartment
250	6-RC-1003-BB1	6-RC-1003-BB1-12	Pressurizer Spray	5A	5.189	20.49	-669.51	1263	Cold	PZR Compartment
251	6-RC-1003-BB1	6-RC-1003-BB1-13	Pressurizer Spray	5A	5.189	12	-678	1251	Cold	PZR Compartment
252	6-RC-1003-BB1	6-RC-1003-BB1-13A	Pressurizer Spray	5A	5.189	12	-678	1236.5	Cold	PZR Compartment
253	6-RC-1003-BB1	6-RC-1003-BB1-14	Pressurizer Spray	5H*	5.189	12	-678	1222	Cold	PZR Compartment
254	6-RC-1003-BB1	6-RC-1003-BB1-PRZ-1-N2-SE	Pressurizer Spray	5F	5.189	12	-678	1222.5	Cold	PZR Compartment
255	6-RC-1004-NSS	6-RC-1004-NSS-1	Pressurizer SRV Line	5H*	5.189	5.95	-721.01	1202.7	Cold	PZR Compartment
256	6-RC-1004-NSS	6-RC-1004-NSS-2	Pressurizer SRV Line	5E	5.189	5.59	-723.61	1208.62	Cold	PZR Compartment
257	6-RC-1004-NSS	6-RC-1004-NSS-3	Pressurizer SRV Line	5E	5.189	5.59	-723.61	1227.28	Cold	PZR Compartment
258	6-RC-1004-NSS	6-RC-1004-NSS-4	Pressurizer SRV Line	5E	5.189	20.1	-711	1227.27	Cold	PZR Compartment
259	6-RC-1004-NSS	6-RC-1004-NSS-5	Pressurizer SRV Line	5A	5.189	20.1	-711	1222.1	Cold	PZR Compartment
260	6-RC-1004-NSS	6-RC-1004-NSS-6	Pressurizer SRV Line	5A	5.189	23.31	-729.95	1222.1	Cold	PZR Compartment
261	6-RC-1004-NSS	6-RC-1004-NSS-7	Pressurizer SRV Line	5A	5.189	23.31	-729.95	1232.5	Cold	PZR Compartment
262	6-RC-1004-NSS	6-RC-1004-NSS-PRZ-1-N3-SE	Pressurizer SRV Line	5F	5.189	5.95	-721.01	1202.7	Cold	PZR Compartment
263	6-RC-1009-NSS	6-RC-1009-NSS-1	Pressurizer SRV Line	5H*	5.189	49.17	-702.14	1206.45	Cold	PZR Compartment
264	6-RC-1009-NSS	6-RC-1009-NSS-2	Pressurizer SRV Line	5E	5.189	51.2	-703.46	1212.19	Cold	PZR Compartment
265	6-RC-1009-NSS	6-RC-1009-NSS-3	Pressurizer SRV Line	5E	5.189	51.2	-703.46	1232.45	Cold	PZR Compartment
266	6-RC-1009-NSS	6-RC-1009-NSS-4	Pressurizer SRV Line	5E	5.189	48.64	-686.29	1232.47	Cold	PZR Compartment
267	6-RC-1009-NSS	6-RC-1009-NSS-5	Pressurizer SRV Line	5A	5.189	48.64	-686.29	1220.3	Cold	PZR Compartment
268	6-RC-1009-NSS	6-RC-1009-NSS-6	Pressurizer SRV Line	5A	5.189	53.56	-679.99	1212.3	Cold	PZR Compartment
269	6-RC-1009-NSS	6-RC-1009-NSS-7	Pressurizer SRV Line	5A	5.189	59.03	-672.99	1212.3	Cold	PZR Compartment
270	6-RC-1009-NSS	6-RC-1009-NSS-8	Pressurizer SRV Line	5A	5.189	63.95	-666.69	1220.3	Cold	PZR Compartment
271	6-RC-1009-NSS	6-RC-1009-NSS-9	Pressurizer SRV Line	5A	5.189	63.95	-666.69	1232.3	Cold	PZR Compartment
272	6-RC-1009-NSS	6-RC-1009-NSS-PRZ-1-N4C-SE	Pressurizer SRV Line	5F	5.189	49.32	-702.24	1206.63	Cold	PZR Compartment
273	6-RC-1012-NSS	6-RC-1012-NSS-1	Pressurizer SRV Line	5H*	5.189	49.79	-654.39	1205.31	Cold	PZR Compartment
274	6-RC-1012-NSS	6-RC-1012-NSS-2	Pressurizer SRV Line	5E	5.189	51.78	-653.15	1210.97	Cold	PZR Compartment
275	6-RC-1012-NSS	6-RC-1012-NSS-3	Pressurizer SRV Line	5E	5.189	51.78	-653.15	1216.43	Cold	PZR Compartment
276	6-RC-1012-NSS	6-RC-1012-NSS-4	Pressurizer SRV Line	5E	5.189	47.03	-652.31	1223.77	Cold	PZR Compartment
277	6-RC-1012-NSS	6-RC-1012-NSS-5	Pressurizer SRV Line	5E	5.189	8.75	-645.56	1240.59	Cold	PZR Compartment
278	6-RC-1012-NSS	6-RC-1012-NSS-6	Pressurizer SRV Line	5E	5.189	5.62	-645.01	1241.25	Cold	PZR Compartment
279	6-RC-1012-NSS	6-RC-1012-NSS-7	Pressurizer SRV Line	5A	5.189	-2.85	-643.51	1241.25	Cold	PZR Compartment
280	6-RC-1012-NSS	6-RC-1012-NSS-8	Pressurizer SRV Line	5A	5.189	-10.72	-642.13	1233.25	Cold	PZR Compartment
281	6-RC-1012-NSS	6-RC-1012-NSS-9	Pressurizer SRV Line	5A	5.189	-10.72	-642.13	1222.53	Cold	PZR Compartment
282	6-RC-1012-NSS	6-RC-1012-NSS-10	Pressurizer SRV Line	5A	5.189	0.69	-626.05	1222.52	Cold	PZR Compartment
283	6-RC-1012-NSS	6-RC-1012-NSS-11	Pressurizer SRV Line	5A	5.189	0.69	-626.05	1225.38	Cold	PZR Compartment
284	6-RC-1012-NSS	6-RC-1012-NSS-PRZ-1-N4B-SE	Pressurizer SRV Line	5F	5.189	49.64	-654.48	1205.13	Cold	PZR Compartment
285	6-RC-1015-NSS	6-RC-1015-NSS-1	Pressurizer PORV Line	5E	5.189	5.6	-635.02	1202.71	Cold	PZR Compartment

No.	Line Number	Location Name	System	Category	Pipe ID	X	Y	Z	Side	Compartment
286	6-RC-1015-NSS	6-RC-1015-NSS-2	Pressurizer PORV Line	5E	5.189	5.23	-632.42	1208.64	Cold	PZR Compartment
287	6-RC-1015-NSS	6-RC-1015-NSS-3	Pressurizer PORV Line	5E	5.189	5.23	-632.42	1217.93	Cold	PZR Compartment
288	6-RC-1015-NSS	6-RC-1015-NSS-4	Pressurizer PORV Line	5E	5.189	6.35	-640.34	1225.93	Cold	PZR Compartment
289	6-RC-1015-NSS	6-RC-1015-NSS-5	Pressurizer PORV Line	5E	5.189	7.58	-649.1	1225.93	Cold	PZR Compartment
290	6-RC-1015-NSS	6-RC-1015-NSS-6	Pressurizer PORV Line	5E	5.189	5.96	-655.14	1225.93	Cold	PZR Compartment
291	6-RC-1015-NSS	6-RC-1015-NSS-7	Pressurizer PORV Line	5E	5.189	2.1	-660.08	1225.93	Cold	PZR Compartment
292	6-RC-1015-NSS	6-RC-1015-NSS-8	Pressurizer PORV Line	5E	5.189	-2.84	-666.4	1233.93	Cold	PZR Compartment
293	6-RC-1015-NSS	6-RC-1015-NSS-9	Pressurizer PORV Line	5E	5.189	-2.84	-666.4	1240.98	Cold	PZR Compartment
294	6-RC-1015-NSS	6-RC-1015-NSS-10	Pressurizer PORV Line	5E	5.189	-6.91	-663.22	1248.46	Cold	PZR Compartment
295	6-RC-1015-NSS	6-RC-1015-NSS-11	Pressurizer PORV Line	5E	5.189	-30.76	-644.59	1259.94	Cold	PZR Compartment
296	6-RC-1015-NSS	6-RC-1015-NSS-12	Pressurizer PORV Line	5E	5.189	-38.88	-645.87	1262.06	Cold	PZR Compartment
297	6-RC-1015-NSS	6-RC-1015-NSS-13	Pressurizer PORV Line	5E	5.189	-40.72	-648.23	1262.06	Cold	PZR Compartment
298	6-RC-1015-NSS	6-RC-1015-NSS-14	Pressurizer PORV Line	5E	5.189	-31.49	-636.41	1262.06	Cold	PZR Compartment
299	6-RC-1015-NSS	6-RC-1015-NSS-15	Pressurizer PORV Line	5E	5.189	-29.64	-634.05	1262.06	Cold	PZR Compartment
300	6-SI-1108-BB1	6-SI-1108-BB1-1	SI	7H	5.189	-394.51	-458.32	483	Hot	Annulus
301	6-SI-1108-BB1	6-SI-1108-BB1-2	SI	7H	5.189	-390.98	-461.85	483	Hot	Annulus
302	6-SI-1108-BB1	6-SI-1108-BB1-3	SI	7H	5.189	-376.83	-461.85	483	Hot	Annulus
303	6-SI-1108-BB1	6-SI-1108-BB1-4	SI	7H	5.189	-337.24	-422.26	483	Hot	SG Compartment
304	6-SI-1111-BB1	6-SI-1111-BB1-1	SI	7H	5.189	-401.01	-237.72	231.01	Cold	Below SG Compartment
305	6-SI-1111-BB1	6-SI-1111-BB1-2	SI	7H	5.189	-401.01	-230.38	231.01	Cold	Below SG Compartment
306	6-SI-1208-BB1	6-SI-1208-BB1-1	SI	7H	5.189	-374.64	478.19	483	Hot	Annulus
307	6-SI-1208-BB1	6-SI-1208-BB1-2	SI	7H	5.189	-378.18	474.65	483	Hot	Annulus
308	6-SI-1208-BB1	6-SI-1208-BB1-3	SI	7H	5.189	-378.18	460.51	483	Hot	Annulus
309	6-SI-1208-BB1	6-SI-1208-BB1-4	SI	7H	5.189	-338.58	420.91	483	Hot	SG Compartment
310	6-SI-1211-BB1	6-SI-1211-BB1-1	SI	7H	5.189	-392.04	236.38	231.01	Cold	Below SG Compartment
311	6-SI-1211-BB1	6-SI-1211-BB1-2	SI	7H	5.189	-392.04	229.38	231.01	Cold	Below SG Compartment
312	6-SI-1308-BB1	6-SI-1308-BB1-1	RH	7H	5.189	514	146.37	230.92	Cold	RHR Compartment
313	6-SI-1308-BB1	6-SI-1308-BB1-2	RH	7H	5.189	454.5	146.37	230.92	Cold	Below SG Compartment
314	6-SI-1308-BB1	6-SI-1308-BB1-3	RH	7H	5.189	446.5	154.37	230.92	Cold	Below SG Compartment
315	6-SI-1308-BB1	6-SI-1308-BB1-4	RH	7H	5.189	446.5	164.37	230.92	Cold	Below SG Compartment
316	6-SI-1327-BB1	6-SI-1327-BB1-1	SI	7H	5.189	407.93	305.38	491.92	Hot	SG Compartment
317	6-SI-1327-BB1	6-SI-1327-BB1-2	SI	7H	5.189	407.9	315.13	491.92	Hot	SG Compartment
318	6-SI-1327-BB1	6-SI-1327-BB1-3	SI	7H	5.189	404.5	323.62	491.92	Hot	SG Compartment
319	6-SI-1327-BB1	6-SI-1327-BB1-4	SI	7H	5.189	371.97	356.14	491.92	Hot	SG Compartment
320	6-SI-1327-BB1	6-SI-1327-BB1-5	SI	7H	5.189	357.12	370.99	491.92	Hot	SG Compartment
321	6-SI-1327-BB1	6-SI-1327-BB1-6	SI	7H	5.189	357.12	379.48	491.92	Hot	SG Compartment
322	6-SI-1327-BB1	6-SI-1327-BB1-7	SI	7H	5.189	363.49	385.84	491.92	Hot	SG Compartment
323	8-RC-1114-BB1	8-RC-1114-BB1-1	SI	7B	6.813	-148.4	-233.45	483	Hot	SG Compartment
324	8-RC-1114-BB1	8-RC-1114-BB1-2	SI	7B	6.813	-134.97	-220.01	483	Hot	SG Compartment
325	8-RC-1114-BB1	8-RC-1114-BB1-3	SI	7B	6.813	-126.48	-211.52	495	Hot	SG Compartment
326	8-RC-1114-BB1	8-RC-1114-BB1-4	SI	7G	6.813	-126.48	-211.52	510	Hot	SG Compartment

No.	Line Number	Location Name	System	Category	Pipe ID	X	Y	Z	Side	Compartment
327	8-RC-1114-BB1	8-RC-1114-BB1-5	SI	7G	6.813	-115.35	-216.02	522	Hot	SG Compartment
328	8-RC-1114-BB1	8-RC-1114-BB1-6	SI	7G	6.813	-107.94	-219.02	522	Hot	SG Compartment
329	8-RC-1214-BB1	8-RC-1214-BB1-1	SI	7B	6.813	-149.63	231.95	483	Hot	SG Compartment
330	8-RC-1214-BB1	8-RC-1214-BB1-2	SI	7B	6.813	-136.91	219.23	483	Hot	SG Compartment
331	8-RC-1214-BB1	8-RC-1214-BB1-3	SI	7B	6.813	-128.42	210.74	495	Hot	SG Compartment
332	8-RC-1214-BB1	8-RC-1214-BB1-4	SI	7G	6.813	-128.42	210.74	510	Hot	SG Compartment
333	8-RC-1214-BB1	8-RC-1214-BB1-5	SI	7G	6.813	-117.29	215.24	522	Hot	SG Compartment
334	8-RC-1214-BB1	8-RC-1214-BB1-6	SI	7G	6.813	-109.12	218.54	522	Hot	SG Compartment
335	8-RC-1324-BB1	8-RC-1324-BB1-1	SI	7B	6.813	169.39	227.71	492	Hot	SG Compartment
336	8-RC-1324-BB1	8-RC-1324-BB1-2	SI	7B	6.813	160.91	219.23	492	Hot	SG Compartment
337	8-RC-1324-BB1	8-RC-1324-BB1-3	SI	7B	6.813	152.42	210.74	504	Hot	SG Compartment
338	8-RC-1324-BB1	8-RC-1324-BB1-4	SI	7G	6.813	152.42	210.74	510	Hot	SG Compartment
339	8-RC-1324-BB1	8-RC-1324-BB1-5	SI	7G	6.813	141.31	215.23	522	Hot	SG Compartment
340	8-RC-1324-BB1	8-RC-1324-BB1-6	SI	7G	6.813	133.12	218.54	522	Hot	SG Compartment
341	8-RH-1108-BB1	8-RH-1108-BB1-1	RH	7G	6.813	-438	-221.37	231.01	Cold	Below SG Compartment
342	8-RH-1108-BB1	8-RH-1108-BB1-2	RH	7G	6.813	-422.5	-221.37	231.01	Cold	Below SG Compartment
343	8-RH-1112-BB1	8-RH-1112-BB1-1	RH	7G	6.813	-375.82	-358.25	483.01	Hot	SG Compartment
344	8-RH-1112-BB1	8-RH-1112-BB1-1A	RH	7G	6.813	-333.39	-400.68	483.01	Hot	SG Compartment
345	8-RH-1112-BB1	8-RH-1112-BB1-2	RH	7G	6.813	-327.03	-407.04	483.01	Hot	SG Compartment
346	8-RH-1208-BB1	8-RH-1208-BB1-1	RH	7G	6.813	-438	221.38	231.01	Cold	Below SG Compartment
347	8-RH-1208-BB1	8-RH-1208-BB1-2	RH	7G	6.813	-422.5	221.38	231.01	Cold	Below SG Compartment
348	8-RH-1212-BB1	8-RH-1212-BB1-1	RH	7G	6.813	-367.47	369.22	483.01	Hot	SG Compartment
349	8-RH-1212-BB1	8-RH-1212-BB1-2	RH	7G	6.813	-331.42	405.27	483.01	Hot	SG Compartment
350	8-RH-1308-BB1	8-RH-1308-BB1-1	RH	7G	6.813	553	170.12	230.92	Cold	RHR Compartment
351	8-RH-1308-BB1	8-RH-1308-BB1-2	RH	7G	6.813	516	170.12	230.92	Cold	RHR Compartment
352	8-RH-1315-BB1	8-RH-1315-BB1-1	RH	7G	6.813	387.53	370.28	491.92	Hot	SG Compartment
353	8-SI-1108-BB1	8-SI-1108-BB1-1	SI	7G	6.813	-337.24	-422.26	483	Hot	SG Compartment
354	8-SI-1108-BB1	8-SI-1108-BB1-2	SI	7G	6.813	-328.77	-413.79	483	Hot	SG Compartment
355	8-SI-1108-BB1	8-SI-1108-BB1-3	SI	7G	6.813	-320.28	-405.3	483	Hot	SG Compartment
356	8-SI-1108-BB1	8-SI-1108-BB1-4	SI	7G	6.813	-177.96	-262.98	483	Hot	SG Compartment
357	8-SI-1108-BB1	8-SI-1108-BB1-5	SI	7C	6.813	-165.23	-250.25	483	Hot	SG Compartment
358	8-SI-1208-BB1	8-SI-1208-BB1-1	SI	7G	6.813	-338.58	420.91	483	Hot	SG Compartment
359	8-SI-1208-BB1	8-SI-1208-BB1-2	SI	7G	6.813	-332.83	415.17	483	Hot	SG Compartment
360	8-SI-1208-BB1	8-SI-1208-BB1-3	SI	7G	6.813	-321.52	403.85	483	Hot	SG Compartment
361	8-SI-1208-BB1	8-SI-1208-BB1-3A	SI	7G	6.813	-177.2	259.54	483	Hot	SG Compartment
362	8-SI-1208-BB1	8-SI-1208-BB1-4	SI	7C	6.813	-163.06	245.4	483	Hot	SG Compartment
363	8-SI-1327-BB1	8-SI-1327-BB1-1	SI	7G	6.813	371.97	385.84	491.92	Hot	SG Compartment
364	8-SI-1327-BB1	8-SI-1327-BB1-2	SI	7G	6.813	363.49	394.33	491.92	Hot	SG Compartment
365	8-SI-1327-BB1	8-SI-1327-BB1-3	SI	7G	6.813	358.23	399.58	491.92	Hot	SG Compartment
366	8-SI-1327-BB1	8-SI-1327-BB1-4	SI	7G	6.813	349.75	408.07	503.92	Hot	SG Compartment
367	8-SI-1327-BB1	8-SI-1327-BB1-5	SI	7G	6.813	349.75	408.07	528	Hot	SG Compartment

No.	Line Number	Location Name	System	Category	Pipe ID	X	Y	Z	Side	Compartment
368	8-SI-1327-BB1	8-SI-1327-BB1-6	SI	7G	6.813	341.26	399.58	540	Hot	SG Compartment
369	8-SI-1327-BB1	8-SI-1327-BB1-7	SI	7G	6.813	329.95	388.27	540	Hot	SG Compartment
370	8-SI-1327-BB1	8-SI-1327-BB1-8	SI	7G	6.813	321.46	379.78	528	Hot	SG Compartment
371	8-SI-1327-BB1	8-SI-1327-BB1-9	SI	7G	6.813	321.46	379.78	504	Hot	SG Compartment
372	8-SI-1327-BB1	8-SI-1327-BB1-10	SI	7G	6.813	312.98	371.3	492	Hot	SG Compartment
373	8-SI-1327-BB1	8-SI-1327-BB1-11	SI	7C	6.813	192.46	250.78	492	Hot	SG Compartment
374	10-RH-1108-BB1	10-RH-1108-BB1-1	RH	7F	8.5	-422.5	-221.38	231.01	Cold	Below SG Compartment
375	10-RH-1108-BB1	10-RH-1108-BB1-1A	RH	7F	8.5	-410.33	-221.38	231.01	Cold	Below SG Compartment
376	10-RH-1108-BB1	10-RH-1108-BB1-2	RH	7F	8.5	-404.08	-221.38	231.01	Cold	Below SG Compartment
377	10-RH-1108-BB1	10-RH-1108-BB1-3	RH	7F	8.5	-386.08	-221.38	231.01	Cold	Below SG Compartment
378	10-RH-1108-BB1	10-RH-1108-BB1-4	RH	7F	8.5	-349.7	-221.38	231.01	Cold	Below SG Compartment
379	10-RH-1108-BB1	10-RH-1108-BB1-5	RH	7F	8.5	-333.7	-221.38	247.01	Cold	Below SG Compartment
380	10-RH-1108-BB1	10-RH-1108-BB1-6	RH	7F	8.5	-333.7	-221.38	257.01	Cold	Below SG Compartment
381	10-RH-1108-BB1	10-RH-1108-BB1-7	RH	7F	8.5	-333.7	-237.38	273.01	Cold	Below SG Compartment
382	10-RH-1108-BB1	10-RH-1108-BB1-8	RH	7F	8.5	-333.7	-368.92	273.01	Cold	Below SG Compartment
383	10-RH-1108-BB1	10-RH-1108-BB1-9	RH	7F	8.5	-338.39	-380.23	273.01	Cold	Below SG Compartment
384	10-RH-1108-BB1	10-RH-1108-BB1-10	RH	7F	8.5	-342.19	-384.03	273.01	Cold	Below SG Compartment
385	10-RH-1208-BB1	10-RH-1208-BB1-1	RH	7F	8.5	-422.5	221.38	231.01	Cold	Below SG Compartment
386	10-RH-1208-BB1	10-RH-1208-BB1-2	RH	7F	8.5	-407.7	221.38	231.01	Cold	Below SG Compartment
387	10-RH-1208-BB1	10-RH-1208-BB1-3	RH	7F	8.5	-395.7	221.38	231.01	Cold	Below SG Compartment
388	10-RH-1208-BB1	10-RH-1208-BB1-4	RH	7F	8.5	-349.7	221.38	231.01	Cold	Below SG Compartment
389	10-RH-1208-BB1	10-RH-1208-BB1-5	RH	7F	8.5	-333.7	221.38	247.01	Cold	Below SG Compartment
390	10-RH-1208-BB1	10-RH-1208-BB1-6	RH	7F	8.5	-333.7	221.38	257.01	Cold	Below SG Compartment
391	10-RH-1208-BB1	10-RH-1208-BB1-7	RH	7F	8.5	-333.7	237.38	273.01	Cold	Below SG Compartment
392	10-RH-1208-BB1	10-RH-1208-BB1-8	RH	7F	8.5	-333.7	327.46	273.01	Cold	Below SG Compartment
393	10-RH-1208-BB1	10-RH-1208-BB1-9	RH	7F	8.5	-333.7	352.87	273.01	Cold	Below SG Compartment
394	10-RH-1208-BB1	10-RH-1208-BB1-10	RH	7F	8.5	-338.39	364.09	273.01	Cold	Below SG Compartment
395	10-RH-1208-BB1	10-RH-1208-BB1-11	RH	7F	8.5	-346.46	372.16	273.01	Cold	Below SG Compartment
396	10-RH-1308-BB1	10-RH-1308-BB1-1	RH	7F	8.5	510	170.12	230.92	Cold	RHR Compartment
397	10-RH-1308-BB1	10-RH-1308-BB1-2	RH	7F	8.5	455.5	170.12	230.92	Cold	Below SG Compartment
398	10-RH-1308-BB1	10-RH-1308-BB1-3	RH	7F	8.5	437.5	170.12	230.92	Cold	Below SG Compartment
399	10-RH-1308-BB1	10-RH-1308-BB1-4	RH	7F	8.5	433	170.12	230.92	Cold	Below SG Compartment
400	10-RH-1308-BB1	10-RH-1308-BB1-5	RH	7F	8.5	417	186.12	230.92	Cold	Below SG Compartment
401	10-RH-1308-BB1	10-RH-1308-BB1-6	RH	7F	8.5	417	331.73	230.92	Cold	Below SG Compartment
402	10-RH-1308-BB1	10-RH-1308-BB1-7	RH	7F	8.5	401	347.73	230.92	Cold	Below SG Compartment
403	10-RH-1308-BB1	10-RH-1308-BB1-8	RH	7F	8.5	345	347.73	230.92	Cold	Below SG Compartment
404	12-RC-1112-BB1	12-RC-1112-BB1-1	RHR-Suction	7E	10.126	-63.57	-236.94	503.31	Hot	SG Compartment
405	12-RC-1112-BB1	12-RC-1112-BB1-2	RHR-Suction	7A	10.126	-53.99	-240.81	492.97	Hot	SG Compartment
406	12-RC-1112-BB1	12-RC-1112-BB1-3	RHR-Suction	7A	10.126	-49.64	-242.57	481.66	Hot	SG Compartment
407	12-RC-1112-BB1	12-RC-1112-BB1-4	RHR-Suction	7A	10.126	-49.64	-242.57	472.04	Hot	SG Compartment
408	12-RC-1112-BB1	12-RC-1112-BB1-5	RHR-Suction	7A	10.126	-38.33	-253.88	456.04	Hot	SG Compartment

No.	Line Number	Location Name	System	Category	Pipe ID	X	Y	Z	Side	Compartment
409	12-RC-1112-BB1	12-RC-1112-BB1-6	RHR-Suction	7A	10.126	-22.7	-269.51	456.04	Hot	SG Compartment
410	12-RC-1112-BB1	12-RC-1112-BB1-7	RHR-Suction	7A	10.126	-18.02	-280.82	456.04	Hot	SG Compartment
411	12-RC-1112-BB1	12-RC-1112-BB1-8	RHR-Suction	7A	10.126	-18.02	-438	456.04	Hot	SG Compartment
412	12-RC-1112-BB1	12-RC-1112-BB1-9	RHR-Suction	7E	10.126	-18.02	-485	456.04	Hot	SG Compartment
413	12-RC-1112-BB1	12-RC-1112-BB1-10	RHR-Suction	7E	10.126	-34.02	-501	456.04	Hot	SG Compartment
414	12-RC-1112-BB1	12-RC-1112-BB1-11	RHR-Suction	7E	10.126	-78.02	-501	456.04	Hot	SG Compartment
415	12-RC-1125-BB1	12-RC-1125-BB1-1	SI-ACC-CL1	7N	10.126	-317.4	-428.18	273.02	Cold	Below SG Compartment
416	12-RC-1125-BB1	12-RC-1125-BB1-2	SI-ACC-CL1	7N	10.126	-299.02	-446.57	273.02	Cold	Below SG Compartment
417	12-RC-1125-BB1	12-RC-1125-BB1-3	SI-ACC-CL1	7N	10.126	-276.39	-446.57	273.02	Cold	Below SG Compartment
418	12-RC-1125-BB1	12-RC-1125-BB1-4	SI-ACC-CL1	7N	10.126	-250.93	-421.11	273.02	Cold	Below SG Compartment
419	12-RC-1125-BB1	12-RC-1125-BB1-5	SI-ACC-CL1	7N	10.126	-250.93	-398.49	273.02	Cold	Below SG Compartment
420	12-RC-1125-BB1	12-RC-1125-BB1-6	SI-ACC-CL1	7N	10.126	-293.63	-355.79	273.02	Cold	Below SG Compartment
421	12-RC-1125-BB1	12-RC-1125-BB1-7	SI-ACC-CL1	7N	10.126	-304.94	-344.48	289.02	Cold	Below SG Compartment
422	12-RC-1125-BB1	12-RC-1125-BB1-8	SI-ACC-CL1	7N	10.126	-304.94	-344.48	428.2	Cold	SG Compartment
423	12-RC-1125-BB1	12-RC-1125-BB1-9	SI-ACC-CL1	7N	10.126	-304.94	-344.48	532.2	Cold	SG Compartment
424	12-RC-1125-BB1	12-RC-1125-BB1-10	SI-ACC-CL1	7N	10.126	-293.63	-333.17	548.2	Cold	SG Compartment
425	12-RC-1125-BB1	12-RC-1125-BB1-11	SI-ACC-CL1	7N	10.126	-220.44	-259.98	548.2	Cold	SG Compartment
426	12-RC-1125-BB1	12-RC-1125-BB1-12	SI-ACC-CL1	7N	10.126	-215.3	-248.6	546.6	Cold	SG Compartment
427	12-RC-1125-BB1	12-RC-1125-BB1-13	SI-ACC-CL1	7N	10.126	-213.67	-194.95	533.24	Cold	SG Compartment
428	12-RC-1212-BB1	12-RC-1212-BB1-1	RHR-Suction	7E	10.126	-60.71	238.07	500.23	Hot	SG Compartment
429	12-RC-1212-BB1	12-RC-1212-BB1-2	RHR-Suction	7A	10.126	-52.9	241.23	491.81	Hot	SG Compartment
430	12-RC-1212-BB1	12-RC-1212-BB1-3	RHR-Suction	7A	10.126	-49.64	242.54	483.33	Hot	SG Compartment
431	12-RC-1212-BB1	12-RC-1212-BB1-4	RHR-Suction	7A	10.126	-49.64	242.54	468.01	Hot	SG Compartment
432	12-RC-1212-BB1	12-RC-1212-BB1-5	RHR-Suction	7A	10.126	-41.17	251.02	456.01	Hot	SG Compartment
433	12-RC-1212-BB1	12-RC-1212-BB1-6	RHR-Suction	7A	10.126	-21.52	270.67	456.01	Hot	SG Compartment
434	12-RC-1212-BB1	12-RC-1212-BB1-7	RHR-Suction	7A	10.126	-18.01	279.07	456.01	Hot	SG Compartment
435	12-RC-1212-BB1	12-RC-1212-BB1-8	RHR-Suction	7A	10.126	-18.01	414.99	456.01	Hot	SG Compartment
436	12-RC-1221-BB1	12-RC-1221-BB1-1	SI-ACC-CL2	7N	10.126	-317.4	427.95	273.01	Cold	Below SG Compartment
437	12-RC-1221-BB1	12-RC-1221-BB1-2	SI-ACC-CL2	7N	10.126	-299.05	446.3	273.01	Cold	Below SG Compartment
438	12-RC-1221-BB1	12-RC-1221-BB1-3	SI-ACC-CL2	7N	10.126	-276.39	446.34	273.01	Cold	Below SG Compartment
439	12-RC-1221-BB1	12-RC-1221-BB1-4	SI-ACC-CL2	7N	10.126	-250.93	420.88	273.01	Cold	Below SG Compartment
440	12-RC-1221-BB1	12-RC-1221-BB1-5	SI-ACC-CL2	7N	10.126	-250.93	398.26	273.01	Cold	Below SG Compartment
441	12-RC-1221-BB1	12-RC-1221-BB1-6	SI-ACC-CL2	7N	10.126	-293.63	355.56	273.01	Cold	Below SG Compartment
442	12-RC-1221-BB1	12-RC-1221-BB1-7	SI-ACC-CL2	7N	10.126	-304.94	344.25	289.01	Cold	Below SG Compartment
443	12-RC-1221-BB1	12-RC-1221-BB1-8	SI-ACC-CL2	7N	10.126	-304.94	344.25	410.59	Cold	SG Compartment
444	12-RC-1221-BB1	12-RC-1221-BB1-9	SI-ACC-CL2	7N	10.126	-304.94	344.25	532.17	Cold	SG Compartment
445	12-RC-1221-BB1	12-RC-1221-BB1-10	SI-ACC-CL2	7N	10.126	-293.63	332.94	548.17	Cold	SG Compartment
446	12-RC-1221-BB1	12-RC-1221-BB1-11	SI-ACC-CL2	7N	10.126	-260.97	300.28	548.17	Cold	SG Compartment
447	12-RC-1221-BB1	12-RC-1221-BB1-12	SI-ACC-CL2	7N	10.126	-221.77	261.08	548.17	Cold	SG Compartment
448	12-RC-1221-BB1	12-RC-1221-BB1-13	SI-ACC-CL2	7N	10.126	-216.79	249.88	546.57	Cold	SG Compartment
449	12-RC-1221-BB1	12-RC-1221-BB1-14	SI-ACC-CL2	7N	10.126	-215.13	196.36	533.24	Cold	SG Compartment

No.	Line Number	Location Name	System	Category	Pipe ID	X	Y	Z	Side	Compartment
450	12-RC-1312-BB1	12-RC-1312-BB1-1	RH	7E	10.126	84.95	238	500.48	Hot	SG Compartment
451	12-RC-1312-BB1	12-RC-1312-BB1-2	RH	7A	10.126	76.9	241.25	491.8	Hot	SG Compartment
452	12-RC-1312-BB1	12-RC-1312-BB1-3	RH	7A	10.126	73.64	242.57	483.31	Hot	SG Compartment
453	12-RC-1312-BB1	12-RC-1312-BB1-4	RH	7A	10.126	73.64	242.57	468	Hot	SG Compartment
454	12-RC-1312-BB1	12-RC-1312-BB1-5	RH	7A	10.126	65.16	251.06	456	Hot	SG Compartment
455	12-RC-1312-BB1	12-RC-1312-BB1-6	RH	7A	10.126	45.51	270.7	456	Hot	SG Compartment
456	12-RC-1312-BB1	12-RC-1312-BB1-7	RH	7A	10.126	42	279.18	456	Hot	SG Compartment
457	12-RC-1312-BB1	12-RC-1312-BB1-8	RH	7A	10.126	42	386.95	456	Hot	SG Compartment
458	12-RC-1312-BB1	12-RC-1312-BB1-9	RH	7E	10.126	42	487.69	456	Hot	SG Compartment
459	12-RC-1312-BB1	12-RC-1312-BB1-10	RH	7E	10.126	54	499.69	456	Hot	SG Compartment
460	12-RC-1312-BB1	12-RC-1312-BB1-11	RH	7E	10.126	199.56	499.69	456	Hot	SG Compartment
461	12-RC-1322-BB1	12-RC-1322-BB1-1	SI-ACC-CL3	7N	10.126	283.34	302.01	548.18	Cold	SG Compartment
462	12-RC-1322-BB1	12-RC-1322-BB1-1A	SI-ACC-CL3	7N	10.126	260.67	279.34	548.18	Cold	SG Compartment
463	12-RC-1322-BB1	12-RC-1322-BB1-2	SI-ACC-CL3	7N	10.126	242.84	261.51	548.18	Cold	SG Compartment
464	12-RC-1322-BB1	12-RC-1322-BB1-3	SI-ACC-CL3	7N	10.126	238	249.97	546.51	Cold	SG Compartment
465	12-RC-1322-BB1	12-RC-1322-BB1-4	SI-ACC-CL3	7N	10.126	238	196.66	533.24	Cold	SG Compartment
466	12-RH-1101-BB1	12-RH-1101-BB1-1	RH	7E	10.126	-108.02	-501	455.7	Hot	SG Compartment
467	12-RH-1101-BB1	12-RH-1101-BB1-2	RH	7E	10.126	-226.24	-501	455.83	Hot	SG Compartment
468	12-RH-1101-BB1	12-RH-1101-BB1-3	RH	7E	10.126	-237.38	-496.32	455.84	Hot	SG Compartment
469	12-RH-1101-BB1	12-RH-1101-BB1-3A	RH	7E	10.126	-328.79	-404.91	455.94	Hot	SG Compartment
470	12-RH-1101-BB1	12-RH-1101-BB1-4	RH	7E	10.126	-372.86	-360.84	455.99	Hot	SG Compartment
471	12-RH-1101-BB1	12-RH-1101-BB1-5	RH	7E	10.126	-408.95	-324.75	456.03	Hot	SG Compartment
472	12-RH-1101-BB1	12-RH-1101-BB1-6	RH	7E	10.126	-413.64	-313.53	456.04	Hot	SG Compartment
473	12-RH-1101-BB1	12-RH-1101-BB1-7	RH	7E	10.126	-413.64	-255.38	456.04	Hot	SG Compartment
474	12-RH-1101-BB1	12-RH-1101-BB1-8	RH	7E	10.126	-429.64	-239.38	456.05	Hot	SG Compartment
475	12-RH-1101-BB1	12-RH-1101-BB1-9	RH	7E	10.126	-479.81	-239.37	456.11	Hot	SG Compartment
476	12-RH-1101-BB1	12-RH-1101-BB1-10	RH	7E	10.126	-571.54	-239.38	456.21	Hot	RHR Compartment
477	12-RH-1101-BB1	12-RH-1101-BB1-11	RH	7E	10.126	-587.53	-239.38	440.23	Hot	RHR Compartment
478	12-RH-1101-BB1	12-RH-1101-BB1-12	RH	7E	10.126	-587.61	-239.38	369.23	Hot	RHR Compartment
479	12-RH-1101-BB1	12-RH-1101-BB1-13	RH	7E	10.126	-587.77	-239.38	225.23	Hot	RHR Compartment
480	12-RH-1101-BB1	12-RH-1101-BB1-14	RH	7E	10.126	-587.85	-239.38	149.71	Hot	RHR Compartment
481	12-RH-1101-BB1	12-RH-1101-BB1-15	RH	7E	10.126	-587.87	-223.38	129.04	Hot	RHR Compartment
482	12-RH-1101-BB1	12-RH-1101-BB1-16	RH	7E	10.126	-587.87	-190.38	129.04	Hot	RHR Compartment
483	12-RH-1201-BB1	12-RH-1201-BB1-1	RH	7E	10.126	-18.01	453.99	456.01	Hot	SG Compartment
484	12-RH-1201-BB1	12-RH-1201-BB1-2	RH	7E	10.126	-18.01	485.99	456.01	Hot	SG Compartment
485	12-RH-1201-BB1	12-RH-1201-BB1-3	RH	7E	10.126	-34.01	501.99	456.01	Hot	SG Compartment
486	12-RH-1201-BB1	12-RH-1201-BB1-4	RH	7E	10.126	-226.44	501.99	456.01	Hot	SG Compartment
487	12-RH-1201-BB1	12-RH-1201-BB1-5	RH	7E	10.126	-237.76	497.31	456.01	Hot	SG Compartment
488	12-RH-1201-BB1	12-RH-1201-BB1-6	RH	7E	10.126	-323.53	411.53	456.01	Hot	SG Compartment
489	12-RH-1201-BB1	12-RH-1201-BB1-7	RH	7E	10.126	-409.38	325.69	456.01	Hot	SG Compartment
490	12-RH-1201-BB1	12-RH-1201-BB1-8	RH	7E	10.126	-414	314.43	456.01	Hot	SG Compartment

No.	Line Number	Location Name	System	Category	Pipe ID	X	Y	Z	Side	Compartment
491	12-RH-1201-BB1	12-RH-1201-BB1-9	RH	7E	10.126	-414	256.38	456.01	Hot	SG Compartment
492	12-RH-1201-BB1	12-RH-1201-BB1-10	RH	7E	10.126	-430	240.38	456.01	Hot	SG Compartment
493	12-RH-1201-BB1	12-RH-1201-BB1-11	RH	7E	10.126	-530.54	240.38	456.01	Hot	RHR Compartment
494	12-RH-1201-BB1	12-RH-1201-BB1-12	RH	7E	10.126	-588	240.38	432.01	Hot	RHR Compartment
495	12-RH-1201-BB1	12-RH-1201-BB1-13	RH	7E	10.126	-588	240.38	423.01	Hot	RHR Compartment
496	12-RH-1201-BB1	12-RH-1201-BB1-14	RH	7E	10.126	-588	240.38	237.01	Hot	RHR Compartment
497	12-RH-1201-BB1	12-RH-1201-BB1-15	RH	7E	10.126	-588	240.38	153.01	Hot	RHR Compartment
498	12-RH-1201-BB1	12-RH-1201-BB1-16	RH	7E	10.126	-588	213.12	129.01	Hot	RHR Compartment
499	12-RH-1201-BB1	12-RH-1201-BB1-17	RH	7E	10.126	-588	191.38	129.01	Hot	RHR Compartment
500	12-RH-1301-BB1	12-RH-1301-BB1-1	RH	7E	10.126	232.84	499.69	456	Hot	SG Compartment
501	12-RH-1301-BB1	12-RH-1301-BB1-2	RH	7E	10.126	251.71	499.69	456	Hot	SG Compartment
502	12-RH-1301-BB1	12-RH-1301-BB1-3	RH	7E	10.126	263.02	495	456	Hot	SG Compartment
503	12-RH-1301-BB1	12-RH-1301-BB1-4	RH	7E	10.126	441.96	316.06	456	Hot	SG Compartment
504	12-RH-1301-BB1	12-RH-1301-BB1-5	RH	7E	10.126	454.32	311.37	456	Hot	SG Compartment
505	12-RH-1301-BB1	12-RH-1301-BB1-5A	RH	7E	10.126	515.15	311.37	456	Hot	RHR Compartment
506	12-RH-1301-BB1	12-RH-1301-BB1-6	RH	7E	10.126	523.96	311.37	456	Hot	RHR Compartment
507	12-RH-1301-BB1	12-RH-1301-BB1-7	RH	7E	10.126	539.96	311.37	435	Hot	RHR Compartment
508	12-RH-1301-BB1	12-RH-1301-BB1-8	RH	7E	10.126	539.96	311.37	415	Hot	RHR Compartment
509	12-RH-1301-BB1	12-RH-1301-BB1-9	RH	7E	10.126	539.96	295.37	399	Hot	RHR Compartment
510	12-RH-1301-BB1	12-RH-1301-BB1-10	RH	7E	10.126	539.96	265.37	399	Hot	RHR Compartment
511	12-SI-1125-BB1	12-SI-1125-BB1-1	SI-ACC-CL1	7O	10.126	-383.87	-361.72	273.02	Cold	Below SG Compartment
512	12-SI-1125-BB1	12-SI-1125-BB1-2	SI-ACC-CL1	7O	10.126	-364.07	-381.51	273.02	Cold	Below SG Compartment
513	12-SI-1125-BB1	12-SI-1125-BB1-3	SI-ACC-CL1	7O	10.126	-355.59	-390	273.02	Cold	Below SG Compartment
514	12-SI-1125-BB1	12-SI-1125-BB1-4	SI-ACC-CL1	7O	10.126	-344.27	-401.31	273.02	Cold	Below SG Compartment
515	12-SI-1218-BB1	12-SI-1218-BB1-1	SI-ACC-CL2	7O	10.126	-383.87	361.49	273.01	Cold	Below SG Compartment
516	12-SI-1218-BB1	12-SI-1218-BB1-2	SI-ACC-CL2	7O	10.126	-365.49	379.87	273.01	Cold	Below SG Compartment
517	12-SI-1218-BB1	12-SI-1218-BB1-3	SI-ACC-CL2	7O	10.126	-354.17	391.18	273.01	Cold	Below SG Compartment
518	12-SI-1218-BB1	12-SI-1218-BB1-4	SI-ACC-CL2	7O	10.126	-344.27	401.08	273.01	Cold	Below SG Compartment
519	12-SI-1315-BB1	12-SI-1315-BB1-1	SI-ACC-CL4	7O	10.126	366.48	385.2	191.01	Cold	Below SG Compartment
520	12-SI-1315-BB1	12-SI-1315-BB1-2	SI-ACC-CL4	7O	10.126	340.31	359.04	191.01	Cold	Below SG Compartment
521	12-SI-1315-BB1	12-SI-1315-BB1-3	SI-ACC-CL4	7O	10.126	329	347.73	207.01	Cold	Below SG Compartment
522	12-SI-1315-BB1	12-SI-1315-BB1-4	SI-ACC-CL4	7O	10.126	329	347.73	225.01	Cold	Below SG Compartment
523	12-SI-1315-BB1	12-SI-1315-BB1-5	SI-ACC-CL1	7O	10.126	329	347.73	237.01	Cold	Below SG Compartment
524	12-SI-1315-BB1	12-SI-1315-BB1-6	SI-ACC-CL4	7O	10.126	329	347.73	379.07	Cold	SG Compartment
525	12-SI-1315-BB1	12-SI-1315-BB1-7	SI-ACC-CL4	7O	10.126	329	347.73	447.73	Cold	SG Compartment
526	12-SI-1315-BB1	12-SI-1315-BB1-8	SI-ACC-CL4	7D	10.126	329	347.73	532.19	Cold	SG Compartment
527	12-SI-1315-BB1	12-SI-1315-BB1-9	SI-ACC-CL4	7D	10.126	317.69	336.41	548.19	Cold	SG Compartment
528	12-SI-1315-BB1	12-SI-1315-BB1-10	SI-ACC-CL4	7D	10.126	309.42	328.15	548.19	Cold	SG Compartment
529	16-RC-1412-NSS	16-RC-1412-NSS-1	Pressurizer Surge Line	4B	12.814	12	-678	688.5	Hot	Surge Line
530	16-RC-1412-NSS	16-RC-1412-NSS-3	Pressurizer Surge Line	4B	12.814	181.01	-678	528.97	Hot	Surge Line
531	16-RC-1412-NSS	16-RC-1412-NSS-4	Pressurizer Surge Line	4B	12.814	205	-654	528.41	Hot	Surge Line

No.	Line Number	Location Name	System	Category	Pipe ID	X	Y	Z	Side	Compartment
532	16-RC-1412-NSS	16-RC-1412-NSS-5	Pressurizer Surge Line	4B	12.814	205	-531	526.97	Hot	SG Compartment
533	16-RC-1412-NSS	16-RC-1412-NSS-6	Pressurizer Surge Line	4B	12.814	180.85	-507	526.41	Hot	SG Compartment
534	16-RC-1412-NSS	16-RC-1412-NSS-7	Pressurizer Surge Line	4B	12.814	91.98	-507	525.37	Hot	SG Compartment
535	16-RC-1412-NSS	16-RC-1412-NSS-8	Pressurizer Surge Line	4B	12.814	12	-400.56	523.22	Hot	SG Compartment
536	16-RC-1412-NSS	16-RC-1412-NSS-9	Pressurizer Surge Line	4C	12.814	89.65	-262.75	522	Hot	SG Compartment
537	16-RC-1412-NSS	16-RC-1412-NSS-PRZ-1-N1-SE	Pressurizer Surge Line	4A	12.814	12	-678	691	Hot	Surge Line
538	27.5-RC-1103-NSS - LOOP 1	27.5-RC-1103-NSS-1	RC Cold Leg 1	3C	27.5	-264.83	-202.37	522	Cold	SG Compartment
539	27.5-RC-1103-NSS - LOOP 1	27.5-RC-1103-NSS-3	RC	7I	3.438	-252.54	-190.08	541.08	Cold	SG Compartment
540	27.5-RC-1103-NSS - LOOP 1	27.5-RC-1103-NSS-4	SI-ACC-CL1	7N	10.126	-212.31	-149.85	522	Cold	SG Compartment
541	27.5-RC-1103-NSS - LOOP 1	27.5-RC-1103-NSS-5	CV	8E	3.438	-201.49	-112.07	522	Cold	SG Compartment
542	27.5-RC-1103-NSS - LOOP 1	27.5-RC-1103-NSS-6	RC Cold Leg 1	3C	27.5	-122.74	-60.28	522	Cold	RX Cavity
543	27.5-RC-1103-NSS - LOOP 1	27.5-RC-1103-NSS-7	RC Cold Leg 1	3C	27.5	-117.38	-54.92	522	Cold	RX Cavity
544	27.5-RC-1103-NSS - LOOP 1	27.5-RC-1103-NSS-RPV1-N2ASE	RC Cold Leg 1	3A	27.5	-108.79	-51.27	522	Cold	RX Cavity
545	27.5-RC-1203-NSS - LOOP 2	27.5-RC-1203-NSS-1	RC Cold Leg 2	3C	27.5	-264.83	202.37	522	Cold	SG Compartment
546	27.5-RC-1203-NSS - LOOP 2	27.5-RC-1203-NSS-3	SI-ACC-CL2	7N	10.126	-214.54	177.45	528.52	Cold	SG Compartment
547	27.5-RC-1203-NSS - LOOP 2	27.5-RC-1203-NSS-4	RC Cold Leg 2	3C	27.5	-122.74	60.28	522	Cold	RX Cavity
548	27.5-RC-1203-NSS - LOOP 2	27.5-RC-1203-NSS-5	RC Cold Leg 2	3C	27.5	-110.41	51.96	522	Cold	RX Cavity
549	27.5-RC-1203-NSS - LOOP 2	27.5-RC-1203-NSS-RPV1-N2BSE	RC Cold Leg 2	3A	27.5	-108.79	51.27	522	Cold	RX Cavity
550	27.5-RC-1303-NSS - LOOP 3	27.5-RC-1303-NSS-1	RC Cold Leg 3	3C	27.5	288.83	202.37	522	Cold	SG Compartment
551	27.5-RC-1303-NSS - LOOP 3	27.5-RC-1303-NSS-3	SI-ACC-CL3	7N	10.126	238	177.01	528.34	Cold	SG Compartment
552	27.5-RC-1303-NSS - LOOP 3	27.5-RC-1303-NSS-4	CV	8E	3.438	198.5	139	522	Cold	SG Compartment
553	27.5-RC-1303-NSS - LOOP 3	27.5-RC-1303-NSS-5	RC Cold Leg 3	3C	27.5	146.74	60.28	522	Cold	RX Cavity
554	27.5-RC-1303-NSS - LOOP 3	27.5-RC-1303-NSS-6	RC Cold Leg 3	3C	27.5	134.41	51.96	522	Cold	RX Cavity
555	27.5-RC-1303-NSS - LOOP 3	27.5-RC-1303-NSS-RPV1-N2CSE	RC Cold Leg 3	3A	27.5	132.79	51.27	522	Cold	RX Cavity
556	27.5-RC-1403-NSS - LOOP 4	27.5-RC-1403-NSS-1	RC Cold Leg 4	3C	27.5	288.83	-202.37	522	Cold	SG Compartment
557	27.5-RC-1403-NSS - LOOP 4	27.5-RC-1403-NSS-3	RC	7I	3.438	273.56	-187.1	541.06	Cold	SG Compartment
558	27.5-RC-1403-NSS - LOOP 4	27.5-RC-1403-NSS-4	RC	7I	3.438	254.15	-186.75	535.48	Cold	SG Compartment
559	27.5-RC-1403-NSS - LOOP 4	27.5-RC-1403-NSS-5	RC Cold Leg 4	3C	27.5	146.74	-60.28	522	Cold	RX Cavity
560	27.5-RC-1403-NSS - LOOP 4	27.5-RC-1403-NSS-6	RC Cold Leg 4	3C	27.5	134.41	-51.96	522	Cold	RX Cavity
561	27.5-RC-1403-NSS - LOOP 4	27.5-RC-1403-NSS-RPV1-N2DSE	RC Cold Leg 4	3A	27.5	132.79	-51.27	522	Cold	RX Cavity
562	29-RC-1101-NSS - LOOP 1	29-RC-1101-NSS-1	RC-Hot Leg 1	1B	29	-36.35	-119.66	522	Hot	RX Cavity
563	29-RC-1101-NSS - LOOP 1	29-RC-1101-NSS-2	SI	7G	6.813	-99.42	-222.46	522	Hot	SG Compartment
564	29-RC-1101-NSS - LOOP 1	29-RC-1101-NSS-3	RHR-Suction	7E	10.126	-67.51	-235.35	507.55	Hot	SG Compartment
565	29-RC-1101-NSS - LOOP 1	29-RC-1101-NSS-4	RC-Hot Leg 1	1B	29	-101.37	-280.59	522	Hot	SG Compartment
566	29-RC-1101-NSS - LOOP 1	29-RC-1101-NSS-5.1	RC-Hot Leg 1	1B	29	-115.72	-316.11	539.86	Hot	SG Compartment
567	29-RC-1101-NSS - LOOP 1	29-RC-1101-NSS-RPV1-N1ASE	RC-Hot Leg 1	1A	29	-34.1	-114.1	522	Hot	RX Cavity
568	29-RC-1101-NSS - LOOP 1	29-RC-1101-NSS-RSG-1A-IN-SE	RC-Hot Leg 1	2	29	-115.85	-316.43	540.28	Hot	SG Compartment
569	29-RC-1201-NSS - LOOP 2	29-RC-1201-NSS-1	RC-Hot Leg 2	1B	29	-36.35	119.66	522	Hot	RX Cavity
570	29-RC-1201-NSS - LOOP 2	29-RC-1201-NSS-2	SI	7G	6.813	-99.84	222.29	522	Hot	SG Compartment
571	29-RC-1201-NSS - LOOP 2	29-RC-1201-NSS-3	RC	7E	10.126	-67.5	235.33	507.55	Hot	SG Compartment
572	29-RC-1201-NSS - LOOP 2	29-RC-1201-NSS-4	RC-Hot Leg 2	1B	29	-101.37	280.59	522	Hot	SG Compartment

No.	Line Number	Location Name	System	Category	Pipe ID	X	Y	Z	Side	Compartment
573	29-RC-1201-NSS - LOOP 2	29-RC-1201-NSS-5.1	RC-Hot Leg 2	1B	29	-115.72	316.11	539.86	Hot	SG Compartment
574	29-RC-1201-NSS - LOOP 2	29-RC-1201-RPV1-N1BSE	RC-Hot Leg 2	1A	29	-34.1	114.1	522	Hot	RX Cavity
575	29-RC-1201-NSS - LOOP 2	29-RC-1201-RSG-1B-IN-SE	RC-Hot Leg 2	2	29	-115.85	316.43	540.28	Hot	SG Compartment
576	29-RC-1301-NSS - LOOP 3	29-RC-1301-NSS-1	RC-Hot Leg 3	1B	29	60.35	119.67	522	Hot	RX Cavity
577	29-RC-1301-NSS - LOOP 3	29-RC-1301-NSS-2	SI	7G	6.813	123.84	222.29	522	Hot	SG Compartment
578	29-RC-1301-NSS - LOOP 3	29-RC-1301-NSS-3	RC	7E	10.126	91.51	235.35	507.55	Hot	SG Compartment
579	29-RC-1301-NSS - LOOP 3	29-RC-1301-NSS-4	RC-Hot Leg 3	1B	29	125.37	280.6	522	Hot	SG Compartment
580	29-RC-1301-NSS - LOOP 3	29-RC-1301-NSS-5.1	RC-Hot Leg 3	1B	29	139.72	316.12	539.86	Hot	SG Compartment
581	29-RC-1301-NSS - LOOP 3	29-RC-1301-RPV1-N1CSE	RC-Hot Leg 3	1A	29	58.1	114.11	522	Hot	RX Cavity
582	29-RC-1301-NSS - LOOP 3	29-RC-1301-RSG-1C-IN-SE	RC-Hot Leg 3	2	29	139.85	316.44	540.28	Hot	SG Compartment
583	29-RC-1401-NSS - LOOP 4	29-RC-1401-NSS-1	RC-Hot Leg 4	1B	29	60.35	-119.66	522	Hot	RX Cavity
584	29-RC-1401-NSS - LOOP 4	29-RC-1401-NSS-2	Pressurizer Surge Line	4C	12.814	95.22	-260.5	522	Hot	SG Compartment
585	29-RC-1401-NSS - LOOP 4	29-RC-1401-NSS-3	RC-Hot Leg 4	1C	29	125.37	-280.59	522	Hot	SG Compartment
586	29-RC-1401-NSS - LOOP 4	29-RC-1401-NSS-4.1	RC-Hot Leg 4	1B	29	139.72	-316.11	539.86	Hot	SG Compartment
587	29-RC-1401-NSS - LOOP 4	29-RC-1401-NSS-RPV1-N1DSE	RC-Hot Leg 4	1A	29	58.1	-114.1	522	Hot	RX Cavity
588	29-RC-1401-NSS - LOOP 4	29-RC-1401-NSS-RSG-1D-IN-SE	RC-Hot Leg 4	2	29	139.85	-316.43	540.28	Hot	SG Compartment
589	31-RC-1102-NSS - LOOP 1	31-RC-1102-NSS-1.1	RC Cold Leg 1	3D	31	-195.08	-364.07	538.7	Cold	SG Compartment
590	31-RC-1102-NSS - LOOP 1	31-RC-1102-NSS-2	RC Cold Leg 1	3D	31	-206.74	-363.05	506.56	Cold	SG Compartment
591	31-RC-1102-NSS - LOOP 1	31-RC-1102-NSS-3	RC Cold Leg 1	3D	31	-206.74	-363.05	441.31	Cold	SG Compartment
592	31-RC-1102-NSS - LOOP 1	31-RC-1102-NSS-4	RC Cold Leg 1	3D	31	-234.4	-338.57	404.31	Cold	SG Compartment
593	31-RC-1102-NSS - LOOP 1	31-RC-1102-NSS-5	RC	7K*	1.689	-252	-323	425.33	Cold	SG Compartment
594	31-RC-1102-NSS - LOOP 1	31-RC-1102-NSS-6	RC	7K	1.689	-271.12	-306.08	383.29	Cold	SG Compartment
595	31-RC-1102-NSS - LOOP 1	31-RC-1102-NSS-7	RC	7J	2.626	-278.44	-299.61	425.33	Cold	SG Compartment
596	31-RC-1102-NSS - LOOP 1	31-RC-1102-NSS-8	RC Cold Leg 1	3D	31	-289.67	-289.67	404.31	Cold	SG Compartment
597	31-RC-1102-NSS - LOOP 1	31-RC-1102-NSS-9	RC Cold Leg 1	3D	31	-322.81	-260.35	448.56	Cold	SG Compartment
598	31-RC-1102-NSS - LOOP 1	31-RC-1102-NSS-RSG-1A-ON-SE	RC Cold Leg 1	3B	31	-195.04	-364.07	538.75	Cold	SG Compartment
599	31-RC-1202-NSS - LOOP 2	31-RC-1202-NSS-1.1	RC Cold Leg 2	3D	31	-195.08	364.07	538.7	Cold	SG Compartment
600	31-RC-1202-NSS - LOOP 2	31-RC-1202-NSS-2	RC Cold Leg 2	3D	31	-206.74	363.05	506.56	Cold	SG Compartment
601	31-RC-1202-NSS - LOOP 2	31-RC-1202-NSS-3	RC Cold Leg 2	3D	31	-206.74	363.05	441.31	Cold	SG Compartment
602	31-RC-1202-NSS - LOOP 2	31-RC-1202-NSS-4	RC Cold Leg 2	3D	31	-234.43	338.54	404.31	Cold	SG Compartment
603	31-RC-1202-NSS - LOOP 2	31-RC-1202-NSS-5	RC	7K	1.689	-249.25	325.43	425.33	Cold	SG Compartment
604	31-RC-1202-NSS - LOOP 2	31-RC-1202-NSS-6	RC	7J	2.626	-278.44	299.61	425.33	Cold	SG Compartment
605	31-RC-1202-NSS - LOOP 2	31-RC-1202-NSS-7	RC	7K	1.689	-271.15	306.06	383.29	Cold	SG Compartment
606	31-RC-1202-NSS - LOOP 2	31-RC-1202-NSS-8	RC Cold Leg 2	3D	31	-289.7	289.65	404.31	Cold	SG Compartment
607	31-RC-1202-NSS - LOOP 2	31-RC-1202-NSS-9	RC Cold Leg 2	3D	31	-322.81	260.35	448.56	Cold	SG Compartment
608	31-RC-1202-NSS - LOOP 2	31-RC-1202-NSS-RSG-1B-ON-SE	RC Cold Leg 2	3B	31	-195.05	364.07	538.74	Cold	SG Compartment
609	31-RC-1302-NSS - LOOP 3	31-RC-1302-NSS-1.1	RC Cold Leg 3	3D	31	219.08	364.07	538.7	Cold	SG Compartment
610	31-RC-1302-NSS - LOOP 3	31-RC-1302-NSS-2	RC Cold Leg 3	3D	31	230.74	363.05	506.56	Cold	SG Compartment
611	31-RC-1302-NSS - LOOP 3	31-RC-1302-NSS-3	RC Cold Leg 3	3D	31	230.74	363.05	441.29	Cold	SG Compartment
612	31-RC-1302-NSS - LOOP 3	31-RC-1302-NSS-4	RC Cold Leg 3	3D	31	258.45	338.53	404.31	Cold	SG Compartment
613	31-RC-1302-NSS - LOOP 3	31-RC-1302-NSS-5	RC	7K	1.689	272.81	325.82	425.33	Cold	SG Compartment

No.	Line Number	Location Name	System	Category	Pipe ID	X	Y	Z	Side	Compartment
614	31-RC-1302-NSS - LOOP 3	31-RC-1302-NSS-6	RC	7J	2.626	302.44	299.61	425.33	Cold	SG Compartment
615	31-RC-1302-NSS - LOOP 3	31-RC-1302-NSS-7	RC	7I	3.438	295.13	306.07	383.29	Cold	SG Compartment
616	31-RC-1302-NSS - LOOP 3	31-RC-1302-NSS-8	RC Cold Leg 3	3D	31	313.67	289.67	404.31	Cold	SG Compartment
617	31-RC-1302-NSS - LOOP 3	31-RC-1302-NSS-9	RC Cold Leg 3	3D	31	346.81	260.35	448.56	Cold	SG Compartment
618	31-RC-1302-NSS - LOOP 3	31-RC-1302-NSS-RSG-1C-ON-SE	RC Cold Leg 3	3B	31	219.08	364.07	538.7	Cold	SG Compartment
619	31-RC-1402-NSS - LOOP 4	31-RC-1402-NSS-1.1	RC Cold Leg 4	3D	31	219.08	-364.07	538.7	Cold	SG Compartment
620	31-RC-1402-NSS - LOOP 4	31-RC-1402-NSS-2	RC Cold Leg 4	3D	31	230.74	-363.05	506.56	Cold	SG Compartment
621	31-RC-1402-NSS - LOOP 4	31-RC-1402-NSS-3	RC Cold Leg 4	3D	31	230.74	-363.05	441.31	Cold	SG Compartment
622	31-RC-1402-NSS - LOOP 4	31-RC-1402-NSS-4	RC Cold Leg 4	3D	31	258.45	-338.53	404.31	Cold	SG Compartment
623	31-RC-1402-NSS - LOOP 4	31-RC-1402-NSS-5	RC	7K	1.689	273.37	-325.32	425.33	Cold	SG Compartment
624	31-RC-1402-NSS - LOOP 4	31-RC-1402-NSS-6	RC	7J	2.626	302.44	-299.61	425.33	Cold	SG Compartment
625	31-RC-1402-NSS - LOOP 4	31-RC-1402-NSS-7	RC	7K	1.689	295.15	-306.06	383.29	Cold	SG Compartment
626	31-RC-1402-NSS - LOOP 4	31-RC-1402-NSS-8	RC Cold Leg 4	3D	31	313.67	-289.67	404.31	Cold	SG Compartment
627	31-RC-1402-NSS - LOOP 4	31-RC-1402-NSS-9	RC Cold Leg 4	3D	31	346.81	-260.35	448.56	Cold	SG Compartment
628	31-RC-1402-NSS - LOOP 4	31-RC-1402-NSS-RSG-1D-ON-SE	RC Cold Leg 4	3B	31	219.05	-364.07	538.74	Cold	SG Compartment

5.3.3 Statistical Fit of NUREG-1829 LOCA Frequencies

NUREG-1829 provides a set of LOCA frequency uncertainties (corresponding to the 5th percentile, median, mean, and 95th percentile) for six different break sizes (½", 1-5/8", 3", 7", 14", and 31") (37). The values corresponding to each break size were fit with a bounded Johnson distribution to define the full range of epistemic uncertainty associated with LOCA frequencies (8). This is illustrated in Figure 5.3.2.

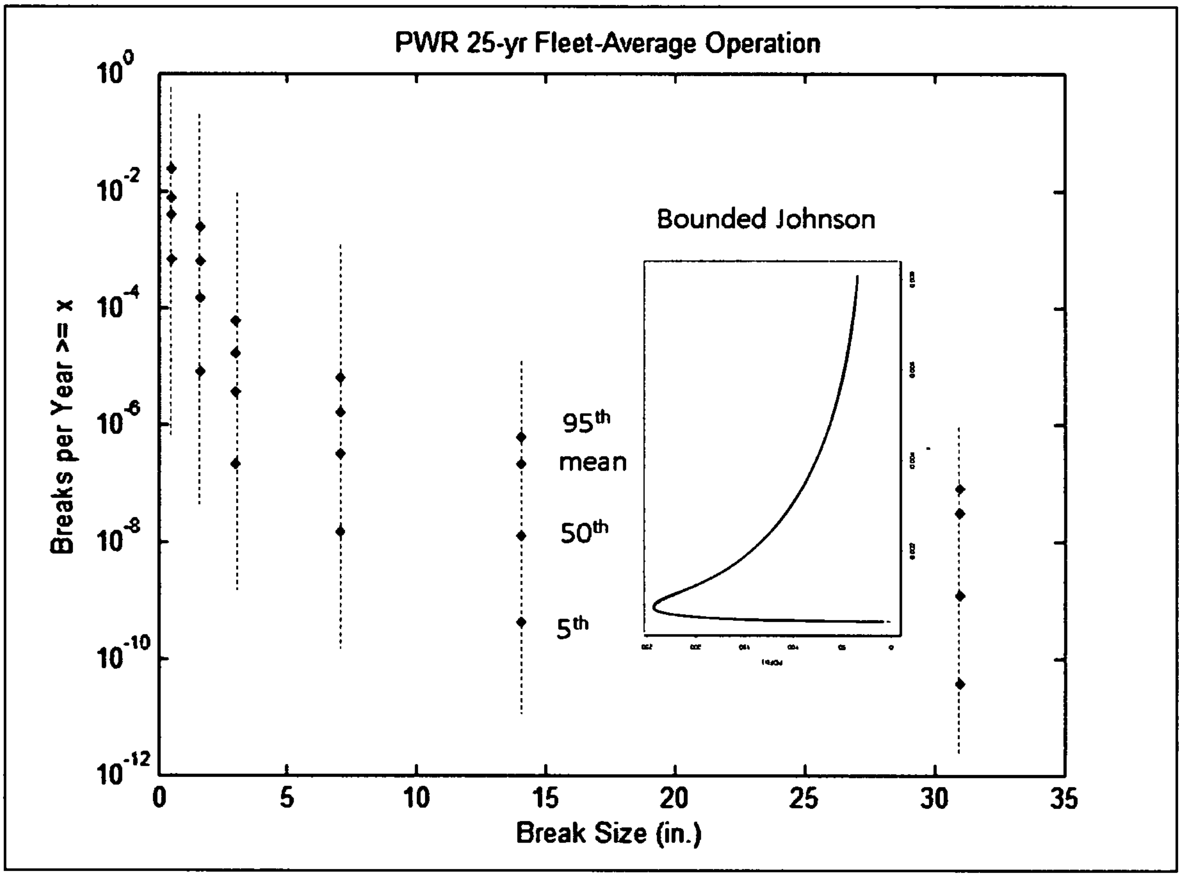

Figure 5.3.2 – Illustration of bounded Johnson fit for NUREG-1829 break frequencies

The bounded Johnson cumulative distribution function and optimization model are shown in Equation 23 and Equation 24 (8), and the fitted parameters are provided in Section 2.2.3.

$F[x] = \Phi\{\gamma + \delta f[(x - \xi)/\lambda]\}$ Equation 23 where $\Phi[x]$ is the cumulative distribution function of a standard normal random variable, γ and δ are shape parameters (with γ driving the distribution's skewness), ξ is a location parameter, λ is a scale parameter, and $f(z) = \log[z / (1-z)]$ for $\xi \le x \le \xi + \lambda$.

$$\begin{aligned} \min_{\gamma,\delta,\xi,\lambda} \quad & (F[x_{0.05}] - 0.05)^2 + (F[x_{0.50}] - 0.50)^2 + (F[x_{0.95}] - 0.95)^2 \\ \text{s.t.} \quad & \xi \le x_{0.05} \\ & \lambda + \xi \ge x_{0.95} \\ & \delta, \xi, \lambda \ge 0 \end{aligned} \qquad \text{Equation 24}$$

5.3.4 Sample Epistemic Uncertainty of LOCA Frequencies

Given the fitted distribution parameters, the epistemic uncertainty of the LOCA frequency data in NUREG-1829 can be sampled. For example, if the 62nd percentile is selected, the LOCA frequencies can be calculated based on Equation 23 and the parameters in Section 2.2.3. The calculated 62nd percentile values are shown in Table 5.3.4. Figure 5.3.3 shows the LOCA frequency vs. break size for the 62nd percentile assuming linear interpolation between the values in Table 5.3.4. (Note that the shape of the interpolated curves appears to be non-linear on a semi-log plot.)

Table 5.3.4 – Example calculation of LOCA frequencies vs. break size for 62nd Percentile

Break Size (in)	**62nd Percentile LOCA Frequencies (year^{-1})**
0.5	1.06E-03
1.625	1.66E-04
3	6.35E-06
7	5.92E-07
14	2.74E-08
31	2.89E-09

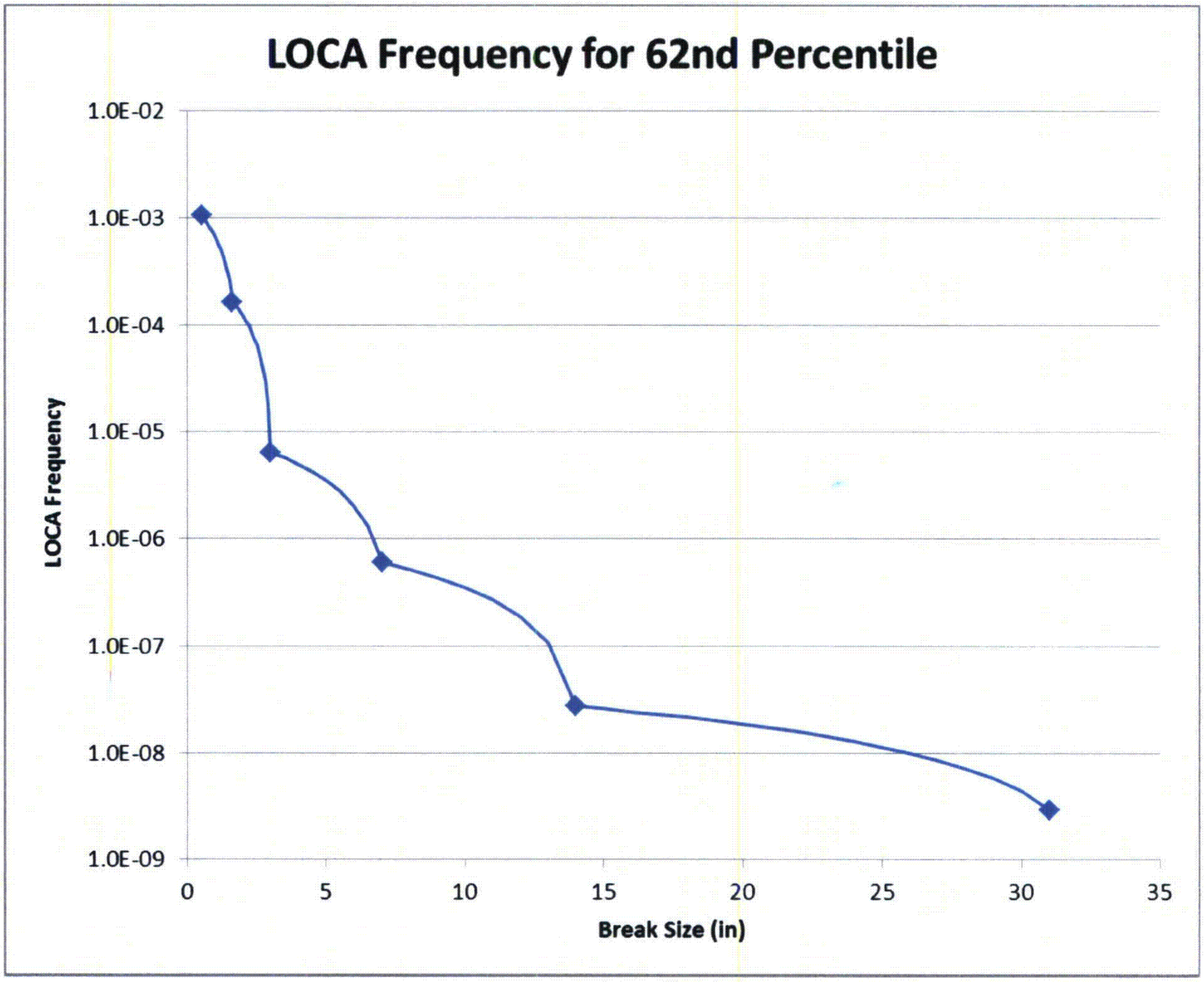

Figure 5.3.3 – Illustration of LOCA frequency vs. break size for 62nd percentile

5.3.5 Sample Break Sizes at Each Weld Location

CASA Grande evaluates multiple sizes of breaks at every weld in containment, and it always includes the DEGB condition for every weld. The total number of break scenarios investigated for each weld is determined based on user input for the maximum desired number of breaks in the largest pipe, N_L. One of these breaks is assigned to the DEGB condition, and the remaining number are selected from $N_L - 1$ strata defined across the large break size range. The range of break sizes for a given weld was subdivided into a number of intervals proportional to the range of the largest possible LBLOCA. The standard LOCA bins of 0.5 to 2 inches (SBLOCAs), 2 to 6 inches (MBLOCAs), and greater than 6 inches

(LBLOCAs) were used; so the number of breaks in the small and medium range were determined by the following formulas[19]:

$$N_S = ceil\left(\frac{2 - 0.5}{D_{max} - 6} N_L\right) \quad \text{Equation 25}$$

$$N_M = ceil\left(\frac{6 - 2}{D_{max} - 6} N_L\right) \quad \text{Equation 26}$$

where:

N_S = Number of breaks in SBLOCA category
N_M = Number of breaks in MBLOCA category
N_L = Number of breaks in LBLOCA category
D_{max} = Maximum break size in containment (in)

The ceil(x) operator simply rounds up to the nearest integer. This guarantees that there is always at least one small break and at least one medium break at every weld that can support breaks of these sizes.

Given the desired number of breaks in each LOCA category, the conditional probability for breaks in the associated weld case was divided into an equivalent number of non-uniform bins (unequal size), and the probability weights for each bin were recorded. Random percentiles were selected from each probability bin, and the conditional probability was interpolated to find corresponding break sizes. (Neither the probability bins, nor the corresponding size intervals are of equal size.) The set of discrete break sizes are matched with their probability weight and carried throughout the evaluation as independent break scenarios.

When this algorithm is applied to the STP weld population for $N_L = 10$, the total number of scenarios is approximately 3,070. When $N_L = 5$, the number of scenarios is approximately 2,250, and when $N_L = 3$, the number of scenarios is approximately 2,100. For this evaluation, all sampling replicates were run with $N_L = 5$. A given choice of N_L determines the LHS sample size for a single replicate CASA evaluation. Quantitative evaluations presented here are based on 20 replicates for each of 15 Johnson uncertainty percentiles (675,000 break scenarios for each plant failure case).

Figure 5.3.4 illustrates the break-size selection process for Weld Case 1B, which includes the largest pipes in containment. LOCA category limits are marked with vertical solid lines. The DEGB condition, marked with a red dot, represents one of the 10 breaks imposed on the LBLOCA range. The remaining

[19] There are several methods that could be used to select the bins for small, medium, and large breaks. This method emphasizes the contributions of the larger breaks while also ensuring that small and medium breaks are considered.

nine equal break-size intervals are separated by vertical dashed lines between 6 inches and 31.5 inches (the maximum pipe diameter). Note that the size intervals only appear unequal because of the logarithmic scale. By relative proportion of their respective ranges, only two break intervals are assigned to MBLOCAs, and only one is assigned SBLOCAs. Thus, for this example, 13 breaks are simulated at each weld belonging to Weld Case 1B.

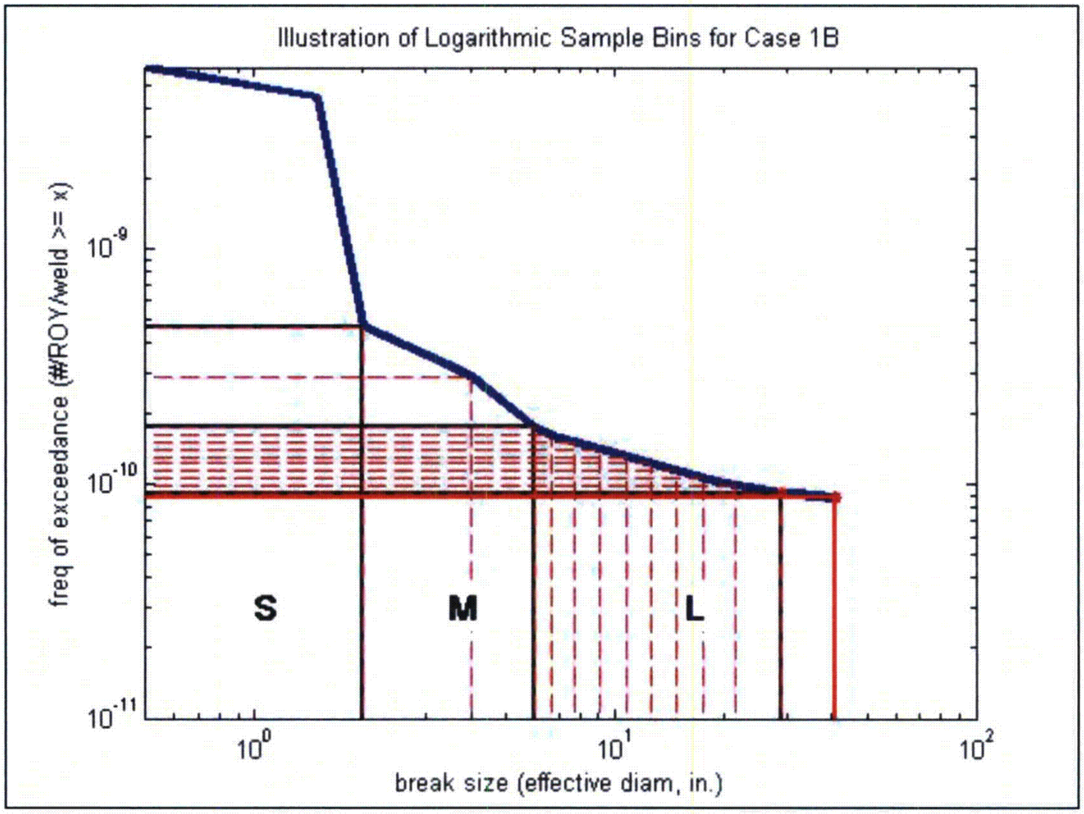

Figure 5.3.4 – Example of non-uniform stratified sampling strategy for one weld case

5.4 Debris Generation

Debris generation analysis includes calculations of the total quantity of insulation, coatings, latent, and miscellaneous debris, as well as a definition of debris characteristics (size and density). These topics are discussed in this section.

5.4.1 ZOI Model

The quantity of insulation debris generated is calculated directly in CASA Grande based on the currently accepted deterministic ZOI model. As described in NEI 04-07 Volume 2, the break jet ZOI can be conservatively modeled as a sphere for a fully offset DEGB or as a hemisphere for anything less than a

DEGB (i.e., a side-wall pipe break) (45). The ZOI radius depends on the destruction pressure of the insulation and the size of the break. As shown in Section 2.2.14, the ZOI sizes for insulation at STP are 2D for Transco RMI, 17D for Nukon and Thermal-Wrap (assumed to be the same as Nukon), and 28.6D for Microtherm (assumed to be the same as Min-K). All insulation that falls within its respective ZOI is assumed to become debris.

Figure 5.4.1 through Figure 5.4.3 show examples of the ZOIs for a large 31-inch DEGB, a medium 6-inch side-wall break, and a small 2-inch side-wall break. Because of the spherical ZOI assumption, the direction of the jet is irrelevant for DEGBs (see Figure 5.4.1). The jet direction and orientation of the hemispherical ZOI for side-wall breaks is dependent on the break location radially around the pipe, but the ZOI is constrained along the axis of the pipe (see Figure 5.4.2 and Figure 5.4.3).

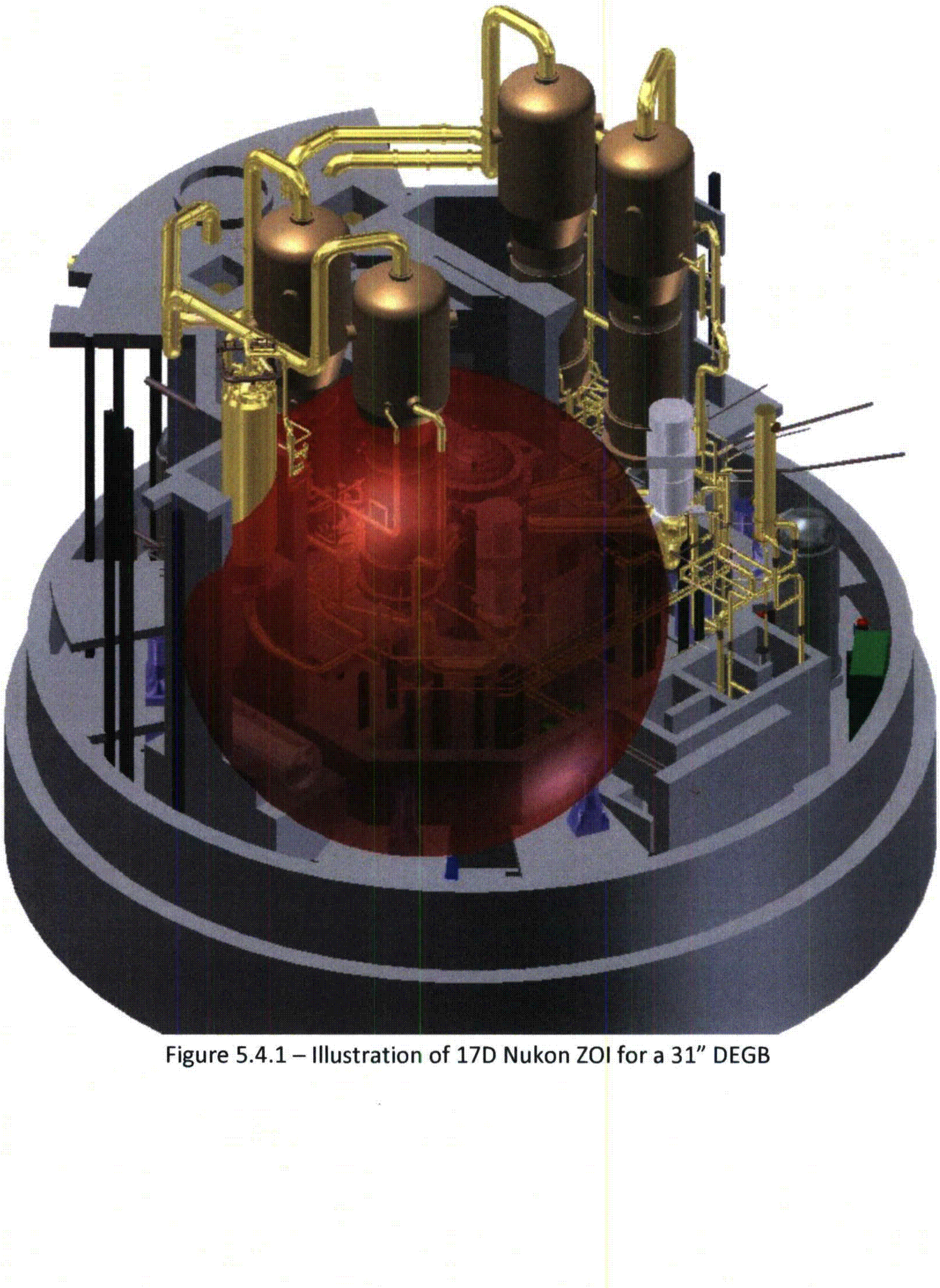

Figure 5.4.1 – Illustration of 17D Nukon ZOI for a 31" DEGB

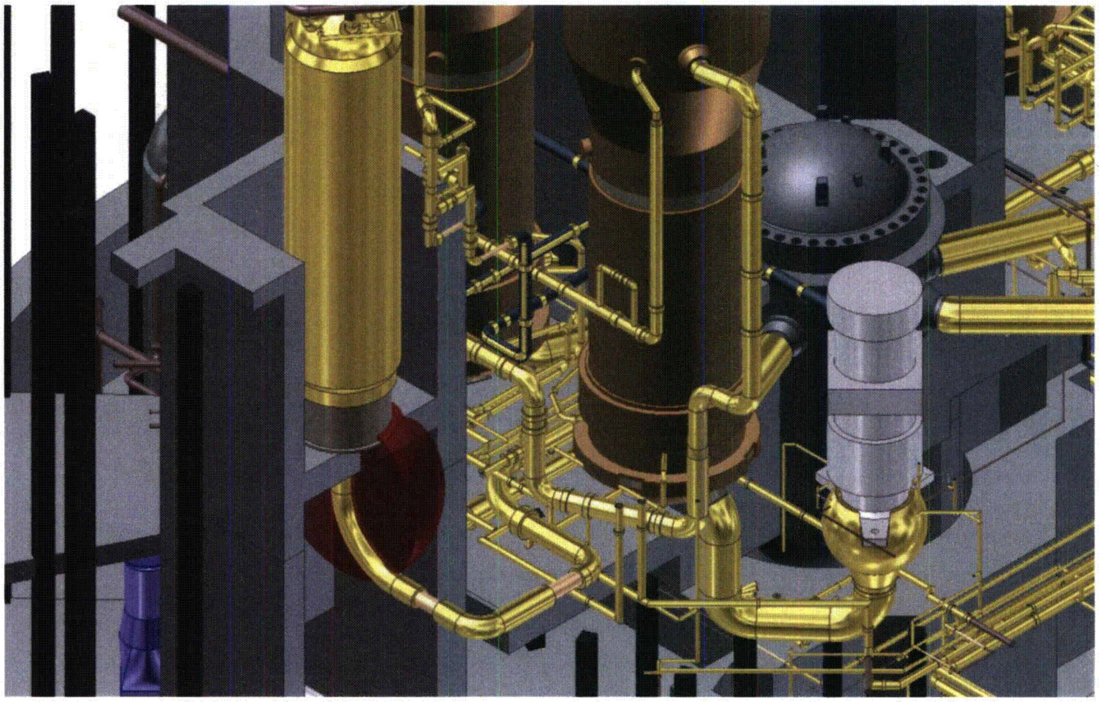

Figure 5.4.2 – Illustration of 17D Nukon ZOI for a 6" side-wall break

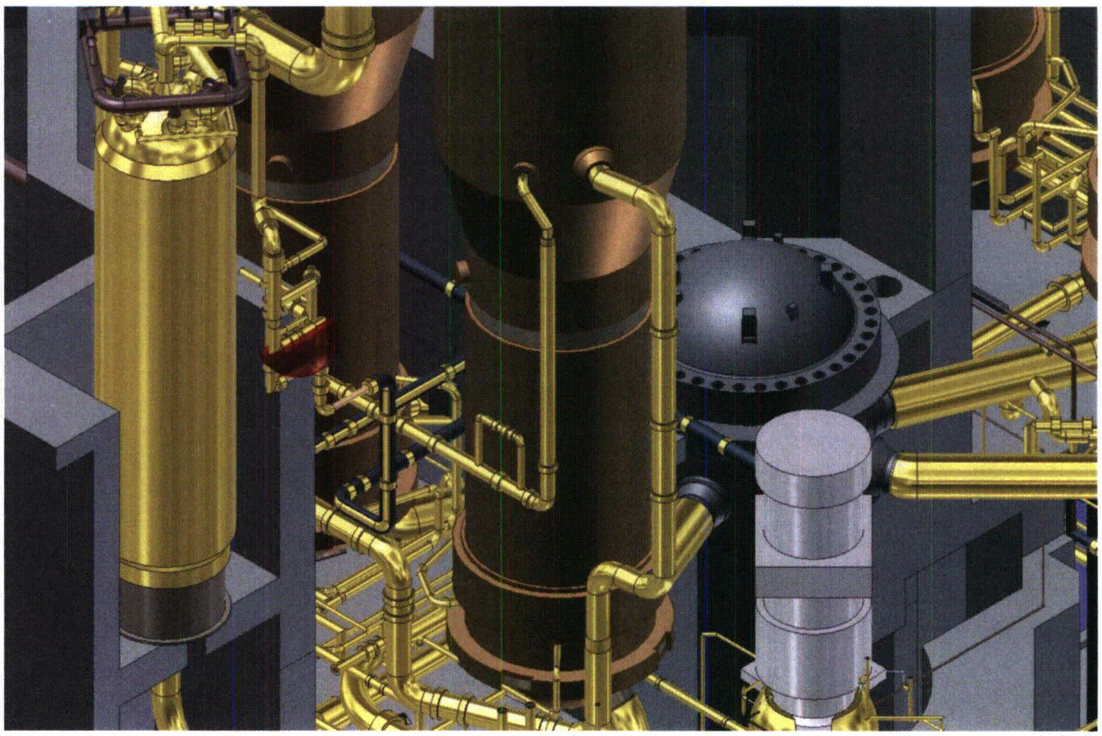

Figure 5.4.3 – Illustration of 17D Nukon ZOI for a 2" side-wall break

Jet formation modeling was conducted to evaluate the potential conservatism in the ZOI size and shape (10). However, the effects of realistic jets on the ZOIs were not explicitly considered in this evaluation.

5.4.2 Insulation Debris Size Distribution Model

To implement the fiberglass debris size distribution described in Section 2.2.15, the fiberglass ZOI was split into three sub-zones. The quantity of fiberglass insulation in each sub-zone was multiplied by the appropriate percentage of fines, small pieces, large pieces, and intact blankets as defined in Table 4.1 of the Alion debris size distribution report (46). Figure 5.4.4 shows an example of the size distribution sub-zones.

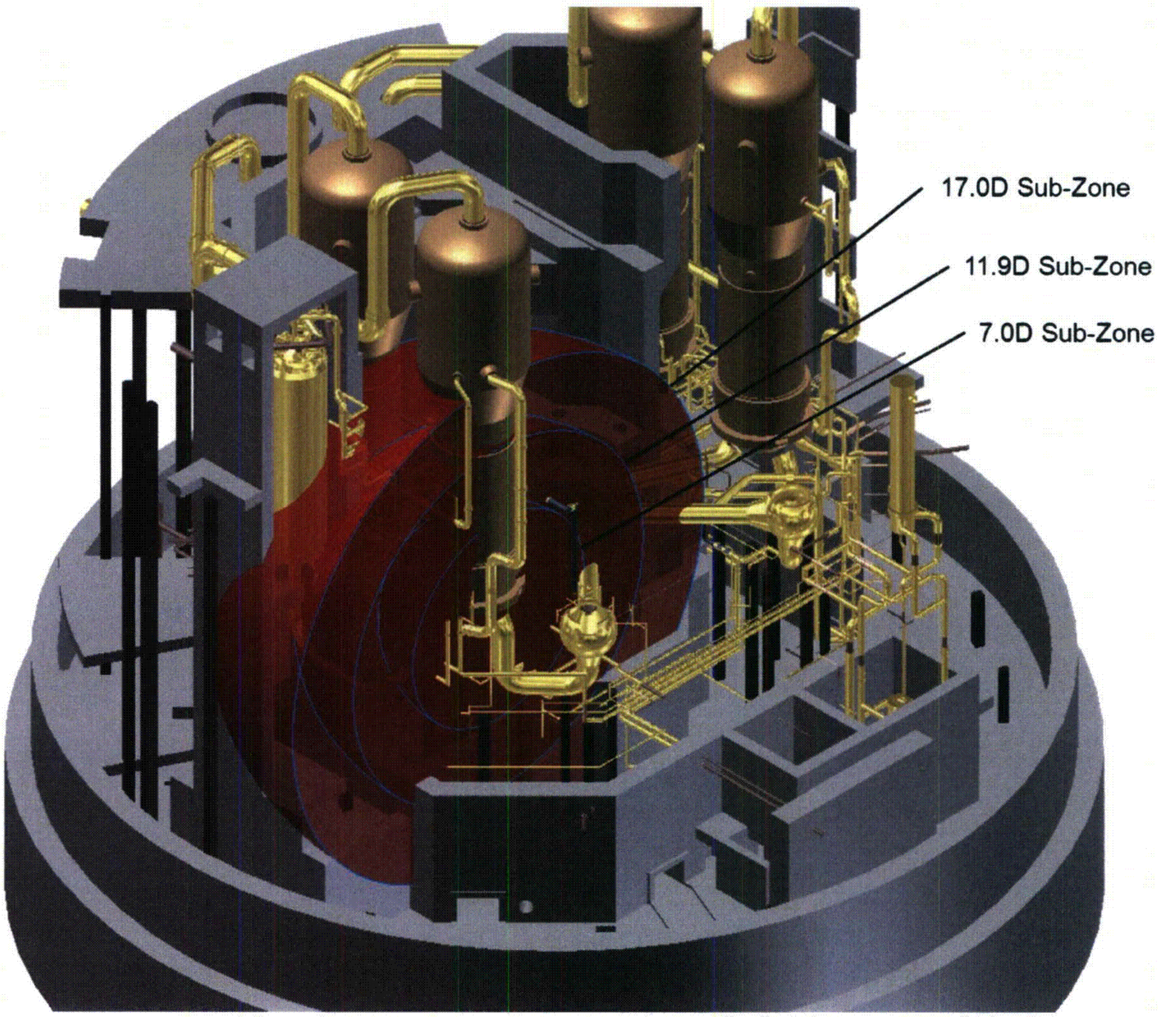

Figure 5.4.4 – Illustration of sub-zones used for fiberglass debris size distribution

The Microtherm debris was assumed to fail as 100% fines with components of SiO_2, TiO_2, and fibers as described in Section 2.2.15.

5.4.3 Insulation Debris

Using the LOCA frequency sampling strategy described in Section 5.3, three replicates of approximately 2,250 break scenarios each were sampled to illustrate the probability distribution associated with ZOI debris volume. These calculations assumed a 17D ZOI for Nukon and Thermal Wrap insulation. Figure 5.4.5 shows the complementary cumulative probability distribution function formed from the fiberglass debris quantities calculated for these scenarios with the relative initiating event frequencies included as probability weights. As shown on this figure, the maximum quantity of fiberglass debris that can be generated approaches 3,000 ft^3, but 99.9% of the scenarios generate less than 10 ft^3 of fiberglass debris.

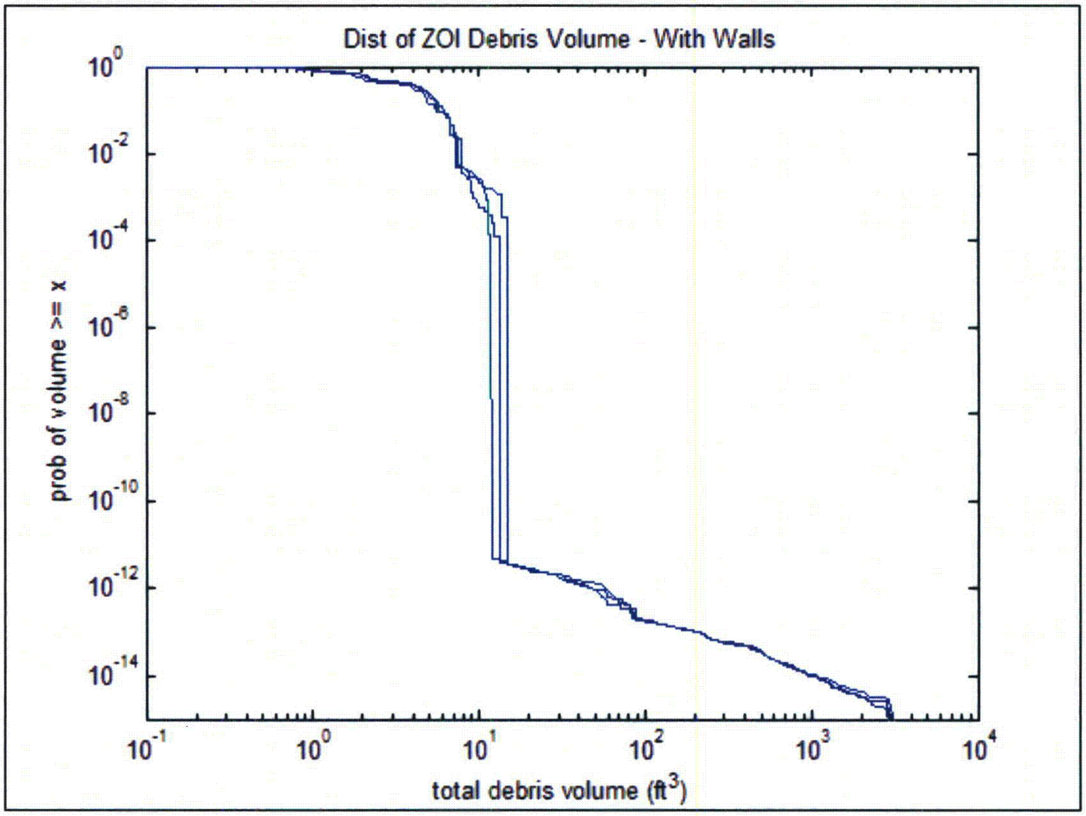

Figure 5.4.5 – Distribution of potential fiberglass debris quantities

5.4.4 Qualified Coatings Debris

Similar to insulation debris, the quantity of qualified coatings debris is calculated based on the quantity of coatings within the ZOI. However, due to the difficulty of accurately modeling all of the coated surfaces within CASA Grande, the qualified coatings debris calculations were performed outside of CASA Grande using the CAD model. As described in Section 2.2.9, bounding quantities of qualified epoxy and IOZ coatings debris were determined for break sizes of 2-inch, 6-inch, 15-inch, and 31-inch DEGB. In CASA, the bounding 31-inch DEGB quantities were applied for all breaks.

5.4.5 Unqualified Coatings Debris

The inputs for unqualified epoxy, alkyd, IOZ, and baked enamel coatings failure are provided in Section 2.2.10. For each of the unqualified coatings, the total quantity is multiplied by the failure fraction (100%) to determine the actual quantity of unqualified coatings debris generated. The quantity of unqualified coatings debris that transports to the strainers (as well as the arrival time at the strainers) is dependent on both the failure location and failure timing. Therefore, these inputs were provided in Section 2.2.10 also. The following equations illustrate the method for calculating the time-dependent and cumulative coatings failure:

$$M_{ij}(t) = M_{total,ij} \cdot F_{fail,i} \cdot F(t) \qquad \text{Equation 27}$$

$$M_{ij,cum} = \frac{M_{ij}(t)}{F(t)} = M_{total,ij} \cdot F_{fail,i} \qquad \text{Equation 28}$$

where:

$M(t)$ = Mass of unqualified coatings that fail during a specific time period
t = Specific time period following the start of the accident
Subscript i = Unqualified coating type (epoxy, IOZ, alkyd, or baked enamel)
Subscript j = Coating location (upper containment, lower containment, or reactor cavity)
M_{total} = Total mass of unqualified coatings
F_{fail} = Total failure fraction
$F(t)$ = Fraction of coatings that fail during a specific time period
$M_{ij,cum}$ = Cumulative mass of unqualified coatings that fail

Although the failure fraction could realistically range from 0% to 100% for the various types of coatings, the failure fraction implemented in CASA was conservatively set at 100% for all unqualified coatings. As described in Section 5.5.7, however, the transport fractions for unqualified coatings take into consideration the coatings location and the failure timing (e.g., unqualified coatings that fail in upper containment after containment sprays are secured would not be washed down). Since sprays are secured prior to 24 hours (see Section 2.2.1), the quantity of coatings that fail prior to securing sprays would be 6% or less (see Section 2.2.10). Therefore, a washdown transport fraction of 6% was used for unqualified coatings in upper containment. All of the unqualified coatings that were calculated to transport to the strainer over a total of 30 days were conservatively introduced to the pool at a uniform rate starting at 10 minutes and ending at 36 hours (i.e., approximately 2.8% per hour).

5.4.6 Latent Debris

The quantities of latent fiber and latent dirt/dust were entered as input parameters in CASA Grande based on the values specified in Section 2.2.12. The total quantity of latent debris is applicable to all LOCA scenarios.

5.4.7 Miscellaneous Debris

Unqualified tags, labels, plastic signs, tie wraps, etc. are assumed to fail for all LOCA scenarios. The total quantity of miscellaneous debris was entered as an input parameter in CASA Grande based on the value specified in Section 2.2.13.

5.4.8 Debris Characteristics

The important debris properties were entered as input parameters in CASA Grande based on the values specified in Section 2.2.16. The parameters that are important for GSI-191 calculations include the characteristic diameters of particles and fibers, the macroscopic (or bulk) density of debris, and the microscopic (or particle) density of debris.

5.5 Debris Transport

Debris transport is the estimation of the fraction of debris that is transported from the location where it is generated to the sump strainers. The four major debris transport modes are:

- *Blowdown transport* – the vertical and horizontal transport of debris to all areas of containment by the break jet.
- *Washdown transport* – the vertical (downward) transport of debris by the containment sprays and break flow.
- *Pool fill transport* – the horizontal transport of debris during the RWST injection phase to regions of the pool that may be active or inactive during recirculation.
- *Recirculation transport* – the horizontal transport of debris from the active portions of the recirculation pool to the sump strainers.

The four transport modes, potential upstream blockage, fiberglass debris erosion, and time-dependent transport are all discussed in this section.

5.5.1 Upstream Blockage

Potential upstream blockage points at STP include the four 30-inch vent holes in the secondary shield wall (see Figure 5.2.7 and Figure 5.5.1) and the two 6-inch refueling canal drain lines. These potential blockage points were previously evaluated as part of the deterministic GSI-191 analysis, and it was shown that they would not be clogged with debris (65; 76).

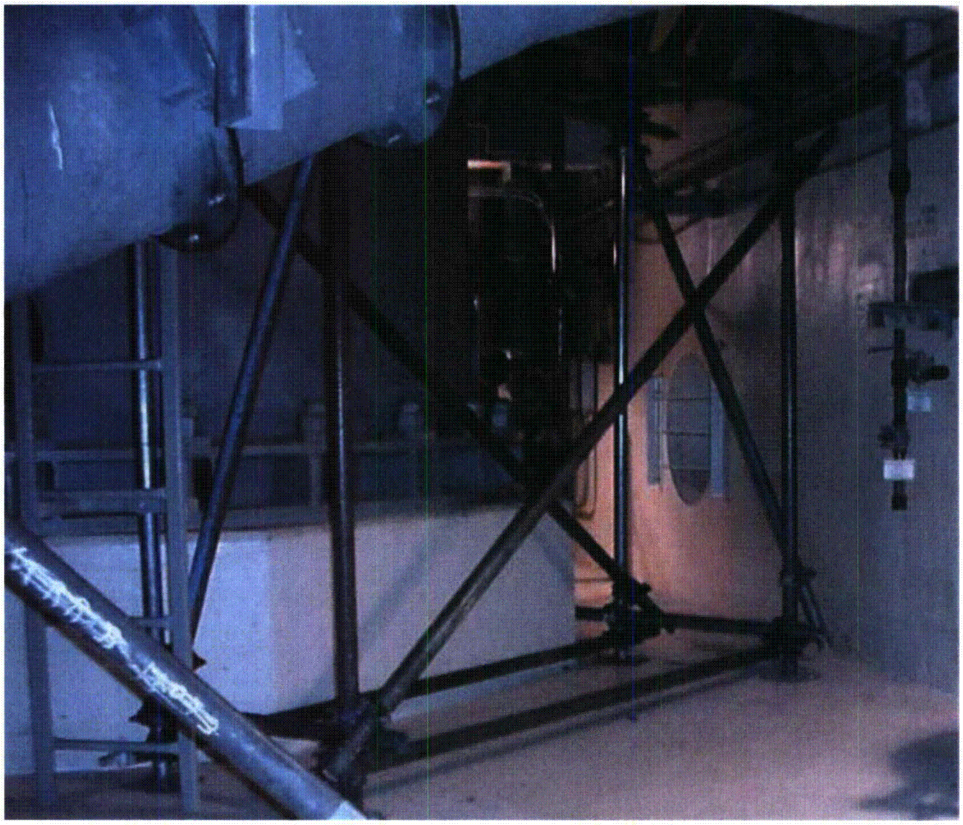

Figure 5.5.1 – Photograph of 30-inch vent hole in secondary shield wall

5.5.2 Blowdown Transport

The blowdown transport fractions are provided in Section 2.2.17. As described in Assumption 6.h, the bounding, large break, steam generator compartment blowdown fractions were used for all breaks. These values are shown below in Table 5.5.1.

Table 5.5.1 – Blowdown transport fractions used in CASA Grande

Debris Type	Blowdown Transport Fractions		
	Upper Containment	Upper Containment	Remaining in Compartments
Fines	70%	30%	0%
Small LDFG	60%	25%	15%
Large LDFG	22%	0%	78%

5.5.3 Washdown Transport

The washdown transport fractions are provided in Section 2.2.18. As described in Assumption 6.h, the bounding washdown transport fractions (assuming sprays are always initiated) were used for all breaks. These values are shown below in Table 5.5.2.

Table 5.5.2 – Washdown transport fractions used in CASA Grande

Debris Type	Washdown Transport Fractions	
	Washed Down in Annulus	**Washed Down inside Secondary Shield Wall**
Fines	47%	53%
Small LDFG	19%	27%
Large LDFG	0%	0%

5.5.4 Pool Fill Transport

The pool fill transport fractions are provided in Section 2.2.19. As described in Assumption 6.h, the pool fill transport fractions for breaks inside the secondary shield wall were used for all breaks. These values are shown below in Table 5.5.3.

Table 5.5.3 – Pool fill transport fractions used in CASA Grande

Debris Type	Pool Fill Transport Fractions	
	Each Sump	**Inactive Cavities**
Fines	2%	5%
Small LDFG	0%	0%
Large LDFG	0%	0%

5.5.5 Recirculation Transport

The recirculation transport fractions are provided in Section 2.2.20. As described in Assumption 6.h, the bounding, large break, steam generator compartment recirculation fractions were used for all breaks. These values are shown below in Table 5.5.4.

Table 5.5.4 – Recirculation transport fractions used in CASA Grande

Debris Type	Size	Recirculation Transport Fractions		
		Debris in Lower Containment	Washed in Annulus	Washed inside Secondary Shield Wall
LDFG	Fines	100%	100%	100%
	Small Pieces	64%	58%	64%
	Large Pieces	0%	NA	NA
Qualified Coatings	Fines	100%	100%	100%
Unqualified Coatings[20]	Fines	100%		
Unqualified Epoxy[20]	Fine Chips	41%		
	Small Chips	0%		
	Large Chips	0%		
	Curled Chips	100%		
Crud	Fines	100%	100%	100%
Dirt/Dust	Fines	100%	100%	100%
Latent Fiber	Fines	100%	100%	100%

5.5.6 Debris Erosion

Pieces of fiberglass debris that are held up on grating and exposed to spray, and pieces of fiberglass debris that settle in the recirculation pool would be subject to erosion. The erosion fractions are described in Section 2.2.21.

5.5.7 Strainer Transport

The total transport to the ECCS strainers was determined based on the logic tree method described in NEI 04-07 (44). The transport fractions can be calculated using Equation 29 for debris generated inside the ZOI, Equation 30 for unqualified coatings debris generated outside the ZOI, and Equation 31 for latent debris.

[20] The recirculation transport is assumed to be the same for unqualified coatings washed down to the pool and unqualified coatings that are initially in lower containment since the locations where debris would be washed down and the locations where unqualified coatings exist in lower containment are spread out and can be reasonably treated as a uniform distribution (23).

$$
\begin{aligned}
DTF_{ZOI} = F_{BD(upper)} & \\
& \cdot \{(1 - F_{WD(inside)} - F_{WD(annulus)}) \cdot F_{Erosion(spray)} + F_{WD(inside)} \\
& \cdot [F_{Recirc(WDinside)} + (1 - F_{Recirc(WDinside)}) \cdot F_{Erosion(pool)}] \\
& + F_{WD(annulus)} \\
& \cdot [F_{Recirc(WDannulus)} + (1 - F_{Recirc(WDannulus)}) \cdot F_{Erosion(pool)}]\} \\
& + (1 - F_{BD(upper)} - F_{BD(lower)}) \\
& \cdot \{(1 - F_{WD(BCinside)} - F_{WD(BCannulus)}) \cdot F_{Erosion(spray)} \\
& + F_{WD(BCinside)} \\
& \cdot [F_{Recirc(WDinside)} + (1 - F_{Recirc(WDinside)}) \cdot F_{Erosion(pool)}] \\
& + F_{WD(BCannulus)} \\
& \cdot [F_{Recirc(WDannulus)} + (1 - F_{Recirc(WDannulus)}) \cdot F_{Erosion(pool)}]\} \\
& + F_{BD(lower)} \\
& \cdot \{(1 - 3 \cdot F_{PF(sump)} - F_{PF(inactive)}) \\
& \cdot [F_{Recirc(lower)} + (1 - F_{Recirc(lower)}) \cdot F_{Erosion(pool)}] + N_{Sumps} \\
& \cdot F_{PF(sump)}\}
\end{aligned}
\qquad \text{Equation 29}
$$

where:

DTF_{ZOI} = Total debris transport fraction (for particular type/size of debris generated in the ZOI)
$F_{BD(upper)}$ = Blowdown fraction to upper containment
$F_{BD(lower)}$ = Blowdown fraction to lower containment
$F_{WD(inside)}$ = Washdown fraction inside secondary shield wall
$F_{WD(annulus)}$ = Washdown fraction in annulus
$F_{WD(BCinside)}$ = Washdown fraction from break compartment to inside secondary shield wall
$F_{WD(BCannulus)}$ = Washdown fraction from break compartment to annulus
$F_{PF(sump)}$ = Pool fill fraction to each sump strainer
$F_{PF(inactive)}$ = Pool fill fraction to inactive cavities
N_{sumps} = Number of ECCS sumps in operation during recirculation
$F_{Recirc(lower)}$ = Recirculation fraction for debris initially blown to lower containment
$F_{Recirc(WDinside)}$ = Recirculation fraction for debris washed down inside secondary shield wall
$F_{Recirc(WDannulus)}$ = Recirculation fraction for debris washed down in annulus
$F_{Erosion(spray)}$ = Erosion fraction for debris held up above the pool
$F_{Erosion(pool)}$ = Erosion fraction for non-transporting debris in the pool

$$
\begin{aligned}
DTF_{UC} = F_{fail} \cdot [F_{upper} \cdot F_{spray} \cdot F_{Recirc} + F_{lower} \cdot F_{Recirc} + F_{reactor} & \\
\cdot F_{Recirc(reactor)}] &
\end{aligned}
\qquad \text{Equation 30}
$$

where:

DTF_{UC} = Total debris transport fraction (for particular type/size of unqualified coatings debris)
F_{fail} = Total failure fraction
F_{upper} = Fraction located in upper containment
F_{lower}= Fraction located in lower containment
$F_{reactor}$ = Fraction located in the reactor cavity
F_{spray} = Fraction of coatings that would fail prior to securing containment sprays
F_{Recirc} = Recirculation fraction for debris washed to or initially in lower containment
$F_{Recirc(reactor)}$ = Recirculation fraction for debris in reactor cavity

$$DTF_{LD} = F_{upper} \cdot F_{WD} \cdot F_{Recirc} + F_{lower} \cdot \left[\left(1 - 3 \cdot F_{PF(sump)} - F_{PF(inactive)} \right) \cdot F_{Recirc} + N_{Sumps} \cdot F_{PF(sump)} \right] \qquad \text{Equation 31}$$

where:

DTF_{LD} = Total debris transport fraction (for particular type/size of latent debris)
F_{upper} = Fraction located in upper containment
F_{lower}= Fraction located in lower containment
F_{WD} = Total washdown fraction
$F_{PF(sump)}$ = Pool fill fraction to each sump strainer
$F_{PF(inactive)}$ = Pool fill fraction to inactive cavities
N_{sumps} = Number of ECCS sumps in operation during recirculation
F_{Recirc} = Recirculation fraction for debris washed to or initially in lower containment

Figure 5.5.2 through Figure 5.5.7 show the transport logic trees for each type and size of debris generated inside the ZOI for a large break in the steam generator compartments. The washdown transport fractions are based on the actuation of containment sprays (i.e., CS flow is greater than 0 gpm), and the pool fill transport fractions are based on all three sumps being active (i.e., at least one pump is running on three different trains).

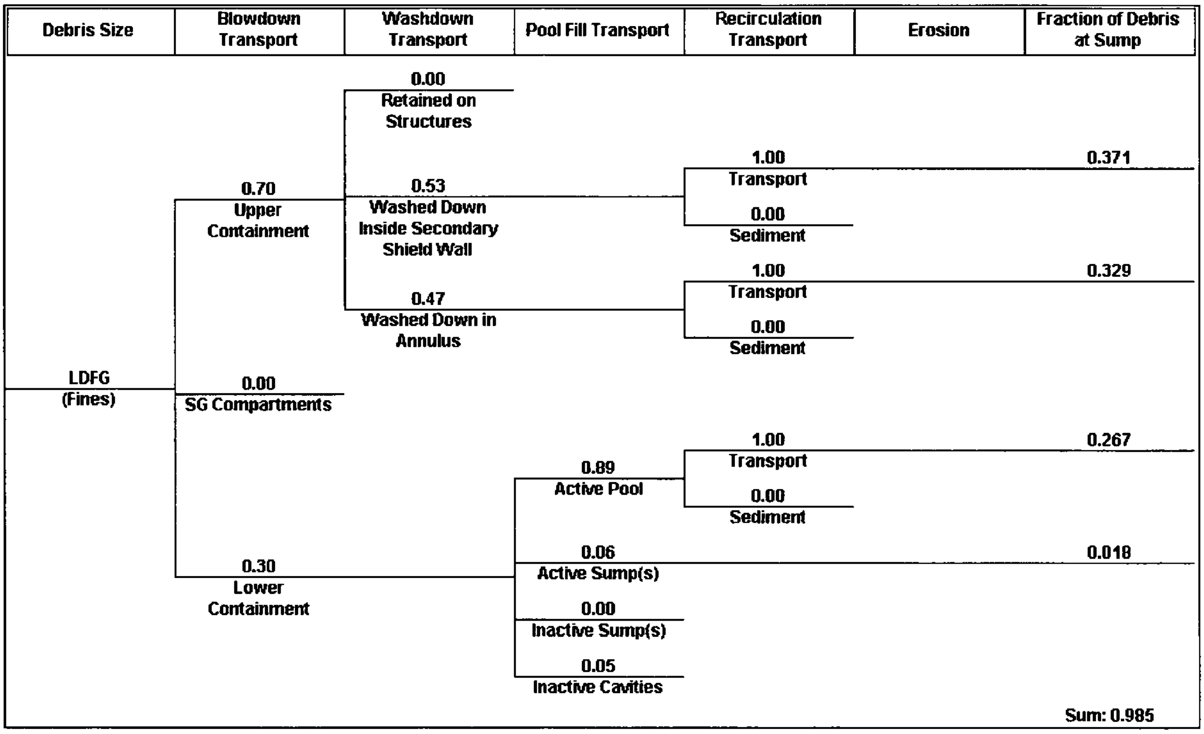

Figure 5.5.2 – Logic tree for LDFG fines showing total transport fraction implemented for all breaks

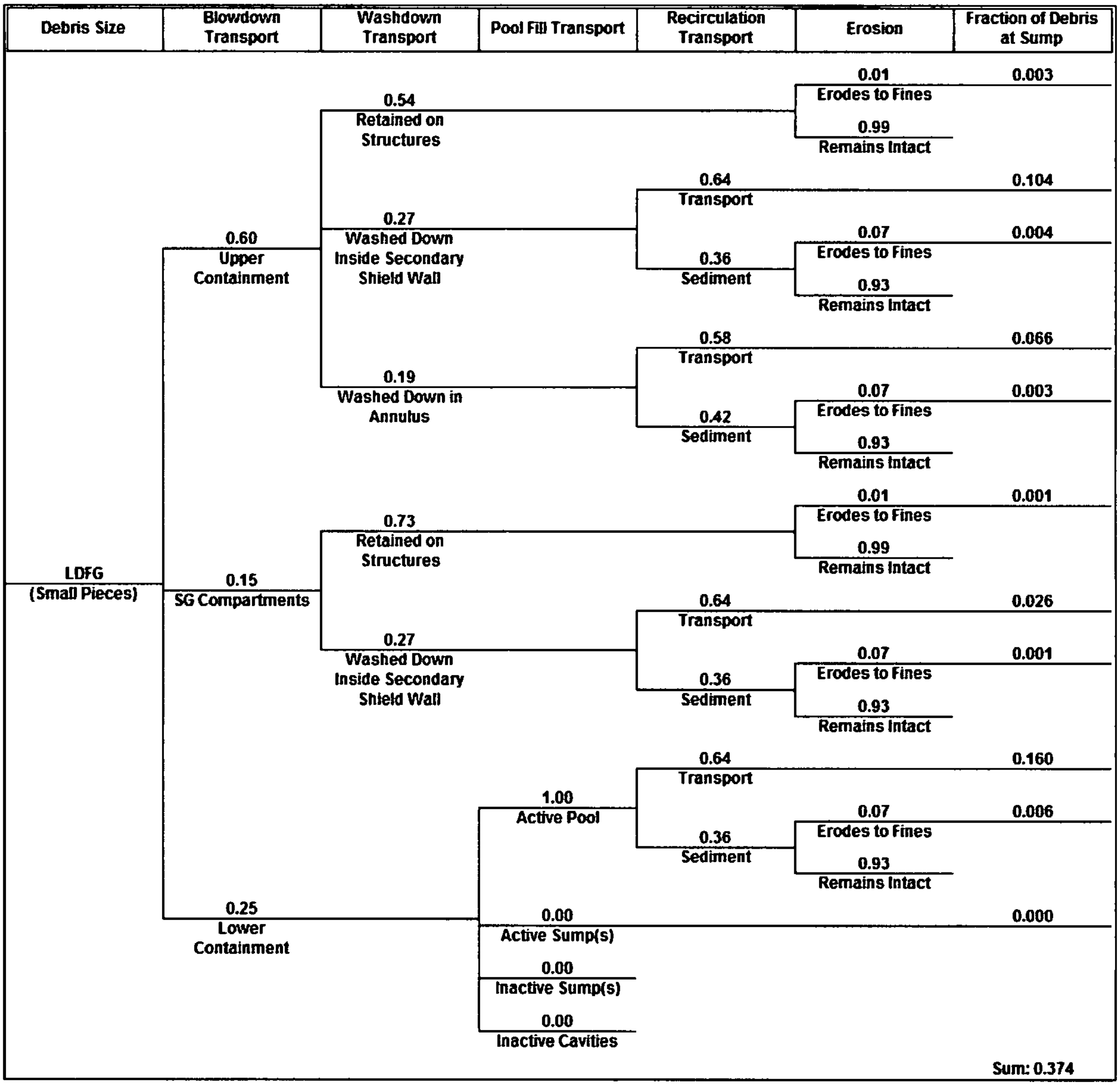

Figure 5.5.3 – Logic tree for LDFG small pieces showing total transport fraction implemented for all breaks

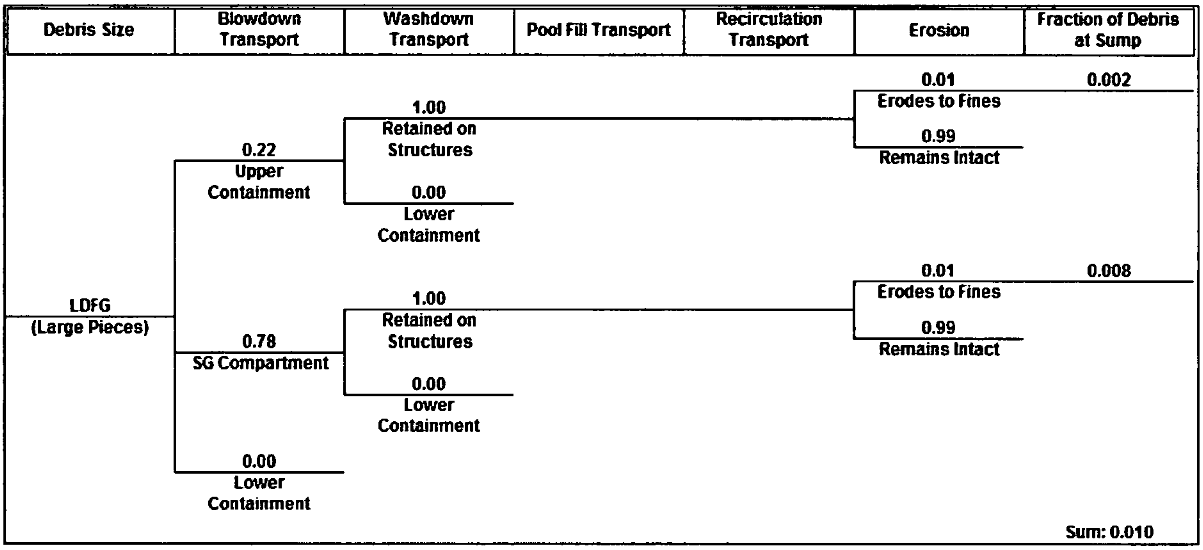

Figure 5.5.4 – Logic tree for LDFG large pieces showing total transport fraction implemented for all breaks

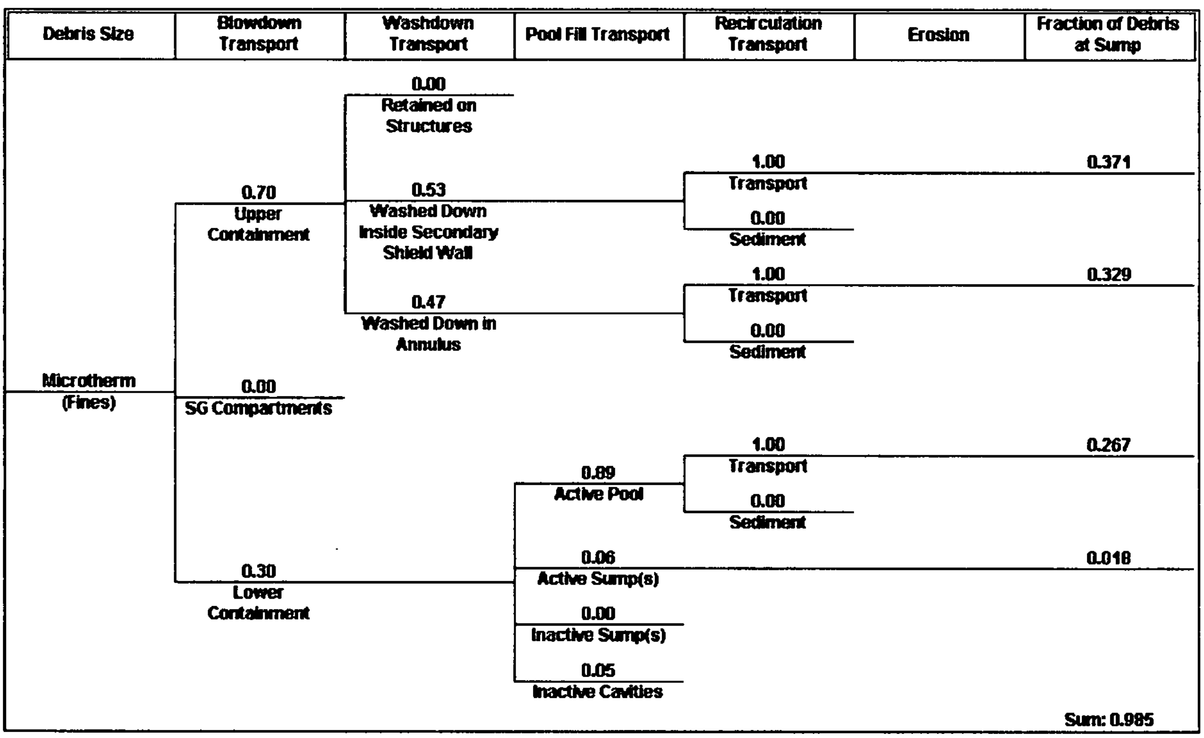

Figure 5.5.5 – Logic tree for Microtherm fines showing total transport fraction implemented for all breaks

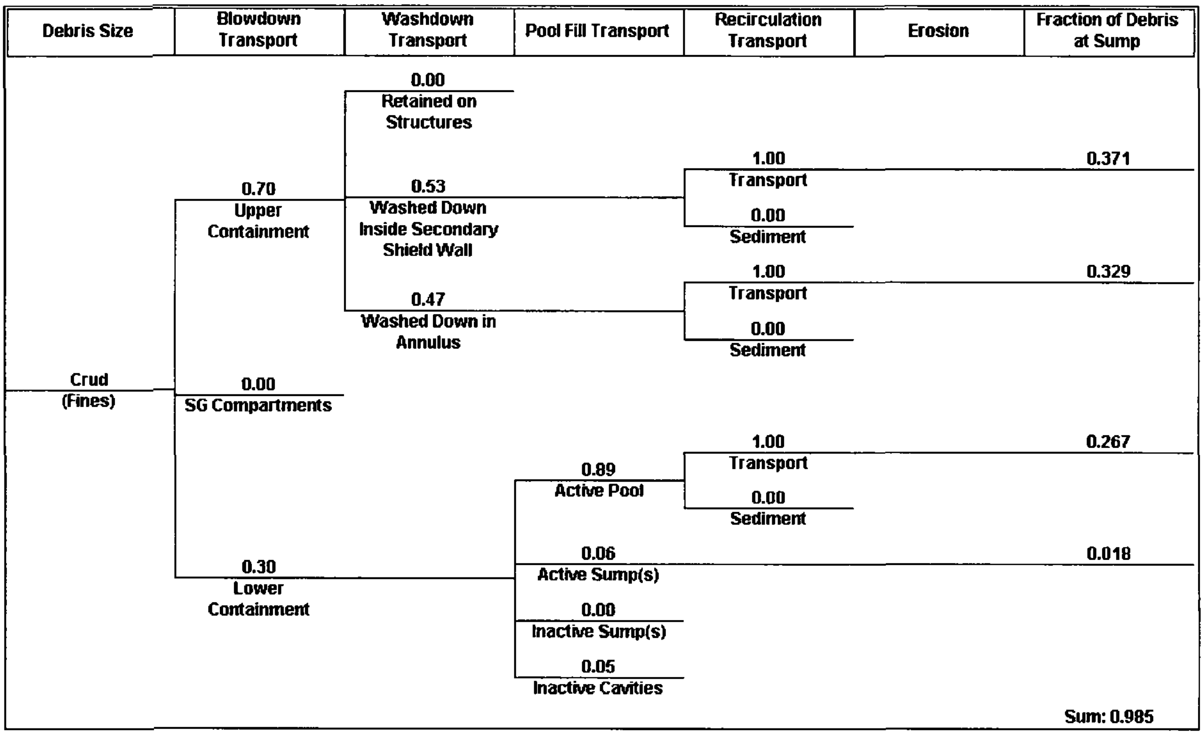

Figure 5.5.6 – Logic tree for crud fines showing total transport fraction implemented for all breaks

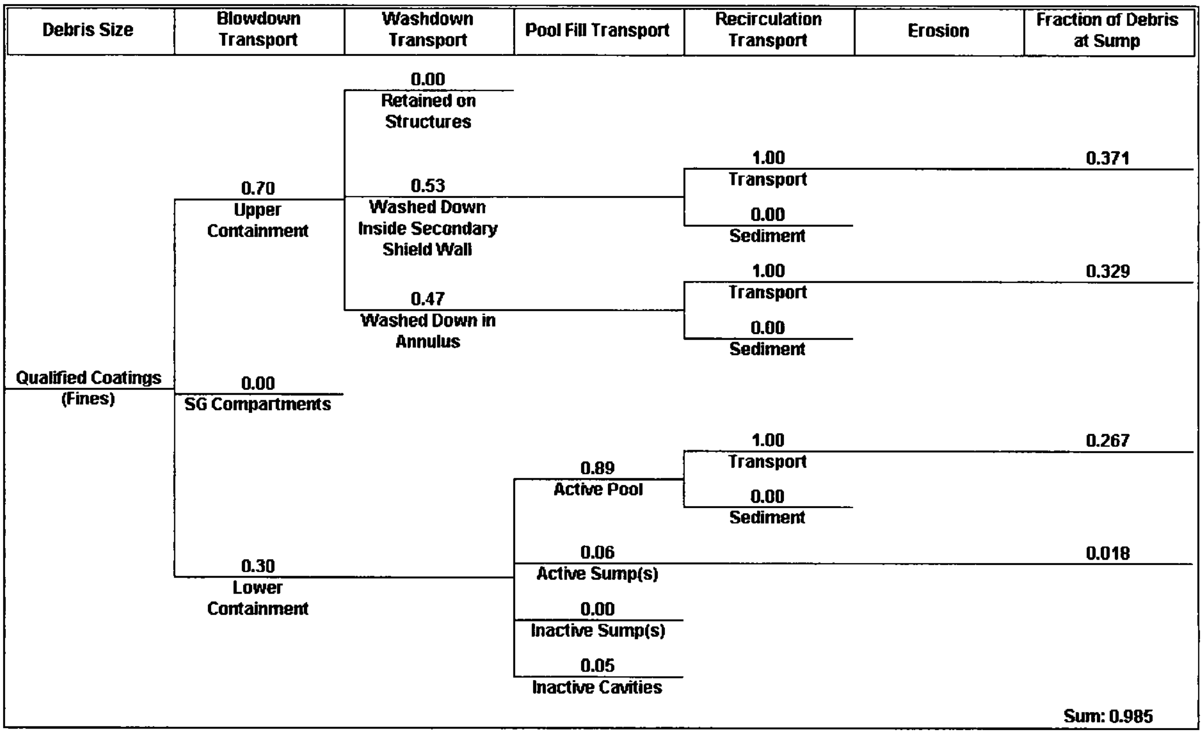

Figure 5.5.7 – Logic tree for qualified coatings fines showing total transport fraction implemented for all breaks

Figure 5.5.8 through Figure 5.5.15 show transport logic trees for each type and size of debris generated outside the ZOI for a large break in the steam generator compartments. The transport fraction for the unqualified coatings is based on a failure fraction of 100%, as well as the failure timing for the coatings in upper containment. Since the majority of unqualified coatings would fail after 24 hours (approximately 94% as shown in Section 2.2.10), and the sprays would generally be secured within a few hours, most of the unqualified coatings in upper containment would not be washed down to the pool.

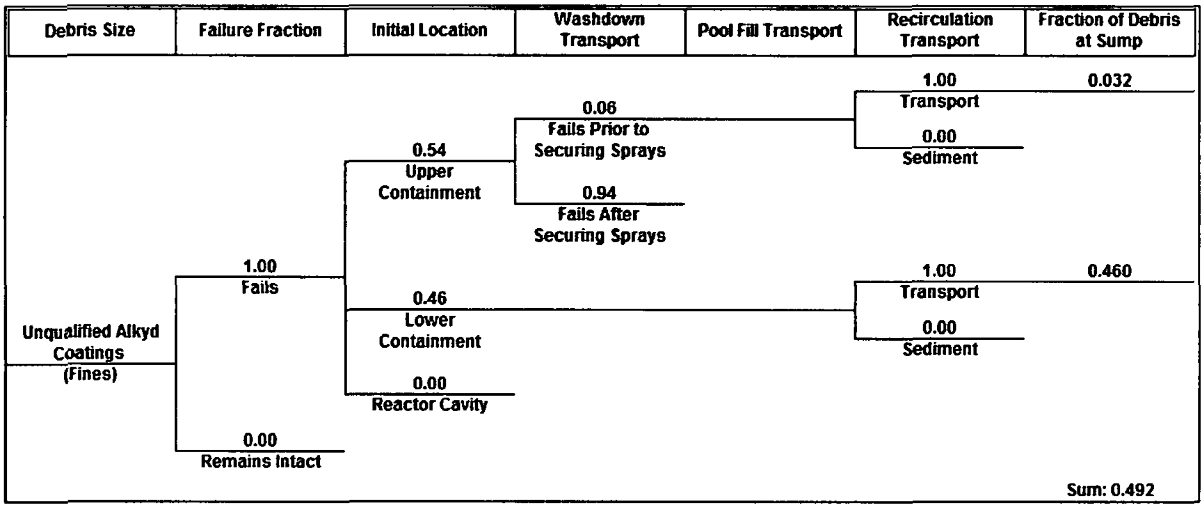

Figure 5.5.8 – Logic tree for unqualified alkyd coatings fines showing total transport fraction implemented for all breaks

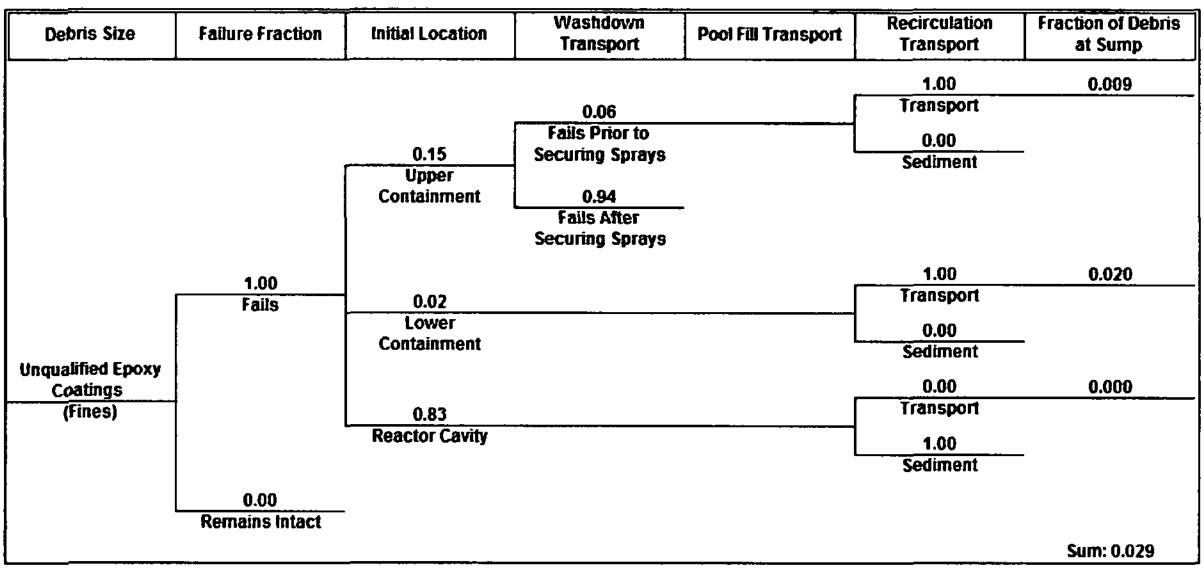

Figure 5.5.9 – Logic tree for unqualified epoxy coatings fines showing total transport fraction implemented for all breaks

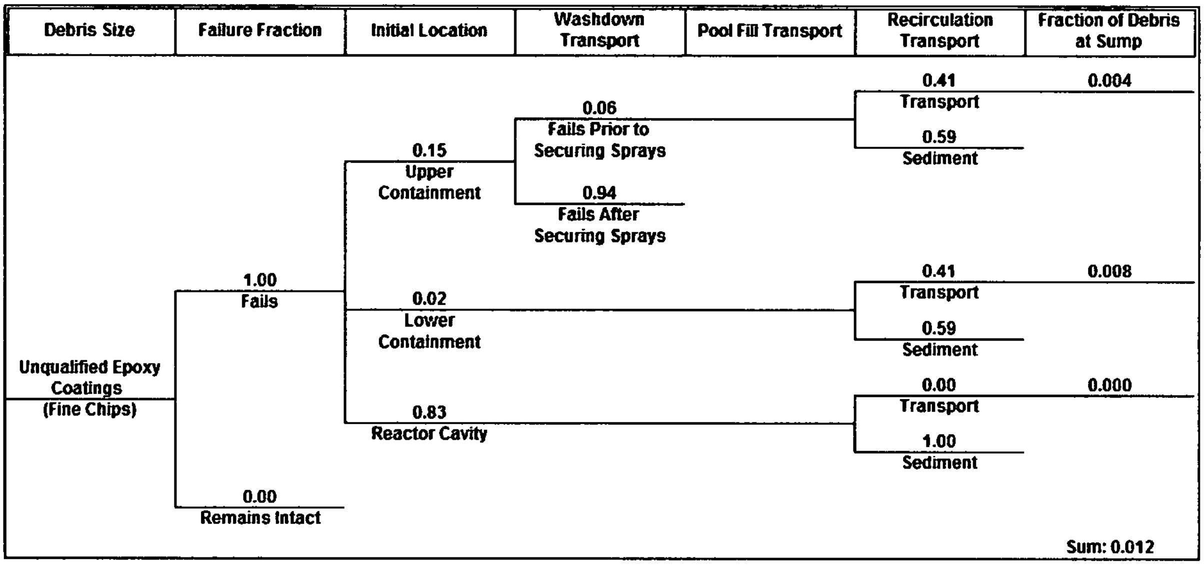

Figure 5.5.10 – Logic tree for unqualified epoxy coatings fine chips showing total transport fraction implemented for all breaks

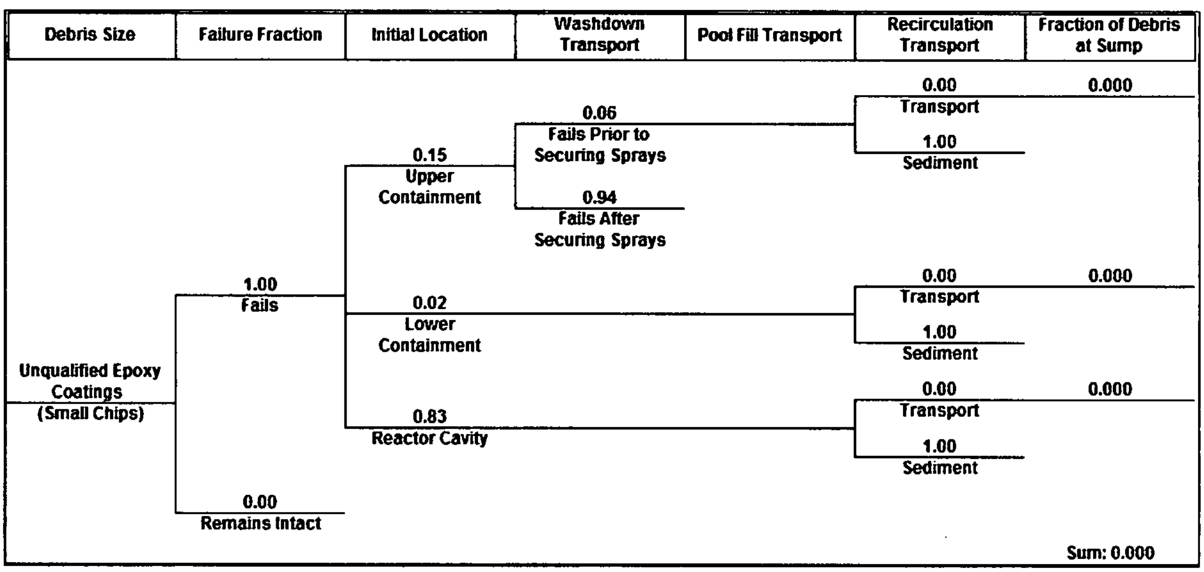

Figure 5.5.11 – Logic tree for unqualified epoxy coatings small chips showing total transport fraction implemented for all breaks

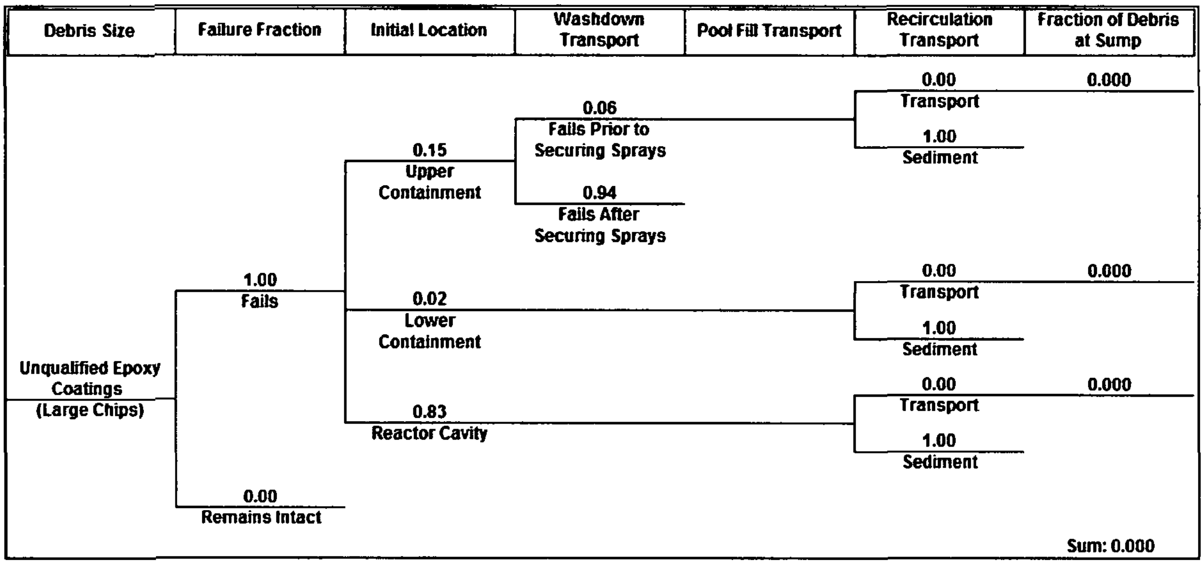

Figure 5.5.12 – Logic tree for unqualified epoxy coatings large chips showing total transport fraction implemented for all breaks

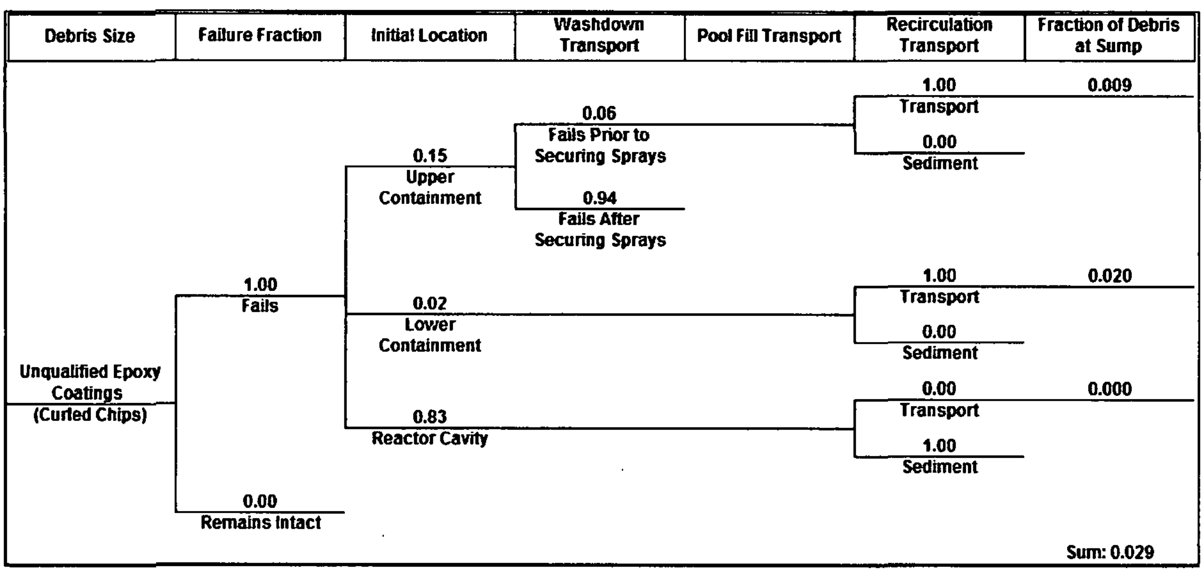

Figure 5.5.13 – Logic tree for unqualified epoxy coatings curled chips showing total transport fraction implemented for all breaks

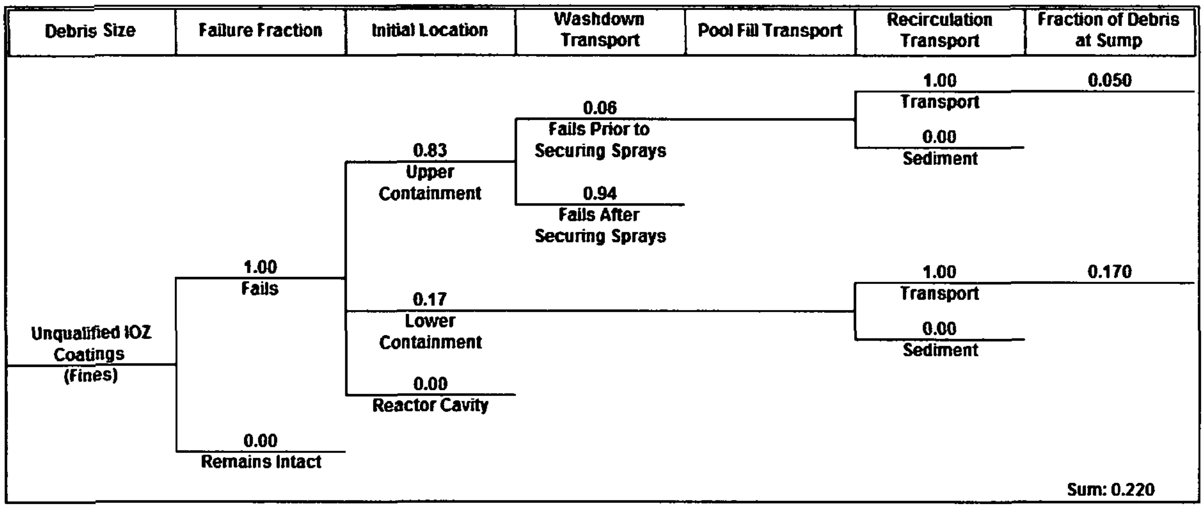

Figure 5.5.14 – Logic tree for unqualified IOZ coatings fines showing total transport fraction implemented for all breaks

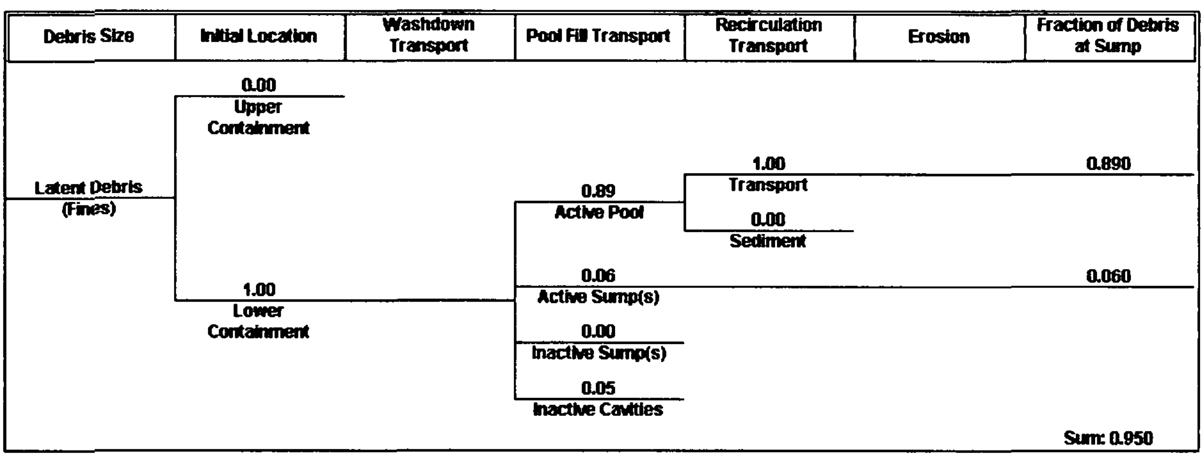

Figure 5.5.15 – Logic tree for latent fines showing total transport fraction implemented for all breaks

As discussed in Assumption 6.e, debris accumulation on the strainers is assumed to be proportional to the strainer flow split. Therefore, the debris accumulation on each individual strainer can be calculated as shown in Equation 32.

$$DTF_{Sump(X)} = DTF \cdot \frac{Q_{Sump(X)}}{Q_{Sump(A)} + Q_{Sump(B)} + Q_{Sump(C)}} \qquad \text{Equation 32}$$

where:

$DTF_{Sump(X)}$ = Recirculation transport to Sump(X) for a particular type/size of debris in pool

Sump(X) = Sump(A), Sump(B), or Sump(C)
DTF = Recirculation transport for a particular type/size of debris in pool
$Q_{Sump(X)}$ = Flow rate to Sump(X)
$Q_{Sump(A,B,C)}$ = Flow rate to Sump(A,B,C)

If all pumps are operating at the same flow rate in all three trains, 33.3% of the transported debris would accumulate on each strainer. However, if the pumps in two trains failed, 100% of the transported debris would accumulate on the active strainer.

5.5.8 Time-Dependent Debris Arrival Model

There are several factors that must be taken into consideration to analyze time-dependent arrival of debris at the strainers or in the core. These factors were addressed in the debris transport calculation as summarized in Table 5.5.5 and illustrated in Figure 5.5.16 (23).

Table 5.5.5 – Time-dependent transport

Source	Time or Equation	Comments
Inactive Cavity Fill	t = ~0 s (no curbs around inactive cavity entrances)	Assume only applies for debris blown to pool and latent debris
Sump Strainer Fill	t ~ 425 s (based on a flow rate of 14,040 gpm and a pool volume of 13,325 ft^3)	Assume only applies to debris blown to pool and latent debris
Total Fill (Switchover)	t ~ 20 min (LBLOCA)	
Initial Washdown	6 s – 1000 s (fines); 2 min – 50 min (small pieces)	Assume washdown occurs after inactive and sump cavities are filled, but before recirculation is initiated
Unqualified Coatings Failure	0 min – 30 days	Conservatively introduced at a constant rate from 10 minutes to 36 hours
Recirculated Spray Flow Debris Washdown	t ~ 300s	Assume instant washdown
Recirculated Break Flow Debris Washdown	t < 300s	Assume instant washdown
Spray Erosion Washdown	t < 15 min	Assume during pool fill
Pool Erosion Recirculation	0-30 days	Assume during pool fill
Initial Debris in Pool at start of recirculation (x_i)	x_i = blowdown + initial washdown - pool fill	Total debris in pool from blowdown and initial washdown minus the debris transported to inactive cavities or the strainer during pool fill
Debris Recirculation Time (x(t))	Described in Section 5.8	Based on arrival time, flow rate, pool volume, debris penetration, and core bypass.

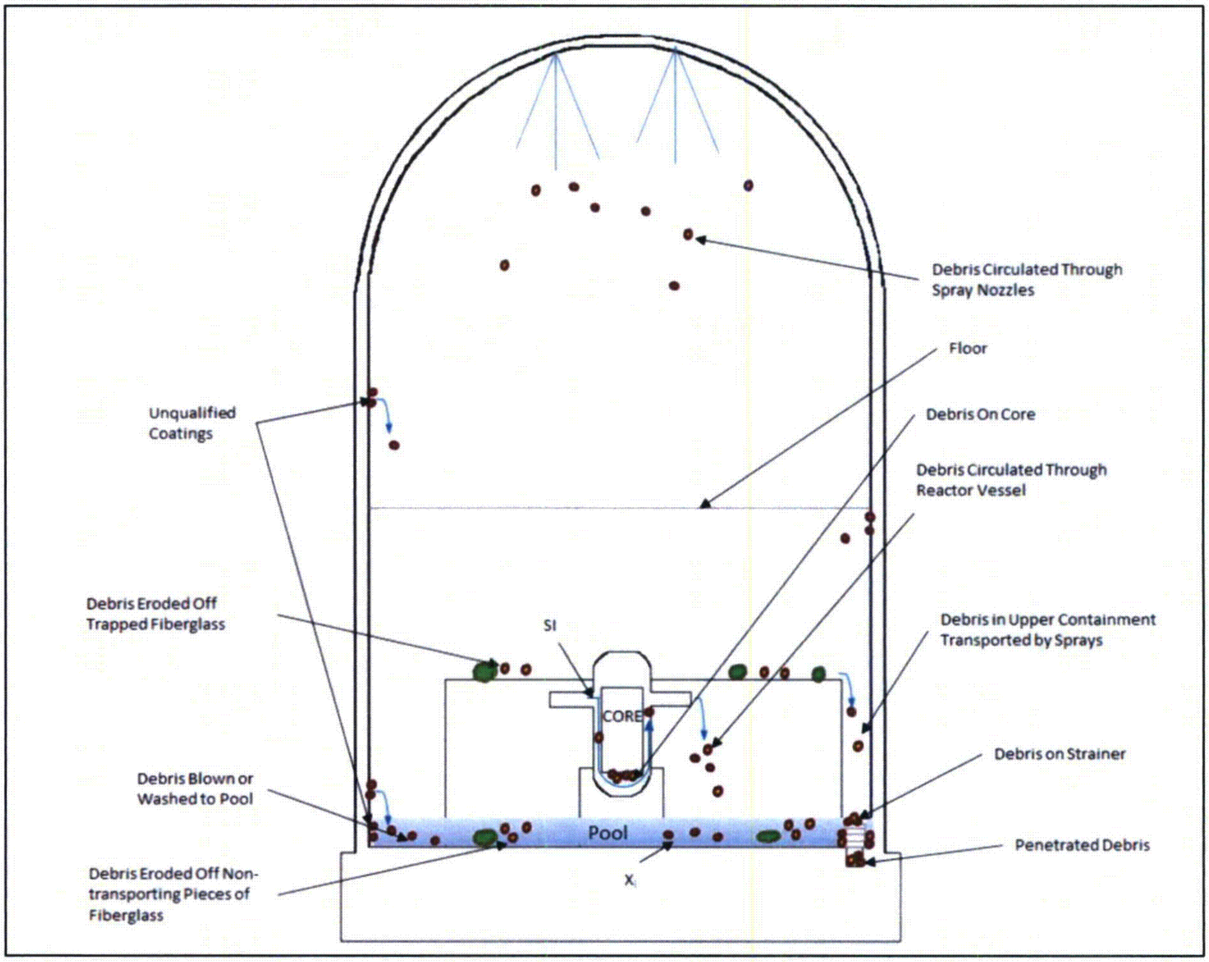

Figure 5.5.16 – Illustration of time-dependent transport

5.6 Strainer Head Loss

Overall head loss across the strainer includes the clean strainer head loss as well as the debris bed head loss from both conventional debris (fiber, particulate, RMI, paint chips, etc.) and chemical precipitates. If the strainer head loss exceeds the NPSH margin of the pumps, the pumps would fail. Similarly, if the head loss exceeds the structural margin of the strainers, the strainers would fail potentially allowing large quantities of debris to be ingested into the ECCS.

5.6.1 Clean Strainer Head Loss

As described in Section 2.2.23, a constant clean strainer head loss value of 0.220 ft was used in CASA. This is the maximum clean strainer head loss that was measured for an equivalent approach velocity of

0.013 ft/s. Note that the maximum strainer approach velocity at STP is 0.0086 ft/s based on a maximum flow rate of 7,020 gpm (see Section 2.2.8) and a strainer area of 1,818.5 ft^2 (see Section 2.2.22).

5.6.2 Conventional Debris Head Loss Model

The NUREG/CR-6224 correlation was selected for the CASA computation of conventional debris head loss[21] across the strainer. This correlation is a semi-theoretical head loss model and is described in detail in Appendix B of NUREG/CR-6224 (70). The correlation is based on theoretical and experimental research for head loss across a variety of porous and fibrous media carried out since the 1940s. The NUREG/CR-6224 head loss correlation was developed in support of the NRC evaluation of the strainer clogging issue in BWRs and has been extensively validated for a variety of flow conditions, water temperatures, experimental facilities, types and quantities of fibrous insulation debris, and types and quantities of particulate matter debris. The types of fibrous insulation material tested include Nukon, Temp-Mat, and mineral wool. The particulate matter debris tested includes iron oxide particles from 1 to 300 μm in characteristic size, inorganic zinc, and paint chips. In all of these cases, the NUREG/CR-6224 head loss correlation has bounded the experimental results. Due to the semi-empirical nature of the correlation STP performed confirmatory head loss tests to demonstrate the applicability of the correlation to STP conditions (24).

<u>NUREG/CR-6224 Head Loss Correlation</u>

The NUREG/CR-6224 head loss correlation, applicable for laminar, turbulent, and mixed flow regimes through mixed debris beds (i.e., debris beds composed of fibrous and particulate matter) is given by Equation 33:

$$\Delta H = \Lambda\left[3.5 S_v{}^2 \alpha_m{}^{1.5}(1 + 57\alpha_m{}^3)\mu U + 0.66 S_v \frac{\alpha_m}{1-\alpha_m}\rho U^2\right]\Delta L_m \qquad \text{Equation 33}$$

where:

- ΔH = Head loss
- S_v = Surface to volume ratio of the debris
- μ = Dynamic viscosity of water
- U = Fluid approach velocity
- ρ = Density of water
- α_m = Mixed debris bed solidity (one minus the porosity)
- ΔL_m = Actual mixed debris bed thickness
- Λ = Conversion factor:

[21] The term "conventional debris head loss" is used to distinguish between the debris bed head loss caused by typical fiber and particulate debris vs. the head loss caused by chemical effects.

Λ = 1 for SI units
Λ = 4.1528x10^{-5} (ft-water/in)/(lb_m/ft^2-s^2) for English units

The fluid approach velocity, U, is given simply in terms of the volumetric flow rate and the effective surface area:

$$U = \frac{Q}{A}$$ Equation 34

where:

Q = Total volumetric flow rate through the screen
A = Screen surface area

The screen surface area (A) is the submerged (wetted) surface area of the screen. The available surface area may change with time, particularly in the case of the STP strainer design. As more debris reaches the strainer the surface area may eventually evolve to the circumscribed area as the debris starts to fill up the interstitial volume. If the debris load is sufficient to fill the entire interstitial volume, the head loss for the STP strainer is calculated using the circumscribed area with a debris load equal to the total debris load transported to the strainer less the quantity of debris required to fill in the interstitial volume of the strainer.

The mixed debris bed solidity (α_m) is given by:

$$\alpha_m = \left(1 + \frac{\rho_f}{\rho_p}\eta\right)\alpha_o \frac{c}{c_o}$$ Equation 35

where:

α_o = Solidity of the original fiber blanket (i.e., the "as fabricated" solidity)
η = Particulate to fiber mass ratio in the debris bed (m_p/m_f)
ρ_f = Fiber density
ρ_p = Average particulate material density
c = Actual packing bed density corresponding to a pressure gradient of $\Delta H/\Delta L_o$
c_o = Reference packing density or theoretical packing density

For debris deposition on a flat surface of a constant size, the compression (c) relates the actual debris bed thickness (ΔL_m) and the theoretical fibrous debris bed thickness (ΔL_o) via the relation:

$$c = c_o \frac{\Delta L_o}{\Delta L_m}$$ Equation 36

Compression of the fibrous bed due to the pressure gradient across the bed is also taken into consideration. The relation that accounts for this effect, which must be satisfied in parallel to the previous equation for the head loss, is given by the following equation valid for $(\Delta H/\Delta L_o) > 0.5$ ft-water/inch-insulation:

$$\frac{c}{c_o} = 1.3\left(\frac{\Delta H}{\Delta L_o}\right)^{0.38}$$ Equation 37

It should be noted that this formulation for debris bed compression may over predict compression significantly in the case of very thick debris layers (roughly 6-inches or more). Thus, in these cases, it is conservative.

For very large pressure gradients, the compression has to be limited such that a maximum solidity is not exceeded. In NUREG/CR-6224, this maximum solidity is defined to be:

$$\alpha_m = \frac{65\, lb_m/ft^3}{\rho_p}$$ Equation 38

This is equivalent to having a debris layer with a density of 65 lb_m/ft^3. Note that 65 lb_m/ft^3 is the macroscopic, or bulk density of a granular media such as sand or gravel and clay.

Each debris constituent has a surface-to-volume ratio based on the characteristic shape of that debris type. For typical debris types, this includes:

Cylindrically-shaped debris:	S_v = 4/diam
Spherically-shaped debris:	S_v = 6/diam
Flakes (flat-plates):	S_v = 2/thick

where:

'diam' = Diameter of the fiber or spherical particle, and
'thick' = Thickness of the flake/chip.

The average surface to volume ratio for several debris constituents was calculated in CASA Grande using the following equation:

$$S_v = \frac{\sum(S_{v_n} \cdot m_n)}{\sum m_n}$$ Equation 39

where the subscript 'n' refers to the n^{th} constituent, and m_n is the mass of each constituent. Linear mass weighting was used because CASA Grande tracks the mass of each debris constituent in the pool, and the individual proportion of S_v contribution to the composite depends on the quantity of each constituent that is present in the bed at any point in time. Many alternative composite weighting schemes could be considered including some based on volume fractions rather than mass fractions that incorporate geometric weighting like the square-root of the sum of squared contributions. Note that using a mass-weighted averaging to calculate the surface to volume ratio deviates from the guidance in NEI 04-07 Volume 2 Appendix V, which specifies a volumetric-weighted averaging (45). Also note that performing the averaging using a linear term rather than a squared term results in a lower S_v value (45).

Debris Parameters Required for Head Loss Calculations

The NUREG/CR-6224 head loss correlation requires the following debris parameters:

- Microscopic density, also referred to as "material" density
- Macroscopic density, also referred to as "bulk" density
- Characteristic size, which is the dimension to be used in computing the surface to volume ratio (i.e., diameter for fibers and particulates, and thickness for chips)

Table 5.6.1 and Table 5.6.2 show the parameter values that were used for the head loss calculations in CASA Grande. These parameters are largely based on the debris characteristics provided in Section 2.2.16. However, there were some modifications to some of the values:

- As described in Assumption 1.f, the small and large pieces of Nukon were treated the same as the fiber fines (i.e., 7 micron diameter with an S_v of 571,429 m^{-1}).
- As described in Assumption 1.d, Thermal-Wrap LDFG was assumed to be identical to Nukon LDFG (i.e., 7 micron diameter, 175 lb_m/ft^3 microscopic density, and 2.4 lb_m/ft^3 macroscopic density).
- Since the Microtherm debris would fail as fines, the density of the Microtherm fiber that accumulates on the strainer would be essentially the same as the density of the other fiberglass fines (i.e., 2.4 lb_m/ft^3).
- A crud diameter of 15 μm was used to represent the size range of 8 to 63 μm. This diameter on the conservatively low end of the range.
- An unqualified coatings diameter of 10 μm was used to represent the size range of 4 to 20 μm for unqualified alkyd, enamel and IOZ coatings. This diameter is on the conservatively low end of the range.
- A crud density of 350 lb_m/ft^3 was used to represent the density range of 325 to 556 lb_m/ft^3. This density is on the conservatively low end of the range.

Table 5.6.1 – Head loss characteristics for fibrous debris

Debris Type	Size	Geometry	Size	S_v (m^2/m^3)	Microscopic Density (lb_m/ft^3)	Macroscopic Density (lb_m/ft^3)
LDFG	Fines	cylinder	7 microns	571,429	175	2.4
	Small Pieces	cylinder	7 microns	571,429	175	2.4
	Large Pieces	cylinder	7 microns	571,429	175	2.4
Microtherm Fiber	Fines	cylinder	6 microns	666,667	165	2.4
Latent Fiber	Fines	cylinder	7 microns	571,429	175	2.4

Table 5.6.2 – Head loss characteristics for non-fibrous debris

Debris Type	Size	Geometry	Size	S_v (m^2/m^3)	Microscopic Density (lb_m/ft^3)	Macroscopic Density (lb_m/ft^3)
Microtherm TiO_2	Fines	sphere	20 microns	300,000	262	52.40[22]
Microtherm SiO_2	Fines	sphere	2.5 microns	2,400,000	137	27.40[22]
Qualified Epoxy	Fines	sphere	10 microns	600,000	94	36.66[23]
Qualified IOZ	Fines	sphere	10 microns	600,000	208	81.12[23]
Crud	Fines	sphere	15 microns	400,000	350	70.00[22]
Unqualified Epoxy	Fines	sphere	152 microns	39,474	124	48.36[23]
	Fine Chips	chip[24]	15 mil thick	5,249	124	48.36[23]
	Small Chips	chip[24]	15 mil thick	5,249	124	48.36[23]
	Large Chips	chip[24]	15 mil thick	5,249	124	48.36[23]
	Curled Chips	chip[24]	15 mil thick	5,249	124	48.36[23]
Unqualified Alkyd	Fines	sphere	10 microns	600,000	207	80.73[23]
Unqualified Enamel	Fines	sphere	10 microns	600,000	93	36.27[23]
Unqualified IOZ	Fines	sphere	10 microns	600,000	244	95.16[23]
Latent Dirt/Dust	Fines	sphere	17.3 microns	346,821	169	33.80[22]

Geometric Strainer Loading

Compact strainer designs like the PCI stacked plate modules used at STP are designed to maximize the surface area available to accommodate a debris load while minimizing the containment floor space taken up by the strainer manifold. The large surface area is intended to distribute total suction flow so that the face velocity of water entering the strainer is very low. For large volumes of fibrous debris, the interstitial gaps between strainer plates can load with debris, the effective surface area of a strainer

[22] Calculated based on a packing fraction of 0.20 for iron oxide sludge (70). See Assumption 7.b.
[23] Calculated based on packing fraction of 0.39 for acrylic coatings debris (24). See Assumption 7.b.
[24] Since CASA Grande does not include an S_v calculation for chips, the chip debris was treated as particles with a spherical diameter of 1,143 microns, which provides an equivalent S_v value as a 15 mil thick chip.

module transitions to a circumscribed shape, and the velocity of water entering the debris bed increases causing additional head loss.

To emulate geometric loading on the STP strainers and conservatively approximate potential increased approach velocity, a table was constructed to relate fibrous debris volume with idealized bed thickness and circumscribed surface area. The approximation treats each STP strainer train as a rectangular box with a clean strainer area, A_0, of 1,818.5 ft^2 (see Section 2.2.22). When the strainer is loaded with a perfectly uniform thickness of 0.5 in., interstitial gaps are full and total flow must cross the circumscribed area. At this thickness the strainer bed is assumed to have the following dimensions (see Section 2.2.22):

- x = 0.5 in (debris thickness)
- A = 419 ft^2 (debris area)
- V = 81.8 ft^3 (debris volume)
- H = 26 in (loaded strainer height with a half inch of debris on the top and bottom of the strainer)
- W = 29 in (loaded strainer width with a half inch of debris on each side)
- L = 44.6 ft (loaded strainer length)

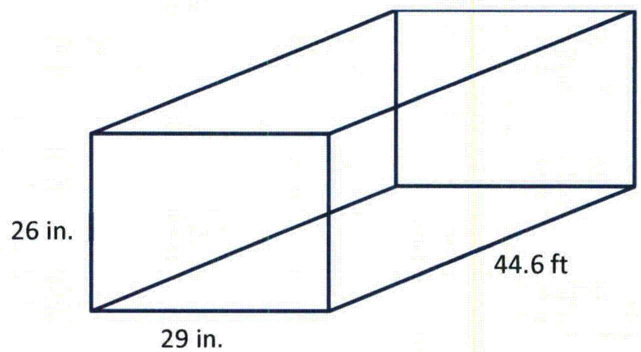

Figure 5.6.1 – Circumscribed strainer dimensions

While debris continues to load on all faces, incremental bed thickness and bed area can be calculated using the following equations for an incremental volume of debris, ΔV:

$$\Delta x = \frac{\Delta V}{2(HW + HL + WL)} \quad \text{Equation 40}$$

$$A = 2[(H + 2\Delta x)(W + 2\Delta x) + (H + 2\Delta x)(L + 2\Delta x) + (W + 2\Delta x)(L + 2\Delta x)] \quad \text{Equation 41}$$

After the incremental thickness exceeds 2 inches, the bottom surface of the strainer is assumed to become inaccessible to further debris loading and the incremental bed thickness and bed area obey the following formulas for an incremental volume of debris, ΔV:

$$\Delta x = \frac{\Delta V}{2H(W+L)+WL} \qquad \text{Equation 42}$$

$$A = 2(H+\Delta x)(W+2\Delta x) + 2(H+\Delta x)(L+2\Delta x) + (W+2\Delta x)(L+2\Delta x) \qquad \text{Equation 43}$$

Incremental thickness is then always added to the initial fully loaded thickness of 0.5 inches. It is assumed that pool depth is always sufficient to permit additional debris loading on the top surface. The loading formulas were evaluated for a wide range of debris volumes to produce the following table that was used in CASA to interpolate bed thickness and area for any time-dependent debris volume.

Table 5.6.3 – Strainer loading table

Volume (ft^3)	Thickness (in)	Area (ft^2)
0	0	1,818.5
81.790	0.5000	419.00
81.800	0.5010	419.31
280.16	8.1421	447.18
478.53	15.783	592.56
676.89	23.424	747.68
875.26	31.065	912.53
1,073.6	38.706	1,087.1
1,272.0	46.348	1,271.4
1,470.3	53.989	1,465.5
1,668.7	61.630	1,669.2
1,867.1	69.271	1,882.7
2,065.4	76.912	2,106.0
2,263.8	84.553	2,338.9
2,462.2	92.194	2,581.6
2,660.5	99.835	2,834.1
2,858.9	107.48	3,096.2
3,057.3	115.12	3,368.1
3,255.6	122.76	3,649.7
3,454.0	130.40	3,941.1
3,652.4	138.04	4,242.2
3,850.7	145.68	4,553.0
4,049.1	153.32	4,873.5
4,247.4	160.96	5,203.8
4,445.8	168.60	5,543.8

4,644.2	176.25	5,893.5
4,842.5	183.89	6,253.0
5,040.9	191.53	6,622.2

Figure 5.6.2 illustrates the relationship between debris volume, bed thickness, and bed surface area that is embodied in the interpolation table.

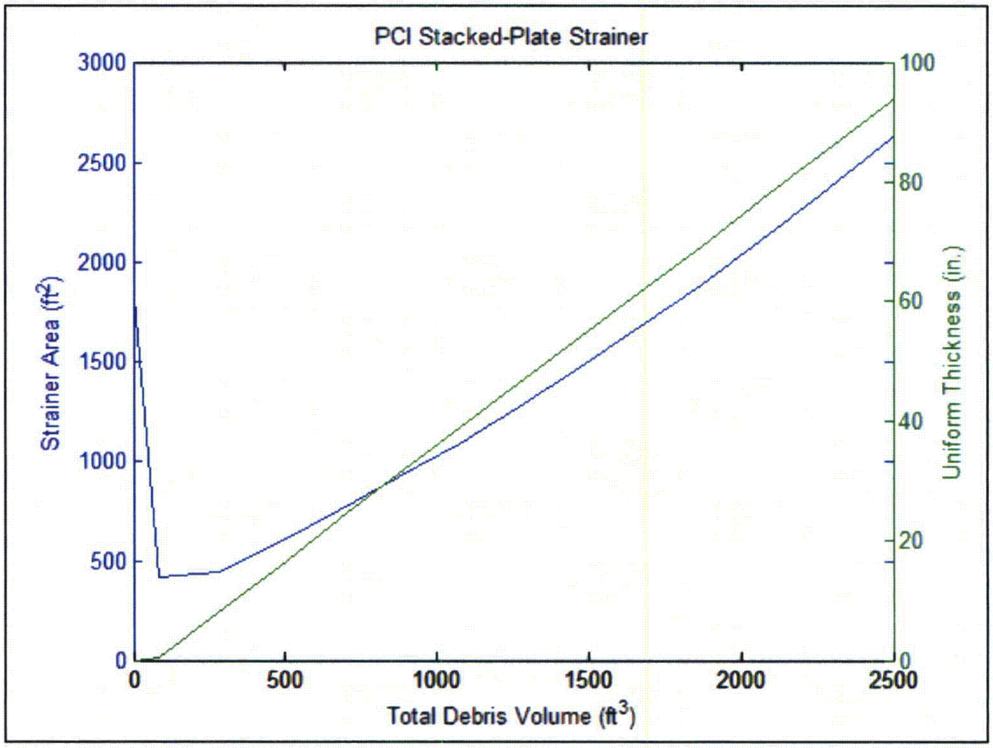

Figure 5.6.2 – Relationship between bed thickness and circumscribed surface area for idealized strainer loading of fiber debris

Applicability of the NUREG/CR-6224 Head Loss Correlation to STP Conditions

The NUREG/CR-6224 head loss correlation has been validated over a large range of approach velocities and debris types. However, there were specific STP conditions where the NUREG/CR-6224 head loss correlation had not been compared to experimental data. In particular, experimental data did not exist to evaluate the impact on the NUREG/CR-6224 head loss correlation for the following conditions:

- Low approach velocities prototypical of the STP strainers – most of the data used to develop the NUREG/CR-6224 head loss correlation was based on tests at higher approach velocities characteristic of the small conical strainers installed in the BWRs before 1992.
- Buffered borated demineralized water – most of the data used to develop the NUREG/CR-6224 head loss correlation was based on tests with tap water. There were some studies done recently that suggested that water chemistry has a significant impact on head loss (77).
- Temperature – most of the data used to develop the NUREG/CR-6224 head loss correlation was based on tests at room temperature.
- NEI fiber debris preparation – most of the data used to develop the NUREG/CR-6224 head loss correlation was based on tests conducted with mechanically shredded fiber debris prior to the development of the NEI debris preparation protocol.

In order to ascertain the applicability of the NUREG/CR-6224 head loss correlation to STP specific conditions, a series of vertical head loss tests were performed (24). The experiments were conducted at STP conditions including the strainer flow approach velocity of 0.0086 ft/s or less, STP-specific water chemistry, a range of temperatures prototypical of the post-LOCA conditions, and STP-specific debris loads.

The application of a head loss correlation to head loss data requires the measurements of head loss, water temperature, and flow velocity for a relatively uniform and homogeneous fibrous/particulate debris bed of known composition at relatively stable conditions. Turbidity measurements, as well as water clarity, are used to judge the completeness of the filtration process.

The correlation validation process depends on knowing the input hydraulic characteristics of each type and size category of debris introduced into the test. Debris size characterization can be used to approximate the hydraulic characteristics of simple forms of debris, such as Nukon fibers, but not for complex particulates. A typical particulate consists of roughly shaped particles of varied sizes making the analytical assessment of the surface to volume ratio, S_v, somewhat difficult and uncertain. Some insulation materials such as calcium silicate, Microtherm, Min-K, and amorphous chemical precipitates have complex forms that simply cannot be assessed analytically, and their impact on head loss has to be addressed experimentally. The solid density of a particle is based on the material properties and the particulate bulk density can be deduced by weighing a known volume of the particulate. The S_v value is deduced by applying a head loss correlation to head loss test data where all parameters are known except the S_v value for the material in question. As such, inaccuracies in the form of the correlation become inherent in the experimentally deduced input parameters. Therefore, the correlation and the hydraulic characteristics become somewhat interdependent.

A total of eleven exploratory head loss tests were performed (24). All testing was done using fibers from a single-side baked Nukon blanket, which was processed using the NEI debris preparation process. All testing was conducted starting at 200 °F at the STP buffered and borated water conditions. The particulate types tested were green silicon carbide, iron oxide (the BWR sludge simulant used in the development of the NUREG/CR-6224 head loss correlation), tin, and ground acrylic paint. Flow and temperature sweeps were performed at the end of some of the experiments to examine the impact of different flow conditions and temperatures.

The NUREG/CR-6224 head loss correlation was used to replicate the measured head loss of the test conducted with iron oxide and a debris bed thickness similar to the test parameters used in the development of the NUREG/CR-6224 head loss correlation (24). The iron oxide S_v value was adjusted until the calculated head loss matched the measured head loss. The final S_v value was in reasonable agreement with the specifications of the size distribution of the sludge simulant indicating that the NUREG/CR-6224 head loss correlation was a reasonable predictor of head losses at STP water and temperature conditions. The iron oxide test, however, was limited to the lowest approach velocity of 0.02 ft/s due to equipment limitations. The NUREG/CR-6224 head loss correlation also generated reasonable estimates of the head loss experiments conducted with ground acrylic paint and extended the approach velocity down to the STP strainer approach velocity of 0.0086 ft/s.

The NUREG/CR-6224 head loss correlation, however, could not replicate the low head losses observed in the tests with tin and/or green silicon carbide. The test report provides a hypothesis for this behavior based on observations of the difference in smooth surfaces noted on SEMs of green silicon carbide and tin as compared to the rough surfaces of iron oxide and ground acrylic paint (24). Further experiments need to be conducted to confirm this hypothesis. This lack of agreement between the NUREG/CR-6224 head loss correlation and testing with green silicon carbide and tin does not impact the STP head loss calculations since there is no green silicon carbide or tin in the STP debris mixture. The green silicon carbide has been used in the past as a simulant of paint, and the tin has been used as a simulant of IOZ coatings. Most of the STP particulate debris comes from coatings, either from qualified coatings in the ZOI or from unqualified coatings elsewhere.

Another anomaly observed in the STP head loss tests was the absence of a direct correlation of the head losses observed in the temperature sweeps with the water viscosity. The test report provides a hypothesis that the temperature also impacts the compression of the fiber debris bed due to the temperature impact on the malleability of the fibers (24). An analytical model was developed to couple the compression to temperature that showed good agreement with the experimentally determined temperature sweep data. The compression algorithm implemented in the NUREG/CR-6224 head loss correlation used in CASA was not modified to incorporate the temperature dependence suggested by the tests. The experiments showed that the measured head losses at lower temperature were lower than the head losses calculated by the NUREG/CR-6224 head loss correlation, hence the CASA calculated head losses are conservative. Additional experiments and analysis need to be performed to validate the temperature dependent compression algorithm prior to its implementation in CASA.

One of the tests conducted (Test 8) was designed to replicate the August 2008 ARL STP prototype test (24; 53). However, this test completely failed to replicate the head losses observed in the previous testing. Both tests used the same primary surrogates of Nukon fibers along with tin and acrylic particulates. Three differences in the tests are: 1) Test 8 had a greater thickness of fiber than was reported in the ARL test, 2) Test 8 used Alion supplied Microtherm and Marinate board particulate instead of the same materials used at ARL, and 3) the ARL fiber debris preparation protocol used a food processor whereas Test 8 used the NEI debris preparation protocol. Based on the experience of the CHLE tests (17), fiber beds with food processor prepared fiber tended to exhibit higher head losses than fiber beds prepared in accordance with the NEI debris preparation protocol. Comparisons of the beds prepared with food processor prepared debris and the NEI debris protocol revealed that the NEI protocol fibers tended to bridge the perforated plate holes and form a debris bed over the perforated plate, while the food processor fibers tended to form low porosity “dimples” at the perforated plate holes. The higher head losses observed with food processor beds was attributed to the formation of the low porosity "dimples". The food processor prepared fibers used in the ARL test could have also formed low porosity "dimples", and allowed the particulate to pack tighter in the ARL test than in Test 8 resulting in a lower porosity bed with higher head losses. The formation of "dimples" in the strainer holes instead of a fiber bed over the perforated plate could also explain the very thin bed observed in the ARL test. The lack of reproducibility of the head losses observed in the Alion vertical loop test compared with the ARL test does not impact the applicability of the NUREG/CR-6224 in calculating the CASA head losses since the differences in the results are attributable to different debris preparation methods. The NUREG/CR-6224 head loss correlation assumes the formation of a debris bed over a perforated plate as was observed with the debris beds prepared in accordance with the NEI debris preparation protocol. Therefore, the NUREG/CR-6224 head loss correlation is considered to be applicable to the debris beds formed with STP prototypical debris.

The test report also addresses the impact of the three main ACRS comments of the NUREG/CR-6224 head loss correlation (24). These ACRS comments were mainly directed at debris beds containing calcium silicate, a known problematic insulation. The test report provides suggested modifications to the NUREG/CR-6224 head correlation to address the three main ACRS concerns (24). Note that all Marinite (similar to calcium silicate) has been removed from containment at STP. Therefore, as shown in the test report, the three main ACRS comments are not significant for STP conditions (24).

Overall, these tests demonstrated that the NUREG/CR-6224 head loss correlation provided reasonable predictions of head loss (as implemented in accordance with the guidance of NEI 04-07) for the prototypical STP debris types and loads, water chemistry, temperature, and strainer approach velocities. However, due to the generic concerns regarding the NUREG/CR-6224 correlation, the head loss calculated using the correlation was increased by a factor of five in CASA Grande to account for uncertainties in the head loss predictions.

5.6.3 Chemical Debris Head Loss Model

A predictive chemical effects evaluation model was not fully developed within this version of the analysis. Therefore, the specific conditions associated with each break scenario (pool volume, pool temperature, debris quantities, etc.) could not be explicitly linked to a corresponding chemical head loss. However, a range of conditions were evaluated using the WCAP-16530-NP calculator and estimated solubility limits for expected product formation to determine a relative comparison of the quantity of precipitates for various break scenarios (20).

For nominal temperature profiles, chemical products (aluminum and calcium precipitates) were not predicted to form for any of the small breaks evaluated. However, some of the medium and large break cases evaluated had total aluminum concentrations that were approximately equal to or slightly higher than the estimated solubility limits (20). The calcium concentration was relatively high for cases where a maximum fiberglass quantity of 2,385 ft^3 was assumed. However, for cases with 60 ft^3 of fiber or less, the calcium concentration was approximately equal to the solubility limit (20). As discussed in Section 5.4.3, the quantity of fiberglass insulation debris generated is less than 10 ft^3 for 99.9% of the scenarios evaluated in CASA Grande. This indicates that even if chemical products form for the nominal scenarios, the effects on strainer head loss would be relatively benign. An evaluation of the chemical concentrations for a maximum temperature profile, however, indicated that the concentration of aluminum would be significantly higher (on the order of 20 times greater than the nominal scenarios). It is possible that these scenarios could result in significant chemical head loss. However, the maximum temperature profiles were developed based on a highly unlikely scenario where the CCW temperature is at the maximum level, four out of six fan coolers fail to operate, and all of the RHR heat exchangers fail (5). Extreme temperature profiles like this have not been fully evaluated, so the current limited testing does not completely preclude the possibility that chemical products may form and arrive at a debris-laden strainer in sufficient quantity to cause unacceptable head loss.

To account for the presence of extreme conditions in the scenario sample space, exponential probability distributions were defined and applied as direct multipliers to the estimated conventional head loss. The probability distributions were developed based on the current results from the CHLE testing (18; 19), WCAP-16530-NP calculations (20), and reasonable engineering judgment. The chemical effects model that was implemented in CASA Grande is described below:

- No bump-up factor is applied if the fiber quantity on a given strainer is less than 1/16 of an inch (see Assumption 7.c).
- No bump-up factor is applied prior to the temperature dropping below 140 °F (see Assumption 5.a). Note that since only two temperature profiles were implemented in CASA Grande (see Section 2.2.6), the increase in head loss would occur approximately 5 hr after the start of the event for large breaks, and approximately 16 hr after the start of the event for small and medium breaks.
- As shown in Table 5.6.4 and Figure 5.6.3 through Figure 5.6.5, the probability distributions for the chemical effects bump-up factors were developed with mean bump-up factors of approximately 2x for small breaks, 3x for medium breaks, and 3x for large breaks, and maximum bump-up factors of approximately 15x for small breaks, 18x for medium breaks, and 24x for large breaks.

The exponential probability density function is defined by a single parameter, the mean, and is continuous on the interval from zero to infinity. The chemical effects bump-up factor should never be less than one, and there is a practical maximum above which all events will lead to sump failure, so the following strategy was adopted. Samples of chemical factor are taken from exponential probability density functions defined using the "formal" parameters given in Table 5.6.4. Manual iteration in a side calculation is used to determine a formal maximum endpoint for each formal mean above which the cumulative tail probability is approximately 1E-5. Thus, the maximum chemical effects bump-up factor is always assigned a weight of 1E-5. Sampling is performed on a logarithmic scale with an emphasis on large values. This means that a much higher proportion of samples are taken from the high end of the range, but each individual sample has a small probability contribution. Finally, all samples from the formal exponential probability density functions are shifted by one unit to guarantee that the applied factors are never less than one.

Shifting all samples by a unit of one has the somewhat unintended consequence of inflating the potential effect of chemical products more than desired. While the desired means are reported as "formal" parameters, the effective means applied in the quantification are actually closer to the "shifted" values given in the table.

Table 5.6.4 – Exponential probability distribution parameters applied to chemical effects bump-up factors for each LOCA category

Parameters		SBLOCA	MBLOCA	LBLOCA	Tail Probability
Formal	Min	0	0	0	~1e-5
	Mean	1.25	1.5	2.0	~1e-5
	Max	14.3	17.2	23	~1e-5
Shifted	Min	1	1	1	~1e-5
	Mean	2.25	2.5	3.0	~1e-5
	Max	15.3	18.2	24	~1e-5

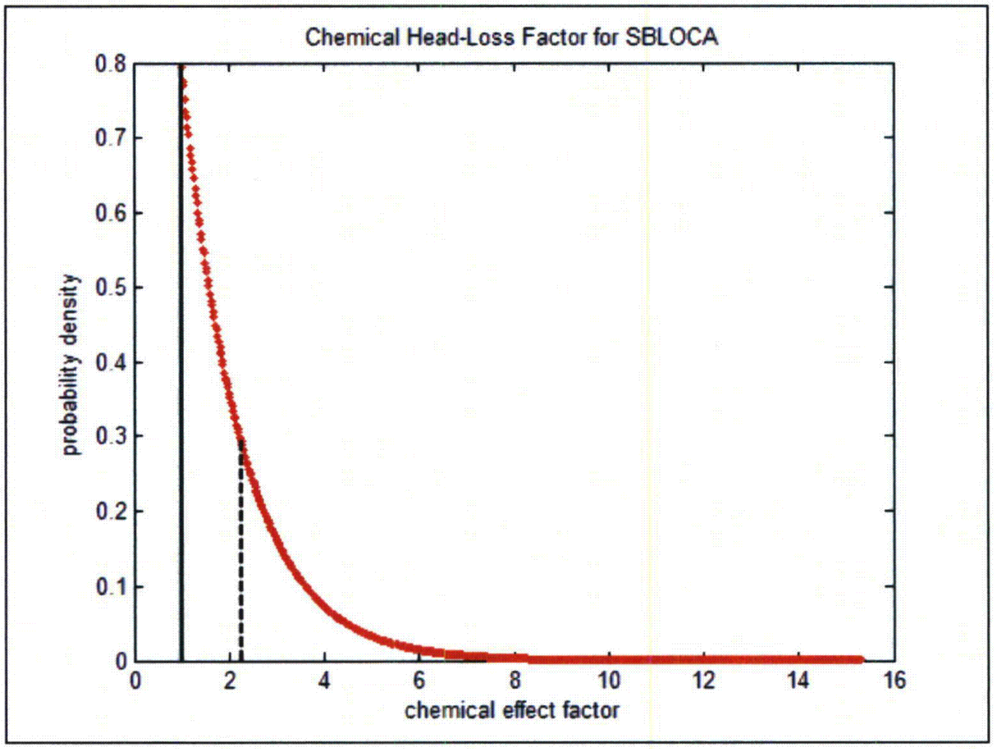

Figure 5.6.3 – Exponential probability density function for chemical effects bump-up factors applied to SBLOCAs

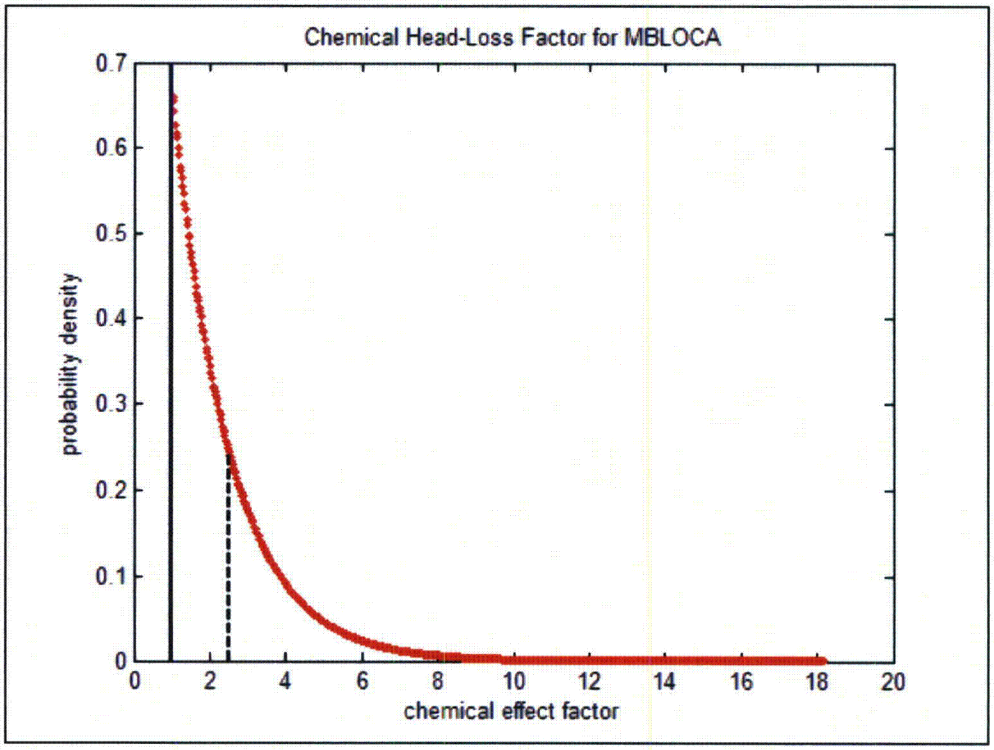

Figure 5.6.4 – Exponential probability density function for chemical effects bump-up factors applied to MBLOCAs

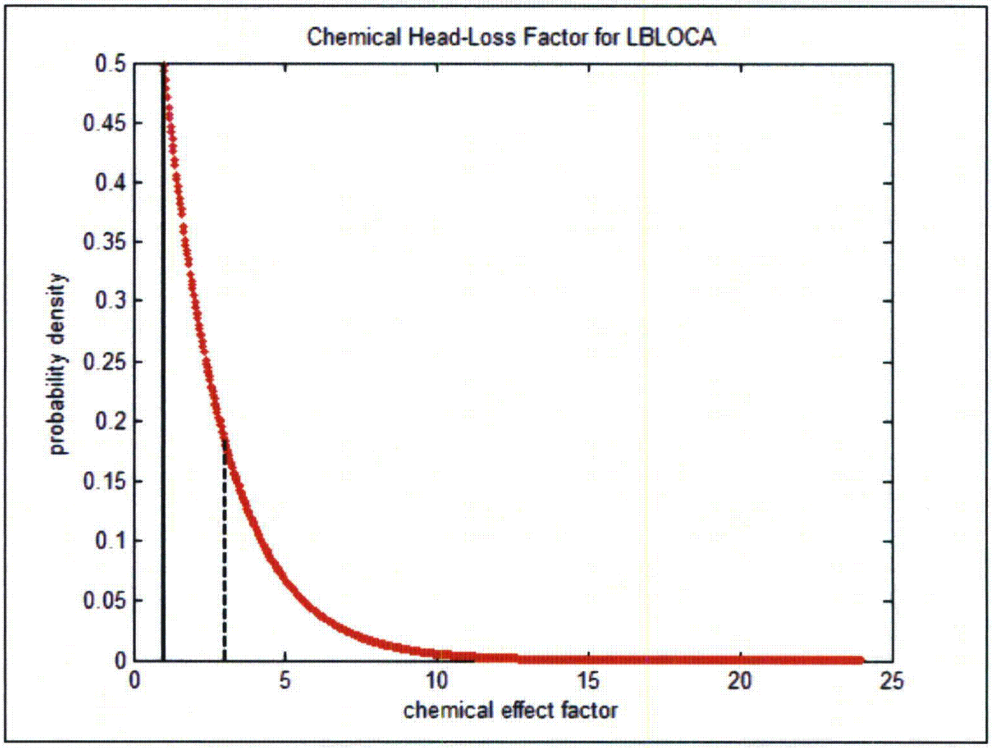

Figure 5.6.5 – Exponential probability density function for chemical effects bump-up factors applied to LBLOCAs

5.6.4 Strainer Head Loss

The overall strainer head loss includes a combination of the clean strainer, debris bed, and chemical head losses as shown in the following equation:

$$\Delta H_S = \Delta H_{CS} + \Delta H_{DB} \cdot B_{CE} \qquad \text{Equation 44}$$

where:

ΔH_S = Total strainer head loss
ΔH_{CS} = Clean strainer head loss
ΔH_{DB} = Conventional debris bed head loss
B_{CE} = Bump-up factor for chemical effects

Figure 5.6.6 shows an example of the time-dependent head loss for random cases evaluated in CASA. Note that the head loss spikes up at approximately 5 hours when the temperature drops below 140 °F and chemical precipitation is assumed to occur, and then spikes back down at approximately 6.5 hours when the containment sprays are secured.

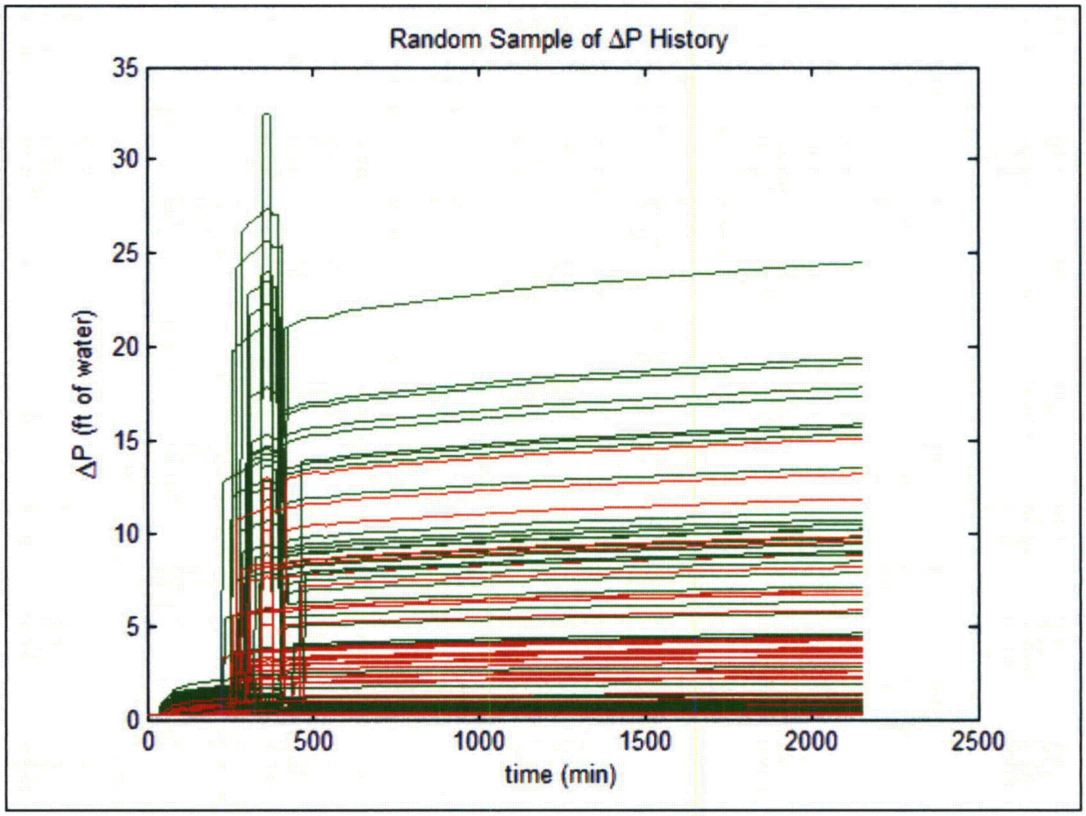

Figure 5.6.6 – Typical sample of sump-strainer head loss histories generated under the assumption of exponential chemical effects factor and artificial head-loss inflation

5.6.5 Acceptance Criterion: NPSH Margin Module

The pump NPSH margin is the difference between the NPSH available and the NPSH required, as shown in Figure 5.6.7 and Equation 45 through Equation 47. Note that the NPSH margin does not include the clean strainer or debris bed head losses. Therefore, the strainer head losses are compared to the NPSH margin to determine whether or not pump cavitation will occur due to loss of NPSH.

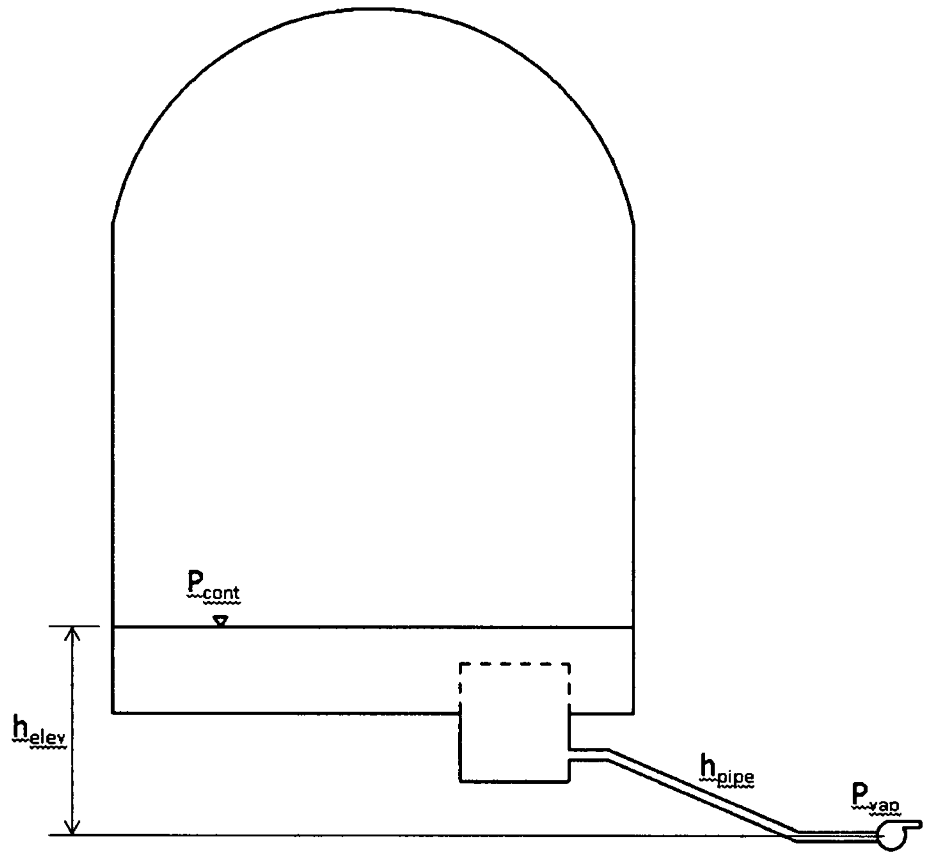

Figure 5.6.7 – Illustration of parameters that affect pump NPSH

$$NPSH_M = NPSH_A - NPSH_R \qquad \text{Equation 45}$$

$$NPSH_A = \frac{P_{cont}}{\rho g} + H_{elev} - H_{piping} - \frac{P_{vap}}{\rho g} \qquad \text{Equation 46}$$

$$NPSH_{R(\alpha_p^* \le 2\%)} = NPSH_{R(\alpha_p^* = 0\%)} \times \left(1 + 0.5\alpha_p^*\right) \qquad \text{Equation 47}$$

where:

$NPSH_M$ = NPSH margin
$NPSH_A$ = NPSH available
$NPSH_R$ = NPSH required
P_{cont} = Containment pressure
ρ = Water density

g = Gravitational acceleration
H_{elev} = Head of water from the pump to the surface of the pool
H_{piping} = Head losses between the strainer and the pump (not including strainer losses)
P_{vap} = Vapor pressure
α_p^* = Volumetric percentage of air in the fluid at the pump inlet ($\alpha_p^* = 100 \cdot \alpha_p$)
α_p = Void fraction of air in the fluid at the pump inlet[25]

As discussed in Assumption 1.c, no credit was taken for containment overpressure. The pressure was assumed to be 14.7 psia, except for cases where the containment pool temperature is greater than 212 °F, where the containment pressure was assumed to be equal to the vapor pressure. The water density and vapor pressure are determined as a function of the containment pool temperature based on standard water properties.

The head of water above the pumps is the sum of the water level above the containment floor and the elevation of the containment floor above the pumps as shown in the equation below. The water level is determined as discussed in Section 2.2.5. The elevation of the pumps below the containment floor is provided in Section 2.2.24.

$$H_{elev} = H_{pool} + H_{pump}$$ Equation 48

where:

H_{pool} = Water level above the containment floor
H_{pump} = Elevation of pumps below the containment floor

The piping flow losses include both major and minor losses, which are a function of cumulative and individual pump flow rates for each train as well as the pool temperature and piping geometry. A schematic of the ECCS suction piping geometry at STP is shown in Figure 5.6.8. The piping flow losses can be calculated using Equation 49 through Equation 51 (25).

[25] As discussed in Assumption 8.i, the void fraction used in CASA was the void fraction at the strainers rather than the void fraction at the pump inlet.

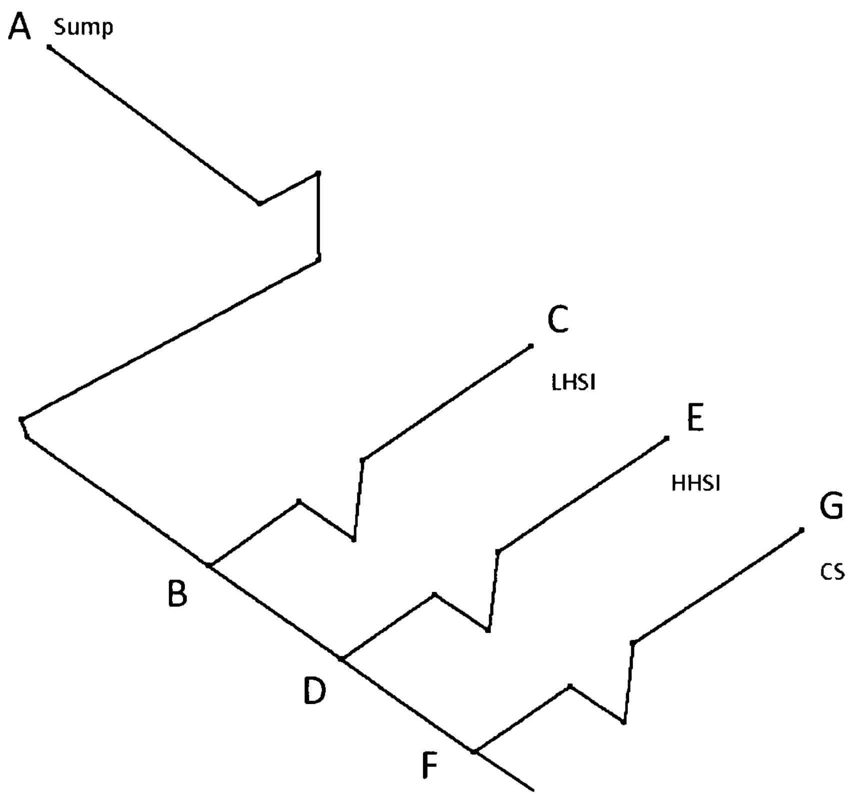

Figure 5.6.8 – Schematic of STP ECCS sump suction piping

$$H_{piping,LHSI} = \left(2.06\frac{s^2}{ft^5}\cdot f_{AB} + 0.005\frac{s^2}{ft^5} + 0.58\frac{s^2}{ft^5}\cdot f_{BC}\right)\cdot (Q_{LHSI} + Q_{HHSI} + Q_{CS})^2 + 2.97\frac{s^2}{ft^5}\cdot f_{BC}\cdot (Q_{LHSI})^2 \quad \text{Equation 49}$$

$$H_{piping,HHSI} = \left(2.06\frac{s^2}{ft^5}\cdot f_{AB} + 0.005\frac{s^2}{ft^5} + 0.19\frac{s^2}{ft^5}\cdot f_{BD}\right)\cdot (Q_{LHSI} + Q_{HHSI} + Q_{CS})^2 + \left(0.09\frac{s^2}{ft^5}\cdot f_{BD} + 0.58\frac{s^2}{ft^5}\cdot f_{DE}\right)\cdot (Q_{HHSI} + Q_{CS})^2 + 6.24\frac{s^2}{ft^5}\cdot f_{DE}\cdot (Q_{HHSI})^2 \quad \text{Equation 50}$$

$$H_{piping,CS} = \left(2.06\frac{s^2}{ft^5}\cdot f_{AB} + 0.005\frac{s^2}{ft^5} + 0.19\frac{s^2}{ft^5}\cdot f_{BD}\right)\cdot(Q_{LHSI} + Q_{HHSI} + Q_{CS})^2 + \left(0.09\frac{s^2}{ft^5}\cdot f_{BD} + 0.19\frac{s^2}{ft^5}\cdot f_{DF}\right)\cdot(Q_{HHSI} + Q_{CS})^2 + \left(0.09\frac{s^2}{ft^5}\cdot f_{DF} + 0.58\frac{s^2}{ft^5}\cdot f_{FG} + 2.95\frac{s^2}{ft^5}\cdot f_{FG}\right)\cdot(Q_{CS})^2 \quad \text{Equation 51}$$

where:

$H_{piping,xx}$ = Flow losses in piping for the LHSI, HHSI, and CS pumps respectively
f_{xx} = Friction factor for various pipe segments illustrated in Figure 5.6.8
Q_{xx} = Flow rate for LHSI, HHSI, and CS pumps respectively

The friction factor is dependent on the Reynolds number, and can be determined using the following equations (25; 78). Note that the implicit form of the friction factor equation in the NPSH calculation (25) was replaced with an explicit equation (78) in CASA to improve runtime.

$$f_{AB} = \left\{-2\cdot\log\left[\frac{\varepsilon}{3.7\cdot D_{AB}} - \frac{5.02}{Re_{AB}}\cdot\log\left(\frac{\varepsilon}{D_{AB}} - \frac{5.02}{Re_{AB}}\cdot\log\left(\frac{\varepsilon}{3.7\cdot D_{AB}} + \frac{13}{Re_{AB}}\right)\right)\right]\right\}^{-2} \quad \text{Equation 52}$$

$$Re_{AB} = \frac{4\cdot\rho\cdot(Q_{LHSI} + Q_{HHSI} + Q_{CS})}{\mu\cdot\pi\cdot D_{AB}} \quad \text{Equation 53}$$

$$f_{BC} = \left\{-2\cdot\log\left[\frac{\varepsilon}{3.7\cdot D_{BC}} - \frac{5.02}{Re_{BC}}\cdot\log\left(\frac{\varepsilon}{D_{BC}} - \frac{5.02}{Re_{BC}}\cdot\log\left(\frac{\varepsilon}{3.7\cdot D_{BC}} + \frac{13}{Re_{BC}}\right)\right)\right]\right\}^{-2} \quad \text{Equation 54}$$

$$Re_{BC} = \frac{4\cdot\rho\cdot(Q_{LHSI})}{\mu\cdot\pi\cdot D_{BC}} \quad \text{Equation 55}$$

$$f_{BD} = \left\{-2\cdot\log\left[\frac{\varepsilon}{3.7\cdot D_{BD}} - \frac{5.02}{Re_{BD}}\cdot\log\left(\frac{\varepsilon}{D_{BD}} - \frac{5.02}{Re_{BD}}\cdot\log\left(\frac{\varepsilon}{3.7\cdot D_{BD}} + \frac{13}{Re_{BD}}\right)\right)\right]\right\}^{-2} \quad \text{Equation 56}$$

$$Re_{BD} = \frac{4\cdot\rho\cdot(Q_{HHSI} + Q_{CS})}{\mu\cdot\pi\cdot D_{BD}} \quad \text{Equation 57}$$

$$f_{DE} = \left\{-2\cdot\log\left[\frac{\varepsilon}{3.7\cdot D_{DE}} - \frac{5.02}{Re_{DE}}\cdot\log\left(\frac{\varepsilon}{D_{DE}} - \frac{5.02}{Re_{DE}}\cdot\log\left(\frac{\varepsilon}{3.7\cdot D_{DE}} + \frac{13}{Re_{DE}}\right)\right)\right]\right\}^{-2} \quad \text{Equation 58}$$

$$Re_{DE} = \frac{4\cdot\rho\cdot(Q_{HHSI})}{\mu\cdot\pi\cdot D_{DE}} \quad \text{Equation 59}$$

$$f_{DF} = \left\{-2 \cdot \log\left[\frac{\varepsilon}{3.7 \cdot D_{DF}} - \frac{5.02}{Re_{DF}} \cdot \log\left(\frac{\varepsilon}{D_{DF}} - \frac{5.02}{Re_{DF}} \cdot \log\left(\frac{\varepsilon}{3.7 \cdot D_{DF}} + \frac{13}{Re_{DF}}\right)\right)\right]\right\}^{-2} \quad \text{Equation 60}$$

$$Re_{DF} = \frac{4 \cdot \rho \cdot (Q_{CS})}{\mu \cdot \pi \cdot D_{DF}} \quad \text{Equation 61}$$

$$f_{FG} = \left\{-2 \cdot \log\left[\frac{\varepsilon}{3.7 \cdot D_{FG}} - \frac{5.02}{Re_{FG}} \cdot \log\left(\frac{\varepsilon}{D_{FG}} - \frac{5.02}{Re_{FG}} \cdot \log\left(\frac{\varepsilon}{3.7 \cdot D_{FG}} + \frac{13}{Re_{FG}}\right)\right)\right]\right\}^{-2} \quad \text{Equation 62}$$

$$Re_{FG} = \frac{4 \cdot \rho \cdot (Q_{CS})}{\mu \cdot \pi \cdot D_{FG}} \quad \text{Equation 63}$$

where:

Re_{xx} = Reynolds number for various pipe segments illustrated in Figure 5.6.8
ρ = Water density as a function of temperature, lb_m/ft^3
μ = Water viscosity as a function of temperature, lb_m/ft-sec
f_{xx} = Friction factor for various pipe segments illustrated in Figure 5.6.8
Q_{xx} = Flow rate for LHSI, HHSI, and CS pumps respectively
D_{xx} = Pipe diameter, ft
ε = Pipe roughness, ft

The NPSH required is a fixed value dependent on the pump specifications. However, if gas voids are present (see Section 5.7), the NPSH required must be adjusted as discussed in Regulatory Guide 1.82 (59).

For each scenario, the time-dependent strainer head loss was compared to the time-dependent NPSH margin to determine whether any failures occur. As discussed in Assumption 12.a, the failure of one pump in any train was assumed to be equivalent to the failure of all pumps in all trains.

5.6.6 Acceptance Criterion: Structural Margin

The strainer structural margin is 9.35 ft (see Section 2.2.25). If the strainer head losses exceed the structural margin, the strainer may fail allowing large quantities of debris to be ingested. As discussed in Assumption 12.b, the structural failure of one strainer was assumed to lead to complete ECCS failure.

5.7 Air Intrusion

The presence of air or other gasses in the ECCS, CSS, or other systems can result in the failure of those systems to perform their intended safety functions. Gas intrusion and accumulation issues have been evaluated in response to Generic Letter 2008-01 (GL 08-01), which identifies concerns with gas upstream of pumps causing potential pump failure, gas downstream of pumps causing water hammer effects when the pump is started, and other potential issues (79). Some of these issues are directly related to GSI-191, since it is possible for air to enter the ECCS and CSS through vortexing or degasification at the strainers during recirculation.

5.7.1 Vortex Formation

Vortex formation can appear to be an almost random variable since it is strongly influenced by minor variations in the local flow conditions. However, as discussed in a series of NUREGs (80; 81; 82; 83; 84), vortex formation is somewhat related to the Froude number. In general, vortexing is dependent on the strainer flow rate, the submergence depth, the strainer geometry, and to some extent the containment geometry (which could either induce or inhibit swirling as the flow approaches the strainer). Vortexing can be easily prevented with simple structures that disrupt swirling motion in the flow.

ECCS strainer vortexing has been evaluated at STP, and based on the strainer design, it has been determined that vortexing would not occur under even under bounding conditions (56). Therefore, there would be no air ingestion due to vortexing.

5.7.2 Degasification

Under a given set of conditions (temperature, pressure, humidity, etc.), a certain quantity of air can be dissolved in water. If these conditions change, some of the dissolved air may be released from the water. In a LOCA scenario, some air would be dissolved in the containment pool, and as the water passes through the ECCS strainer, the head loss across the strainer would cause some of the air to be released.

The following generic properties of air and water are necessary for calculating degasification:

- The composition of air is approximately 78.08% nitrogen (N_2), 20.95% oxygen (O_2), 0.93% argon (Ar), and 0.04% carbon dioxide (CO_2) with trace amounts of other gasses (85).
- The critical temperature of water is 647.14°K (86).
- The molecular weight of water is 18.01528, the molecular weight of nitrogen is 28.01348, the molecular weight of oxygen is 31.9988, the molecular weight of Argon is 39.948, and the molecular weight of carbon dioxide is 44.010 (86). The overall molecular weight of air is approximately 28.97.

The quantity of air released from a given volume of water across an ECCS strainer can be determined by subtracting the concentration of air dissolved in water in the containment pool by the concentration of air dissolved in water downstream of the strainer. The concentration of air is calculated using Henry's Law:

$$C_G = K_G(T) \cdot P_G$$ Equation 64

where:

C_G = Saturation concentration of air
K_G = Henry's constant for air at a given temperature
T = Temperature
P_G = Partial pressure of air

Henry's Constant for Air-Water Solutions

Henry's constant for air (K_G) can be determined based on the individual Henry's constant for each component of air (N_2, O_2, Ar, and CO_2). The volatility constant for each of these components can be calculated using the following semi-empirical correlation (87):

$$ln(k_c) = ln(P_{SAT}) + \frac{A_C}{T^*} + \frac{B_C \cdot (1 - T^*)^{0.355}}{T^*} + C_C \cdot e^{(1-T^*)} \cdot (T^*)^{-0.41}$$ Equation 65

where:

k_c = Volatility constant in units of pressure
P_{SAT} = Saturation pressure at the given temperature
A_C, B_C, C_C = Constants provided in Table 5.7.1
T^* = T/T_c where T is the temperature and T_c is the critical temperature of water (°K)

Table 5.7.1 – Semi-empirical correlation parameters to calculate Henry's constants in aqueous solvent (87)

Solute	A_C	B_C	C_C	Maximum T (K)
Nitrogen	-11.6184	4.9266	13.3445	636.5
Oxygen	-9.4025	4.4923	11.3387	616.48
Argon	-7.4316	4.2239	9.6803	568.4
Carbon Dioxide	-9.4234	4.0087	10.3199	631.7

The relationship between the volatility constant and the Henry's solubility constant is shown in Equation 66.

$$K_c = M_c \cdot \frac{\rho_{H_2O}}{k_c \cdot M_{H_2O}}$$ Equation 66

where:

K_c = Henry's solubility constant for gas component
k_c = Volatility constant for gas component
ρ_{H2O} = Density of water
M_C = Molecular weight of gas component
M_{H20} = Molecular weight of water

The overall solubility constant for air can be calculated using the individual solubility constants as shown in Equation 67.

$$K_{Air} = K_{N_2} \cdot F_{N_2} + K_{O_2} \cdot F_{O_2} + K_{Ar} \cdot F_{Ar} + K_{CO_2} \cdot F_{CO_2}$$ Equation 67

where:

K = Henry's solubility constant for each gas component
F = Mole fraction of each gas component

<u>Concentration of Air in Containment Pool</u>

The partial pressure of air in the containment atmosphere can be calculated as shown in Equation 68 using the containment pressure (P_0) and the vapor pressure ($P_{V,0}$). Note that the subscript 0 is used to designate conditions upstream of the ECCS strainer.

$$P_{G,0} = P_0 - P_{V,0}$$ Equation 68

The vapor pressure can be calculated based on the saturation pressure (P_{SAT}) at the pool temperature, and the relative humidity in containment (ϕ_0) as shown in Equation 69.

$$P_{V,0} = \emptyset_0 \cdot P_{SAT}(T_0)$$ Equation 69

Combining Equation 69 into Equation 68 and Equation 68 into Equation 64 yields the following:

$$C_{G,0} = K_G(T_0) \cdot [P_0 - \emptyset_0 \cdot P_{SAT}(T_0)]$$ Equation 70

where:

$C_{G,0}$ = Saturation concentration of air in the containment pool
K_G = Henry's constant for air at the pool temperature
T_0 = Temperature of the containment pool
P_0 = Containment pressure
ϕ_0 = Relative humidity in containment
P_{SAT} = Saturation pressure at the pool temperature

Concentration of Air Downstream of ECCS Strainer

The pressure downstream of the ECCS strainer can be calculated using the containment pressure (P_0), the hydrostatic head of water above the strainer, and the pressure loss across the strainer (ΔP_{LOSS}) as shown in Equation 71. The subscript 1 is used to designate conditions downstream of the strainer. Note that if the pressure downstream of the strainer is less than the saturation pressure, boiling will occur resulting in a gas void fraction of essentially 100%. This condition is identified with a flag in CASA Grande.

$$P_1 = P_0 + \rho_L(T_0) \cdot g \cdot H_L - \Delta P_{LOSS} \qquad \text{Equation 71}$$

Similar to the containment pool calculation, the partial pressure of air and the vapor pressure downstream of the ECCS strainer can be calculated using Equation 72 and Equation 73. Note that the temperature downstream of the strainer is assumed to be the same as the temperature in the containment pool.

$$P_{G,1} = P_1 - P_{V,1} \qquad \text{Equation 72}$$
$$P_{V,1} = \emptyset_1 \cdot P_{SAT}(T_1) = \emptyset_1 \cdot P_{SAT}(T_0) \qquad \text{Equation 73}$$

Combining Equation 71 and Equation 73 into Equation 72 and Equation 72 into Equation 64 yields the following:

$$C_{G,1} = K_G(T_0) \cdot [P_0 + \rho_L(T_0) \cdot g \cdot H_L - \Delta P_{LOSS} - \emptyset_1 \cdot P_{SAT}(T_0)] \qquad \text{Equation 74}$$

where:

$C_{G,1}$ = Saturation concentration of air downstream of the strainer
K_G = Henry's constant for air at the pool temperature
T_0 = Temperature of the containment pool
P_0 = Containment pressure
ρ_L = Water density at the pool temperature
g = Gravity
H_L = Pool height above the strainer

ΔP_{LOSS} = Pressure drop across the strainer
ϕ_1 = Relative humidity downstream of the strainer
P_{SAT} = Saturation pressure at the pool temperature

Quantity of Gas Released

After determining the concentration of air in solution before and after the strainer, the gas released can be simply calculated as shown in Equation 75.

$$\Delta C_G = C_{G,0} - C_{G,1} \qquad \text{Equation 75}$$

Note that the concentration of air released is in units of mass of air per unit volume of water. Therefore, the mass rate (Δm_G) that air is released from the water can be calculated by multiplying the concentration of gas released by the flow rate through the strainer (Q_L) as shown in Equation 76.

$$\Delta m_G = \Delta C_G \cdot Q_L \qquad \text{Equation 76}$$

The ideal gas law can then be used to convert the mass of gas released to a volume.

$$Q_G = \frac{\Delta m_G}{M} \cdot \frac{R \cdot T_0}{P_{G,1}} \qquad \text{Equation 77}$$

where:

Q_G = Volumetric flow rate of air released
Δm_G = Mass flow rate of air released
M = Molecular weight of air
R = Ideal gas constant
T_0 = Temperature of the containment pool
$P_{G,1}$ = Partial pressure of air downstream of the strainer

The void fraction (α_s) can be calculated as shown in Equation 78.

$$\alpha_s = \frac{Q_G}{Q_G + Q_L} \qquad \text{Equation 78}$$

It is important to note that this void fraction is the void fraction just downstream of the strainers. However, the concern is the void fraction at the pump inlet (α_p). Since the temperature between the strainer and pumps would be roughly constant, the volume of the gas voids at the pumps can be calculated based on the ideal gas law:

$$\alpha_{pX} = \frac{P_s}{P_{pX}} \cdot \alpha_{sX}$$ Equation 79

where:

α_{pX} = Void fraction at Pump X
P_s = Pressure inside the strainer
P_{pX} = Pressure at Pump X

In CASA Grande, the void fraction at the pumps was conservatively assumed to be the same as the void fraction downstream of the sump strainers (see Assumption 8.i).

5.7.3 Gas Transport and Accumulation

Depending on the strainer, plenum, sump pit, and suction piping geometry, the local flow conditions, and the size of the gas bubbles released due to the strainer head loss, it is possible that the gas bubbles would either transport through the ECCS pumps or accumulate at a high point upstream of the pumps. Figure 5.7.1 shows an isometric view of one of the ECCS strainers, and Figure 5.7.2 shows a cross-section of the strainer and sump pit. Air bubbles that are released due to degasification would have to transport horizontally or vertically through the stacked disks into the core tube, horizontally through the core tube to the plenum, vertically through the plenum and sump pit to the ECCS suction pipe, and horizontally and vertically through the suction pipe to the pumps.

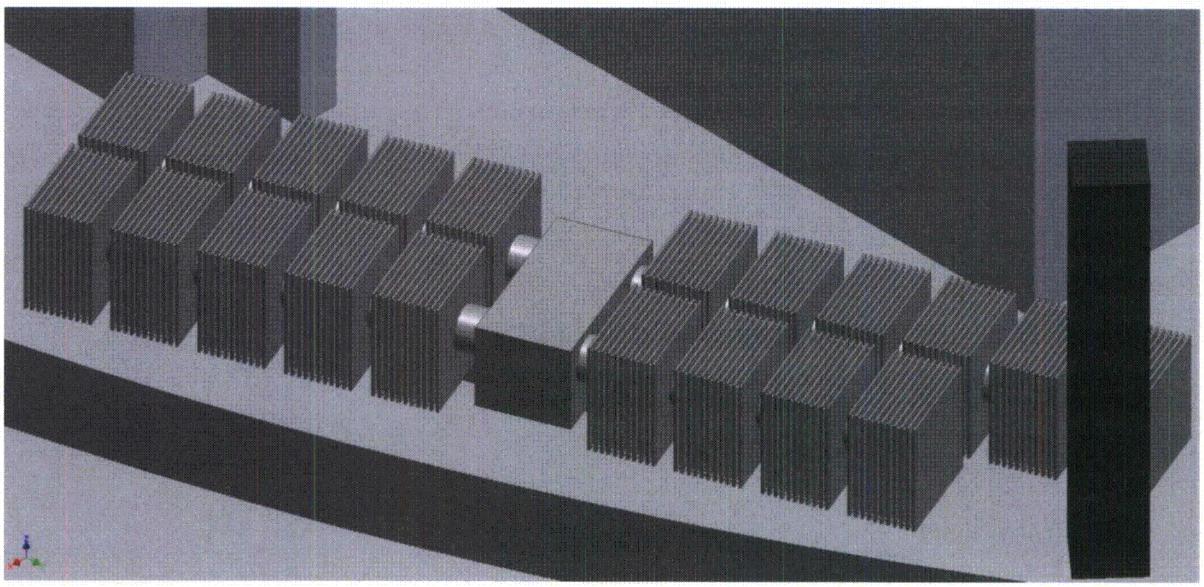

Figure 5.7.1 – Isometric view of ECCS strainer

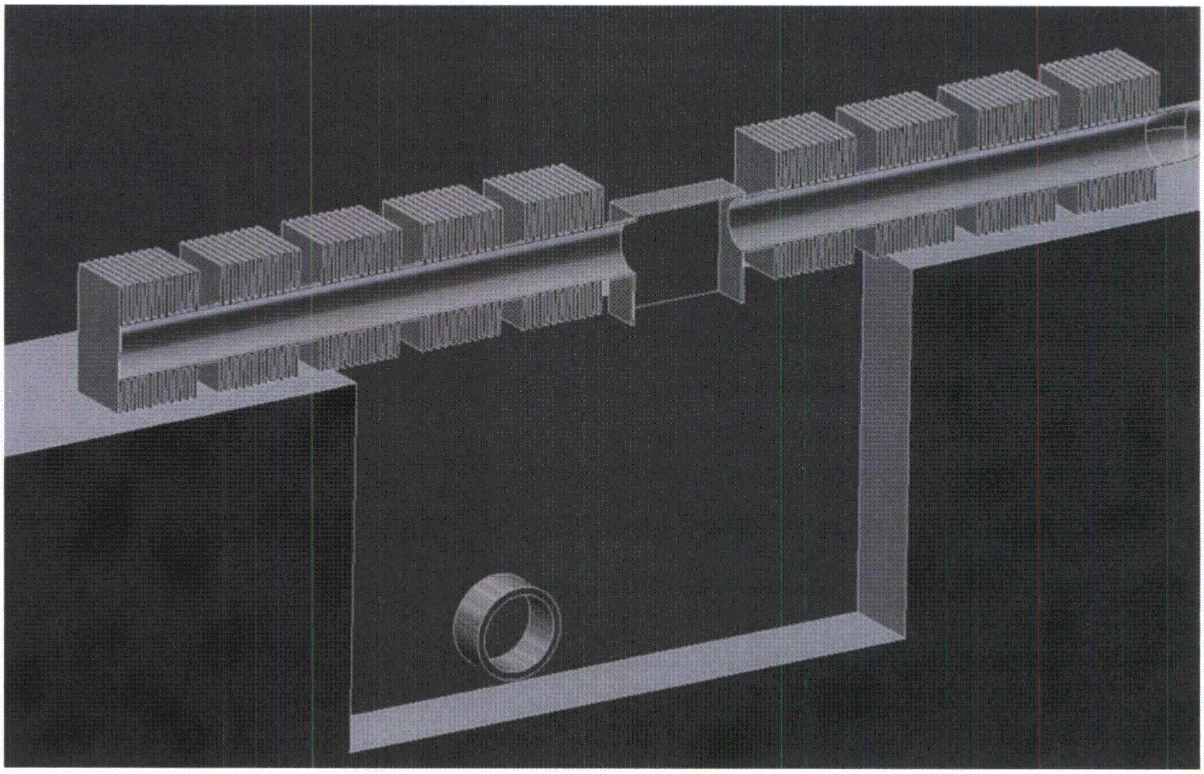

Figure 5.7.2 – Cross-section view of ECCS strainer and sump pit

Bubble transport can be reasonably estimated based on the Froude number. For a horizontal pipe, partial bubble transport will occur when the Froude number is greater than 0.35, and full transport will occur when the Froude number is greater than 0.55 (see Section 2.2.27). The Froude number can be calculated using the following equation:

$$Fr = \frac{v}{\sqrt{g \cdot l}} \qquad \text{Equation 80}$$

where:

Fr = Dimensionless Froude number
v = Velocity (in the core tube, plenum, sump pit, or suction pipe)
g = Acceleration of gravity
l = Characteristic length (hydraulic diameter of the core tube, plenum, sump pit, or suction pipe)

The diameter of the strainer core tube is approximately 0.9 ft (see Section 2.2.22). Assuming a maximum sump flow rate of 7,020 gpm (see Section 2.2.8) split evenly between the four strainer core tubes, the maximum flow rate to each core tube would be 1,755 gpm. The Froude number within the core tubes (near the strainer plenum) is 1.14 as shown in the following calculation:

$$Fr = \frac{1{,}755 gpm}{7.48 \, {}^{gal}/_{ft^3} \cdot 60 \, {}^{s}/_{min} \cdot \pi \cdot \left(\frac{0.9ft}{2}\right)^2 \cdot \sqrt{32.2 \, {}^{ft}/_{s^2} \cdot 0.9ft}} = 1.14 \quad \text{Equation 81}$$

Since the maximum Froude number is greater than 0.55, it is possible that some air would be transported through the core tubes into the plenum. For vertical bubble transport from the plenum to the suction pipe, partial bubble transport will occur when the Froude number is greater than 0.35, and full transport will occur when the Froude number is greater than 1.0 (see Section 2.2.27). The diameter of the suction pipe is approximately 1.3 ft (see Section 2.2.22), and the maximum sump flow rate is 7,020 gpm (see Section 2.2.8). The maximum Froude number within the suction pipe is 1.82 as shown in the following calculation:

$$Fr = \frac{7{,}020 gpm}{7.48 \, {}^{gal}/_{ft^3} \cdot 60 \, {}^{s}/_{min} \cdot \pi \cdot \left(\frac{1.3ft}{2}\right)^2 \cdot \sqrt{32.2 \, {}^{ft}/_{s^2} \cdot 1.3ft}} = 1.82 \quad \text{Equation 82}$$

The horizontal cross-sectional area of the sump pit is 40 ft^2 (see Section 2.2.22). Since the hydraulic diameter of the sump pit (approximately 5.7 ft) is significantly larger than the suction pipe, the Froude number within the sump pit is only 0.03 as shown in the following calculation:

$$Fr = \frac{7{,}020 gpm}{7.48 \, {}^{gal}/_{ft^3} \cdot 60 \, {}^{s}/_{min} \cdot 40ft^2 \cdot \sqrt{32.2 \, {}^{ft}/_{s^2} \cdot 5.7ft}} = 0.03 \quad \text{Equation 83}$$

Therefore, if the bubbles transported to the sump suction piping, they would easily transport to the pumps. However, at the prototypical STP flow rates, it is not likely that the bubbles would transport vertically down through the sump pit. For conservatism in the evaluation of potential pump failures due to air ingestion, and the negative effects of gas voids on the NPSH required, it was assumed that any gas voids caused by degasification would be transported to the ECCS pumps (see Assumption 8.h).

If the velocity within the strainer and sump is not high enough to transport the air bubbles, the air would accumulate at high points within the strainer or plenum. There is a small area at the top of the strainer plenum where it is possible for air to collect. It is also possible that air pockets could form at the top of the strainer disks. As shown in Figure 5.7.3, if a large enough gas void forms at the top of the plenum, air would migrate to the strainer disks closest to the plenum. If the buoyancy of the voids in the strainer disks is greater than the pressure drop across the debris bed on the strainer, the gas voids would break through the debris bed and be vented to the containment pool.

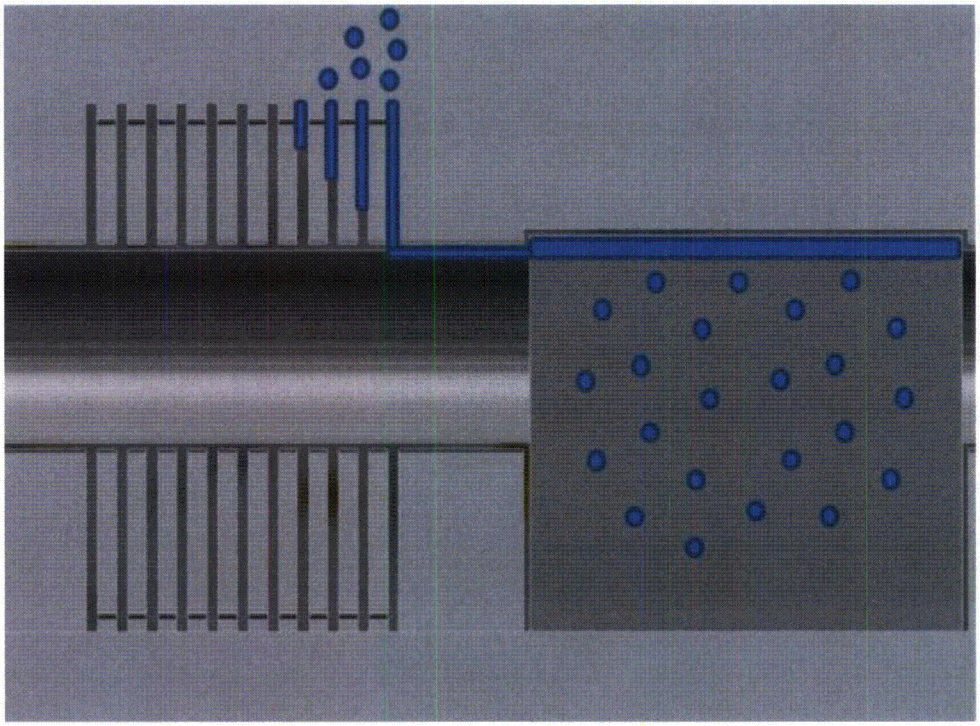

Figure 5.7.3 – Illustration of air bubble accumulation and venting

5.7.4 Acceptance Criterion: Pump Gas Void Limits

As discussed in Section 2.2.28, the acceptance criterion for a steady-state gas void fraction at the pump suction inlet is 2%. As described in Assumption 8.i, the void fraction at the pumps was conservatively assumed to be the same as the void fraction at the strainer.

5.8 Debris Penetration

Debris penetration is a function of two mechanisms. The first mechanism is direct passage of debris as it arrives on the strainer. A portion of the debris that initially arrives at the strainer will pass through, and the remainder of the debris will be captured by the strainers. The direct passage penetration is inversely proportional to the combined filtration efficiency of the strainer and the initial debris bed that forms. The second mechanism is shedding, which is the process of debris working its way through an existing bed and passing through the strainer. By definition, the fraction of debris that passes through the strainer by direct penetration will go to zero after the strainer has been fully covered with a fiberglass debris bed. Shedding, however, is a longer term phenomenon since particulate and small fiber debris may continue to work its way through the debris bed for the duration of the event. These processes are illustrated in Figure 5.8.1.

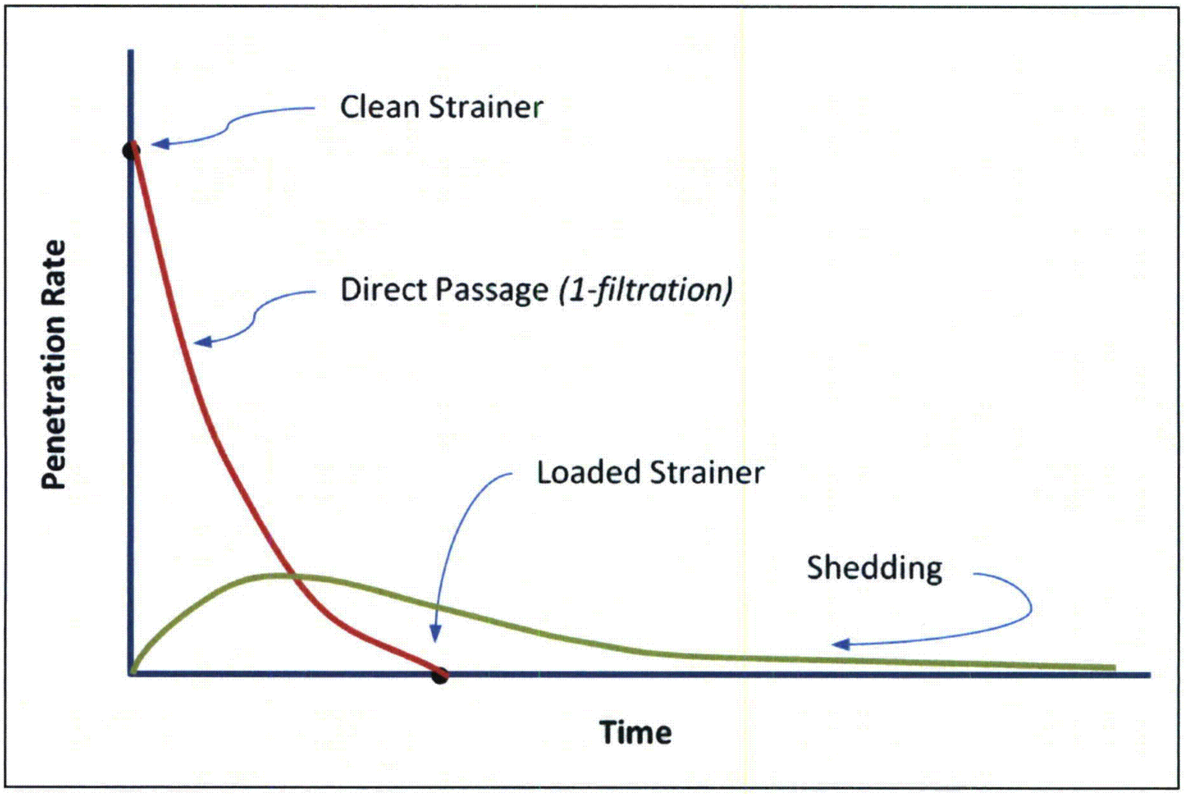

Figure 5.8.1 – Illustration of direct passage and shedding

Debris that penetrates the strainer can cause both ex-vessel and in-vessel problems. Ex-vessel effects are addressed in Section 5.9, and in-vessel effects are addressed in Section 5.10 and Section 5.11. The most significant downstream effects concern is related to the quantity of fiberglass debris that accumulates in the core. This is a highly time-dependent process due to the following time-dependent parameters:

- Initiation of recirculation with cold leg injection
- Switchover to hot leg recirculation
- Arrival of debris at the strainer
- Accumulation of debris on the strainer
- Direct passage
- Debris shedding
- Flow changes when pumps are secured

- Decay heat boil-off

The timing for initiation of recirculation, switchover to hot leg injection, and procedurally securing pumps is described in Section 2.2.1. The time-dependent arrival of debris at the strainer is described in Section 5.5.8. The decay heat boil-off curve, which defines the flow split to the core for cold leg breaks during cold leg injection, is described in Section 5.10.3. Debris accumulation on the strainer and debris penetration through the strainer (including both direct passage and shedding) are described in more detail within this section.

The various parameters associated with time-dependent debris accumulation on the strainer and core are illustrated in Figure 5.8.2, where $S_n(t)$ is the source rate for initial introduction of debris type n, V(t) is the pool volume, $m_n(t)$ is the mass of debris n in the pool, $f_n(t)$ is the filtration efficiency for debris n at the strainer, $s_n(t)$ is the shedding rate for debris n from the existing debris bed, Q(t) is the volumetric flow rate passing through the strainers, γ is the fraction of SI flow compared to the total flow, λ is the fraction of flow passing through the core compared to the total SI flow, and $g_n(t)$ is the filtration efficiency for debris n at the core.

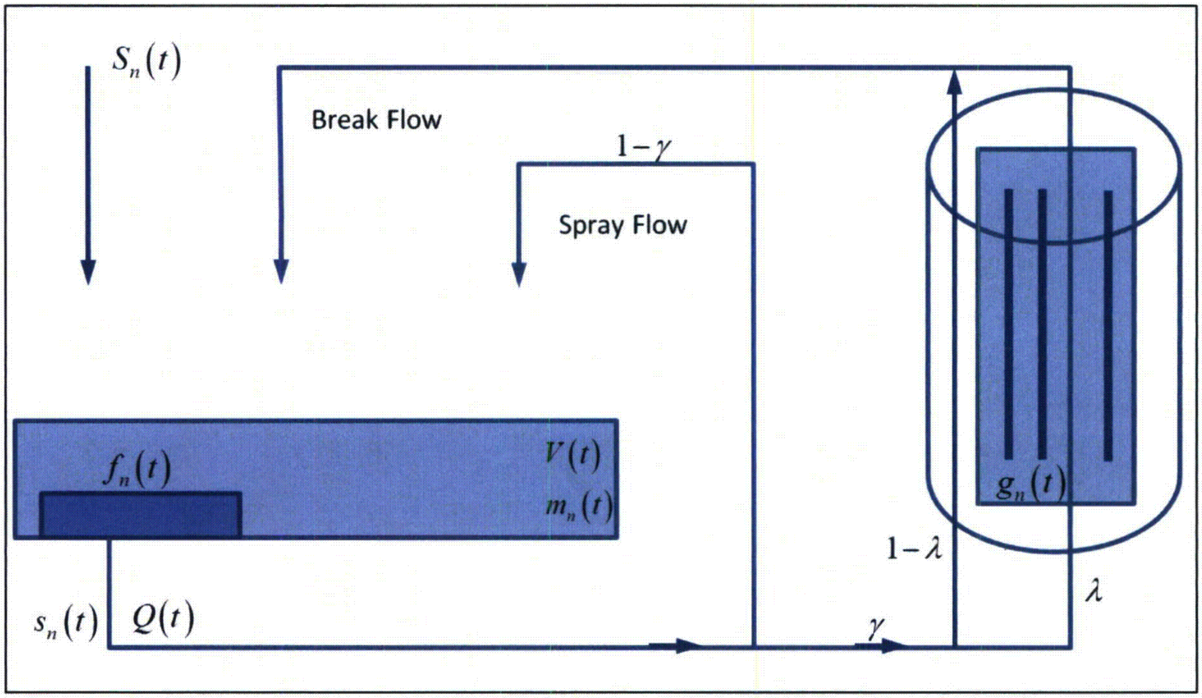

Figure 5.8.2 – Illustration of time-dependent parameters associated with debris accumulation on the strainer and core

As illustrated by Figure 5.8.2, debris that passes through the strainer will not necessarily end up on the core. A portion of the debris could pass through the containment spray pumps, and a portion could either bypass or pass directly through the core and spill out the break. The debris that doesn't accumulate in the core may end up back in the pool where it could transport and potentially pass through the strainer again. The differential rate of change for each debris type in the pool (assuming a homogenous mixing volume) can be described using the following equation (28):

$$\frac{dm_n}{dt} = S_n - f_n \frac{Q}{V} m_n - \gamma \lambda g_n (1 - f_n) \frac{Q}{V} m_n + s_n - \gamma \lambda g_n s_n \qquad \text{Equation 84}$$

where all of the properties can be time-dependent and have the following definitions:

m_n = Mass of debris type n suspended in the pool
t = Time
f_n = Filtration efficiency for debris type n at the strainer
Q = Volumetric flow rate passing through strainers
V = Total volume of the pool
S_n = Source rate for initial introduction of debris type n
s_n = Shedding rate for debris type n from existing bed
g_n = Filtration efficiency for debris type n at the core
γ = Fraction of the total flow going to the SI pumps
λ = Fraction of SI flow going to the core

Note that 100% filtration efficiency at the strainer, f_n, for non-fibrous debris (i.e., particulate or chips) is used in CASA. This is conservative since it maximizes the strainer head loss, and the particulate debris quantity is not considered in the core blockage and boron precipitation acceptance criteria.

Based on Equation 84, the total quantity of debris that accumulates on the strainer or the core can be described by the following equations (28):

$$M_n^S(t) = \int_0^t \left[f_n(t') m_n(t') \frac{Q(t')}{V(t')} - s_n(t') \right] dt' \qquad \text{Equation 85}$$

$$M_n^C(t) = \int_0^t \gamma(t') \lambda(t') g_n(t') \left[\left(1 - f_n(t')\right) \frac{Q(t')}{V(t')} m_n(t') + s_n(t') \right] dt' \qquad \text{Equation 86}$$

where:

M_n^S = Cumulative mass of debris type n on the strainer
M_n^C = Cumulative mass of debris type n on the core
t' = Dummy integration variable where t' ≤ t denotes all times from the start to t of interest

Equation 84 through Equation 86 can be determined using the following analytical solution, where the subscript n has been dropped for simplification:

$$m(t_i) = \frac{S(t_{i-1})}{H(t_{i-1})} \cdot \left[1 - e^{-H(t_{i-1})\cdot\Delta t_{i-1}}\right] + m(t_{i-1}) \cdot e^{-H(t_{i-1})\cdot\Delta t_{i-1}} \quad \text{Equation 87}$$

$$M_j^S(t_i) = M_j^S(t_{i-1}) + f_j(t_{i-1}) \cdot h_j(t_{i-1}) \cdot m(t_{i-1}) \cdot \Delta t_{i-1} - s_j(t_{i-1}) \cdot \Delta t_{i-1} \quad \text{Equation 88}$$

$$M_j^C(t_i) = M_j^C(t_{i-1}) + \Delta t_{i-1} \cdot \sum_{j=1}^{N} \left[s_j(t_{i-1}) + \left(1 - f_j(t_{i-1})\right) \cdot h_j(t_{i-1}) \cdot m(t_{i-1})\right] \cdot \gamma_j(t_{i-1}) \cdot \lambda(t_{i-1}) \cdot g(t_{i-1}) \quad \text{Equation 89}$$

$$S(t_{i-1}) = \sum S_k(t_{i-1}) + \sum_{j=1}^{N} \left[s_j(t_{i-1}) \cdot \left(1 - \gamma_j(t_{i-1}) \cdot \lambda(t_{i-1}) \cdot g(t_{i-1})\right)\right] \quad \text{Equation 90}$$

$$H(t_{i-1}) = \sum_{j=1}^{N} h_j(t_{i-1}) \cdot \left[\frac{\gamma_j(t_{i-1}) \cdot \lambda(t_{i-1}) \cdot g(t_{i-1})}{1 - \gamma_j(t_{i-1}) \cdot \lambda(t_{i-1}) \cdot g(t_{i-1})} + f_j(t_{i-1})\right] \cdot \left[1 - \gamma_j(t_{i-1}) \cdot \lambda(t_{i-1}) \cdot g(t_{i-1})\right] \quad \text{Equation 91}$$

$$h_j(t_{i-1}) = \frac{Q_j(t_{i-1})}{V(t_{i-1})} \quad \text{Equation 92}$$

$$\Delta t_{i-1} = t_i - t_{i-1} \quad \text{Equation 93}$$

where:

t_i = End of specific time step interval
t_{i-1} = Beginning of specific time step interval
N = Number of ECCS strainers
Subscript j = Variables specific to a given ECCS strainer
S_k = Source rate for initial introduction of fiber type k

Each of these equations can be solved by explicit forward integration assuming that the integrands are known at the beginning of each time step and that they remain constant during each time step. Variables such as the source rate of debris to the pool (S), the strainer flow rate (Q), the pool volume (V), the SI and CS flow split (γ), and the SI flow vs. boil-off flow split (λ) are defined in other sections. The filtration efficiency for the core (g) is conservatively assumed to be 100% (i.e., all debris that transports to the core is trapped). Therefore, the primary unknowns in Equation 87 through Equation 93 are the filtration efficiency at the strainer (f) and the shedding rate (s).

The shedding rate can be defined as a function of time as described in the following equation (28):

$$s_n(t) = \nu_n \eta_n e^{-\eta_n t} \int_0^t f_n(t') \frac{Q(t')}{V(t')} m_n(t') e^{\eta_n t'} dt' \qquad \text{Equation 94}$$

where:

ν_n = Fraction of debris type n that is "sheddable" (i.e., able to pass through a debris bed)
η_n = Time constant associated with the shedding process

Similar to the analytical solution above, Equation 94 can be solved as follows where the subscript n has been dropped for simplification:

$$m_j^{sh}(t_i) = m_j^{sh}(t_{i-1}) \cdot e^{-\eta \cdot \Delta t_{i-1}} + \frac{\nu}{\eta} \cdot f_j(t_{i-1}) \cdot h_j(t_{i-1}) \cdot m(t_{i-1}) \left[1 - e^{-\eta \cdot \Delta t_{i-1}}\right] \qquad \text{Equation 95}$$

$$s_j(t_i) = \eta \cdot m_j^{sh}(t_i) \qquad \text{Equation 96}$$

where:

m_j^{sh} = Mass of sheddable debris in the bed

To determine the filtration efficiency and shedding rate, a series of penetration tests were conducted at Alden Research Laboratory (ARL) (26). A combination of 100% capture filter bags and isokinetic grab samples were used to gather data regarding the change in penetration as a function of strainer loading and time. A series of sensitivity tests were also conducted at Texas A&M University (TAMU) and ARL, which showed that penetration is not strongly dependent on water chemistry (27) or debris concentration and flow rate within the range of conditions tested (26). The ARL test data was statistically evaluated to determine appropriate fitting parameters to describe the shedding and filtration terms as a function of the debris load on the strainer and time (60). The filtration equation and fitting parameters for filtration and shedding are provided in Section 2.2.29.